High rate reactive magnetron sputtering

HIGH RATE REACTIVE MAGNETRON SPUTTERING

by

ALARIC GRAHAM SPENCER

A doctoral thesis submitted in partial fulfilment of the requirements for the award of Doctor of Philosophy of the Loughborough University of Technology.

December 1988

Supervisor: Dr R.P. Howson B.Sc. Ph.D.
Department of Physics

ABSTRACT

Glow discharge sputtering has been used for many years to produce thin films but its commercial applications are severely limited by low deposition rates. The DC planar magnetron, developed a decade ago, allows much higher deposition rates and its commercial use has expanded rapidly. Non-reactive magnetron sputtering of metallic thin films is well understood and utilized. However when a reactive gas is introduced the process becomes harder to control and can switch between two stable modes. Often films are produced simply by using one of these stable modes even though this does not lead to optimum film properties or high deposition rates.

This work gives a model of reactive magnetron sputtering and verifies experimentally its predictions. A 0.5 m long magnetron was designed and built specifically to allow reactive sputtering onto A4 rigid substrates. This magnetron has a variable magnetic field distribution which allows plasma bombardment of the substrate during film growth. This was shown to activate reactions at the substrate. The target lifetime was extended in our design by broadening the erosion zone and increasing the target thickness. The reactive sputtering process was shown to be inherently unstable and a control system was designed to maintain the magnetron in an unstable state. Light emission by the plasma at metal line emission wavelengths changes across the instability and so with this control signal a feedback system was built.

The accuracy of control was shown experimentally and theoretically to depend on the delay time between measurement, action and effect. In practice this delay was limited by the time constant of the gas distribution manifold. The time constant of such manifolds was measured and calculated. Using our controller high quality films were produced at high rates in normally unstable deposition systems. Conducting indium oxide was produced at 6 nm/s with a resistivity of 6 x 10^{-6} ohm.metres onto A4 glass sheets. Tin oxide was produced at increased rates onto 2.5 m by 3 m substrates.

ACKNOWLEDGEMENTS

I would particularly like to thank my supervisor Dr R.P. Howson and I am grateful to my director of research Prof. K.R.A. Ziebeck and to E.M. Stenlake, Dr K Oka, R. Lewin and Dr C.A. Bishop, for help and guidance. I would like to thank the many people who have helped me both in Loughborough, Everest Double Glazing, and elsewhere. I would also like to acknowledge the financial support of Everest Double Glazing and my wife. Thankyou Lyn.

UNITS

S.I. units are used throughout for theory and calculation. In practice archaic units are still used and consequently are easier to visualize. My experimental results are therefore presented using mTorr (0.132 Pa) for pressure and sccm (1.667 Pa.l/s) for gas flow rates. All other practical units are S.I.

CONTENTS

2. INTRODUCTION

D.C. Magnetron sputtering is one technique among many for production of thin films onto solid substrates. These coatings are generally 1 nm to 1000 nm thick (10,000 nm for some applications) and can be deposited onto most substrates that can be exposed to vacuum. The starting material must be conducting (usually metallic) and from this can be formed films of metals or metal compounds. In practice this allows the production of a wide choice of coatings to alter many material properties.

Industry profile

Production costs for vacuum deposition of thin films are usually dominated by equipment costs. This is because of the high cost of vacuum apparatus. A single coater may cost anything from £1000,000 to M£ 10. Taking an approximate figure of M£ 1, with interest charges of 10% p.a. and writing off the cost over five years gives per year:-

£100,000	interest
£200,000	to write off cost
£300,000	Total

This is approximately £1000/day. This is a very rough estimate of cost and neglects several important factors (ref. 1) (housing and staffing the machine, consumables, maintenance and down time) but it does give an idea of the costs involved. Now if the production volume is considered we begin to get an overall view of the vacuum coating industry. The above costs may be covered either by high volume production of low cost items or low volume production of high cost items. The industrial use of vacuum for coating can then be arranged according to the production volume.

Table 2.1: Unit Cost of Coating

Market Area	Items per day	Cost per item
Military, Aerospace	1	£1000
	10	£100
Industrial equipment	100	£10
	1000	£1
Consumer goods	10,000	£0.1
	100,000	£0.01
Packaging	1000,000	£0.001

The above analysis considers only the fixed costs (machine payments, buildings, etc). In certain cases the variable costs (materials, substrates, personnel, etc) can dominate eg thicker films of precious metals or high cost substrates such as germanium lenses or aircraft canopies. The cost scalings with production volume will then still occur but not as drastically. The production volume alters the emphasis so that at the high volume end, production rate and downtime are critical whereas at the high cost end, quality and repeatability are paramount. This consequently alters the choice of deposition technique.

Size of markets

The application of thin films to various products is proceeding. A recent U.S. market study (ref. 2) placed the thin film market at B$ 3.0 per annum. The bulk of this is for electronic, opto-electronic and optical products (B$ 2.6). The remainder is for wear resistance, corrosion resistance and decorative coatings. The projected market growth was 15% a year until 1992. The product areas and applications are detailed in table 2.2.

Table 2.2: Major Current Markets

Semiconductors
Micro Electronics
Photo-voltaics
Electro-magnetics (storage media)
Optical (storage media, precision optics, Infra-red coatings)
Architectural Glass
Opto-electronics

Other techniques

To indicate the position of D.C. magnetron sputtering it can be ranked with other techniques in terms of deposition rate and film quality and controllability. For each technique the deposition rate may vary by a few orders of magnitude so there is considerable overlap between techniques. The units given on the left of table 2.3 indicate orders of magnitude only.

Table 2.3: Deposition Rates

Evaporation	micron/sec
Arc evaporation	
Evaporation with ion or plasma bombardment	
Magnetron sputtering	nm/s
Chemical Vapour Deposition (C.V.D.)	
Diode sputtering	
Ion Beam Sputtering	
Molecular Beam Epitaxy (M.B.E.)	Angstrom/hour

The film quality and controllability are vague terms used here to indicate the defect density (dislocations, voids, inclusions) and the degree of independent control over various parameters (film stoichiometry, ion bombardment during growth, energy of depositing species, crystal phases and orientations). The highest film quality and controllability is generally achieved at the lowest rates so a table of film quality (table 2.4) is almost table 2.3 in reverse order.

Table 2.4: Film Quality and Controllability

Molecular Beam Epitaxy	Best
Ion Beam Sputtering	
Chemical Vapour Deposition (C.V.D.)	
Magnetron sputtering	
Diode sputtering	
Evaporation with ion or plasma bombardment	
Evaporation without bombardment	
Arc Evaporation	Worst

Other considerations which may rule out some of the above techniques are the required coating area, and the thermal stability of the substrate. Techniques like M.B.E. or Ion beam sputtering are limited in area and generally coat semiconductor slice sized substrates (currently 200 mm maximum). There are many variants of C.V.D. as the vapour decomposition can be accomplished by many means eg heat, plasmas, or light. These all required substrate heating (to varying degrees) and this is not always possible as some substrates (particularly polymers) cannot be taken to the required temperatures. Diode sputtering also leads to substantial substrate heating that limits its applications.

Magnetron sputtering then comes into its own for coating large areas and giving low substrate heating and/or better film quality and controllability than other techniques. The commercial requirement for a high deposition rate and the considerations for film quality and controllability tend to define the market areas occupied by magnetron sputtering. This can be stated simply as magnetron sputtering will be used for film production when it gives the required film quality and controllability and the faster techniques do not.

Types of Industrial Plant

From this point on we will only consider magnetron sputtering as this is the area covered by this thesis. There are basically three

types of industrial plant used for bulk coating by magnetron sputtering. These have characteristics determined by the substrates and are continuous (load lock) or batch machines for rigid substrates and roll coaters for flexible (usually polymer) substrates (ref 3). All types come in a range of sizes from 0.1 m wide substrates (sometimes smaller) for research to 3 m wide for large area production (coated areas up to 10^5 - 10^6 m^2/year). To get a feel for the deposition rate requirements we can consider the rate needed to give a coating time equal to the pump out time. Rates an order of magnitude faster than this would still be useful as this would approximately half the total process time, double the production volume and so half the unit cost.

The production rate of a load lock machine is generally limited by the pumping cycle of the load lock chamber(s). The deposition rate must then be sufficient to coat a substrate in a time compatible with the pump out time of the lock chamber. This pump out time may be anything from 3 minutes (ref 4) to 10 seconds (ref 5) and the minimum time practical depends on the load lock chamber size ie the substrate size. With coatings in the thickness range 1 nm to 10 microns this is a maximum deposition rate of 10 microns in 10 seconds ie 1 micron/s. This is an enormous rate not achievable with magnetron sputtering, only evaporation comes anywhere near. For a thickness of 100 nm (sufficient for many applications) the required rate falls to 10 nm/s which is high but possible with magnetron sputtering. For the largest substrates with pump out times of around a minute this rate falls further to values well within the capabilities of magnetron sputtering.

Batch coaters must pump out the whole chamber before film deposition starts. A batch coater will generally pump out in the order of hours and so taking a process time of one hour with coatings in the thickness range 1 nm to 10 microns gives a maximum deposition rate of 10 microns/hour ie 2 nm/s which is well within the range of magnetron sputtering.

A roll coater must also pump out the whole chamber before deposition but invariably this contains a large roll of porous or hydroscopic material (ie plastic, paper, fabric) with a large surface

area (refs 3,6). By using cooled surfaces pumping rates up to 10^5 l/s for water can be achieved (ref 3) and the evacuation time may be brought to around 12 hours. The roll may be a km or more in length (ref 7) so taking a deposition zone of 10 cm with a required film thickness of 100 nm means that to coat this length in 12 hours we need a deposition rate of 20 nm/s. This can be met by using more than one cathode (ie two cathodes at 10 nm/s each) but is again towards the high end of rates achievable with magnetron sputtering. If a thicker film or a longer roll is used then the rates available will limit the production volume. The feasibility of using magnetron sputtering will then depend on the value of the product.

Summary

The coating costs of vacuum produced thin film products are usually dominated by the expensive vacuum equipment. This makes high deposition rates desirable and for medium cost products magnetron sputtering can reach or just reach the required deposition rates. Evaporation (and allied techniques) offers higher deposition rates and for this reason dominates in low cost markets and occurs in other markets whenever it can meet the film requirements. The advantages of magnetron sputtering then lie in obtaining as high a rate as possible coupled with better film properties (adhesion, uniformity, controllability, morphology) and often with low substrate temperatures.

REFERENCES: CHAPTER 2

1. Mathews L.A., 'Estimating Manufacturing Costs', McGraw Hill, New York, 1983.

2. Garham International Study, Electro-Optics, P. 7, Nov., 1987.

3. Schiller S., Beister G., Neumann M., and Jaesch G., Thin Solid Films, 96, 199-216, 1982.

4. Spencer A.G., Georgson M., Bishop C.A., Stenberg E. and Howson R.P., Solar Energy Materials, 18, 87-95, 1988.

5. Lavine R.E., 'Thin film sputtering improved by handling disks individually', Research and Development, March 1985 pp 111-116.

6. Kieser J., Schwarz W., and Wagner W., Thin Solid Films, 119, 217-222, 1984.

7. Clow H., 'Evaporated metal film magnetic recording tape', in Proc. 'Vapour deposition - an industrial coating process', Cranfield, U.K., 1983.

3. THEORY AND BACKGROUND

A basic picture of magnetron (fig 3.1) is:- a cooled cathode with a plasma confined above it by a magnetic field. Ions from this plasma are accelerated into the cathode producing secondary electrons which maintain the plasma. The ion/cathode collisions also sputter the cathode material into the chamber where it forms thin films on exposed surfaces. For compound films a reactive gas is admitted and the subsequent reactions form the relevant compound(s) - (unfortunately on the cathode as well as on the substrate).

The processes involved are then, plasma confinement, sputtering by ions (in reactive and non-reactive atmospheres), transport of the sputtered material to the substrate, film formation (reactions at the substrate, film growth). Associated subjects are the occurrence of arcs (these being particularly troublesome in magnetrons), light emission from the plasma (a useful diagnostic), and relevant substrate properties.

3.1 MAGNETRON DESIGN

Development so far

Thin film deposition by sputtering from a cathode has been known and used since 1877 (ref 1). This simply used a glow discharge and sputtered the cathode material onto substrates placed on the anode or in view of the cathode. The deposition rate from such a system is low and there is substantial substrate heating from the plasma. The magnetron uses magnetic confinement of the plasma to increase the deposition rate and reduce substrate heating. The first patent is for a cylindrical magnetron (ref 2) (Telic Corp.) of the penning type. This is not convenient because of the cylindrical deposition region and so is not widely used. The original planar magnetron was designed by Chapin (refs 3,4) (Airco Inc.). This had a simple domed magnetic field to constrain the electrons and so provide a plasma confinement. An essential feature of this is that the $\overline{E} \times \overline{B}$ electron drift path is closed to prevent electron loss from the plasma. This magnetron has a 'v' shaped erosion profile.

Fig. 3·1 : A typical magnetron with hidden poles and the resulting domed magnetic field

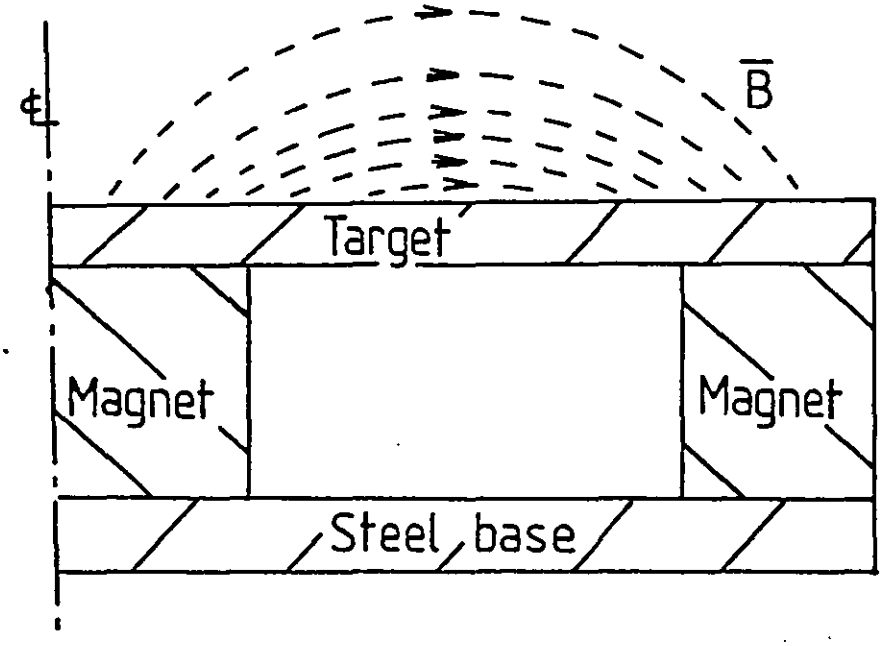

Fig. 3·2 : The effect of an inclined $\overline{B}$ field on the electron motion

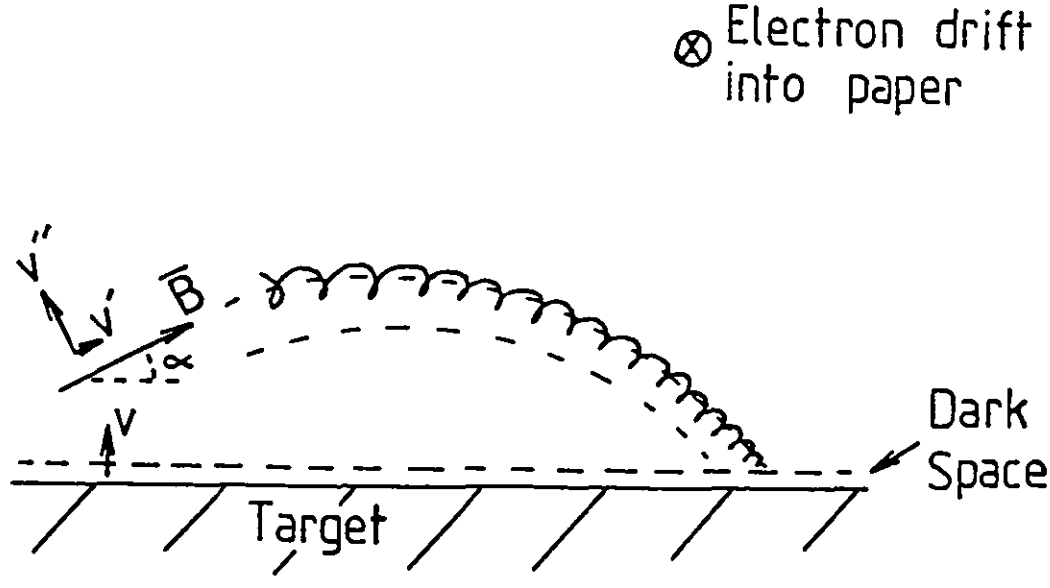

Since 1974 there have been many patents on magnetron design (mostly for small improvements refs 5-19). The list here is not complete but indicates the amount of work done and the trend of developments. Running briefly through these patents we have:- Reference 5 is an improvement of the erosion profile obtained by moving the magnetic field. Reference 6 says a magnetron may be used in a reactive sputtering atmosphere to produce compound films. Reference 7 is an effort to improve the erosion uniformity by modifying the magnetic field shape. Reference 8 covers the use of plasma emission monitoring to control reactive sputtering. References 9 and 10 are similar to Reference 7 from the same company. Reference 11 is another attempt to obtain uniform erosion profiles by modifying the magnetic field. Reference 12 is a means of controlling the discharge characteristics by mechanically varying the magnetic field strength. References 13 are both means of controlling the reactive gas flow either by a feedback loop from a mass spectrometer signal or simply pulsing the reactive gas flow. Reference 14 is a magnetron design using magnetic poles in front of the target designed to circumvent the original patent (ref 4). Reference 15 is an attempt to magnetron sputter ferromagnetic targets. Reference 16 is for reactive magnetron sputtering of conducting oxides and relates to substrate temperature. Reference 17 is a means of obtaining plasma bombardment of the substrates as this is said to activate substrate reactions. Reference 18 covers the detection of the end of the target life by putting a tracer material behind the target which is sputtered when the target is eroded through. Reference 19 covers the use of magnet poles above the target surface to sputter ferromagnetic targets.

The areas covered by these patents gives the regions of interest and the problems in magnetron sputtering. These are the target erosion profiles (affecting target lifetime and material utilization), control of reactive sputtering (often an unstable process), the sputtering of ferromagnetic targets and lastly the problem of drifting deposition conditions as the target ages.

There has also been significant adaption by Windows and Savvides who developed the idea of the unbalanced magnetron (ref 20). In this the central return path for the magnetic field is saturated and so the

B field from the outside magnets is forced forward towards the substrate. This results in plasma bombardment which can be used to modify the film properties (ref 21) or to activate reactions (ref 22). Such plasma bombardment had been used before with the sputter-gun (s-gun) and neatly controlled by an auxiliary electrode between the s-gun and the substrate (ref 23).

There is the rotating magnetron which claims improved target utilization but suffers from engineering difficulties and odd shaped targets. This may have real advantages for ferromagnetic materials if these can be formed into tube targets (ref 83).

Application to reactive sputtering

There are no magnetron designs specifically for reactive sputtering and the same magnetron designs are generally used for both reactive and non-reactive sputtering. The bulk of process development in reactive sputtering is aimed at controlling the film composition and not directly at modifying the magnetron.

In wide ranging reviews written only four years after the invention of the planar magnetron, Waits (ref 24) and Thornton (ref 25) give the general principles for magnetron sputtering of metals. The areas where information is lacking are mainly coating specific and process details for reactive sputtering, if known at this time, are still proprietary and unpublished. This is shown by the single paragraph given to this important area by Waits in his review. Indeed he concludes that R.F. is preferable to D.C. for reactive sputtering. This may be true for low volume production or for research but R.F. is not suitable for large area industrial production because of its cost, safety and reliability.

At the end of his review Waits poses several questions that required answering in 1978. These are:-

1. What is the energy distribution of the sputtered atoms?
2. What percentage are ionized?
3. How can the magnetic field pattern by optimized?
4. What is the effect of controlling the substrate bias?

and in R.F. sputtering:-

5. What is the effect of an anode?
6. Can direct reactive sputtering of dielectrics produce high quality films at high rates?

These seem to be fairly astute questions and if the last two are re-directed towards D.C. sputtering, then the set of six questions covers many of the subsequent advances in magnetron sputtering.

Future development

With the enormous range of alloys and compounds that can be sputtered it is difficult to talk about possible advances in materials and applications. The main areas of interest at present are superconductors, sensors, optical coatings, devices, memories, barrier coatings and displays. The progress with specific coatings in these areas and the development of new markets is likely to be significant. The areas of work on the coating process are known and will hopefully lead to advances. Understanding of the processes involved must increase and this should lead to improved system designs (or vice versa). It is to be hoped that the transfer of 'know how' from machine to machine will become easier as understanding improves. The introduction of new control techniques should expand the range of materials available as sputtered thin films. This should also allow the use of simplified (and therefore cheaper) coater designs with higher deposition rates.

Summary

- A magnetron uses a magnetic field to trap a plasma created and maintained by an applied potential.
- Ions from this plasma sputter the target material into the chamber.
- A simple magnetic trap leads to a localized plasma and therefore to a narrow target erosion profile giving short target lifetimes, low utilization of the target and a high localized heat load.
- Developments in magnetron design are generally aimed at giving a wider erosion profile or allowing the sputtering of ferromagnetic

targets. This is typically done by modifying the arrangement of the magnet pole pieces.

- Novel developments in magnetron design include the use of cylindrical rotating targets and also the deliberate leakage of the magnetron plasma to bombard the growing film.
- In reactive magnetron sputtering the main requirement is for process control.

3.2 PLASMAS AND PLASMA CONFINEMENT

Plasma confinement can be initially discussed in terms of the motion of isolated electrons (refs 26-28). In this guiding centre approach to electron paths the electron circulation about the magnetic field lines is considered as a current loop and the trajectory of the centre of this loop is calculated. The magnetic moment of the current loop opposes the applied magnetic field ie the plasma is diamagnetic. The magnetic moment M_e of the current loop is

$$M_e = \frac{2.q.P}{B}$$

where q = electron charge (C)
P = electron energy (eV)
B = magnetic field strength (T)

Taking an electron energy of 10 eV (ref 21) and a magnetic field strength of 0.03 T (300 Gauss, H = 24 kA/m) gives $M_e = 5 \times 10^{-17}$ A.m^2. A magnetron plasma has typically (ref 29) an electron density of 2×10^{15} m^{-3} and this then gives a total plasma magnetization of only 0.1 A/m. This is negligible compared to the applied fields of 24 kA/m and so we can say that in a magnetron the diamagnetism of the plasma has no effect on the magnetic field.

The plasma must be electrically neutral with deviations from neutrality possible only on short time scales over distances smaller than the Debye length λ_0 (ref 30).

$$\lambda_0 = \sqrt{\frac{k.T_e.\varepsilon_0}{n_e.e^2}}$$

where k = Boltzmann constant
= 1.38×10^{-23} J/K
T_e = electron temperature (k)
ε_0 = permittivity of free space
= 8.84×10^{-12} F/m
n_e = electron density (m^{-3})
e = electronic charge
= 1.6×10^{-19} C

Again taking $K.T_e$ to be 10 eV (ref 21) and n_e to be 2 x 10^{15} m^{-3} (ref 29) gives a Debye length of 0.7 mm. The Debye length loses its definite meaning in magnetron plasmas as the ion and electron temperatures are not in equilibrium (ref 31) but it is a reasonable indicator of distances. In magnetron plasmas the Debye length is small and ion movements are therefore 'tied' to the electron motions (ref 21). This is equivalent to saying that the plasma is coulomb dominated as the ion/electron interaction occurs over the Debye length whereas the ion/electron interaction by collision occurs over much larger distances (ref 27).

The isolated electron picture provides an explanation of the sharp 'V' erosion seen in simple domed B field magnetrons (fig 3.1), (refs 26, 28). Where the B field is angled to the magnetron surface, the ejected electrons acquire a component of velocity parallel to the target surface (fig 3.2). This leads to an electron density maximum where the B field is parallel to the target surface and so to maximum ion bombardment and erosion rate at this point. We have previously used an electro-magnetron to vary the confinement magnetic field (ref 26) and the operating potential against magnetic field strength is shown in fig 3.3. This shows that for higher current densities higher magnetic field strengths are required. For our electro-magnetron a field of at least 0.03 T (300 Gauss) is best. To scale this for other magnetrons a dimensionless parameter is needed (ref 32) and a reasonable quantity is the ratio of the cyclotron radius to the width L of the electron trap (20 mm for the electro-magnetron). The cyclotron radius scales as 1/B so our dimensionless parameter reduces to B.L = const. and as the magnetron racetrack is widened we would expect to be able to reduce B accordingly.

Bulk electron and ion movements (oscillations) disturb this picture and provide electron transfer across magnetic field lines which would not be expected for isolated electrons (ref 32). There are a multitude of possible oscillations in magnetized plasmas. The basic types of electrostatic waves, Alfven waves, Magneto-acoustic waves and electro-magnetic waves are discussed in Hoyaux (ref 33) and in more detail in Cap (ref 34).

The Penning discharge has many similarities with planar magnetron discharges and has been investigated for plasma oscillations (ref 31).

Fig. 3·3 : The effect of varying magnetic field strength on magnetron operation.

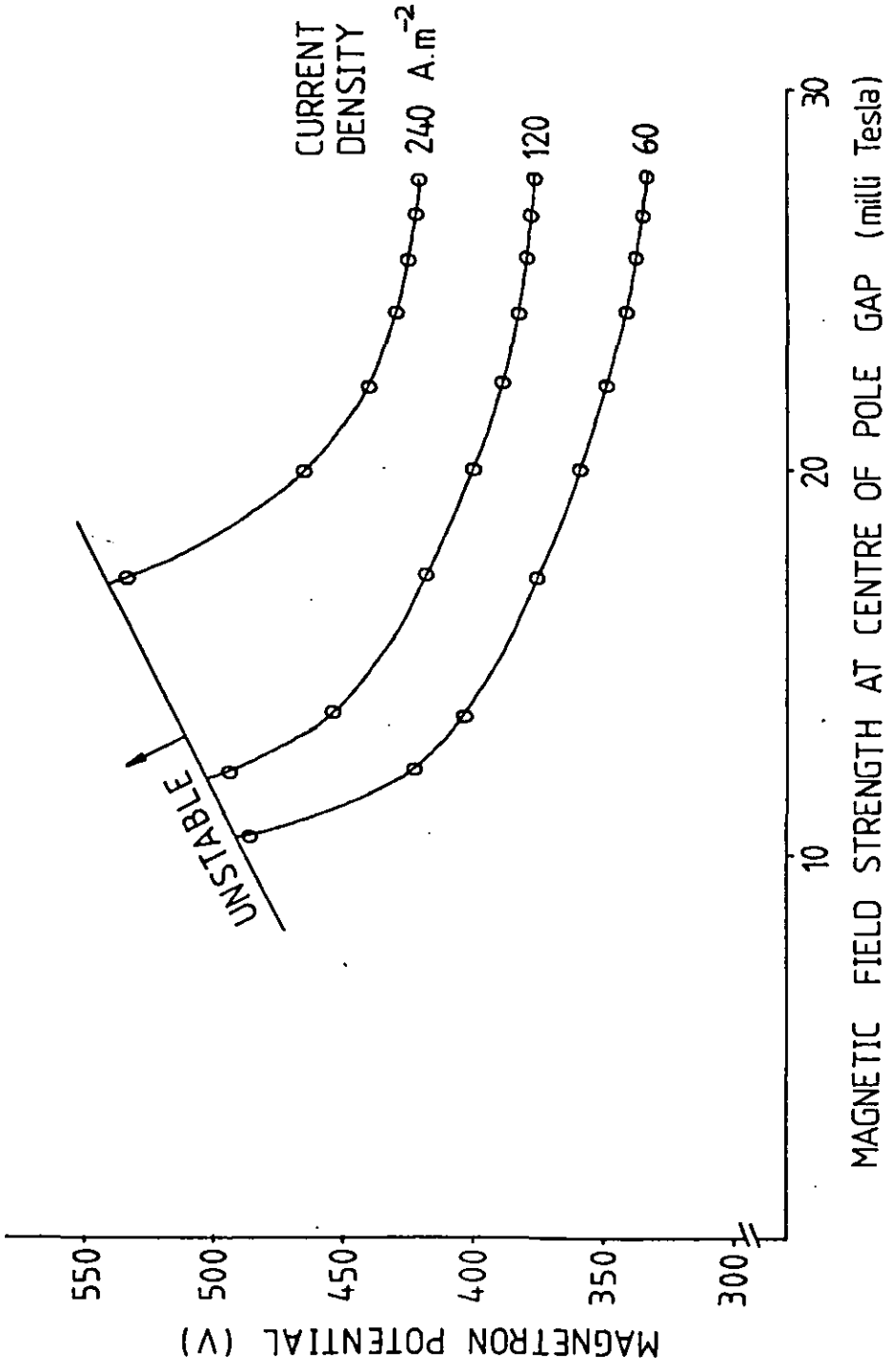

A stability criterion for oscillations has been derived for the Penning discharge (ref 35). This criterion is confirmed for the general case by Cap (ref 34). The electron cloud is stable if

$$\omega_p < \omega_{CYCLO}$$

where ω_p = plasma frequency

ω_{CYCLO} = cyclotron frequency.

We have ω_{CYCLO} = q.B/m (q electron charge, B magnetic field strength, and m electron mass) so in a magnetron with B typically 0.03 T (300 Gauss) ω_{CYCLO} = 5 GHz. The plasma frequency is $\omega_p^2 = e^2.n_e/(m.\varepsilon_0)$ and taking for a magnetron $n_e = 2 \times 10^{15}$ m^{-3} (ref 29) gives ω_p = 3 GHz. This indicates the ω_{CYCLO} and ω_p are approximately equal and so we are close to the onset of electron electro-static oscillations (electron cyclotron resonance). We have observed the onset of such oscillations at high currents when a low magnetic field strength is used (fig 3.4 and ref 36). This would be expected as reducing B will reduce ω_{CYCLO}. Increasing the magnetron current will increase n_e (and ω_p) hence the onset of oscillations as the magnetron current is increased (fig 3.4).

These electron electro-static waves observed by us lead to an increase in the plasma impedance. This is consistent with the work of Thornton (ref 37) where an increasing loss of electrons leads to an increasing operating potential. The onset of the oscillation will lead to electron transfer loss from the plasma. The roll off of the magnetron current with increasing voltage associated with these oscillations has been observed before (ref 38). By increasing the magnetic field strength it was found that higher magnetron currents could be achieved before the roll over. This is again consistent with the condition for stability $\omega_p < \omega_{CYCLO}$.

Also Rossnagel and Kaufmann (ref 39) showed that large electron currents flow around the racetrack of a DC magnetron (150 mm diameter magnetron, 8 A current, circulating current 25-35 A depending on pressure). They analyzed their results in terms of the electron diffusion out of the electron trap. This analysis produces results in agreement with their experiment and is based on the electron diffusion coefficient D_b across a magnetic field (ref 40). This scales as D_b is inversely proportional to B so again a dimensionless parameter L.B can be justified. Also Rossnagel and Kaufmann conclude that collective

Fig. 3·4 : The onset of plasma oscillations in a D.C. planar magnetron.

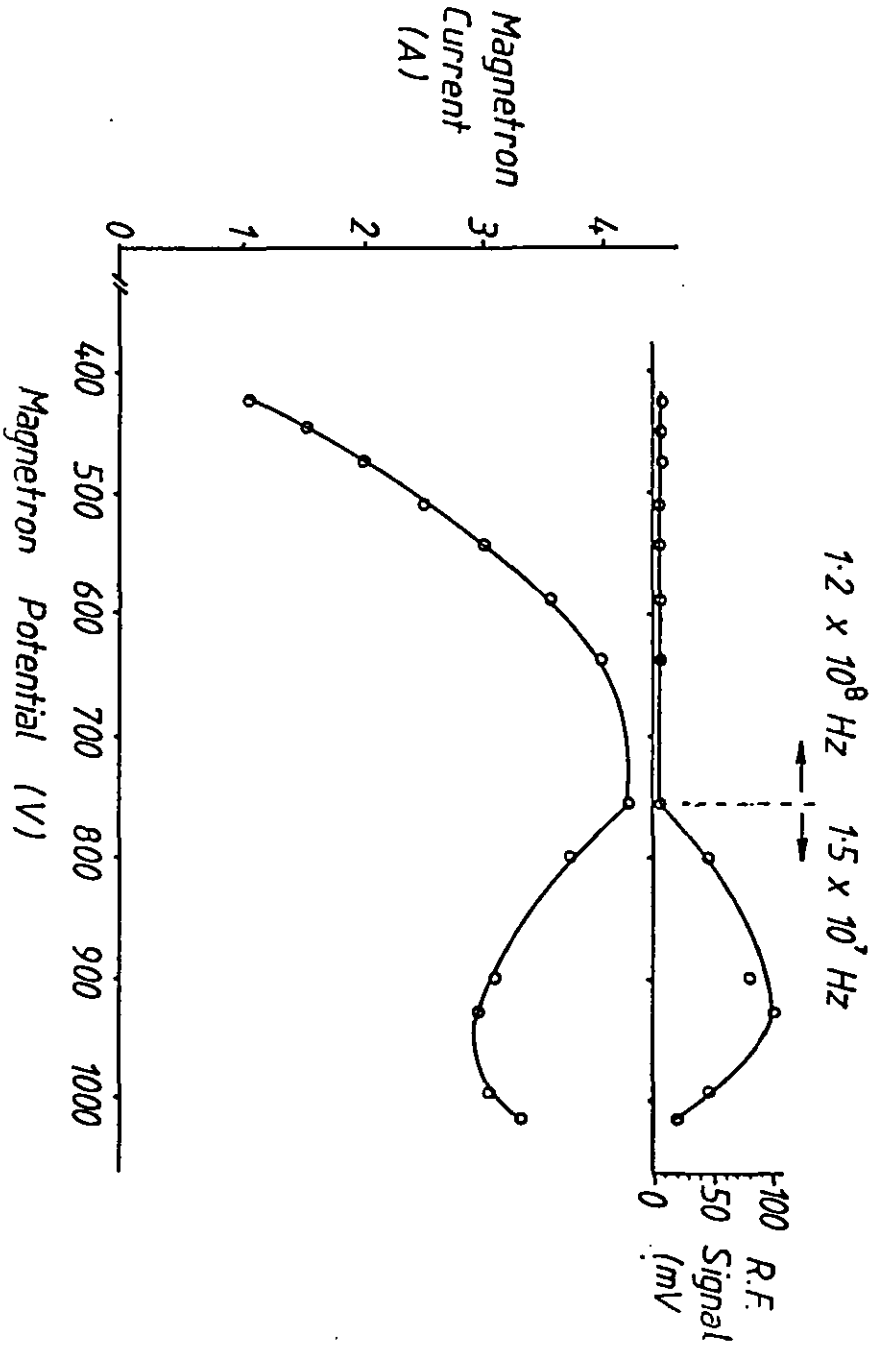

processes ie oscillations are responsible for electron transfer across the B field.

Summary

- Plasma trapping can be discussed in terms of single particle motions. This will explain the interaction of the magnetic trap and the erosion profile.
- The electron and ion bulk movements are linked together by the need to maintain the plasma electrically neutral. (The Debye length is small compared to the magnetron dimensions).
- Electron oscillations occur in the plasma and lead to transfer of electrons across the field lines of the magnetic trap. At low magnetic field strengths this will limit the current density achievable in the magnetron.
- The magnetic field strength B required in a trap of width L should scale as B.L = constant. The value of this constant is around 0.001 T.m (1 kG.cm).

3.3 SPUTTERING BY IONS

Non-reactive sputtering

In D.C. magnetron sputtering the operating potential is typically 300-600 V. The potential across the plasma dark space is close to the applied potential and the sputtering ions are accelerated across this dark space. We therefore are using ions with an energy of 300-600 eV to sputter the target atoms (as doubly charged ions are rare (ref 41) and collisions on crossing the dark space unlikely). When ions of this energy are incident on a solid target then a cascade of collisions occurs as shown in fig 3.5 (ref 41). Looking at such a process it is obvious that the bulk of the incoming ion's energy is absorbed and only a small fraction is available to eject material from the target. This ejected material forms the sputtered flux from a magnetron.

The basis of sputtering theory was laid by P. Sigmund and is covered in depth in his 1981 article (ref 41). The parameter that is most dealt with is the sputter yield Y which is defined as the number of atoms (or ions) ejected from the surface per incident ion. Since Sigmund developed his theoretical model many numerical models have appeared and these are reviewed by Zalm (ref 42). He states that Sigmund's formula for Y (ref 43) still gives the closest agreement with experiment. Biersack and Eckstein (ref 44) conclude from computer modelling that Sigmund's formula is not applicable for ion energies below 500 eV. The discrepancy is small though, down to 300 eV, and accuracies of +/- 5% are achievable in our range of interest. Biersack and Eckstein's results show that in the range 100-1000 eV the sputtered material comes from only 1 nm (or less) below the surface. This agrees with Sigmund and means that a large surface dependence would be expected. The sputtered flux is mainly atomic species as shown by the low secondary ion yields (ref 45). For instance, for 3 KeV Ar ions, Cu and Ni have secondary ions yields of 3×10^{-3} and 6×10^{-3} respectively (ref 46). The sputter yields for the same conditions are 4 and 3 respectively (ref 47) so we would expect the sputtered flux to contain around 0.1% ions.

Sigmund's formula contains many terms that are not immediately calculable (ref 43). A more convenient formula is given by Steinbruchel (ref 48) who, by combining results from various papers (including Sigmund's), arrives at the formula

Fig. 3·5 : A typical collision cascade for the ion energies found in magnetron sputtering (ref. 41).

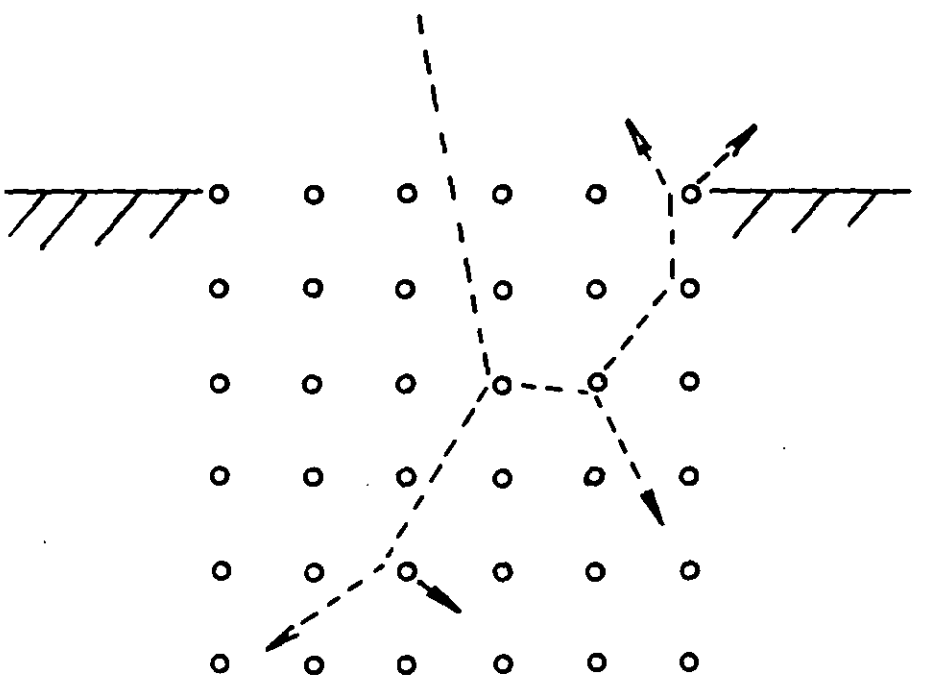

$$Y = \frac{5.2}{U} \cdot \frac{Z_t}{(Z_t^{2/3} + Z_p^{2/3})^{3/4}} \cdot \left(\frac{Z_p}{Z_t + Z_p}\right)^{0.67} \cdot E^{1/2}$$

Where E = ion energy (keV)
U = target binding energy (eV)
Z_t & Z_p = atomic number of target atoms and projectile ions

The sputter yield (Y) is proportional to the square root of the ion energy and inversely proportional to the target binding energy. This has immediate consequences for reactive sputtering. We have already said that the sputter yield is very surface sensitive and now we see that it depends strongly on the target binding energy. In reactive sputtering almost by definition, the target material and the reactive gas react together to form a stable compound ie one with a negative heat of formation. This indicates that our reaction products will have larger binding energies than the original metal and so a lower sputter yield. Therefore the arrival of a reactive gas at the target must result in a reduction of the sputter yield and this reduction will be most severed for the more reactive systems eg Al + O, or Ti + O (see ref 48).

With multi-component targets the sputtered material reaches an equilibrium such that the sputtered flux has the same composition as the target (ref 49). At this point the target surface is enriched in the species which sputter more slowly. This result is very important when considering non-reactive deposition from alloy targets as we need only use the required alloy as a target to form the required film.

We can show with a simple experiment how the actual sputter flux relates to the values calculated from the sputter yield and the magnetron current and voltage. We used a Pd target (four nines purity) and sputtered this for 49 minutes at 0.52 A and 356 V. The target lost a mass of 1.7420 +/- 0.0002 g which with an atomic mass of 106.4 g/mol is 9.860×10^{21} atoms. The total charge delivered by the supply was 1500 C which for singly charged particles (ie 1.6×10^{-19}) is a particle flow of 9.4×10^{21}. Taking measured values of the sputter yield (ref 47) and interpolating gives a sputter yield at 356 eV of 1.58. For a magnetron current carried by ions only, we would expect the number of sputtered atoms to be the sputter yield times the particle flow. This

gives the expected number of sputtered Pd atoms as 1.5×10^{22}. We in fact measured 9.86×10^{21} atoms which is 65% of the predicted figure. This confirms a value of 60% obtained by Schiller et al when sputtering Cu (ref 50).

Possible reasons for this discrepancy are:-

1. The magnetron current is not carried across the dark space solely by ions.
2. The ion energy is less than the energy gained by the fall across the applied potential.
3. The target has some oxidation.
4. There is backscattering of the sputtered material onto the target.
5. There is argon included in the sputtered target.

The first is true, the magnetron current I (as carried across the dark space) is not solely an ion current. Schiller et al (ref 50) have measured this and give a figure of 75% ion current across the dark space. The ion current I_i can be represented as

$$I_i = I/(1 + \gamma)$$

where γ = secondary electron coefficient.

The secondary electron coefficient changes with the target surface usually increasing as an oxide or nitride forms (with a resulting change in the discharge voltage). For a metal γ is typically 0.1 (ref 30) and for an oxide or nitride it may rise to around 0.2 (ref 51).

Davies and Vanderslice (ref 52) have measured ion energies at the cathode of an Ar glow discharge (fig 3.6). They conclude that the dominant factor is the ratio of the ion mean free path to the cathode dark space. A magnetron generally has a dark space an order of magnitude smaller than a glow discharge (0.5 mm to 5 mm) and operates at pressures two orders of magnitude less than a glow discharge (5 mTorr to 0.5 mTorr). The ratio of mean free path to dark space in our case will then be around three orders of magnitude larger than in the glow discharge of fig 3.6. The collision cross section for Ar+ is greater by one order of magnitude than that for Ar++ (ref 53). The

Fig. 3·6 : Ion energies at the cathode of a glow discharge (ref. 52).

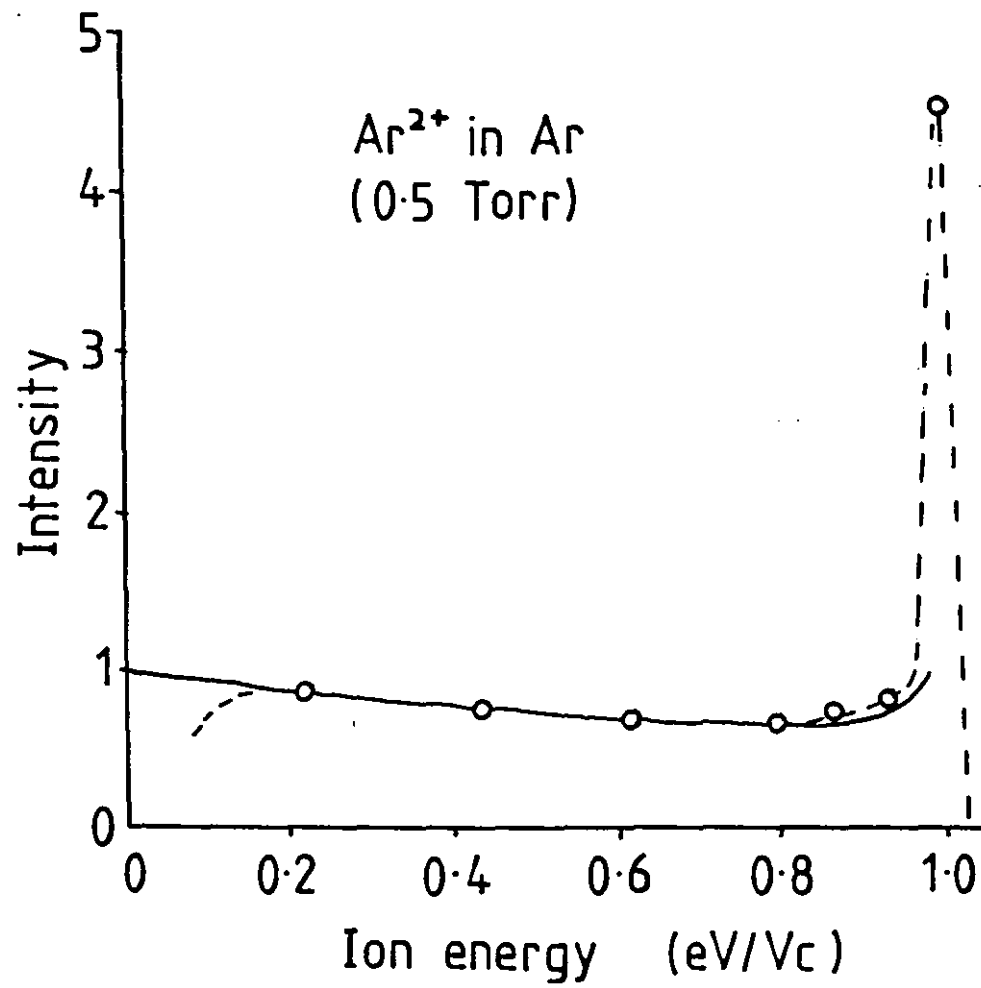

Vc = Applied Potential

results for Ar++ are shown in fig 3.6 and Davis and Vanderslice state that for this graph the dark space is about 2 mean free paths wide. Our two orders of magnitude then gives a dark space for Ar+ that should be 0.02 mean free paths wide. So in a magnetron the ions at the cathode will have energies close to that gained by falling through the applied potential.

A Pd target is unlikely to be significantly oxidized due to its low reactivity (ref 48). At low pressures (3 mTorr) the amount of backscattering onto the target will be negligible (ref 54). Ar inclusion in the target will also occur but the penetration depth will only be a few interatomic spacings (ref 55) ie around 1 nm. In our case we sputtered away around 10^{22} Pd atoms from an area of 3 x 10^{-3} m^2. Taking an atomic radius of 137 pm (ref 56) gives an atomic volume of 2 x 10^{-29} m^3. The sputtered volume should then be 2 x 10^{-7} m^3 and the sputter depth 7 x 10^{-5} or 70,000 nm ie the implanted Ar is not significant.

Summary

- In the sputtering process the bulk of the energy of the incoming ion is dumped into the target. Only a small fraction is usefully employed in producing sputtered atoms.
- The number of atoms produced per incoming ion (the sputtering yield) can be calculated and is inversely proportional to the binding energy of the atom(s) to be sputtered.
- The sputtering collisions occur in the top few mono-layers of the target and so the sputter yield is very surface dependant.
- The formation of compounds on the target surface can therefore have a drastic effect on the sputter yield.
- Electrons created by ion/target collisions carry some of the current to the magnetron (generally 10-20%). The number of ions bombarding the magnetron is then around 80% of the total charged particle flow.

Reactive sputter deposition

There have been many investigations of the reactive sputter deposition process, some of a general nature and some related to a specific material. The more general papers are reviewed here (ref 57-83) and these cover ion beam, diode and magnetron sputtering (dc and rf for the last two). Where equations are taken from papers the symbols assigned to various parameters have been changed to be consistent.

Reactive diode or triode sputtering systems are significantly different from magnetrons in that the sputter rate across the target is uniform. The target then poisons (ie is covered with reaction products) as the reactive gas pressure is increased. Experimentally this is seen as a drop in deposition rate above some critical reactive gas pressure p*. Early references to this phenomena (the first in 1952) are given by Heller (ref 57) and by Abe and Yamashima (ref 58).

The critical pressure p* depends on the sputter rate of reaction products off the target (R(d)) and the formation rate of reaction products on the target (Y(d)). When R(d) > Y(d) the target is metallic and when R(d) < Y(d) the target is poisoned (ref 57). These parameters then reach equilibrium at some thickness d of reaction products on the target. From the time taken to sputter away the oxide layer Heller estimated its thickness as 5 nm for the Fe + O system.

Abe and Yamashima (ref 58) extended Heller's model with an improved description of the reactive gas/target interaction and tested their model on the metals Mo, Ti, Al and Fe with O and N. Their results do not indicate as sharp a transition as Heller's results for Fe and Co with O but a smooth fall over half a decade of reactive gas pressure. Both papers mention the fact that the Ag + O system shows no transition at all and Abe et al attribute this to thermal decomposition of the reaction products on the target. Abe and Yamashima also introduce the idea of an effective sputtering rate R(p) determined from the metal and compound sputter rates (R_m and R_c) and the fraction f(p) of the target that remains metallic.

$$R(p) = R_m \cdot f(p) + R_c \cdot (1 - f(p)$$

where p is the reactive gas pressure.

Experimentally f(p) shows a transition over half a decade of reactive gas pressure (fig 3.7). They derive an equation for f(p) but this has more free variables than calculable quantities and so not surprisingly fits their experimental data.

Shinoki and Itoh (ref 59) using an rf diode system sputtering ZrN continued the work above. They show that if the gettering of the reactive gas by the film growth is considered then this leads to a sharp transition form a metallic to a poisoned target. Their deposition system has a mass spectrometer at the substrate position and they measure the ion intensities as a function of reactive gas pressure (fig 3.8). The sharp transition in the target state is shown by the step in the Zr+ peak. They also saw from the poisoned target the arrival of ZrN+ with an intensity of 10% of the Zr+. They derive an equation for the critical reactive gas pressure p* which has a dependence p* proportional to I_i the ion current density and proportional to $S^{-1/2}$ where S is the reactive gas pumping rate.

Hrbek (ref 60) looked at ion beam sputtering of Ti, Ta, Mo and W with a partial pressure of oxygen or nitrogen. In all cases similar curves to figure 3.7 from Abe and Yamashima were obtained and the decrease in yield occurred over half to one decade of reactive gas pressure. The reactive gas pressure at which the transition occurred was found to depend on the ion bombardment density.

Bomchil et al (ref 61) analyze the system In + O in a triode deposition system. Here the deposition rate is higher than in the previous works and Bomchil et al identify the interaction of the decomposition rate and the reactive gas pressure through getter pumping of the reactive gas. Now the transition in deposition rate is matched by a transition in reactive gas pressure (fig 3.9).

All the papers so far have related to a diode or triode system with a uniform plasma density across the target surface. Schiller et al (ref 62) pointed out that because the magnetron plasma is highly localized in the racetrack region, the magnetron target will have a variety of oxidation states across the racetrack. Their diagram is reproduced in fig 3.10. It shows a peak in the metal sputtering rate at the centre of the racetrack while the poisoning rate is fairly uniform. The consequence of this is that the centre of the racetrack

Fig. 3·7 : Target poisoning in diode sputtering (ref. 58).

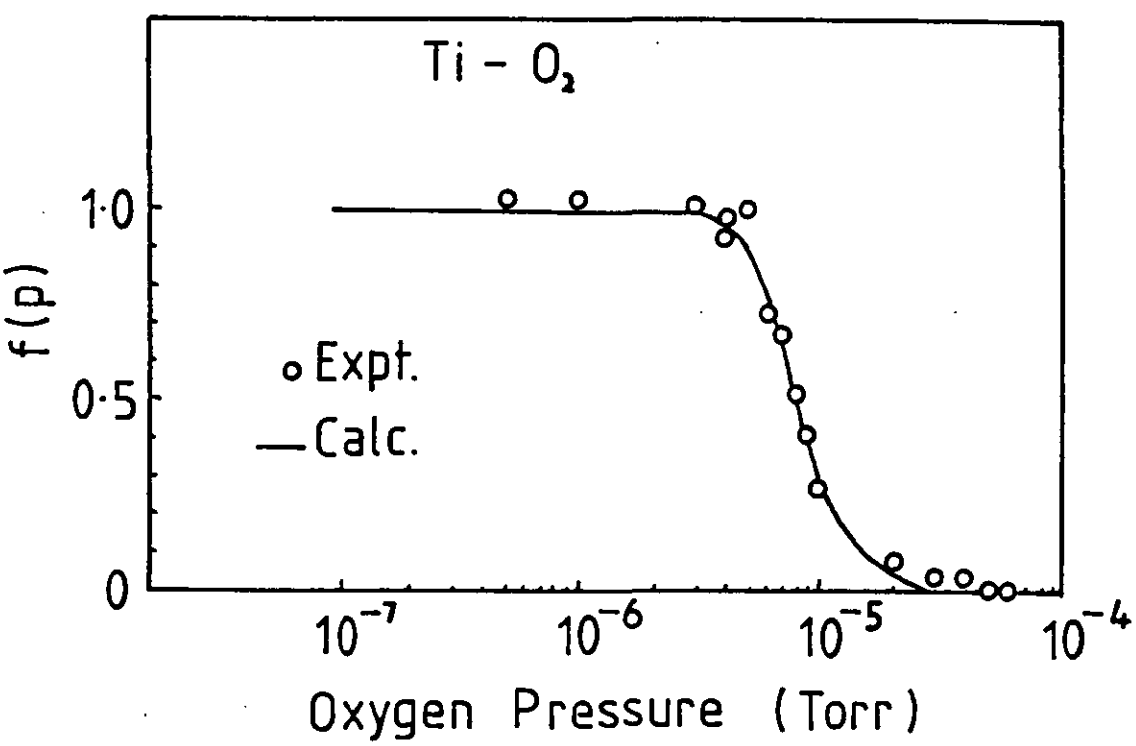

f(p) = Fraction of target surface remaining metallic.

Fig. 3·8 : Species at the substrate in rf sputtering of Zr + N_2 (ref. 59).

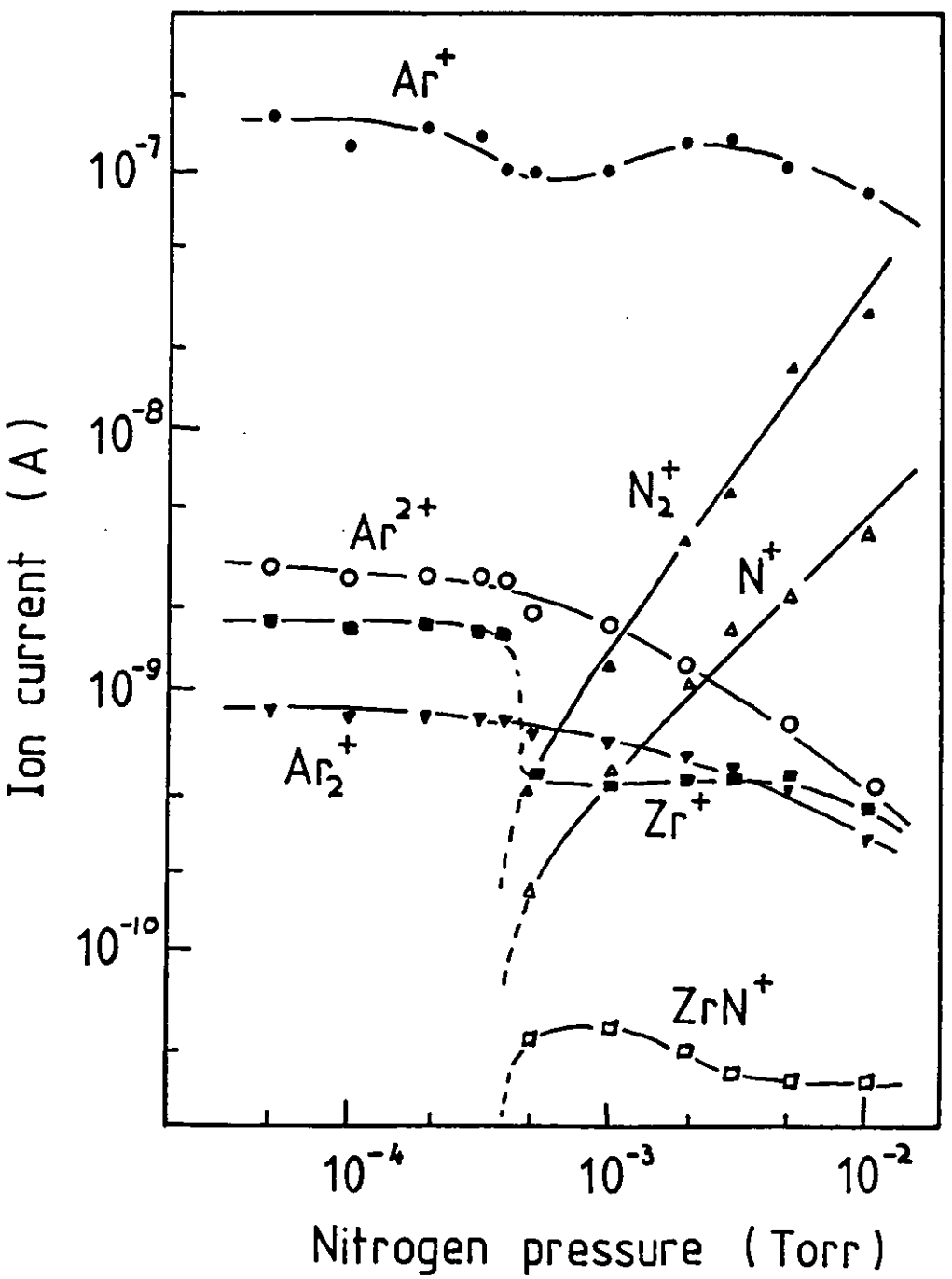

Fig. 3·9 : Gettering of gas in reactive triode sputtering (ref. 61).

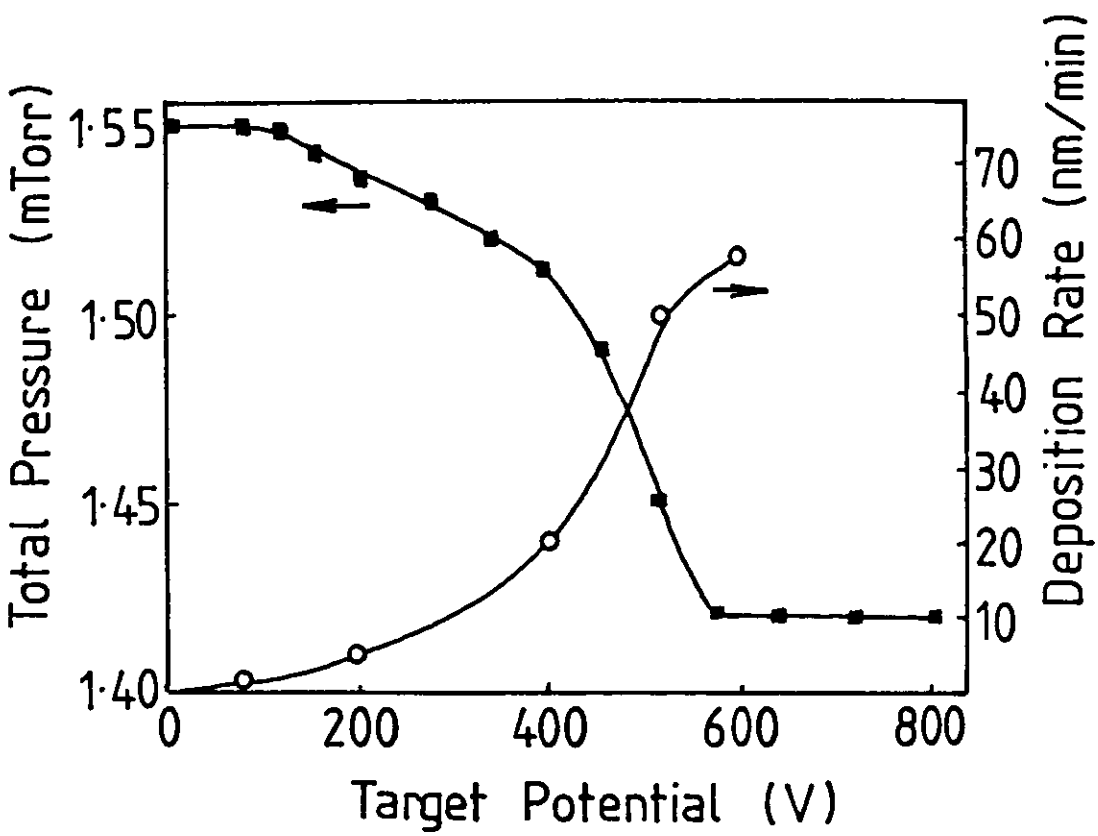

Fig. 3·10 : Magnetron target poisoning (ref. 62).

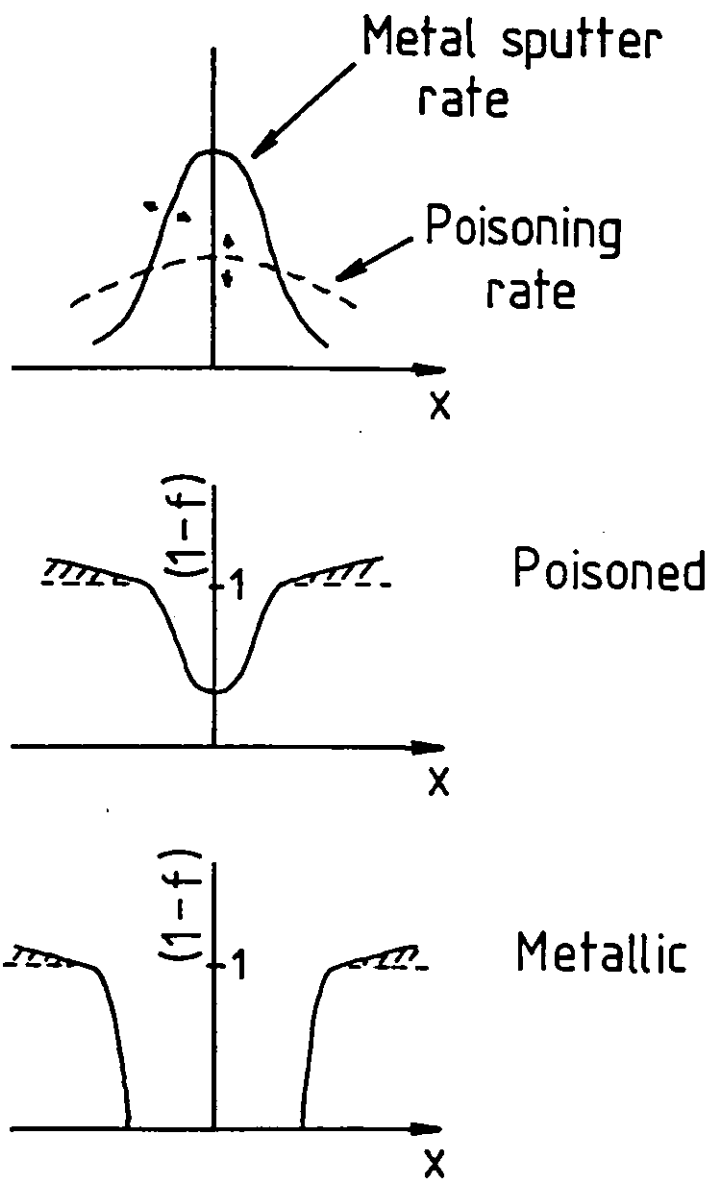

f = Fraction of target surface remaining metallic.

▨ = Bulk compound growth.

stays metallic while the edges become poisoned with reaction products. This often becomes visible on well used reactive sputtering targets.

Natarajan et al (ref 63-65) produced a series of three papers in which optical spectroscopy was used to investigate reactive diode sputtering of In in N (ref 63, 64) and O (ref 64) atmospheres and the results of this were extended to a general model for reactive diode sputtering (ref 65). The equation for the sputtering rate R(p) given by Eltoukhy et al, although based on the equation of Abe and Yamashima (ref 58) above, contains many less free variables and still gives a reasonable fit to the experimental data. The equation is

$$R(p) = I_i(p) \cdot \frac{[R_m(p) \cdot A(p) \cdot (p + p^*) + R_c(p) \cdot p^2]}{p^2 + A(p) \cdot (p + p^*)}$$

where I_i = ion bombardment density
= $I(p)/(1+\gamma)$
I = total current
γ = secondary electron coefficient
R_m = metal sputter rate
R_c = compound sputter rate
p = reactive gas pressure
p^* = critical reactive gas pressure
A = $I_i \cdot R_c/\beta$
$\beta.p$ = incident flux density of reactive species
= $p/(2.\pi.m.k.T)^{1/2}$ (see section 3.7).

The sticking coefficient has been removed from this equation by a simplifying assumption leaving the free variable p* (no definite physical meaning is given to p*). By iteratively fitting this equation to their experimental data with p* and R_c as variables Eltoukhy et al derive values for R_c. They show that in their system running at 2.5 keV InN (heat of formation 4.6 kcal/mol) has a sputter yield of 1.3 while In_2O_3 (heat of formation 221 kcal/mol has a sputter yield of 0.27. These two sputter yields do not scale as 1/U (U = binding energy = heat of formation) as predicted from Sigmund's formula (section 3.3, non reactive sputtering) and do not match values calculated from Sigmund's formula. The model then fits the experimental results but this cannot be reconciled with Sigmund's sputtering theory. The equation above does have a dependence on the ion current density to the target I_i which

fits in well with Schiller's observation of the poisoning on magnetron racetracks.

Despite the range of poisoning seen on magnetron targets at a given reactive gas pressure, a sharp discontinuous transition between a metallic (or partly metallic) target surface and a poisoned target surface is often observed (see for example fig 3.11) (ref 66, 67). With the metallic target we have a high rate deposition of a metal rich film (and a low oxygen pressure). When the target has a surface oxide layer ('poisoned') there is a low rate deposition of a gas rich film (and a higher oxygen pressure).

Aronson et al (ref 67) proposed a solution to this problem based on a pulsed reactive gas flow. With the reactive gas flow switched on and off periodically the target switched from poisoned to metal and back again. The average target condition is then intermediate between the two extremes and a higher rate deposition of a compound film (TiN was claimed. Obviously the switching time could not be too long otherwise the film produced was of alternate layers of metal and compound.

Maniv et al (ref 68) found a different solution. They reasoned that the unstable transition occurred at some critical reactive gas flow and that this was before a compound film was formed on the substrate. To prevent the target poisoning, the oxygen flux to the target was reduced by a mask placed between the magnetron and substrate (this also reduces the metal flux to the substrate). Stoichiometric films could then be deposited before the metal to poisoned target transition.

Steenbeck et al (ref 69) produced another model for reactive magnetron sputtering, this time with more than one magnetron in the chamber. Their model was fitted to the observed current voltage relationships and they derive equations for the current and voltage. They consider gettering of the reactive gas by the film formation and observe pressure changes as the f(p) changes but do associate this with the cause of the instability. The gettering of the reactive gas is dealt with as a certain number of sputtered metals which, after arrival at the substrate, acquire a degree of reaction midway between zero and stoichimetric compound. Their model does not then give any information

Fig. 3·11 : Hysteresis in reactive magnetron sputtering of Al + O_2 (ref. 66).

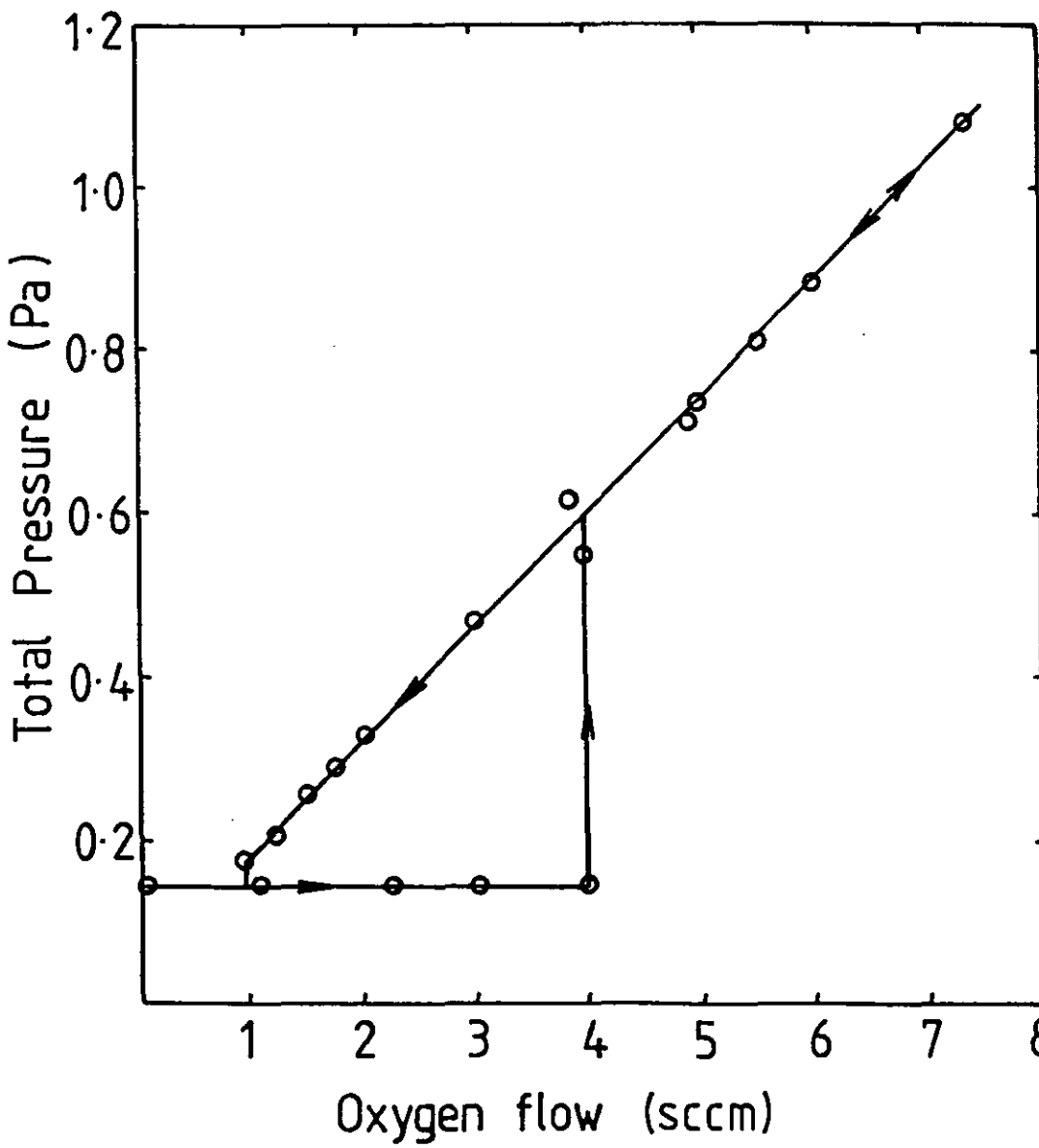

about reactive gas sticking coefficients at the substrate.

Howson et al (ref 70) in 1984 offered an explanation of the discontinuous transition between magnetron target states. "Consider there is a small random rise in the pressure of oxygen, it will cause a slight increase in the area of the cathode which is oxidised, which will lower the rate of metal sputtering. This will result in less oxygen being required to make oxide on the substrate so that for a fixed oxygen input into the chamber the pressure will rise and the process will 'lock on' to a fully oxidized target".

Schiller et al (ref 71) in 1984 produced an important paper covering many aspects of reactive sputter deposition from magnetrons. They briefly state that the metal line emission intensity can be used as a control for the reactive gas flow and that this removes the instability. This statement is not elaborated on but this idea becomes important in later papers. Films of TiO_2 deposited from a poisoned target are shown to have Ti/O ratios as high as 2.4 ie they are gas rich or over-stoichiometric. This means that for many films optimum properties cannot be obtained from a poisoned target. The effects of varying the target substrate distance are investigated experimentally (fig 3.12). They find that at larger target substrate distances the stoichiometric film (TiO_2) is formed at a lower reactive gas pressure (the metal flux density decreases with distance as the metal flux spreads out). At these lower reactive gas pressures less target poisoning occurs and so Schiller et al conclude that the target substrate distance should be made large. Lastly, they evaluate the ratio of arrival rates of Ti and O for the different target substrate distances. As the target substrate distance increases from 80 mm to 380 mm the ratio of the oxygen arrival rate to the titanium arrival rate increases by an order of magnitude. This implies that excited species are required to form the compound and that these are de-excited by gas collisions during transfer to the substrate.

Lemperiere and Poitevin (ref 72) have investigated dc diode sputtering of TiN and produced another model for the target coverage [1-f(p)]. Their model now incorporates the interaction between the sputter flux and the reactive gas pressure by getter pumping. The reactive gas pressure p is given as

Fig. 3·12 : TiO_2 deposition at various target to substrate distances (ref. 71).

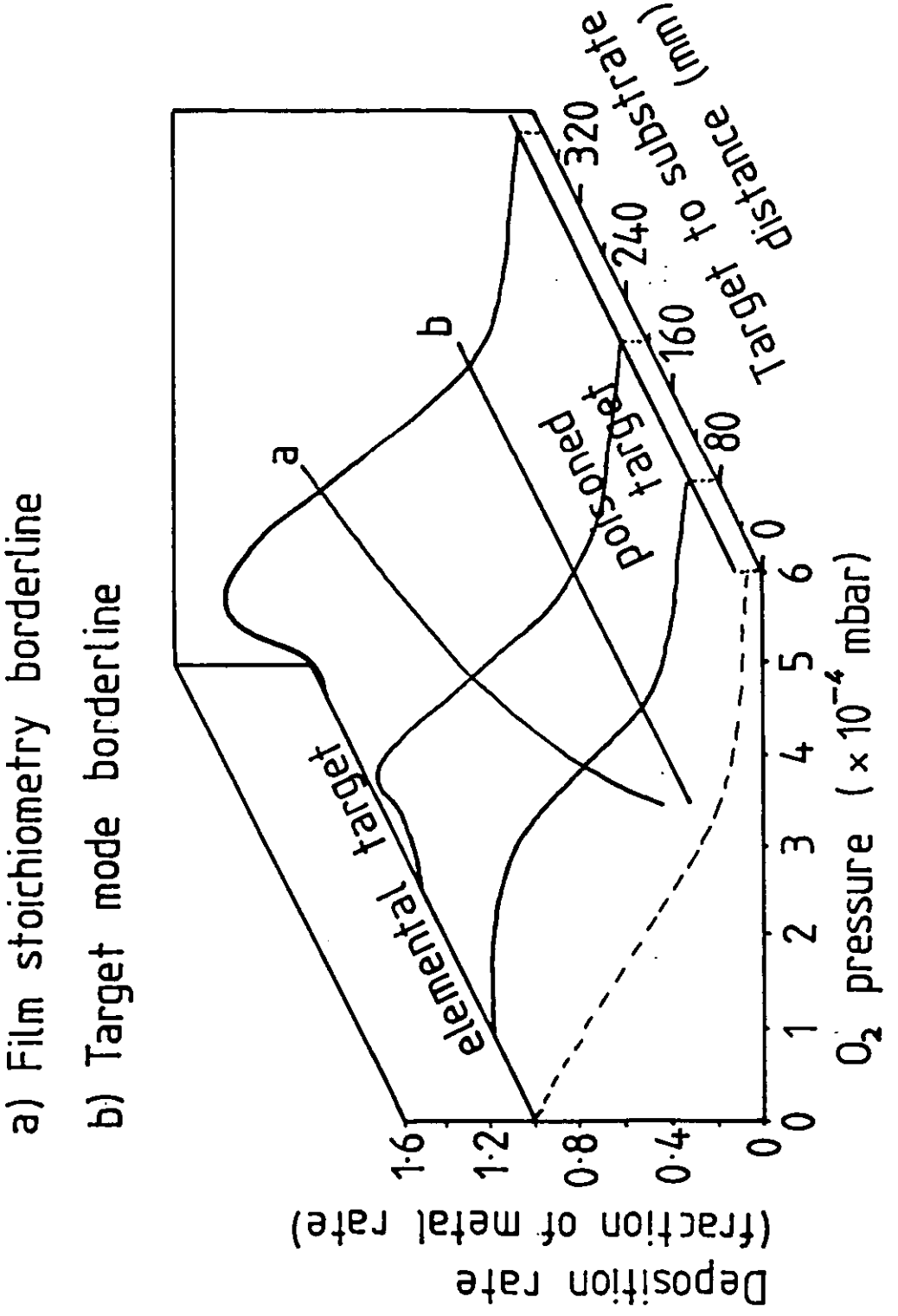

$$p = p_0 - \frac{[\alpha . a . R . I_i . f(p)]}{S}$$

where p_0 = reactive gas pressure without the plasma
α = number of reactive gas atoms absorbed by one sputtered metal atom
a = area of the target
R = target sputter rate
I_i = ion current density to target
$f(p)$ = fraction of target remaining metallic
S = pumping rate of main pumps.

This equation is a simplification of the one used by Steenbeck et al (ref 69) who used a version integrated for varying I_i over the magnetron racetrack. Lemperiere and Poitevin found that α could be represented by

$$\alpha = \alpha_0 . p/(p + p^*)$$

where p* is again the critical pressure. The final equation derived for f(p) is more complex than that of Eltoukhy and so is not quoted here. The agreement between Lemperiere and Poitevin's equation and their data is reasonable and they do not use a large number of free variables. Yet again they find a decrease in f(p) over a decade of reactive gas pressure. It is worth noting that p* now has a physical meaning (the pressure at which the film absorption of reactive gas saturates) and roughly corresponds to the mid point of the target poisoning.

Schiller et al (ref 73) published a review paper in 1984 and this concisely summarizes the instability behaviour of reactive magnetron sputtering (see fig 3.13). They also conclude again that the instability can be removed by reactive gas flow control based on the metal line emission intensity. The details of this are again not given. The basic parameter for reactive sputtering is stated to be the ratio

$$\frac{\text{reactive gas arrival rate}}{\text{metal arrival rate}}$$

Fig. 3·13 : The unstable behaviour of reactive magnetron sputtering (ref. 73).

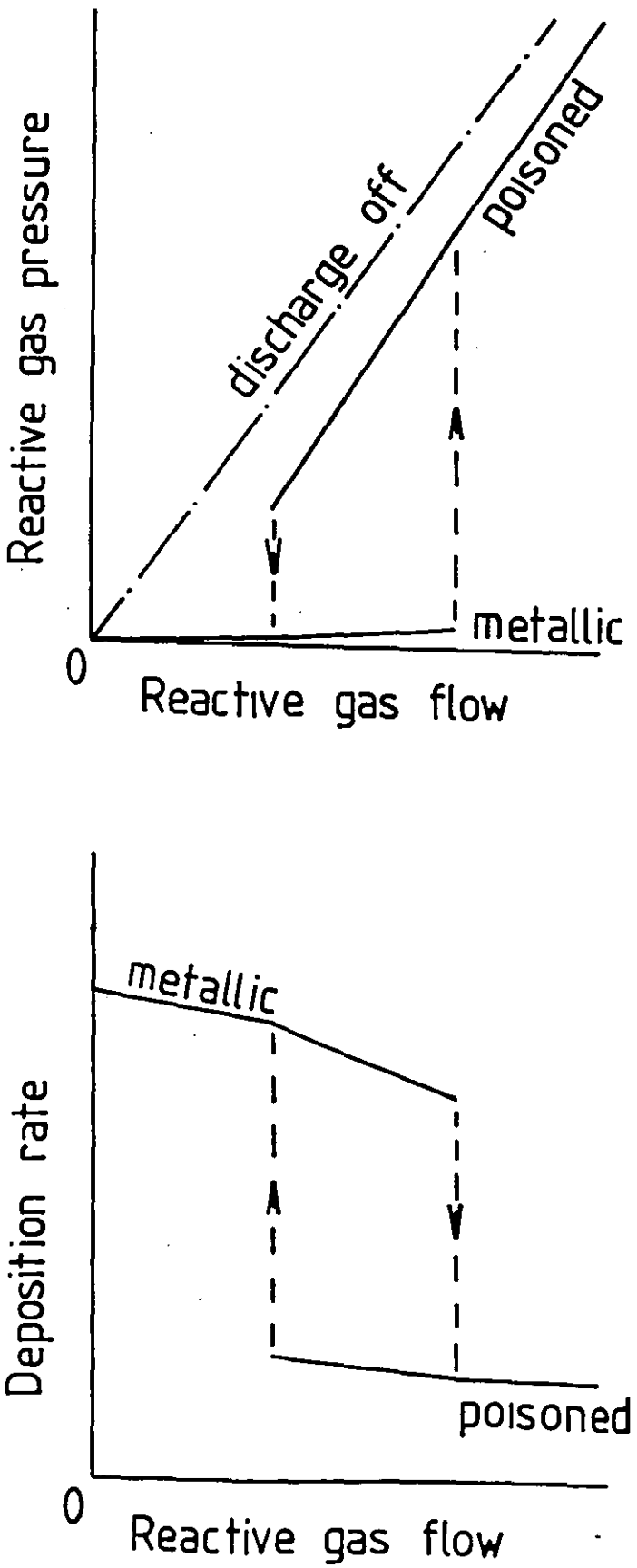

Hohnke et al (ref 74) produced an elegant model for reactive sputtering but unfortunately based it on special conditions in their coater which are not generally satisfied. Their model is based on a curve very similar to Schiller's graph of reactive gas pressure vs reactive gas flow. For some unspecified reason the manage to form their stoichiometric film (TiO_2 or TiN) at a very low reactive gas pressure ie the reactions are highly activated. Ignoring this for now the rest of their model is reasoned as:-

The consumption of reactive gas by the pumps is very small therefore all the input reactive gas (Q) is consumed by the growing film. The compound formation reaction is

$$m.M + (n/2).N_2 \dashrightarrow M_mN_n$$

therefore each sputtered metal atom removes n/m reactive gas atoms. The number of sputtered metal atoms is approximately proportional to the magnetron power W. So for a stoichiometric film (W.n)/(Q.m) must be kept constant. They derive a value for this constant as

$$\frac{W.n}{Q.m} = \frac{2.N.e}{R_m}$$

where N = number of gas atoms per unit flow
e = electronic charge
R_m = metal sputter rate per eV of ion energy

For their calculations Hohnke et al use R_m for the metallic target ie they neglect target poisoning (only possible because they operate at a low reactive gas pressure and take Q as the total input gas flow). However, if instead of R_m we use R(p) from Abe and Yamashima and instead of Q we use the gas consumption by the growing film (ie subtract the amount consumed by the pumps $Q' = Q-p.S$) the model becomes quite general.

Poiteving and Lemperiere (ref 75) performed an interesting set of experiments on the Ti + N system in a dc diode apparatus. At the substrate position was the entrance port to a mass spectrometer which they used to analyze ionic species arriving from the plasma. They could not detect neutrals and their use of a diode (ie higher pressures) means that gas phase collisions are more significant.

Despite this their graph of ion arrival rates vs the nitrogen partial pressure is interesting (fig 3.14). Firstly it is significant that no TiN+ peak is seen re-affirming the film formation as a reaction at the substrate. Yet again the metal component (Ti+) falls away over half a decade of reactive gas pressure. When the metal falls the gas arrival rates increase dramatically. The TiN film formation occurs where the metal arrival rate is decreasing and the gas arrival rate increasing. To form the required stoichiometry we must balance these two arrival rates and so we must have a good control of the reactive gas pressure (or flow) as the arrival rates are a strong function of these.

Blom et al (ref 76) sputtered ZrN in an rf diode system and concluded that the reactive gas flow was a much more consistent parameter for controlling the film stoichiometry than was the reactive gas pressure. This is interesting in the light of the model of Hohnke et al (ref 74). Enlarging on their previous results Berg, Larsson and Blom (ref 77) fixed the film stoichiometry and show that the reactive gas flow is proportional to the deposition rate (fig 3.15). With the deposition rate proportional to power this is equivalent to Hohnke's statement.

This takes us to 1986 and around this time detailed explanations for the instability in reactive sputtering began to appear. In April Kadlec et al (ref 1986) published a letter and Penfold (ref 79) presented essentially the same ideas (presumably both are independent), later came a paper by Berg et al (ref 80). In early 1987 Danvac et al (ref 81) presented the same ideas in France and I presented a paper in London (ref 82) (independent but late).

The basic idea in all these papers is that we consider the reactive gas consumption by both the growing film and the pumps. This is summarized in fig 3.16 taken from Kadlec et al. The consumption by the growing film (bottom curve in fig 3.16) falls as the target poisons and if this is allowed to dominate the pump consumption we have a total reactive gas consumption (middle curve in fig 3.16) that falls with increasing reactive gas pressure. As the reactive gas supply is constant this causes the unstable transitions A-B and C-D in fig 3.16. This simply means that the discontinuous curve shown by Schiller in 1984 (ref 73) (fig 3.13a) is in fact continuous but in parts has a negative gradient (A-C). To control in the region A-C we must then use a method other than the balance between the input gas flow and the

Fig. 3·14 : Species at the substrate in diode sputtering of Ti + N_2 (ref. 75).

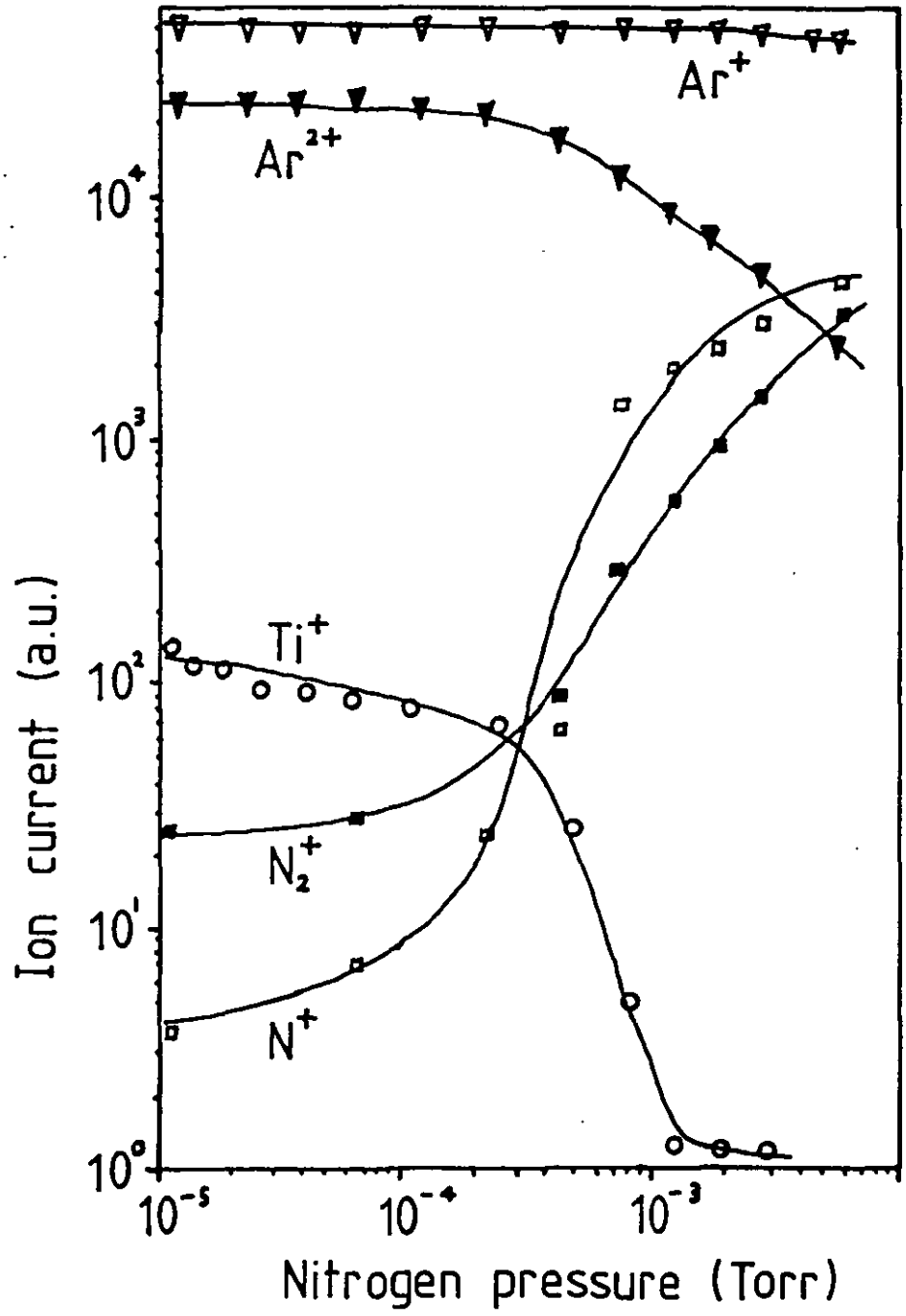

Fig. 3·15 : Deposition parameters for constant film stoichiometry in reactive r.f. sputtering (ref. 76).

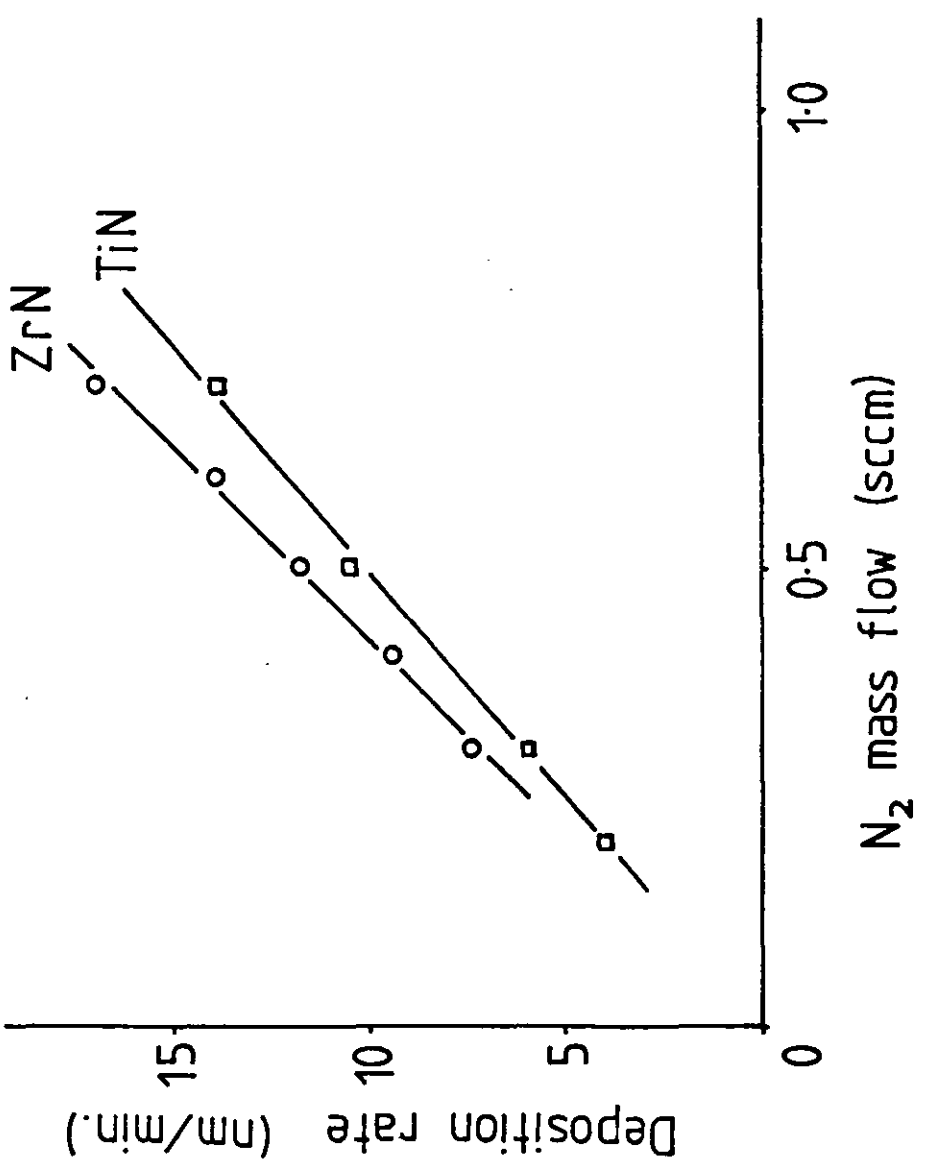

Fig. 3·16 : Instability and hysteresis in reactive sputtering (ref. 78).

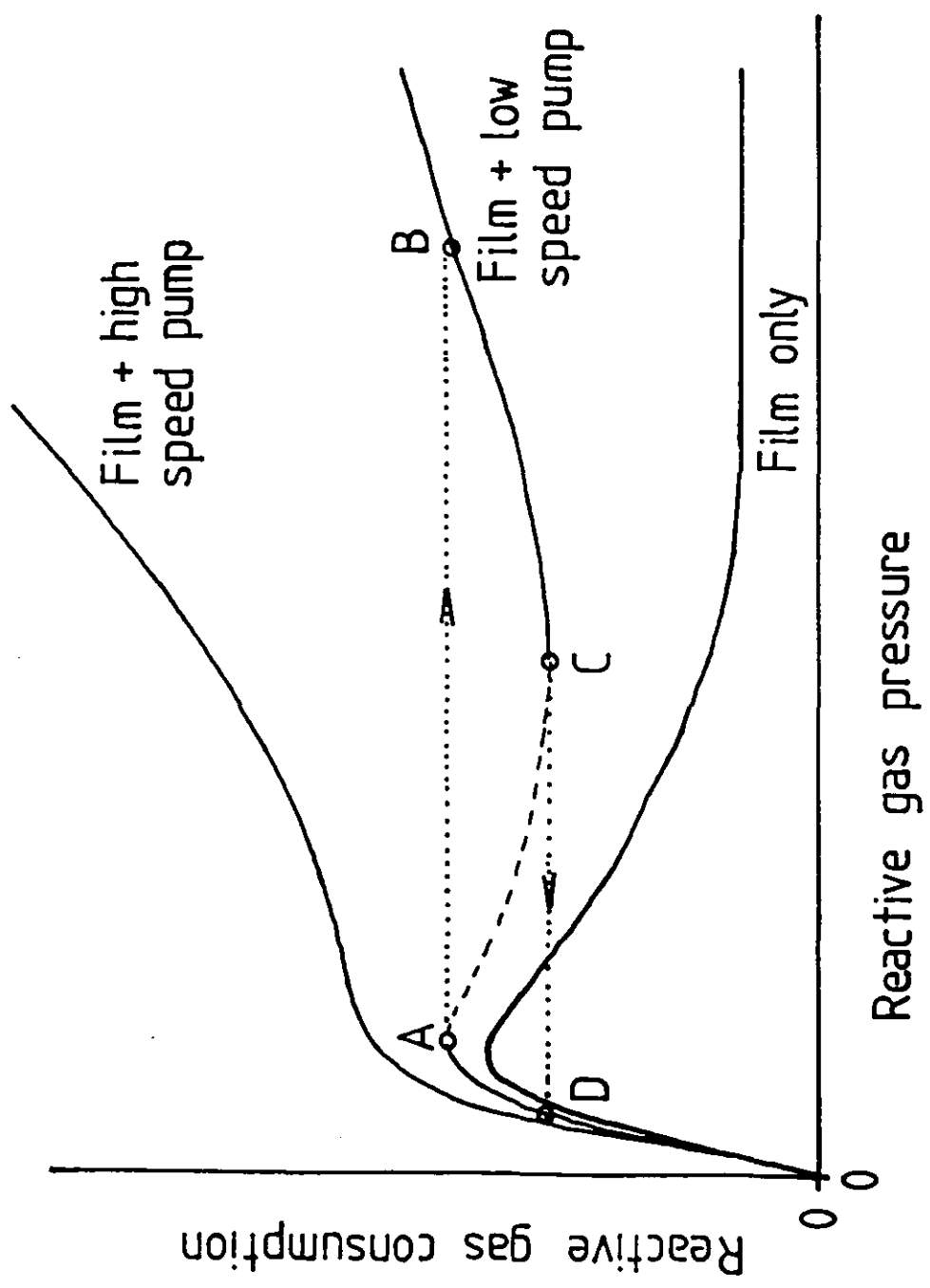

pumping rate (with perfect hindsight this is what Schiller was saying in 1984 but without a coherent explanation). Alternatively we can use very high pumping rates which dominate the reactive gas consumption by the process.

Summary

- As the reactive gas pressure is increased the metal flux from a sputtered surface falls smoothly.
- Getter pumping by the sputtered metal can consume significant quantities of the reactive gas.
- On a magnetron target the current density varies strongly across the erosion profile. The high current density in the centre will keep the target clean there while reaction products form at the edges of the erosion profile.
- Despite the smooth changes in target condition with increasing reactive gas pressure, discontinuous changes are seen in the target condition with increasing reactive gas flow.
- These discontinuous changes are due to a mutual dependence of the reactive gas pressure and the target condition. This mutual dependence can lead to positive feedback and a runaway reactive gas pressure.
- By considering the metal and reactive gas arrival rates and/or consumption, models predicting the film stoichiometry can be produced.

3.4 GAS PHASE REACTIONS

Associative reactions (fig 3.17) in the free space between source and substrate are not significant as the constraints of conserving energy and momentum make these reactions extremely unlikely at low pressures (ref 84). Material sputtered as ready formed molecules is also not significant (ref 59, 75) unless the molecule bond strength is high eg Al_2O_3 or TiO_2 (ref 85). Our film then forms at the substrate from species arriving from the gas phase. The reactive gas component of these arriving species may arrive in its stable state or any number of excited states, for example oxygen may arrive as O_2, O^-, O_2^-, or O* (a metastable state) (ref 86). The sputtered metal flux from the magnetron may also be similarly excited.

The sputtered flux from the magnetron does not contain many ions but gas phase reactions can ionize the material as it transfers to the substrate. Collisions resulting in excitation of the sputtered flux obviously occur as light emission is observed. Ionization of a sputtered metal atom M can occur through several routes. These are electron ionization, asymmetric charge transfer and Penning ionization. The reactions involved in each of these processes are respectively

$$M + e \longrightarrow M^+ + 2e.$$
$$Ar^+ + M \longrightarrow Ar + M^+$$
$$Ar^* + M \longrightarrow Ar + M^+ + e$$

There are other routes involving multiple reactions but these are less likely and will not be discussed here. In, and close to, the dark space there will be electrons with energies of the order of a hundred eV (ref 29). The ionization cross section with 100 eV electrons is around 3×10^{-20} m^2 (ref 87). The collision cross section for asymmetrical charge exchange is of the order of 10^{-19} m^2 (ref 30, 52). The plasma is electrically neutral so $n_e = n_i$ therefore the high collision cross section for charge exchange means that this will lead to more metal ionization than will electron collisions. The mean free path (λ) for a collision with cross section σ is (ref 87)

Fig. 3·17 : Types of gas phase interaction.

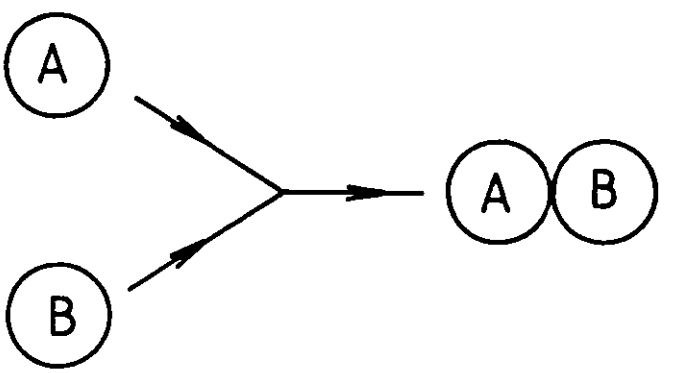

a) Associative reaction.

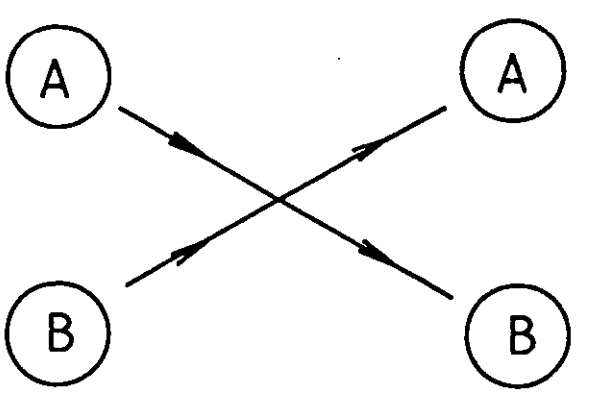

b) Collisions, exchange, and excitation.

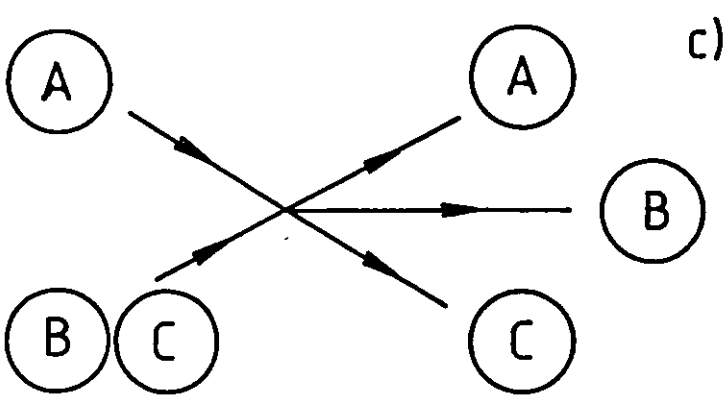

c) Dissociative reaction.

$$\lambda = \frac{1}{n \cdot \sigma}$$

where n = number density of appropriate species

The ion density in the plasma will be of the order of 10^{15} m^{-3} (ref 29) so the mean free path between charge exchange reactions for a sputtered neutral will be around 10 km. This implies that ionization of the sputtered flux by charge exchange or by electron collision is unlikely.

The gas number density is simply n = p/k.T (p = pressure in Pa, T = absolute gas temperature and k = Boltzmann's constant, (ref 84))so at 1 Pa and 300 k we get n = 2.4 x 10^{20} m^{-3}. The mean free path for charge exchange in a magnetron is then around 0.05 m. This implies that there will be significant charge exchange between ions and gas neutrals in the magnetron plasma.

Penning ionization of the sputtered flux is difficult to discuss as the number density of the metastable states Ar^* is unknown and the ionization cross section also unknown. The energies of the Ar^* metastable states are (ref 30) 11.5 eV and 11.7 eV so Penning ionization of most metals is possible as the typical first ionization energy for a metal is 5-9 eV.

Simple scattering collisions are likely and are discussed in my M. Phil. thesis (ref 27). The main effect of these collisions will be to reduce the energy of the sputtered atoms and to increase the range of incidence angles at the substrate. These effects scale with the product of the pressure and target/substrate distance reaching saturation at around 1 Pa.m.

Summary

- Associative reactions in free space are unlikely due to the constraints of conserving energy and momentum.
- Dissociative reactions, exchange reactions and collisions have no such limitations and their probabilities are determined only by

collision cross sections and number densities.

- Charge exchange reactions for the background gas are probable in magnetron plasmas.
- This is not true for the sputtered metal flux which is unlikely to be ionized by charge exchange reactions or by ionizing collisions. Penning ionization is possible but the probability is difficult to evaluate as both the collision cross section and the metastable atom density are unknown.
- Simple scattering collisions will thermalize the sputtered flux over a pressure distance product of around 1 Pa.m. For pressure distance products of less than this the energies and angles of arriving metal atoms are a strong function of pressure and/or distance.

3.5 REACTIONS AT THE SUBSTRATE

General Film Growth

The growth mechanisms of thin film have been discussed in many papers. These discussions can almost be summarized in a few diagrams. The growth of a film in terms of where individual atoms deposit can be monolayer (Frank and Van der Merwe), monolayer + island (Stranski-Krastanov), or island growth (Volmer-Weber). These are discussed by Vook (ref 88) and generally sputtered films form by island growth. During this growth the adsorbed atoms are mobile on the surface until they are desorbed or find a low energy site and bond. In the island mode of growth these low energy sites on the original substrate are termed nucleation sites and once atoms have bonded at these nucleation sites an island starts to form. As the islands grow they coalesce and a continuous (but defect filled) film is formed. Beyond this stage we have growth of the film material on the film material and so we would expect near constant growth rate. The initial nucleation is however a different case and may have growth kinetics drastically different from the continuous film case.

Modelling of this type of film growth has been extensively done by Muller (ref 55). Muller demonstrates that with the assumptions of increasing surface mobility with temperature the structure zone diagram of Thornton (ref 89) can be explained. This well known diagram conveys visually the type of film growth observed for different substrate temperatures and the effects of increasing the deposition pressure (reducing the energy of the depositing species). Muller also demonstrates that low energy ion bombardment leads to film densification by forward scattering of the film material (ref 90).

Reactive Film Growth

The possible rate controlling stages in reactive film growth are discussed by Bunshah (ref 91). He gives these as:-

1. Adequate supply of reactants.
2. Adequate collision frequency between reactants.
3. The rate of reaction at the reaction interface.
4. The rate of removal of reaction products.

In general 1,2 and 4 are easily satisfied and the rate limiting step becomes the rate of reaction. In reactive evaporation Bunshah shows that the presence of a plasma increases the reaction rate ie activates the reaction. In sputtering film formation reactions at the substrate can be activated by the proximity of a plasma (ref 51, 92) or by ion bombardment (ref 93). Where surface reactions dominate the reaction rate (r) we have the Arrhenius equation (ref 94)

$$r = \text{const. } e^{-(\Delta E/kT)}$$

where ΔE = activation energy for the reaction
k = Boltzmann's constant
T = Absolute temperature

The presence of activated species (see section 3.4) will change the activation energy ΔE (ref 51). The arrival of energetic species would add energy to adsorbed atoms on the surface and so increase the effective surface temperature. There are then available mechanisms by which we would expect the presence of a plasma to activate substrate reactions. Stage 1 in Bunshah's list is an adequate supply of reactants. We have at the substrate the arrival rates v(m,g) where m or g indicate metal or gas. Schiller states that we must keep the ratio of these two constant to maintain film stoichiometry (see section 3.3 - reactive sputter deposition). This is enlarged upon by Boenig (ref 85) in the relationship for a film with the composition MmGn

$$n/m = U.V_g/V_m$$

where U = utilization (Boenig uses sticking coefficient here and says generally around 0.01)

This relationship is demonstrated experimentally for evaporated TiN films by Mathews and Teer (ref 95). Their result is shown in figure 3.18 and shows lines of constant stoichiometry (constant n/m) on a graph of the metal evaporation rate vs reactive gas flow. The evaporation rate will be proportional to v_m. The arrival rate of reactive gas at the substrate v_g will be determined by the reactive gas pressure and temperature (see section 3.7). It is not clear how the

Fig. 3·18 : Lines of constant film stoichiometry (ref. 95).

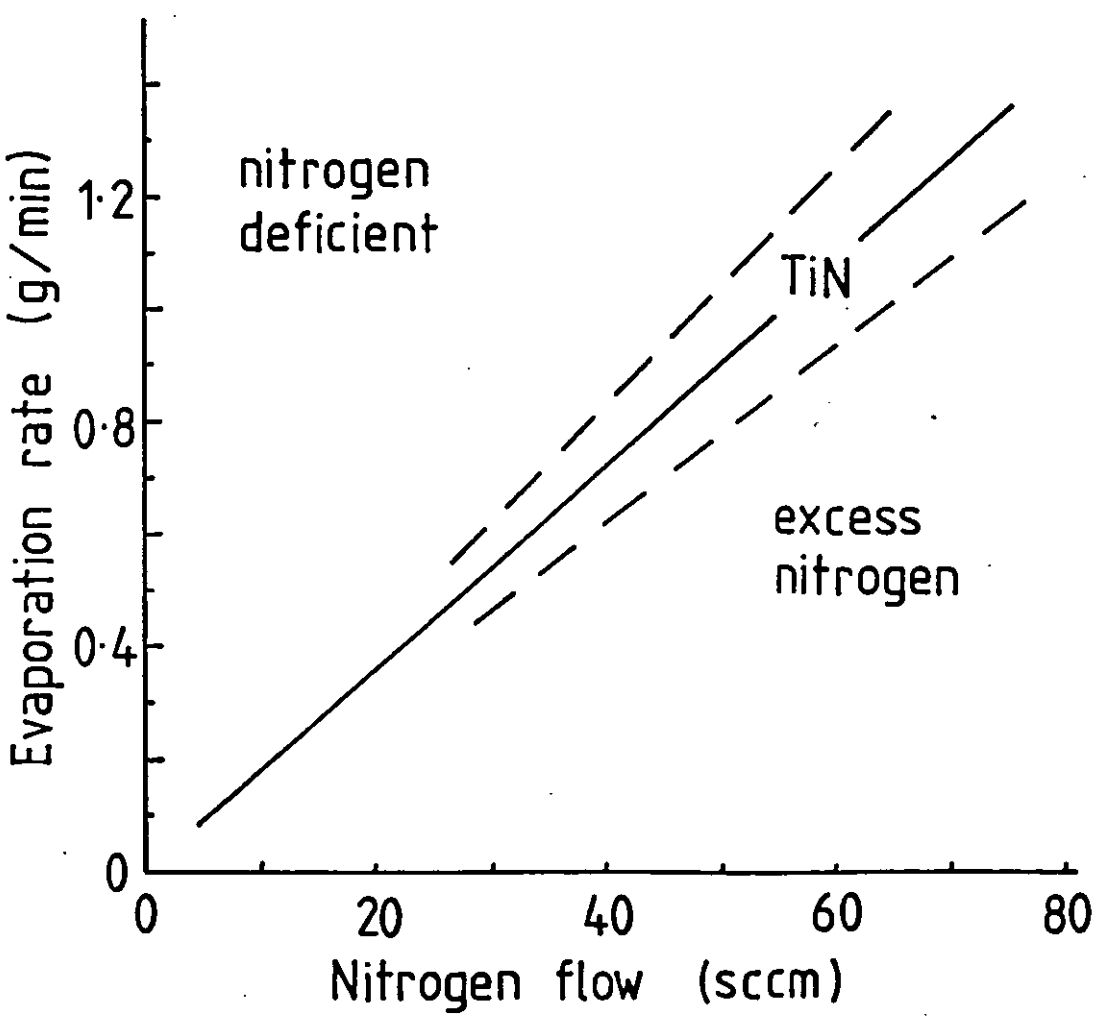

reactive gas pressure depends on the reactive gas flow but for a constant pumping rate the dependence should be linear.

For reactively sputtered a-Si:H there is a simple kinetic model for the hydrogen incorporation (ref 96). The capture rate of hydrogen is

$$\text{capture rate} = \sigma \cdot \theta \cdot v_g \cdot N$$

where σ = capture cross section for reactive sites
θ = sticking coefficient
v_g = hydrogen arrival rate
N = number of reactive sites per unit area.

This equation can be reconciled with the Arrenhuis equation on the basis that the sticking coefficient θ is

$$\theta = e^{-(\Delta E/kT)}$$

The constant in the Arrenhuis equation is then $\sigma . V_g . N$. Also note that here N is a dynamic term for the number of sites ie a balance between metal arrival creating sites and reactions removing them. Now with a film growth rate R (in monolayers per second) a reactive site will have a time 1/R in which to react before it is covered by the next layer of film growth. From the equation above for the capture rate the time dependence of N for a static surface (ie neglecting film growth) will be

$$\frac{dN}{dt} = -\sigma \cdot \theta \cdot v_g \cdot N$$

so after a time 1/R the number surviving will be

$$N = N_0 . \exp(-\sigma \cdot \theta \cdot v_g/R)$$

This then gives the film content of the reactive gas. Tiedje *et al* fitted their result to experimental data they obtained from rf reactive sputtering from a Si target. This is shown in figure 3.19 and using

Fig. 3·19 : H concentration in reactively sputtered α Si:H films (ref. 96).

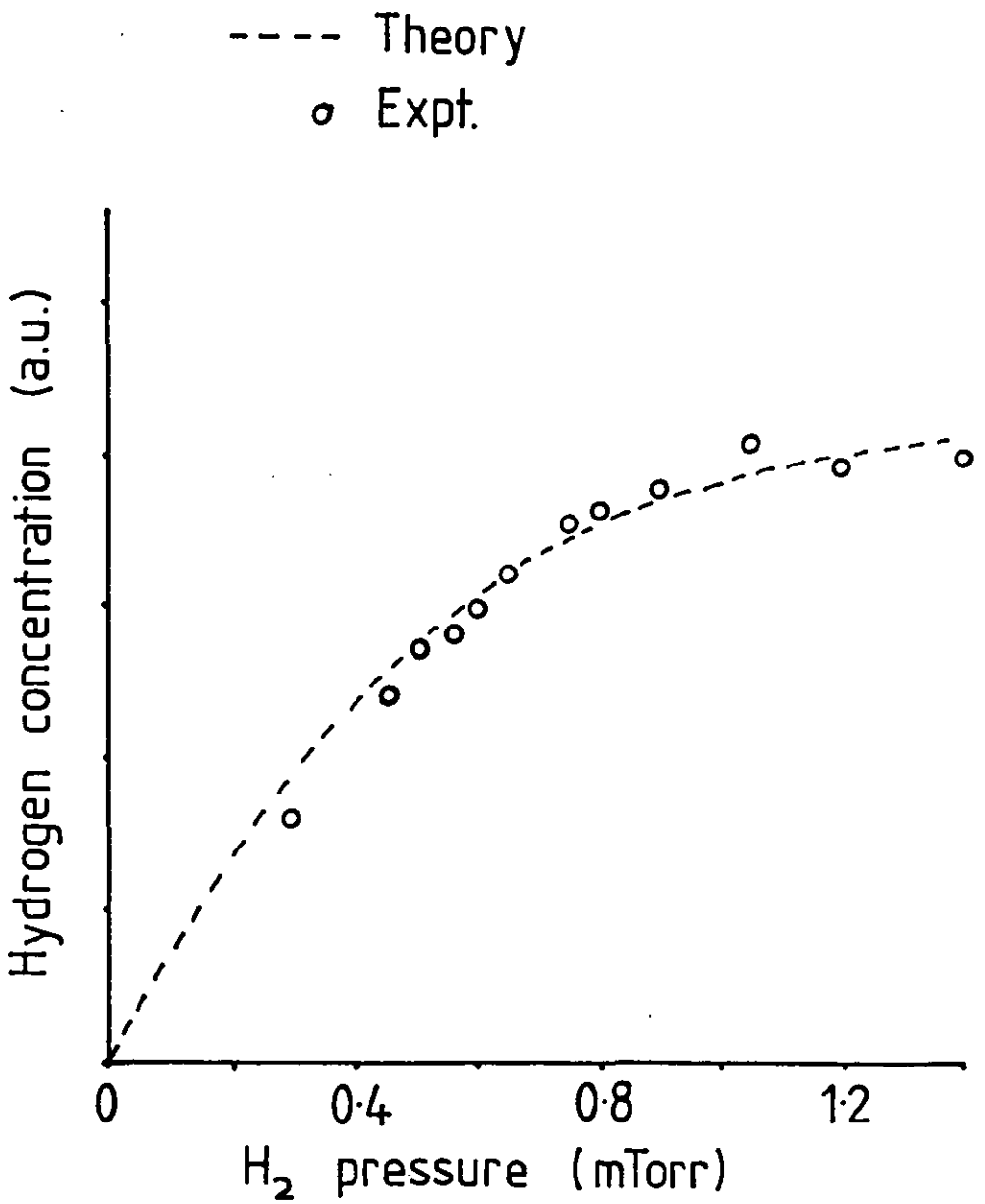

the sticking coefficient as a free variable they obtained from the fit values of θ between 0.02 and 0.06. They attribute this relatively low value to the small fraction of atomic hydrogen arriving at the substrate. They conclude that H is responsible for the reactions at the substrate and not the more abundant H_2.

This metal/gas reaction tends (as the reactive gas pressure is increased) to a film saturated with reactive gas (figure 3.19). This film is in general not the stoichiometric compound but is reactive gas rich eg $TiO_{2.4}$ (ref 97). Deposition of the stoichiometric compound then requires control of the reactive gas pressure in the region approaching saturation. In systems with more than one possible metal/gas compound then many side reactions take place and the film is likely to contain a mixture of compounds. Again the deposition conditions for this film must be optimized experimentally for the required compound or property (ref 98).

Reactive Etching

Reactive etching has some similarity with reactive film growth. Reactive film growth uses two (or more) species from the gas phase to react on a surface to form a solid compound. Reactive etching uses species from the gas phase reacting with a surface to form gaseous compounds. The stages in reactive etching are given by Coburn (ref 99) as:-

1. The gas must adsorb on the surface forming a chemical bond with the surface atoms (ie chemisorption).
2. The atoms on the surface must rearrange themselves to form the product molecule.
3. The product molecule must desorb from the surface.

In reactive film formation we have processes close to all the stages above except that the species that adsorb onto the film surface must react with other adsorbed species or with active sites on the growing film surface. We have seen that in the film growth models ad-atoms react with each other or with active sites of the growing film surface.

Ion bombardment during etching is shown to have large effects on

the etch rate (ie reaction rate) of various mixtures (ref 100) (fig 3.20). This increased reaction rate they attribute to dissociation of adsorbed species and a reduction in the activation energy for the reaction. Each ion may influence many reactions (ref 101, 102) which is consistent with this picture for the ion energies used.

Lastly for ion etching Coburn (ref 99) gives a concise diagram (fig 3.21) showing the relevant parameters for reactive etching. This is reproduced as it is also applicable to reactive deposition.

Summary

- Film growth does not generally occur as consecutive formation of monolayers but as the initial formation of islands at nucleation sites which then grow upwards and out to form a continuous but defect filled film.
- Compound film growth occurs by reaction at the substrate between the sputtered metallic component(s) and the gaseous reactive component(s).
- The film composition can then be controlled by either the metal flux (magnetron power) or the reactive gas (flow and/or pressure).
- The reaction between these species can be significantly enhanced by the provision of energy at the substrate. This can be in the form of ion bombardment, excited reaction species or increased substrate temperature.
- This provision of energy at the substrate will also affect the film structure. In general it will result in a denser film with less defects.

Fig. 3·20 : Ion beam activation of surface reactions in reactive etching (ref. 100).

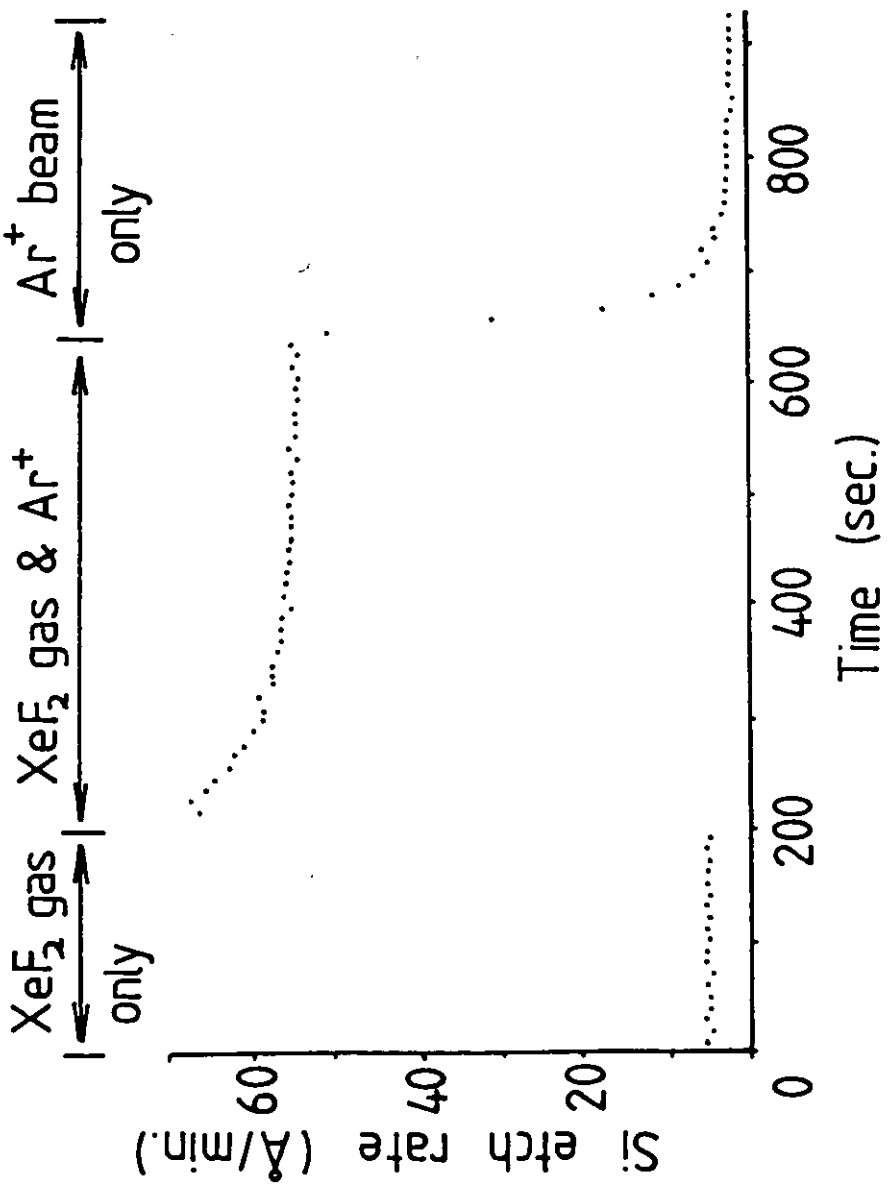

Fig. 3·21 : Significant parameters in plasma etching (ref. 99).
n_e - electron density
f(E) - electron energy distribution
N - gas density
τ - residence time in chamber

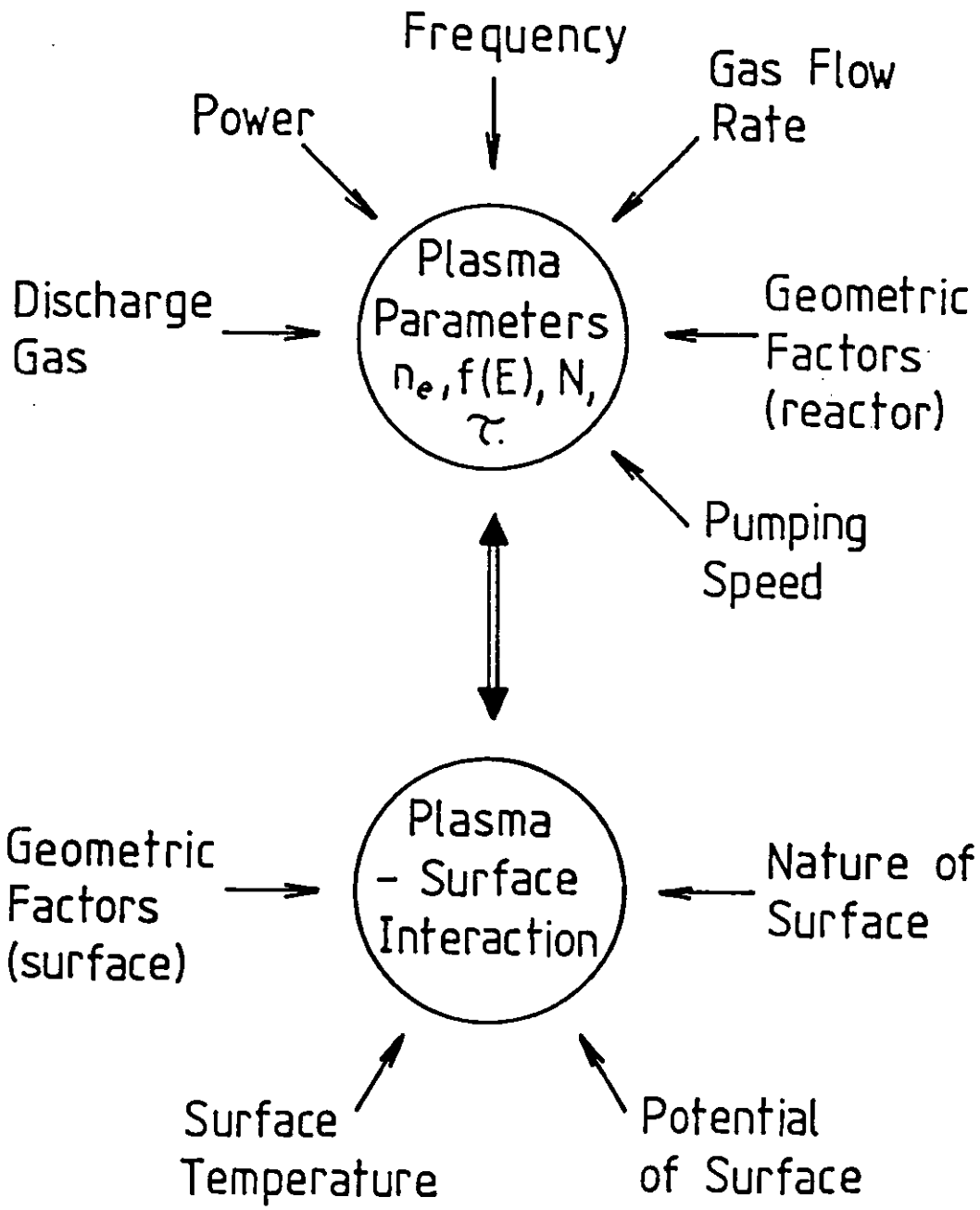

3.6 LIGHT EMISSION BY PLASMAS

Light emission by plasmas in general is discussed by J E Greene (ref 103). Line emission at wavelengths characteristic of a particular species occurs because of a transition between two energy states i and j. The energy of the photon emitted (hence its wavelength - λ) is the energy difference between the two states. A typical spectrum from a reactive sputtering plasma is given by Enjouji et al (fig 3.22) (ref 104). The light intensity I(x) for a particular transition i to j at a position x is given by (ref 103)

$$I(x) = N(x) \cdot P_i(x) \cdot T_{ij} \cdot g(\lambda)$$

where $N(x)$ = number density of relevant species
$P_i(x)$ = excitation probability to state i
T_{ij} = decay probability from state i to state j
$g(\lambda)$ = fraction of emitted photons that are detected.

This equation being reasonable as the product $N(x).P_i(x)$ is the density of the excited species ie emission intensity is proportional to density of excited states (ref 105). T_{ij} is a constant determined by the quantum mechanics of the relevant species. The factor $g(\lambda)$ will be a function of the system geometry, detector sensitivity and plasma transmission. $P_i(x)$ depends on the electron density and energy distribution and can be calculated if these are known. T_{ij} and $g(\lambda)$ are for our purposes unobtainable but should be constant. This forces the use of I(x) on an empirical basis. The equation for $P_i(x)$ is (ref 105)

$$P_i(x) = \int n_e(x,E) \cdot \sigma(E) \cdot dE$$

where E = electron energy
$n_e(x,E)$ = electron density
$\sigma(E)$ = collision cross section for excitation.

It is observed that both the system pressure and the presence of other gases such as hydrogen effect I(x) (ref 106). The most likely mechanism for this then seems to be modification of the electron

Fig. 3·22 : Emission spectrum from a magnetron plasma (In target, Ar/O_2 gas) (ref. 104).

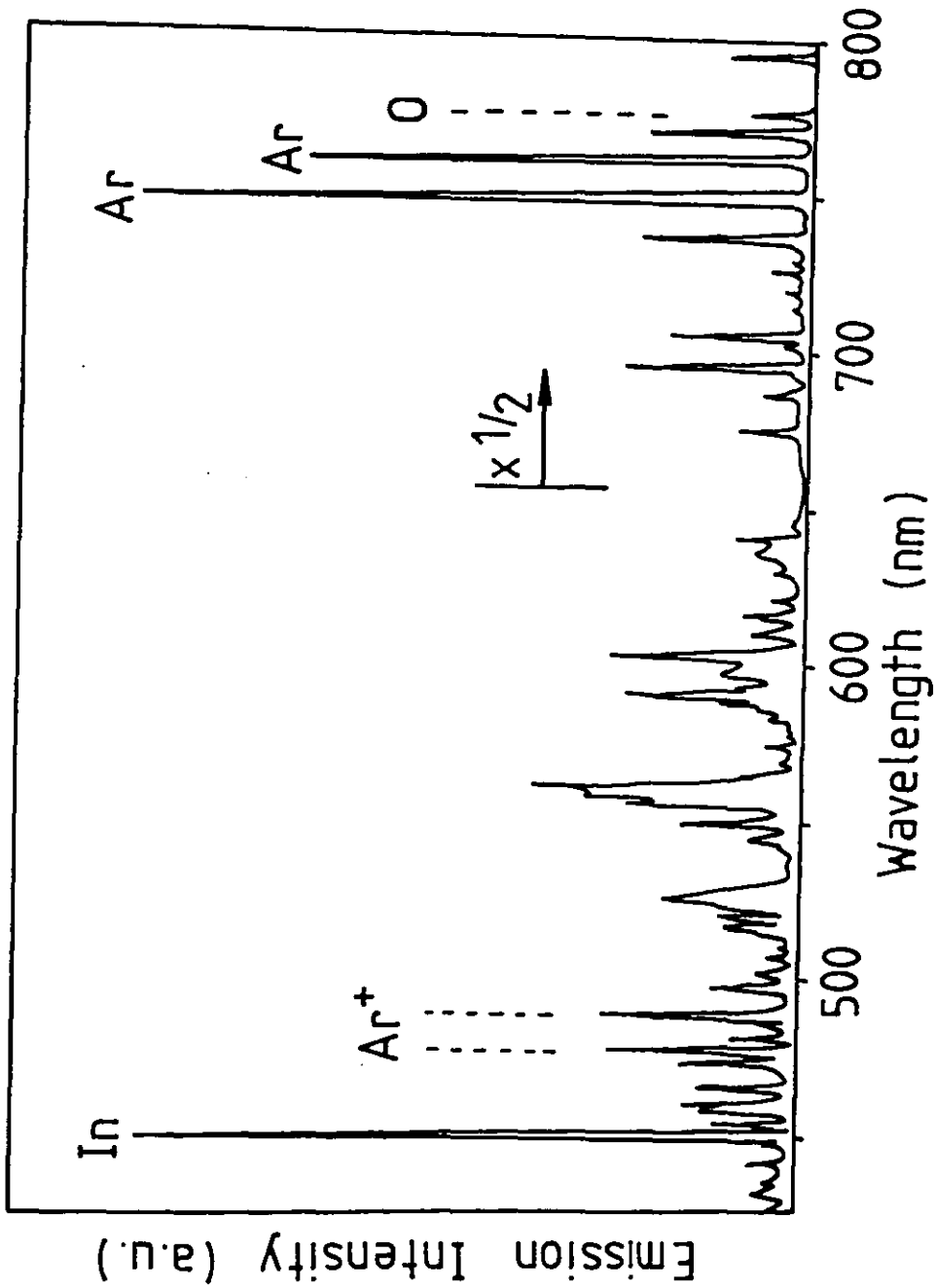

density and/or electron energy distribution (ref 21). Rossnagel and Kaufman found that for increasing pressure T_e increased while n_e decreased (ref 29).

Greene and Sequeda-Osorio (ref 107) show that the emission intensity I(x) is a strong function of position (x), falling away rapidly with increasing distance from the cathode. Presumably this is due to strong variation in $P_i(x)$ as N(x) should not vary strongly with distance from the cathode. Such a variation in $P_i(x)$ is reasonable as secondary electrons created at the cathode surface will arrive at the edge of the dark space with large energies. In their migration away from the cathode the electron density and energy can only fall as in the plasma there are no other large potential gradients to supply energy to the electrons. This was seen experimentally by Rossnagel and Kaufman (ref 29).

Experimentally it has been found that at constant pressure the metal emission intensity is proportional to the deposition rate (ref 104, 106 and 107). Blom et al also found that when depositing ZrN the N emission intensity was linear with increasing nitrogen flow (ref 76). These simple relationships between emission intensities and deposition parameters have led to the use of optical emission spectroscopy to control various plasma deposition techniques (ref 8, 108 and 109).

Optical emission spectroscopy can also be used to monitor gas impurity levels in discharges (ref 110) but as fig 3.22 shows there are a multitude of emission lines and it is by no means a simple matter to identify the species responsible for each line.

There is a US patent covering the use of emission intensity to control reactive sputtering in the unstable transition which was granted in 1979 (ref 8). This technique did not pass into general use and was almost reintroduced by Schiller et al in 1987 (ref 109).

Summary

- The light emission from a plasma is mainly due to atomic transitions and so is composed of emission lines from the excited

species present.

- The intensity of a given line is directly proportional to the number of the appropriate excited species viewed by the detector.
- The relationship between the plasma parameters, detector configuration, species density and line intensity is exact but too complex to yield quantities such as the reactive gas pressure or the metal density in the plasma.
- These quantities can be obtained on an empirical basis as, for example the relationship between the gas emission intensity and the gas pressure, or the metal emission intensity and the deposition rate, is found to be linear.

3.7 PERFECT GAS BEHAVIOUR

In the use of vacuum the behaviour of gases is crucial to the understanding of the process. There are two regimes of gas flow applicable to vacuum: molecular and viscous flow. To define these two regimes the average distance between collisions (the mean free path) λ can be used. When the distances considered are much greater than λ then collisions between particles dominate the properties of the gas and we have viscous flow. At atmospheric pressure (10^5 Pa) viscous flow occurs at all realistic dimensions. As the pressure is reduced λ increases and for a vacuum chamber with dimensions of the order of one metre molecular flow occurs at pressures below 0.01 Pa. In the pumping system the sizes are generally 0.1 to 0.01 m in size and so molecular flow occurs below 0.1 to 1 Pa. There is a broad transition between these two regimes, and about two orders of magnitude up in pressure from those quoted the gas behaviour starts to depart from viscous flow. This can be seen in figure 3.23 which also shows the need to swap between pump types in different regimes.

Various useful relationships can be derived for a perfect gas in these two regimes and some are presented below. Behaviour in the transition region can be calculated by mixing the results from the two extremes (ref 111, 112). For calculation metric units are convenient (ie Pa, l, s, m, K, etc) but most equipment comes with different units eg Torr or bar for pressure, sccm (standard cubic centimetres per minute) for gas flow. These are difficult to reconcile and so in this work calculations are done in metric units and converted. Experimental results are presented in the units of the equipment as these are currently easier to visualize. The conversion factors most often used here are Pa = 7.5 mTorr and 1 Pa.l/s = 0.6 sccm.

A basic quantity is the mean free path λ. This can be calculated as

$$\lambda = \frac{1}{2^{1/2}} \cdot \frac{1}{n \cdot \sigma} \qquad (1)$$

where σ = collision cross section

n = number density.

Fig. 3·23 : Vacuum pumps in different flow regimes (data from Edwards 1988 catalogue).

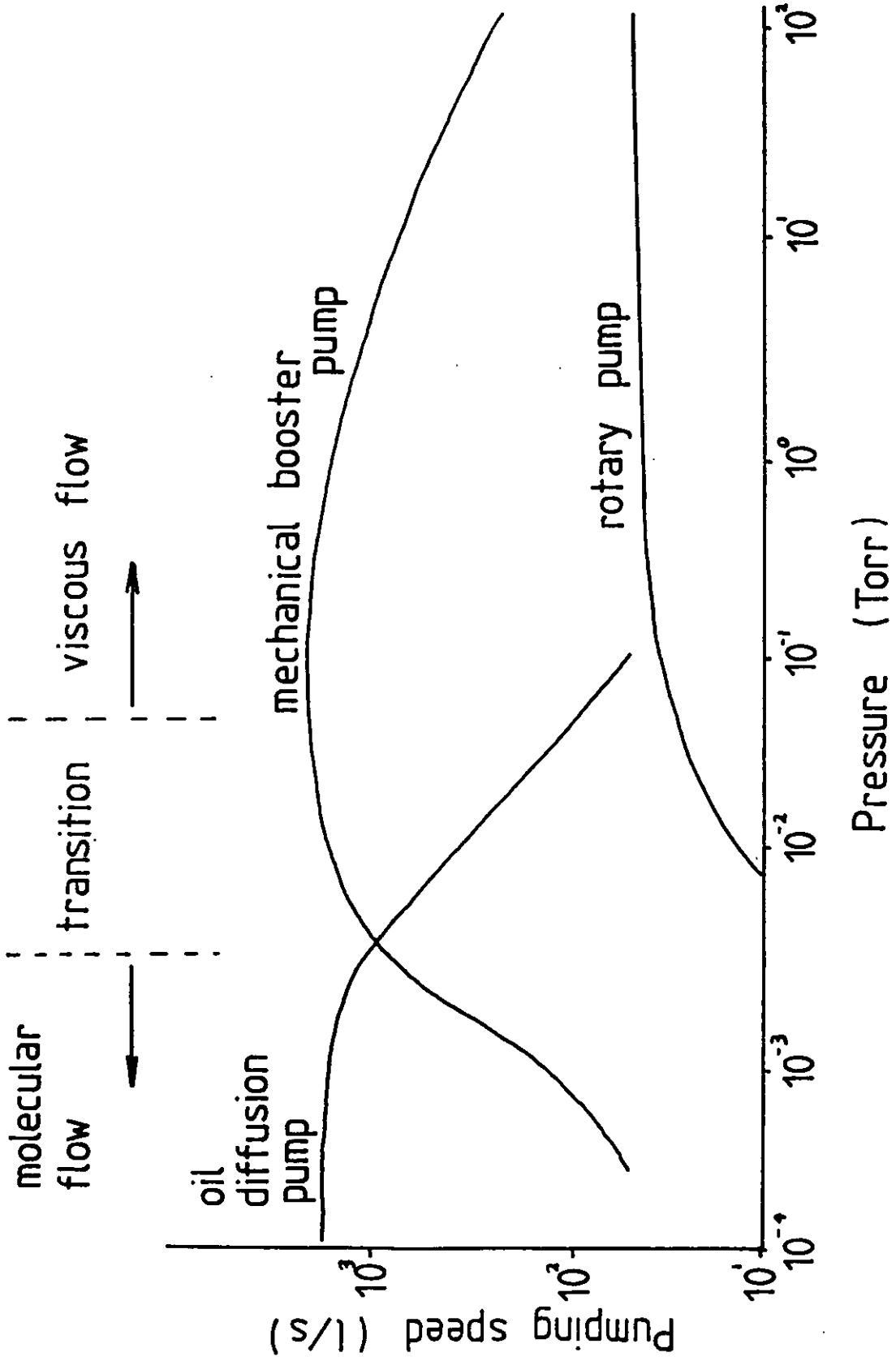

The number and density n of the constituent particles of a perfect gas (atoms or molecules) is

$$n = \frac{p}{k.T} \qquad (2)$$

p = gas pressure (Pa)

k = Boltzmann's constant

= 1.38×10^{-23} J/K

T = Absolute gas temperature (K).

An important quantity in reactive film deposition is the arrival rate of gas atoms at a surface v_g. This is fairly simply expressed in terms of the number density n and average speed $\langle c \rangle$ of the gaseous particles. We have

$$v_g = \frac{n.\langle c \rangle}{4} \qquad (3)$$

Now we need to know the average speed and this is

$$\langle c \rangle^2 = \frac{8.k.T}{\pi.m} \qquad (4)$$

where m = mass of gaseous species (kg).

Combining the relations (2 and 4) for n and $\langle c \rangle$ with that for v_g (3) gives

$$v_g = p.(2.\pi .k.T.m)^{-1/2} \qquad (5)$$

We will use this relationship later to discuss the delivery of the reactive gas atoms to the film surface. The main property of this relationship is that for constant T the delivery rate of a given species to a surface is proportional to the partial pressure of that species.

For now it is interesting to note that with a vacuum pump we have a pumping orifice at which the atoms arrive at a rate v_g and that the volume per atom is 1/n. The volume of gas S arriving per unit area A

of pumping orifice is v_g/n which from (3) is

$$\frac{S}{A} = \frac{\langle c \rangle}{4} \qquad (6)$$

This is independent of pressure and for Ar at 300 K gives a value of 100 m/s. The same number is more usefully expressed as 10.0 l/s/cm^2. In molecular flow this is the volume of gas per unit area that will pass through any orifice. This quantity then puts an upper limit on the volume that can be removed by a pump connected to the chamber through an orifice of a given area. For an orifice of area A (in cm^2) we then get a pumping rate of 10 x A l/s. For a tube or pipe, collisions with the walls reduce this figure (termed the conductance) in a calculable fashion (ref 113, 114).

In the molecular flow regime the pumping rate S of the vacuum pumps expressed in l/s is a constant. If we put in a flow of gas Q (in Pa.l/s) the pressure produced will be

$$P = Q/S \qquad (7)$$

For a chamber of volume V we get two simple relationships. For simply removing the gas within the chamber the pressure will fall exponentially with time:-

$$p = p_0.\exp(-t.S/V) \qquad (8)$$

p_0 = initial pressure.

The quantity S/V is the inverse of the mean residence time of a gas particle in the chamber (V/S). This equation gives a pressure that tends to zero. In practice at small pressures a gas load Q_{OUTGAS} will appear due to material desorbing (outgassing) from the walls. This means that in practical applications our initial pump out will tend to a pressure Q_{OUTGAS}/S. To reach pressures below this we must wait until Q_{OUTGAS} falls (speeded up by heating the walls) or we must increase S.

For a gas diffusion (viscous flow regime) the diffusion rate of gas particles across a density (partial pressure) gradient is given by

the diffusion equation. This is in terms of the gas particle flux density J across the gradient. The one dimensional equation is

$$J = - D.\frac{dn}{dx} \qquad (9)$$

where D = diffusion coefficient.

This diffusion coefficient can be expressed in terms of quantities already derived ie

$$D = 1/3.\langle c \rangle . \lambda . \qquad (10)$$

Typical values for reactive magnetron sputtering

The relationships quoted above can be used to derive figures applicable to the process of reactive magnetron sputtering. The numbers in table 3.1 are appropriate for the 0.5 m bell jar vacuum systems used in this study.

Table 3.1: Typical parameters for our deposition systems

Ar pressure	=	1 to 10 mTorr = 0.1 to 1 Pa
O_2 pressure	=	1 mTorr = 0.1 Pa
Chamber dimensions	=	0.5 m
Pumping rate	=	250 l/s (oxygen)

The collision cross section for molecular oxygen is 1.0×10^{-19} m^2 and the value for argon very similar (ref 115). Assuming a gas temperature of 300 K gives from equations 1 and 2 a mean free path of 300 mm at 0.1 Pa and 30 mm at 1 Pa. The ratio of chamber size to mean free path (the Knudsen number) is then between 2 and 20. This means that the gas behaviour in the deposition chamber is on the viscous flow side of the transition regime.

The mean residence time of an oxygen molecule within the chamber is (from equation 8) 0.4 s and this is also the time constant for pressure fluctuations. With the process running this time will be reduced because of the additional pumping provided by the film growth.

The mean molecular velocity will be (at 300 K) around 450 m/s (from equation 4). So during the residence time our average molecule will make 600 collisions at 0.1 Pa or 6000 collisions at 1 Pa. For a three dimensional random walk process involving z collisions the mean distance travelled is $z^{1/3}.\lambda$ (ref 116). This gives a travelled distance of 2.5 m at 0.1 Pa and 0.5 m at 10 Pa. As these distances are comparable to the chamber dimensions a totally uniform oxygen pressure cannot be taken for granted.

To calculate the pressure gradients within the deposition chamber we would need a complete description of the chamber geometry, pumping by the film and vacuum pumps and accurate calculations within the transitional flow regime. We can estimate the pressure gradients by calculating the pressure gradient along a 0.5 m diameter pipe for viscous flow (equations 9 and 10). With a pumping rate of 250 l/s and a desired pressure of 0.1 Pa we must (from equation 7) put in an oxygen flow of 25 Pa.l/s/ From equation 2 this is 6.0×10^{18} oxygen molecules per second. A uniform flow along a 0.5 m diameter pipe then gives a flux J = $3.1 \times 10^{19}/m^2/s$. From equations 9, 10, 1, 2 and 4 we can calculate for viscous flow the pressure gradient necessary to give us a transport of J atoms/unit area. Doing this gives an oxygen pressure gradient along a 0.3 m substrate of 1% at 0.1 Pa total pressure and 10% at 1 Pa total pressure.

This is only an approximation to the real situation but it does indicate that significant pressure gradients are possible within the deposition chamber. The calculation ignores the additional pressure gradients around the small gas inlet(s) (see section 8) and around the pumping orifice. I also assumed that the substrate was placed along the direction of gas flow and in the coater constructed by us we have tried to avoid this.

Summary

- As the distance between gas/gas collisions (the mean free path) approaches the size of the container a perfect gas makes a transition in behaviour from viscous (a fluid) to molecular (non interacting particles).

- In a typical sputter deposition chamber the gas behaviour is in the transition between these two modes.
- The pumping rate of the chamber is proportional to the area of the pumping orifice (given a big enough pump beneath the orifice).
- In the absence of more sophisticated control the gas pressures are maintained simply by a balance between the input gas flow and the chamber pumping rate.
- Gas pressure gradients of a few percent are to be expected in the chamber and so if the film properties are very dependent on the gas pressure then variations are likely.

3.8 ARCING

Arcing is a problem with magnetron sputtering, particularly when using reactive gases and/or high current densities. During an arc the diffuse high voltage magnetron plasma collapses to a bright concentrated low voltage arc discharge. This arc discharge is a source of target material but is localized and usually produces metal rich films in reactive sputtering atmospheres (higher reactive gas pressures are required) (ref 117). The disruption of an arc to the power supply and to the film produced is then fairly severe. The increased occurrence of arcs with increasing current density (ref 3) can be explained empirically from fig 3.24. This shows the various regimes in which plasmas can operate.

A magnetron is operated in the abnormal discharge region and as the current density is increased we move towards the maximum operating potential. Beyond this the differential impedance goes negative leading to a rapid transition into the arc regime. A higher current density means that we are closer to the transition and so less disturbance is required to lead into an arc.

Arcing problems in relation to the power supply used are discussed by Grove (ref 118). Grove gives a graph of currents against time for a 'typical' arc (fig 3.25) showing currents of 50 A flowing on a time scale of 5×10^{-6} s. It is found experimentally that a capacitance across the magnetron greatly reduces problems with arcing (such a capacitance is fitted on the Everest coater by Leybold). Grove also details the performance of the advanced energy MDX supplies which, when an arc occurs, can cut the power and then restart the magnetron discharge. This is useful for intermittent arcing but with regular persistent arcing means that no power can be supplied to the magnetron.

Grove discusses arcing in terms of 'streamer' theory (ref 119, 120) but this is a high pressure process (ref 121) not applicable to magnetron discharges. His further discussion on target inhomogeneities (mechanical and electrical) as sources of arcing ties in with the details below.

Sharp points on the magnetron surface are to be avoided as these lead to a local increase in current density so increasing the

Fig. 3·24 : The relevant plasma types

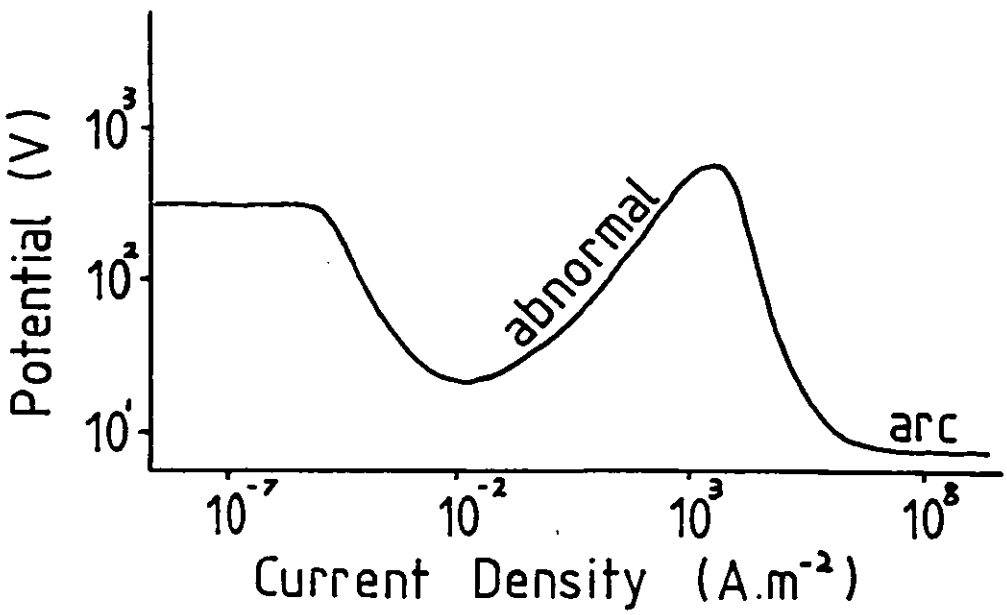

Fig. 3·25 : A typical arc profile (ref. 118).

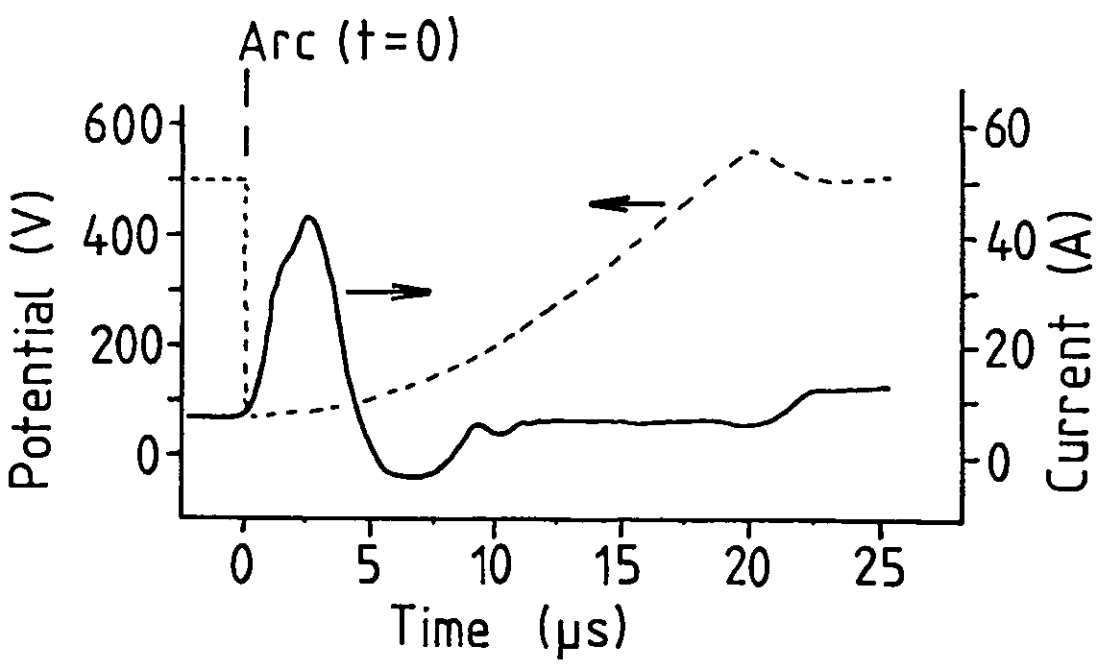

likelihood of arcs. A factor that is almost inherent in magnetron sputtering is the production of debris in the coating zone. The coating on static surfaces within this zone is usually stressed and so at a given thickness the adhesion fails and fragments are ejected from the surface. This debris consequently accumulates over the time between cleaning and leads to increased arcing problems.

Types of arcs and the appropriate mechanisms are given by Brown (ref 121). The three useful classifications are:-

1. Self sustaining thermionic arc (unheated cathode)
2. Non-self sustaining thermionic arc (heated cathode)
3. Field emission arc.

These can be sub-classified as high or low pressure arcs. Magnetrons are operated well into the low pressure region and so high pressure theory (streamers in particular) is not appropriate. At low pressures the main difference is that the electron temperature T_e and the gas temperature T_g are decoupled and we have

$$T_e >> T_g$$

The low pressure variants of the above types of arcs are discussed below.

Mechanism 1

Thermionic arcs of types 1 and 2 are sustained by electron emission from the hot cathode spot (either externally heated (2) or heated by the arc (1)). Evaporation is generally seen from the cathode spot and this immediately implies temperatures that may lead to thermionic emission (this is discussed below). Due to the magnetron magnetic field an arc, once formed, usually moves (ref 121, 122). This makes self sustaining thermionic arcs less likely in a magnetron as the arc movement gives less time for the target temperature to rise to the point of significant thermionic emission (ref 121). A feature of arcs is that their motion in a magnetic field is not always in the direction of the lorentz force ($\overline{I} \times \overline{B}$). The arcs may be stationary or retrograde and can change direction as $|\overline{B}|$ is altered, an explanation for this is offered by Ohtsuka (ref 122). This provides an interaction mechanism between the magnetron magnetic field (strength and

distribution) and the tendency for sustained arcs.

Mechanism 2

Flakes of sputtered material in contact with the target (see debris) have sharp corners and poor cooling. It is often seen that the plasma can heat the points of such debris to red heat (1000-2000 K). These heated points may then form ideal arc initiators by mechanism 2. The temperature required for thermionic emission is material dependent and also affected by impurity levels (eg thoriated tungsten). The Richardson-Dushman equation for the saturated thermionic emission current density (J_{SAT}) is (ref 30):-

$$J_{SAT} = A.T^2.\exp(-e.\phi/k.T)$$

A = Richardson's const.
= 1.2×10^6 A/m^2/K^2
T = Absolute temperature (K)
ϕ = work function (eV)
k = Boltzman's const.
= 1.38×10^{-23} J/K
e = electronic charge
= 1.6×10^{-16} C

An arc can have current densities greater than 10^8 A/m^2 (ref 128). Work functions lie in the range 2-6 eV (ref 123) so tabulating J_{SAT} as a function of ϕ and T gives table 3.2.

Table 3.2: Thermionic saturation current density (A/m^2)

Temperature (K)	500	1000	2000	3000
Work function (eV)				
2	2×10^{-9}	100	4×10^7	4×10^9
3	2×10^{-19}	10^{-3}	10^5	10^8
4	2×10^{-29}	10^{-8}	400	2×10^6
5	1×10^{-39}	10^{-13}	1	4×10^4
6	1×10^{-49}	10^{-18}	4×10^{-3}	1000

magnetron current density (400 A/m^2)

Only the high temperature, low work function region (the top right hand corner) gives current densities equal to or greater than the magnetron current density. Points in this region might be expected to increase the likelihood of arcs from fig 3.24. For significant thermal emission at 1000 K, a work function of 2 eV is required and although possible (Cs:2.14 eV, Rb:2.16 eV, K:2.3 eV, or Eu:2.5 eV (ref 123)) such low work functions are not common. At 2000 K work functions up to 4 eV provide significant emission and at 3000 K up to 6 eV (ie virtually any metal) gives significant thermal emission. In reactive sputtering a lot of the debris is compound material but this is likely to have work functions higher than the metals ie 4-6 eV (ref 124).

Once initiated, evaporation from the arc spot is often seen implying molten regions of the cathode surface and therefore temperatures compatible with thermionically sustained arcs.

Mechanism 3

Haworth (ref 125) showed that an insulating film on a cathode under ion bombardment greatly reduced the potential necessary to strike an arc (34 V with the insulating film, and more than 6 kV with a metal cathode). The mechanism responsible for this was electric field emission through the insulator. Under ion bombardment the front surface of the insulator charges up until an equilibrium is reached between the ion current and the leakage current through the insulator (fig 3.26). In the magnetron this gives an electric field pattern as shown in fig 3.26 and this leads to electron emission through the insulator. Haworth found current densities in excess of 10^{10} A/m^2 generated by this process. Clark et al (ref 126) have studied the oxide layer formed on silicon during oxygen ion bombardment (2-8 KeV energy ions). The found that field strengths of 8×10^7 V/m were developed across this oxide layer under the ion bombardment responsible for its formation.

This arc formation mechanism has many features which tie in with the observed arcing of magnetrons:-

For instance Al as a target material is very prone to arcing and this is aggravated by the presence of oxygen. When sputter cleaned in Ar the arc rate falls and if oxygen is introduced the arc rate

Fig. 3·26 : Field emission of electrons due to ion bombardment

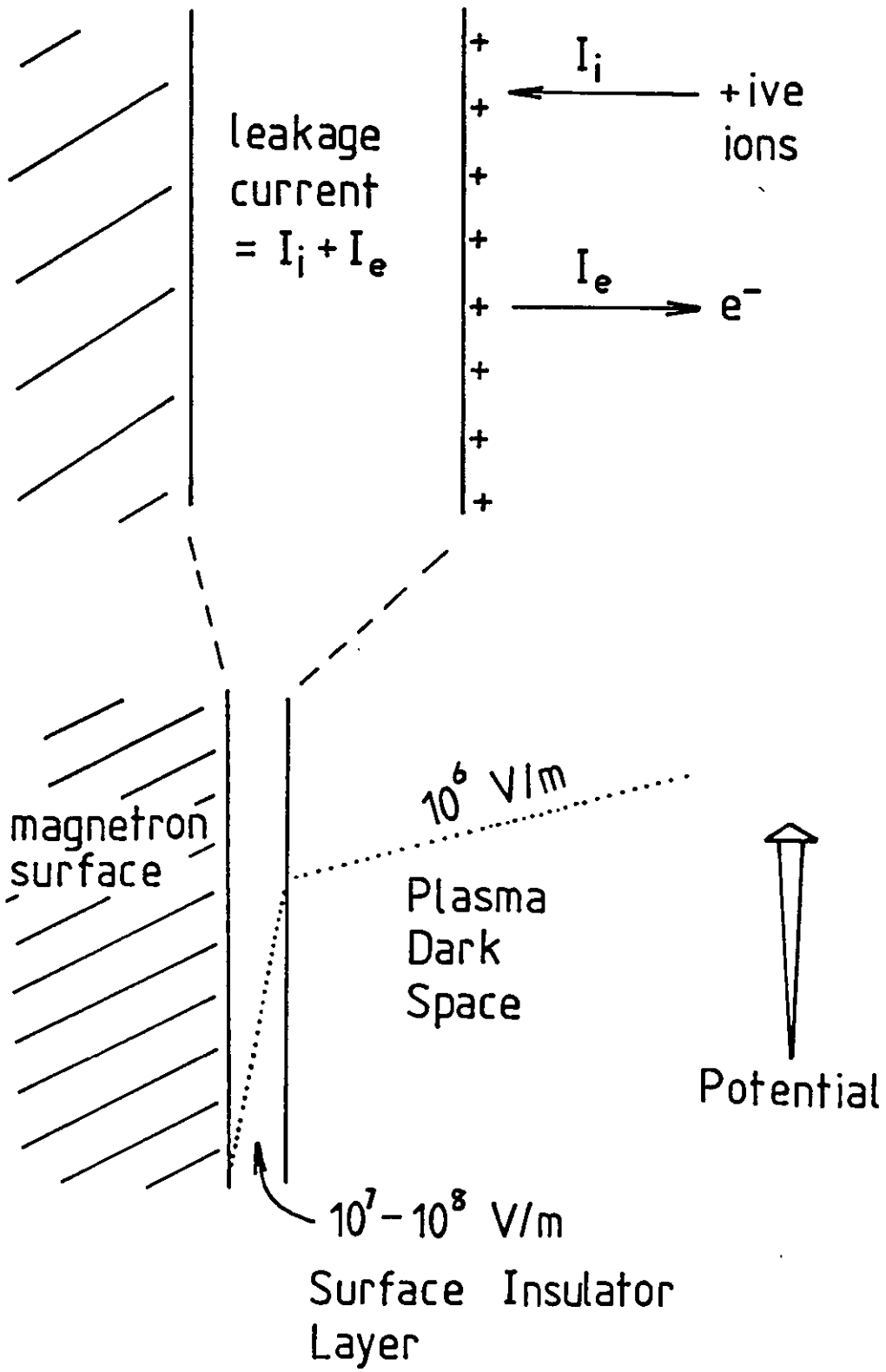

increases again. The dielectric strength of aluminium oxide is particularly high at 4-5 x 10^8 V/m (ref 124) which is consistent with its tendency to arc.

Most magnetron targets arc on operation after exposure to air due to the thermal oxides and as this oxide is sputtered off (seen as a change in magnetron potential) the arcing decreases.

The noble metals Ag, Au and Pt do not show any voltage change as they 'run in' ie no oxide formation, and they do not suffer from arcing.

As a reactively sputtered target ages the arcing gets worse and this may be associated with two effects. Firstly the reaction products build up on the target surface. They appear to increase in thickness and they certainly occupy a greater proportion of the target surface. Secondly the reaction products sputter more slowly than the metal (see section 3.3) and so a patch of oxide develops into a point with an oxide cap as the metal sputters away around the oxide (ref 127). Now not only is there a field emitter but it is on top of a spike leading to a further increase in local current density.

Summary

- Arcs are more likely at high current densities.
- Once formed the arc is likely to be sustained by thermionic emission from the hot cathode spot. This is linked to the magnetic field strength by the interaction between the field and the cathode spot movement.
- Field emission of electrons from insulating layers on the target surface is a possible mechanism for arc initiation and many of the observed features of magnetron arcing indicate that this occurs.

REFERENCES: CHAPTER 3

Section 3.1

1. Wright A. W., Am. J. Sci., 13, 49, 1877.

2. U.K. Pat. 1420061, Telic Corp., filed 4 Sept. 1972.

3. Chapin J.S., Research and Development, pp 37-40, Jan. 1974.

4. U.K. Pat. 1 453 377, Airco Inc., filed 25 Feb. 1974.

5. U.K. Pat. 1 476 079, Airco Inc., filed 8 Dec 1975.

6. U.K. Pat. 1 489 807, Airco Inc. filed 16 April 1975.

7. U.S. Pat. 4 162 954, Vac-Tec Systems, 31 July 1979.

8. U.S. Pat. 4 166 784, Applied Films Lab. Inc., 4 Sept. 1979.

9. U.S. Pat. 4 180 450, Vac-Tec Systems, 25 Dec. 1979.

10. U.S. Pat. 4 265 729, Vac-Tec Systems, 3 May 1981.

11. U.S. Pat. 4 282 083, Hirada Stechnikai Ipari Kutato Intezet, 4 Aug. 1981.

12. U.S. Pat. 4 426 264, Leybold Heraeus GmbH., 17 Jan. 1984.

13. U.S. Pat. 4 428 811/2, Borg/Warner Corp., 31 Jan. 1984.

14. U.K. Pat. 2 143 255 B, Leybold Heraeus GmbH., filed 3 Jul. 1984.

15. U.K. Pat. 2 147 916 A, Leybold Heraeus GmbH., filed 29 Aug. 1984.

16. U.K. Pat. 2 150 599 A, PPG Industries Inc., filed 29 Nov. 1984.

17. U.S. Pat. 4 525 262, Materials Research Corp., 25 Jun. 1985.

18. U.S. Pat. 4 545 882, Shatterproof Glass Corp., 1985.

19. U.S. Pat. 4 572 776, Leybold Heraeus GmbH., 25 Feb. 1986.

20. Window B. and Savvides N., J. Vac. Sci. Technol., A4, 196, 1986.

21. Oka K., "Plasma activated growth of reactively sputtered optical thin films", PhD Thesis, LUT, 1988.

22. Spencer, A.G., Oka K., Howson R.P., and Lewin R.W., Vacuum, 38, 857-859, 1988.

23. Fraser D.B., "The sputter and s-gun magnetron" in 'Thin Film Processes', Ed. Vossen J.L. and Kern W., Academic Press, New York, 1978.

24. Waits R.K., "Planar magnetron sputtering" in 'Thin Film Processes', Ed. Vossen J.L. and Kern W., Academic Press, New York, 1978.

25. Thornton J.A., "Physical Vapour Deposition", in 'Semiconductor materials and process technologies', Ed. McGuire G.E., Noyes, Park Ridge, N.J., U.S.A., 1984.

Section 3.2

26. Spencer A.G., Bishop C.A., and Howson R.P., Vacuum, 37, 3/4, pp 363-366, 1987.

27. Spencer A.G., "The Deposition and Characterization of Sputtered Ferromagnetic Thin Films", MPhil. Thesis, LUT, 1986.

28. Lamont L.T., J. Vac. Sci. Technol., 14, 1, p 122, 1977.

29. Rossnagel S.M., and Kaufmann H.R., J. Vac. Sci. Technol., A4, 1822, 1986.

30. Chapman B., "Glow Discharge Processes", Wiley, New York, 1980.

31. Schuurman W., Physica, 36, pp 136-160, 1967.

32. Kadomstev B.B., Phil. Trans. R. Soc. Lond., A 322, pp 125-131, 1987.

33. Hoyaux M.F., "Plasma Physics and its Applications", in 'Modern Physics', Ed. Webber D., Penguin, Harmondsworth, 1971.

34. Cap F.F., "Handbook on Plasma Instabilities", Academic Press, New York, 1976.

35. Buneman O., Nature, 165, 474, 1950.

36. Spencer A.G., and Howson R.P., Vacuum, 38, 497-498, 1988.

37. Thornton J.A., J. Vac. Sci. Technol., 15, 171, 1978.

38. Kirov K.I., Georgiev S.S., Ivanov N.A., and Minchev G.M., Vacuum, 28, 4, 183-186, 1978.

39. Rossnagel S.M., and Kaufmann H. R., J. Vac. Sci. Technol., A5, 88-91, 1987.

40. Bohm D., in 'The Characteristics of Elelctrical Discharges in Magnetic Fields', Ed. Guthrie A., and Wakerling, McGraw Hill, New York, 1949.

Section 3.3

41. Sigmund P., in 'Sputtering by Particle Bombardment I', Ed. R Behrisch, Topics in Appl. Phys., 47, (Springer, Berlin, Heidelberg, 1981).

42. Zalm P.C., J. Appl. Phys., 54, 5, 2660-2666, 1983.

43. Sigmund P., Phys. Rev., 184, 383, 1969.

44. Biersack J.P., and Eckstein W., Appl. Phys., A34, 73-94, 1984.

45. Benninghoven A., Redenauer F.G., and Werner H.W., "Secondary Ion Mass Spectroscopy", Wiley, New York, 1987.

46. Shimizu H., Hashizume H., Ichimura S., and Kokubun K., Jap. J. Appl. Phys., 27, 4, 1988, pp L502-505.

47. Maissel L.I., and Glang R., "Handbook of thin film technology", McGraw Hill, New York, USA, 1970.

48. Steinbruchel Ch., Appl. Phys., A36, 37-42, 1985.

49. Behrisch R., "Sputtering by Particle Bombardment II", Ed. Behrisch R., Topics in Appl. Phys., 52, (Springer, Berlin, Heidelberg, 1983).

50. Schiller S., Heisig U., Geodicke K., Thin Solid Film, 40, 327-334, 1977.

51. Eltoukhy A.H., Natarajan B.R., Greene J.E., and Barr T.L., Thin Solid Films, 69, 229-235, 1980.

52. Davies W.D., and Vanderslice T.A., Phys. Rev., 131, 1, 219-228, 1963.

53. Bunshah R.F., in 'Deposition Technologies for Films and Coatings', Noyes, Park Ridge, New Jersey, 1982.

54. Laegrid N.D., Wehner G.K., J. Appl. Phys., 32, 365, 1961.

55. Muller K.H., Appl. Phys., A40, 209-213, 1986.

56. Tennent R.M. (Ed.), "Science Data Book", Oliver and Boyd, Edinburgh, 1972.

57. Heller J., Thin Solid Films, 17, 163-176, 1973.

58. Abe T., and Yamashina T., Thin Solid Films, 30, 19-27, 1975.

59. Shinoki F., and Itoh A., J. Appl. Phys., 46, 3381-3384, 1975.

60. Hrbek J., Thin Solid Films, 42, 185-191, 1977.

61. Bomchil G., Buiguez F., Monfret A., and Galzin S., Thin Solid Films, 47, 235-240, 1977.

62. Schiller S., Heisig U., Goedicke K., Schade K., Teschner G., and Henneberger J., Thin Solid Films, 64, 455-467, 1979.

63. Natarajan B.R., Elthoukhy A.H., Greene J.E., and Barr T.L., Thin Solid Films, 69, 201-216, 1980.

64. Natarajan B.R., Elthoukhy A.H., Greene J.E., and Barr T.L., Thin Solid Films, 69, 217-227, 1980.

65. Elthoukhy A.H., Natarajan B.R., Greene J.E., and Barr T.L., Thin Solid Films, 69, 229-235, 1980.

66. Maniv S., and Westwood W.D., J. Vac. Sci. Technol., 17, 3, 743-751, 1980.

67. Aronson A.J., Chen D., and Class W.H., Thin Solid Films, 72, 535-540, 1980.

68. Maniv S., Miner C., and Westwood W.D., J. Vac. Sci. Technol., 18, 2, 195-198, 1981.

69. Steenbeck K., Steinbeiss E., and Ufert K.D., Thin Solid Films, 92, 371-380, 1982.

70. Howson R.P., Suzuki K., Bishop C.A., and Ridge M.I., Vacuum, 34, 291-294, 1984.

71. Schiller S., Beister G., Sieber W., Thin Solid Films, 111, 259, 1984.

72. Lemperiere G., and Poitevin J.M., Thin Solid Films, 111, 339-349, 1984.

73. Schiller S., Heisig U., Beister G., Steinfelder K., Strumpfel J., Kornforfer Chr., and Sieber W., Thin Solid Films, 118, 255-270, 1984.

74. Hohnke D.K., Schmatz D.J., and Hurley M.D., Thin Sold Films, 118, 301-310, 1984.

75. Poitevin J.M., and Lemperiere G., Thin Solid Films, 120, 223-230, 1984.

76. Blom H-O., Berg S., and Larsson T., Thin Solid Films, 130, 307-313, 1985.

77. Berg S., Larsson T., and Blom H-O., J. Vac. Sci. Technol., A4, 3, 594-597, 1986.

78. Kadlec S., Musil J., and Vyskocil H., J. Phys. D: Appl. Phys., 19, L187-190, 1986.

79. Penfold A.S., American Society of Vacuum Coaters' Annu. Tech. Conf. Proc., New Orleans, LA, 381-403, 1986.

80. Berg S., Blom H-O., Larsson T., and Nender C., J. Vac. Sci. Technol., A5, 2, 202-207, 1987.

81. Denvac J., Aubert A., and Gillet R., Proc. Int. Symp. on Trends and New Applications in Thin Films., Strasbourg, Vol. 2, 347-353, 1987.

82. Spencer A.G., "Pressure stability in reactive sputtering", presented at Sputter Deposition Meeting, London, Feb. 1987.

83. Wright M., and Beardow T., J. Vac. Sci. Technol., A4(3), 388-392, 1986.

Section3.4

84. Carpenter L.G., "Vacuum Technology", Adam Hilger, Bristol, 1983.

85. Boenig H.V., "Fundamentals of plasma chenistry and technology", Technomic, Lancaster, U.S.A., 1987.

86. Bardos L., Vacuum, 38, 637-642, 1988.

87. Thornton J., "Plasmas in Depostion Processes", in 'Deposition Technologies for Films and Coatings', Ed. Bunshah R.F., Noyes, Park Ridge, NJ., 1982.

Section 3.5

88. Vook R.W., Opt. Eng., 23, 3, 343-348, 1984.

89. Thornton J.A., J. Vac. Sci. Technol., A4, 6, 3059-3065, 1986.

90. Martin P.J., McKenzie D.R., Netterfield R.P., Swift P., Filipczuk S.W., Muller K. H., Pacey C.G., and James B., Thin Solid Films, 153, 91-102, 1987.

91. Bunshah R.F., Thin Solid Films, 107, 21-38, 1983.

92. Maniv S., Miner C., and Westwood W.D., J. Vac. Sci. Technol., A1, 3, 1370-1375, 1983.

93. Rossnagel S.M., and Cuomo J.J., Vacuum, 38, 2, 73-81, 1981.

94. Pulker H.K., "Coatings on glass", Elsevier, Amersterdam, 1985.

95. Matthews A., and Teer D.G., Thin Solid Films, 72, 541-549, 1980.

96. Tiedje T., Moustakas T.D., and Cebulka J.M., Phys. Rev., B23, 10, 5634-5637, 1981.

97. Schiller S., Beister G., Sieber W., Schirmer G., and Hacker E., Thin Solid Films, 83, 239-245, 1981.

98. Bishop C.A., Edge G., Sutherland I., and Howson R.P., Vacuum, 37, 279-282, 1987.

99. Coburn J.W., "Plasma etching and reactive ion etching", Am. Inst. of Phys., New York, U.S.A., 1982.

100. Coburn J.W., and Winters H.F., J. Appl. Phys., 50, 3189, 1979.

101. Tu Y.Y., Chuang T.J., and Winters H.F., Phys. Rev., B23, 823, 1981.

102. Gerlach-Meyer B. Coburn J.W., and Kay E., Surf. Sci., 103, 177, 1981.

Section 3.6

103. Greene J.E., J. Vac. Sci, Technol., 15, 5, 1718-1729, 1978.

104. Enjouji K., Murata K., and Nishikawa S., Thin Sloid Films, 108, 1-7, 1983.

105. Smith E.V.P., and Jacobs K.C., "Introductory Astronomy and Astophysics", Saunders, Philadelphia, 1973.

106. Schiller S., Heisig U., Steinfelder K., Strumpfel J., Voigt R., Fendler R., and Teschner G., Thin Solid Films, 96, 235-240, 1982.

107. Greene J.E., and Sequeda-Osorio F., J. Vac. Sci. Technol., 10, 6, 1144-1149, 1973.

108. Salmenoja K., and Korhonen A.S., Vacuum 36, 1-3, 33-35, 1986.

109. Schiller S., Heisig U., Steinfelder K., Strumpfel J., Freidrich A., and Fricke R., Proc. Int. Conf. on Ion and Plating and Allied Techniques, Brighton, 1987, CEP Consultants, Edinburgh, 23-31, 1987.

110. Ratinen H., Appl. Phys. Lett., 21, 10, 473-476, 1972.

Section 3.7

111. Tabor D., "Gases, liquids and solids", CUP, Cambridge, 1979.

112. Carpenter L.G., "Vacuum Technology", Adam Hilger, Bristol, 1983.

113. Jananda S., "High Vacua", Van Nostrand, New York, 1947.

114. Kaye G.W.C., and Laby T.H., "Tables of physical and chemical constants", Longman, New York, 1985.

115. DeMuth S.F., and Watson J.S., J. Vac. Sci. Technol., A4 (3), 344-347, 1986.

116. Hablanian M.H., J. Vac. Sci. Technol., A4 (3), 286-292, 1986.

Section 3.8

117. Vyskocil J., Musil J., and Kadlec S., "Comparison of reactive magnetron sputtering and reactive arc evaporation deposition techniques", Research report, Dept. of gas discharges, Czechoslovak Academy of Sciences, Institute of Physics, Prague, 1987.

118. Grove T.C., "Arcing problems encountered during sputter depostion of Aluminium", Advanced Energy Application notes, Advanced Energy, Fort Collins, Co, U.S.A., 1986.

119. Meek J.M., Phys. Rev., 57, 722-730, 1940.

120. Fletcher R.C., Phys. Rev., 76, 1501-1511, 1945.

121. Brown S.C., "Basic data of plasma physics", M.I.T. press, Camb. Ma., U.S.A., 1959.

122. Ohtsuka H., Vacuum, 33, 3, pp 155-157, 1983.

123. "Handbook of Physics and Chemistry", CRC press, Boca Raton, Florida, U.S.A., E79-E80, 1981.

124. Harrop P.J., "Dielectrics", Butterworths, London, U.K., 1972.

125. Haworth F.E., Phys. Rev., 80, 223, 1950.

126. Clark E.A., Dowsett M.G., Augustus P.D., Spiller G.D., Thomas G.R., and Sutherland I., Vacuum, 38, 937-941, 1988.

127. Smith H.I., Proc. IEEE, 62, 1361, 1974.

128. Cobine J.D., and Gallagher C.J., Phys. Rev., 74, 1524, 1948.

4. MEASUREMENT TECHNIQUES

Full characterisation of thin films requires many measurements of their properties. More specifically it is useful to know any or all of the following:- composition, density, microstructure, magnetic, electrical and optical properties. The importance of these will obviously change depending on the application. The properties of the films used in this thesis are extensively studied in other works (refs 1-3). This work concentrates on reactive sputter deposition as a process and the film properties are only measured to confirm that they are consistent with prior work or to provide information about the deposition process.

Surface analysis techniques and various methods for determining film structure are given in references 1-4. Below are given measurement techniques of direct use in studying the deposition process.

4.1 ELLIPSOMETRY

Ellipsometry can be used for transparent and absorbing films (but not opaque) to give the thickness (d) in all cases and to give the film refractive index (n) (ref 5). The apparatus used was a Gaertner L117 ellipsometer. A schematic diagram of this is shown in fig 4.1. There are many ways (of varying complexity) to use this apparatus to provide d and n. For the results given in this work we simply determined the polarizer and analyzer angles (P_1, A_1 and P_2, A_2) which gave minimum detected light levels. There are two minima required, the first is found in the range $0<A_1<90^0$ and $0<P_1<140^0$ and the second is approximately at $A_2 = 180^0-A_1$ and $P_2 = 90^0+P_1$. Having found these values the quantities ψ and Δ are calculated. ψ is the angle between the polarization plane and the plane of incidence and is given by (ref 6)

$$\psi = \frac{180 - (A_2 - A_1)}{2}$$

Δ is the phase change on reflection from the film/surface and is given by

Fig. 4·1 : A schematic of the ellipsometer.

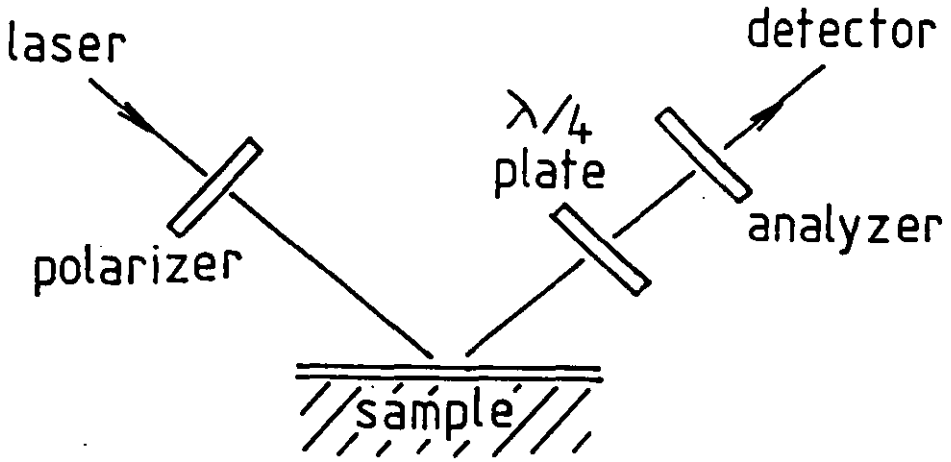

Fig. 4·2 : Δ and ψ for films of varying refractive index (n) and thickness (d) on silicon (ref. 7).

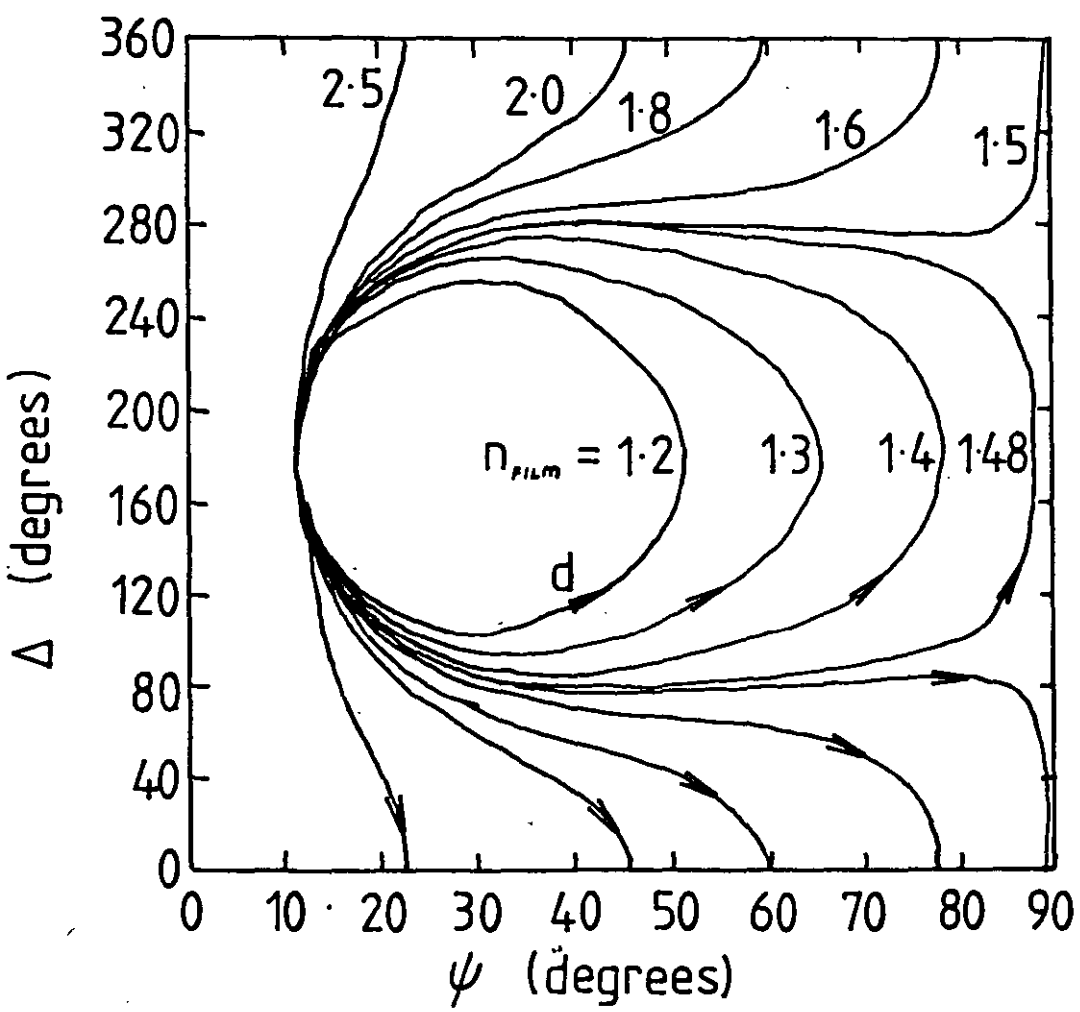

$$\Delta = 360 - (P_1 + P_2)$$

ψ and Δ are related to n and d as shown in fig 4.2 (ref 7). The main feature of this is that the dependence on d is periodic so that the solution is of the form $d = d_1 + k \times \text{period}$, where k is any positive integer. To obtain a unique value for d a second measurement is required and this can be obtained from optical or stylus measurements (refs 8 and 9).

4.2 PRESSURE MEASUREMENT

The measurement of total and partial pressure in reactive sputtering is of great importance as this is one of the primary factors in governing the process. The measurement requirements are high resolution, high long term stability and often a fast time response. Obviously the first two requirements conflict with the last, and in practice two separate gauges may be required. The types of pressure gauge available for the range 0.1 to 1 Pa are thermal conductance (pirani), capacitance, emission or mass spectrometer, and ion gauges (refs 10, 11).

Of these the capacitance manometer provides the best standard and shows no gas selectivity. The models currently available do show significant zero drift over timescales of around an hour. In this work the capacitance manometer available (a Baratron 220BHS-3AL-B-1) was therefore used only as a transfer standard for calibrating other gauges. The newest temperature controlled capacitance manometers have (according to manufacturer's claims) sufficient accuracy and stability for reactive sputtering monitoring and control.

An ion gauge shows excellent time response but when used with reactive gases the attack of the filament leads to a long term drift and a relatively short filament lifetime. The sensitivity for different gases also varies significantly. Ion gauges were therefore not used.

Mass spectrometers provide useful diagnostic information but will not operate at higher pressures due to scattering within the

analyzer. They therefore require separate pumping and a linkage to the process chamber. This linkage complicates analysis of the results as does the use of a separate pump. The sensitivity for various gases can vary a lot due to the selectivity of the ionization process, the variation of conductance to the chamber and the pumping rate for different gases.

The main pressure measurement was therefore made by a computer interfaced pirani gauge (CVC GP-310). The time response of the gauge is poor (time constant 5 seconds) due to the thermal mass of the filament used. The long term stability is however good. The resolution of the gauge was improved by taking 125 measurements over approximately 20 seconds. The standard deviation of these measurements was better than 2×10^{-4} Pa giving a very high resolution. The drift over a coating run (typically 1-2 hours) was within this error.

4.3 SHEET RESISTANCE

For a thin flat sheet of conducting material bounded by insulators the electrical resistance is most easily measured as the sheet resistance. This quantity is size independent. The sheet resistance R_s is measured in Ω/square and can be read directly from a four point probe measurement (fig 4.3) (ref 12). This is related to the film resistivity (p) and thickness (d) as

$$p = R_s.d$$

A four point probe with equal probe spacings S where S>>d and S<<sample size, gives a reading of R_s as

$$R_s = \frac{V.\pi}{I.Ln(2)}$$

Our four point probe was connected to a Schlumberger 7055 or 7066 giving an accuracy in V/I of 0.003%. A larger error than this will arise from the fact that our probe spacings S are not equal. In practice a random error of +/- 10 occurred. Comparison with the Everest four point probe suggests a systematic error of around 5%.

Fig. 4·3 : Four point measurement of sheet resistance.

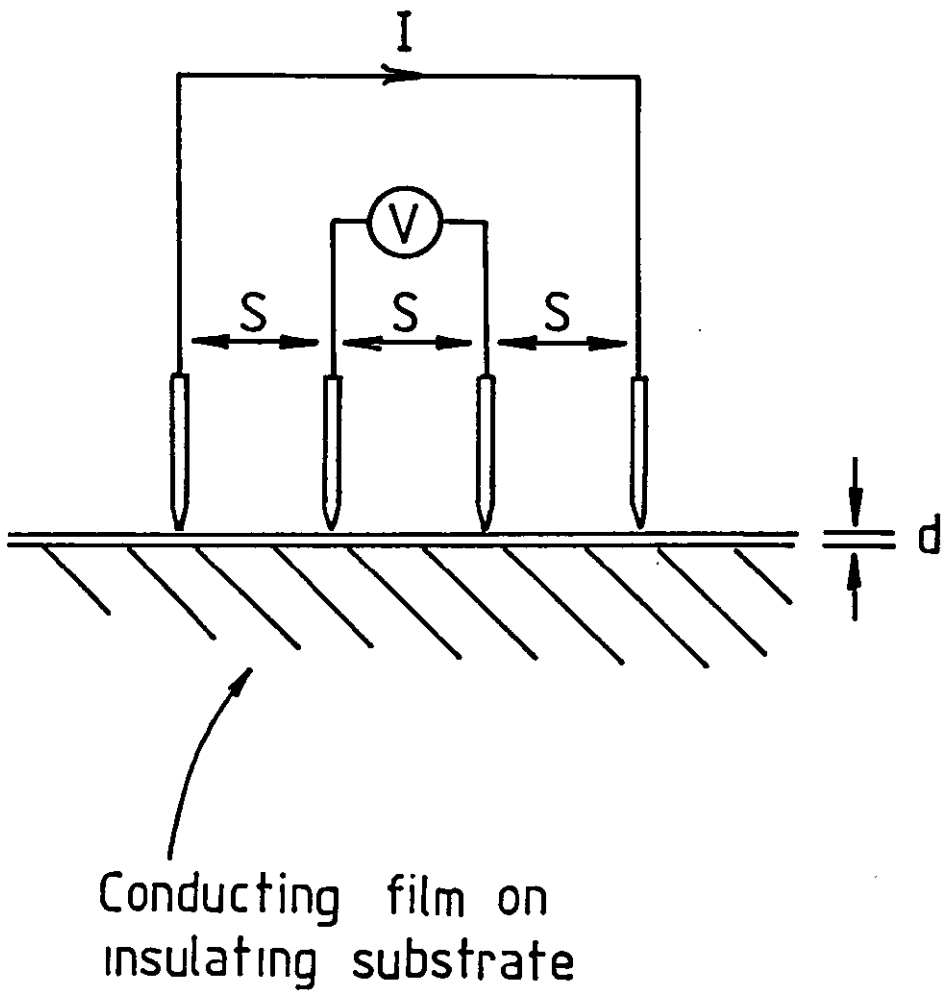

Summary

- Measurements of the film refractive index and thickness were made by ellipsometry combined with stylus or optical transmittance measurements.
- The total and partial pressures in the reactive sputtering chamber were measured by a computer interfaced Pirani gauge. This gave a resolution and medium term (1 hour) stability better than 2×10^{-4} Pa (1×10^{-6} Torr).
- The sheet resistance was measured by a four point probe. This gave a random error of +/- 10% and a systematic error of +/- 5%.

REFERENCES: CHAPTER 4

1. Ridge M.I., PhD Thesis, LUT, 1984.

2. Bishop C.A., "The deposition of coatings onto polymer substrates by planar magnetron sputtering", PhD Thesis, LUT, 1986.

3. Oka, K., "Plasma activated growth of reactively sputtered optical thin films", PhD Thesis, LUT, 1988.

4. Spencer A.G., "The deposition and characterisation of sputtered ferromagnetic thin films", M.Phil. Thesis, LUT, 1986.

5. Heavens O.S., "Optical properties of thin solid films", Dover, New York, 1965.

6. Gaertner L117 Ellipsometer manual, 1977.

7. Archer R.J., J. Opt. Soc. Am., 52, 970-977, 1962.

8. Manifacier J.C., Gasiot J., and Fillard J.P., J. Phys. (E), 9, 1002-1004, 1976.

9. Piegari A., and Masetti E., Thin Solid Films, 124, 249-257, 1962.

10. Redhead P.A., J. Vac. Sci. Technol., A2(2), 132-138, 1984.

11. Hmiel A.F., J. Vac. Sci. Technol., A3(3), 592-595, 1985.

12. Valdes L.B., Proc. I.R.E., 420-427, 1954.

5. DEPOSITION EQUIPMENT

5.1 ROLL COATER

The roll coater used for my initial experiments is that of reference 1 modified to also coat small solid substrates. The coating zone is shown in fig 5.1a. The sheet resistance and film transmission are monitored in situ shortly after the coating zone so that the deposition conditions can be optimized in one coating run. Once optimum conditions have been established the rigid substrate can be coated by opening the shutter. The deposition pressure was monitored by a pirani gauge situated directly below the coating zone and computer interfaced as discussed in section 4.2.

5.2 BATCH COATER

The batch coater used in this work was constructed to coat A4 sized glass substrates with indium oxide and to act as a test bed for ideas suitable for the Everest coater. The design of the batch coater is based on results obtained from the roll coater and is therefore discussed (chapter 8) after these results have been presented (chapters 6 and 7).

The design parameters and requirements we have are summarized in table 5.1.

Fig. 5·1a : The roll coater layout.

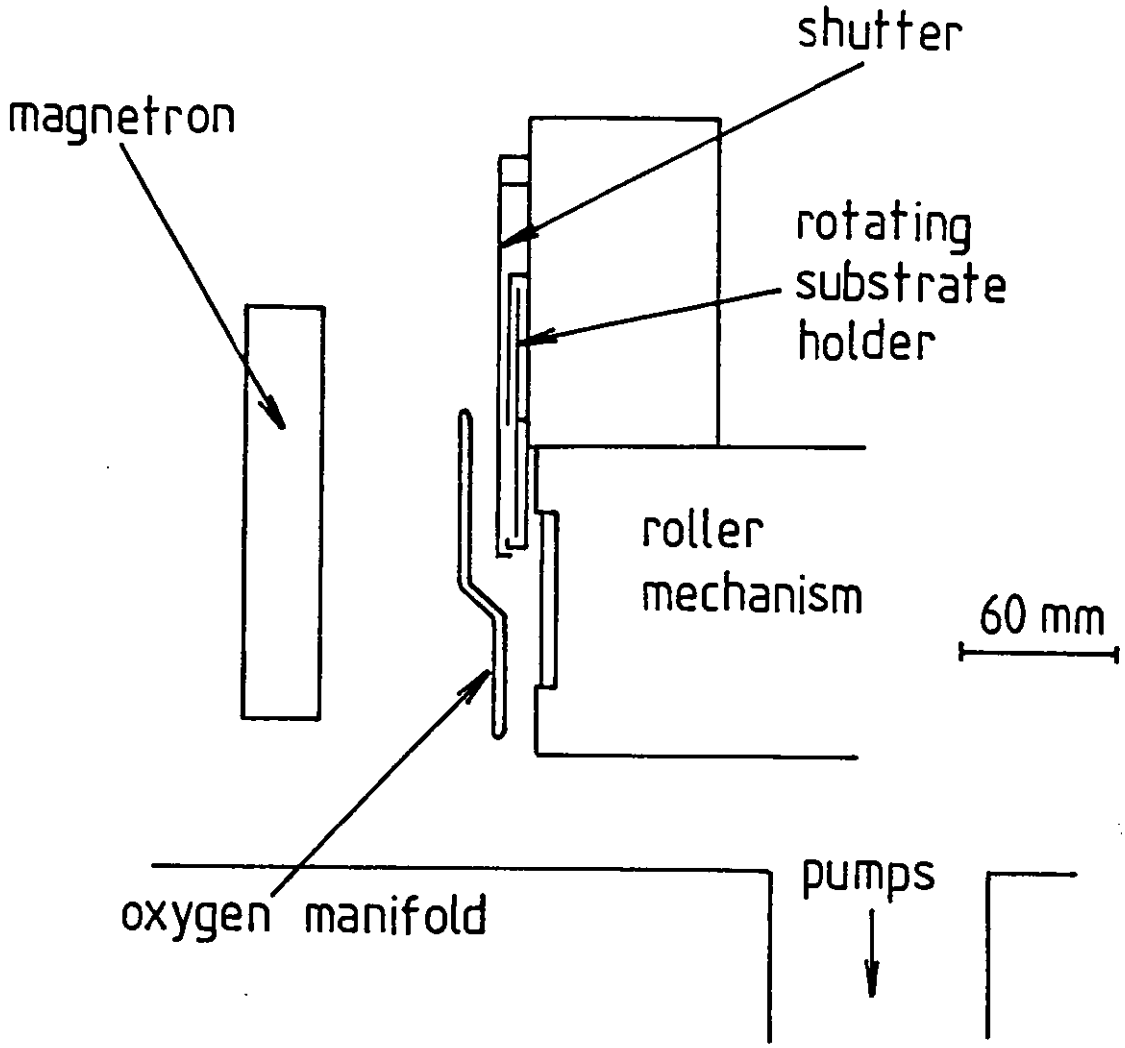

Fig. 5·1b : The magnetron cross section.

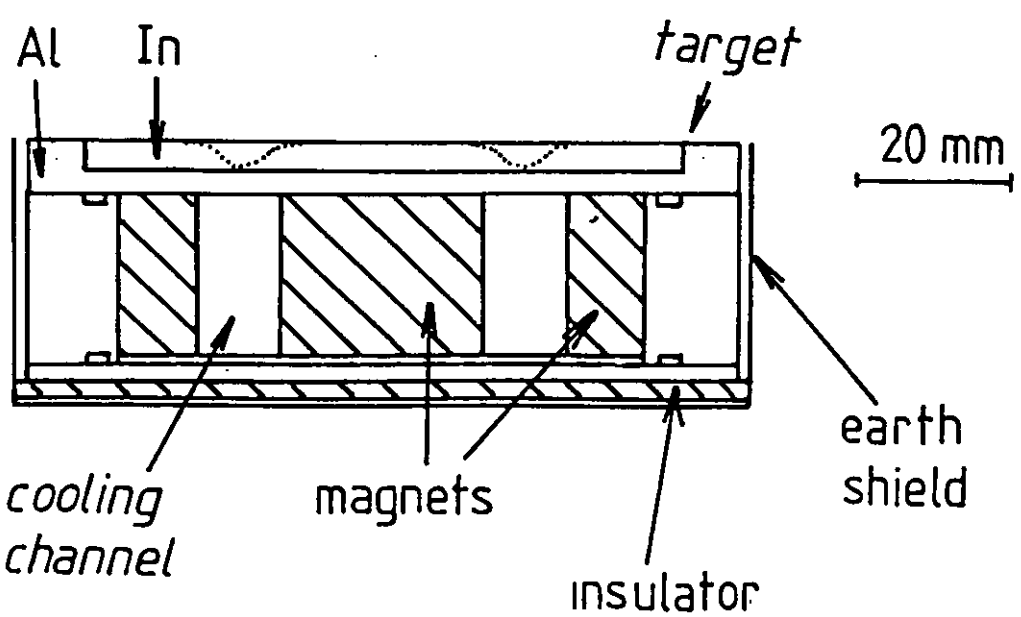

Table 5.1: System Design Parameters and Requirements

Design Parameters	System Requirements
Target thickness	Production Rate
Magnetic Field Distribution	Uniformity
	Pressure Stability
Pumping Surfaces	
	Plasma Bombardment
Target Substrate Distance	No Effect of Substrate Movement on Pumping Rate
Control Mechanisms	
Pump Size and Position	
Gas Admission	
Anode Position	
Substrate Position	

Each of the system requirements may depend on more than one of the design parameters. These dependencies are usually not rigorously specified. A total system design is then done by a combination of experiment, experience and trial and error. Taking the system requirements one by one we can discuss their dependence on the design parameters.

Target lifetime. To maximize the up-time of a coater we must minimize the maintenance and replacement work required. One factor in this is the lifetime of the magnetron target. In line with the Leybold cathodes fitted to the Everest machine a target lifetime of at least 300 hours would be desirable. Our small cathode (fig 5.1b) with a thin target and a highly localized plasma only has a target lifetime of 12 hours. To increase this we must increase the target thickness and widen the erosion profile ie flatten the magnetic field distribution.

Production rate. I have used the term production rate as we are interested in the velocity at which we can move the substrate past the magnetron and obtain a specific thickness of coating. This is determined by the product of deposition rate and coating zone width. The amount of sputtered material will depend on the magnetron power. In reactive sputtering we also have to consider the effects of target poisoning as this can reduce the sputter yield by an order of magnitude. If we use a wide erosion zone (determined by the magnetic field distribution - see section 3.2) and a lower power density this is likely to result in more target poisoning. At large target substrate distances our compound film is formed at lower reactive gas pressures and so less target poisoning occurs. However at large target substrate distances our uniformity is reduced, more material is lost to intermediate surfaces and also the reactive gas utilization goes down.

Uniformity. The film properties should be uniform over the deposition zone both across and along the transport direction. To achieve this we must make all the parameters critical to the film formation uniform. In practice this comes down to a uniform metal arrival rate, a uniform reactive gas pressure and a uniform utilization. The target substrate distance mainly controls the uniformity normal to the linear portions of the racetrack. This is easy to estimate as the sputter flux at an angle θ to a surface varies and as $\sin(\theta)$ (ref 2). At low pressures (1 mTorr, mfp = 100 mm) and smaller target substrate distances (100 mm) gas scattering can be ignored (ref 3). Adding the contributions from each racetrack then gives the thickness profiles at various target substrate distances (fig 5.2). This shows that for maximum uniformity we should design our system with a target/substrate spacing of around 1.4 s (racetrack separation is 2 s). However, Schiller et al (ref 4) (see section 3.3) recommend a larger target/substrate distance as this allows film formation at a lower reactive gas pressure and so gives less target poisoning.

Plasma bombardment. Ion or plasma bombardment has been shown by several authors to alter surface reactions (see section 3.5). To test for this effect in reactive sputtering it would then be useful if we could control plasma bombardment of our substrates. This was achieved by using a wide unbalanced magnetron (ref 5) and the plasma controlled in situ by the use of an anode (ref 6).

Fig. 5·2 : Calculated film thickness distributions for various target/substrate distances.

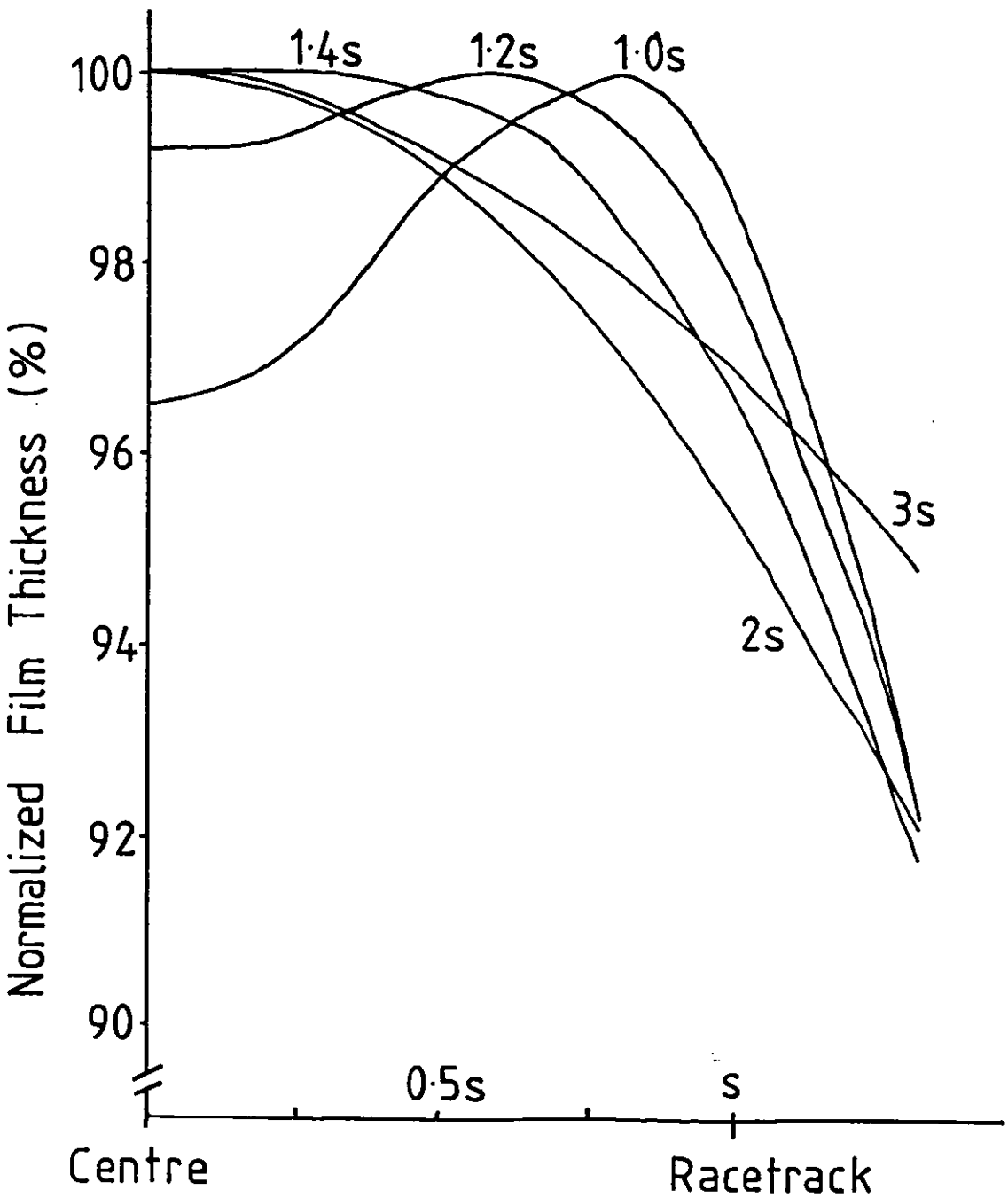

Effect of substrate movement on pumping rate. At its simplest this just means making sure that the substrate does not obstruct the pumping orifice. Also we show later that the surfaces within the vacuum that receive coating flux act as getter pumping surfaces. In high deposition rate systems this means that when absent the substrate should be replaced by a surface in the same position to avoid a change in the reactive gas consumption.

My deposition apparatus is shown in plan view in fig 5.3. Within the constraints of an available 0.5 m bell jar and an A4 substrate size this tries to meet the requirements above. The pump is a 200 mm oil diffusion pump and the pumping speed for oxygen in the chamber is 290 l/s (from measured pressure and input massflow). When absent the substrate is replaced by a metal shield. Louvred pumping surfaces are also used to bring the system closer to stability.

The magnetron used is shown in figs 5.4 and 5.5. This uses magnetic poles infront of the target to give a wide erosion (see section 3.2) and removable bar magnets to give a controllable magnetic field. This later feature allows the plasma bombardment of the substrate.

5.3 EVEREST PRODUCTION COATER

The Everest coater is used for large scale production (10^6 m^2/year) of a dielectric/metal/dielectric heat mirror onto 2.5 m by 3 m glass substrates. The metal used is silver with tin oxide dielectric layers on both sides to anti-reflect it in the visible region of the spectrum. An Al barrier/sacrificial layer is used to protect the Ag in the oxygen rich plasma of the last tin oxide stage. The coater is of modular design with a load lock at both ends. It comprises (in coating order): entrance load lock, glow discharge clean, tin oxide module, metal layer module, tin oxide module and exit load lock.

The main area of interest when considering the production of a semiconductor heat mirror (such as indium oxide or indium/tin oxide) is obviously the tin oxide module as these are already producing a similar material. A tin oxide deposition chamber is shown in fig 5.6 along with its associated pumping chamber. The magnetron target is 2.9 m long with a racetrack 2.7 m long. The magnetic trap design uses a

Fig. 5·3 : A plan view of the A4 batch coater.

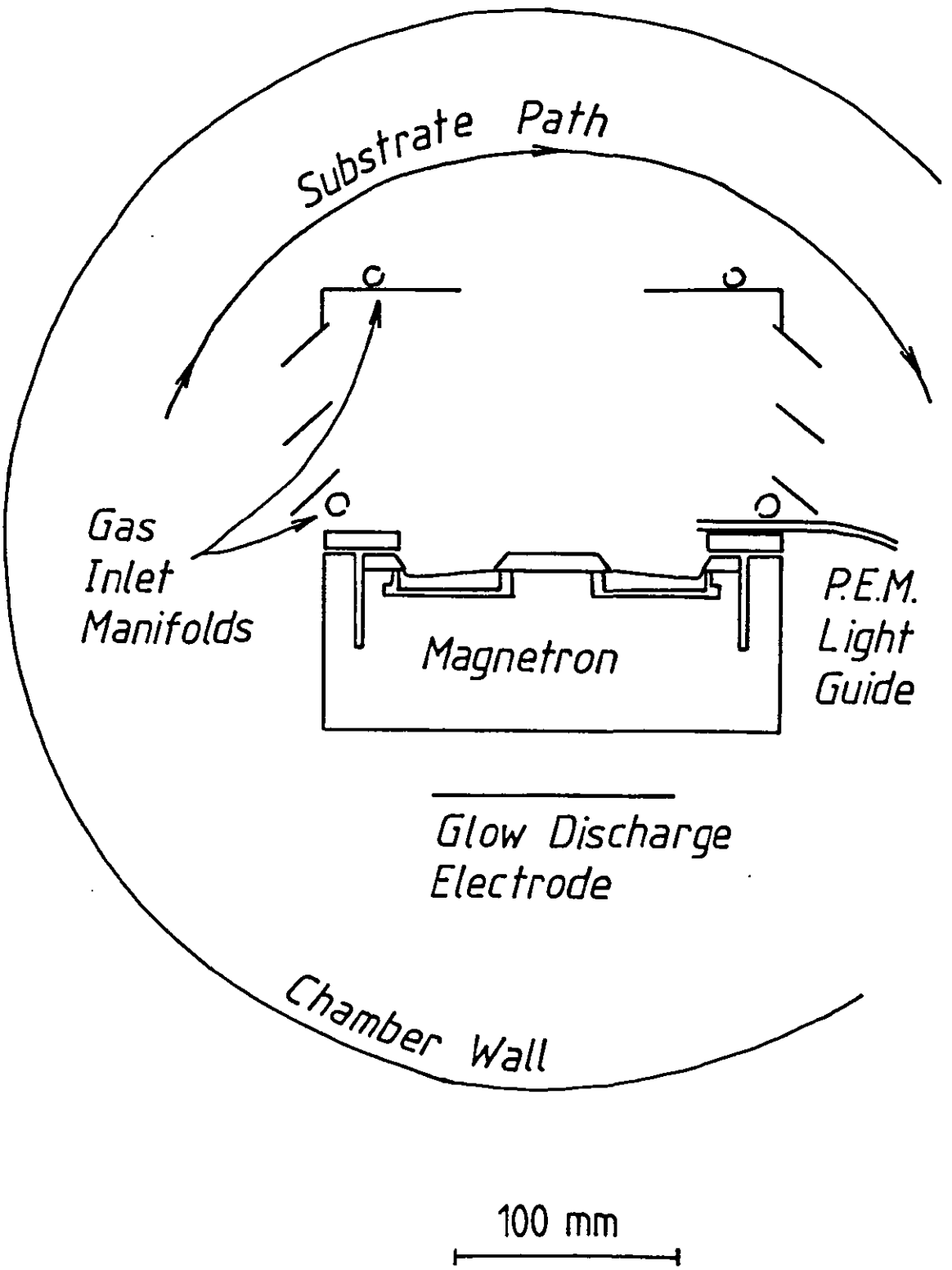

Fig. 5·4 : A cross section of the A4 magnetron.

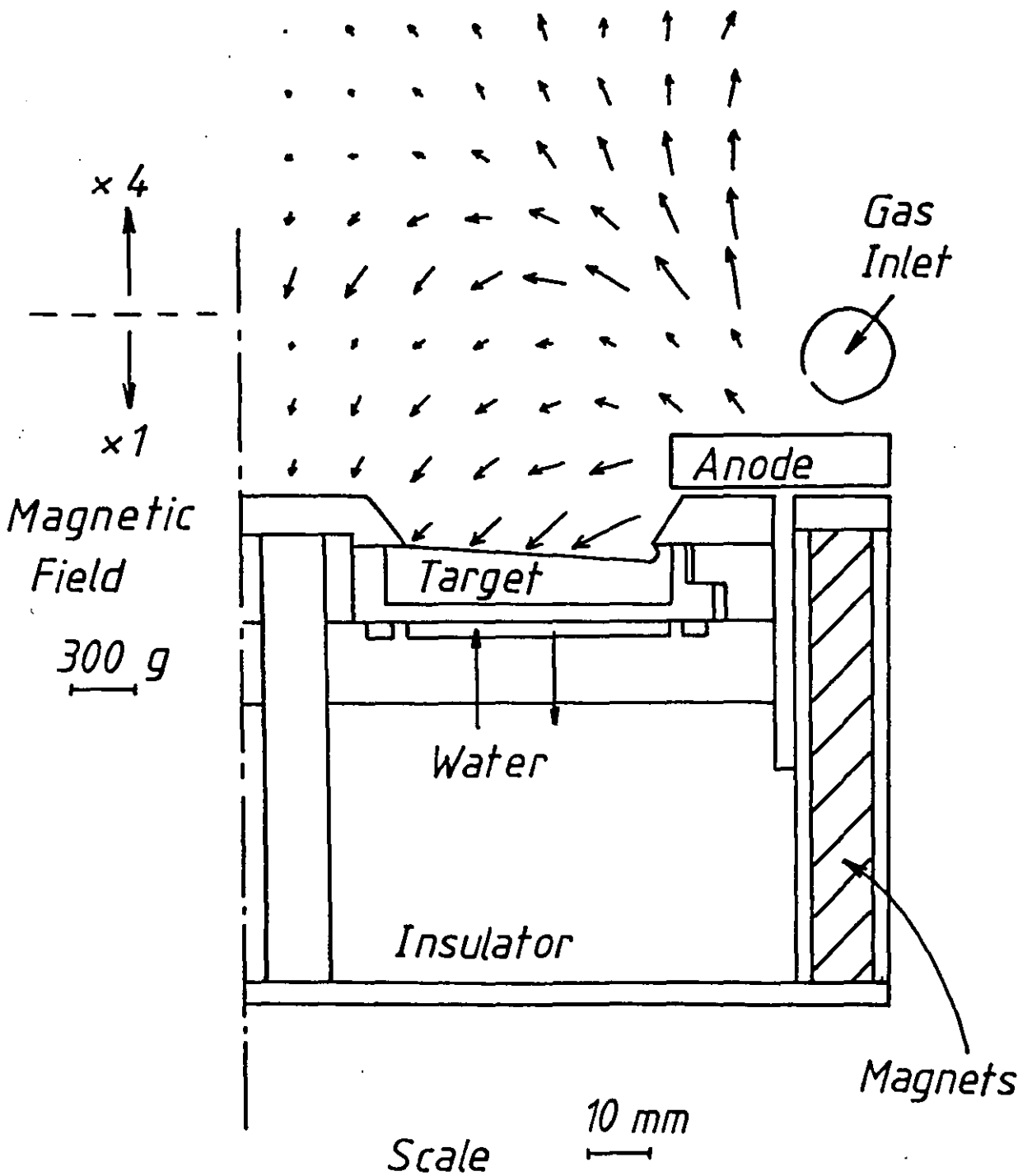

Fig. 5·5 : Detail of the 0·5 m magnetron showing removable magnets and poles and anode affixed.

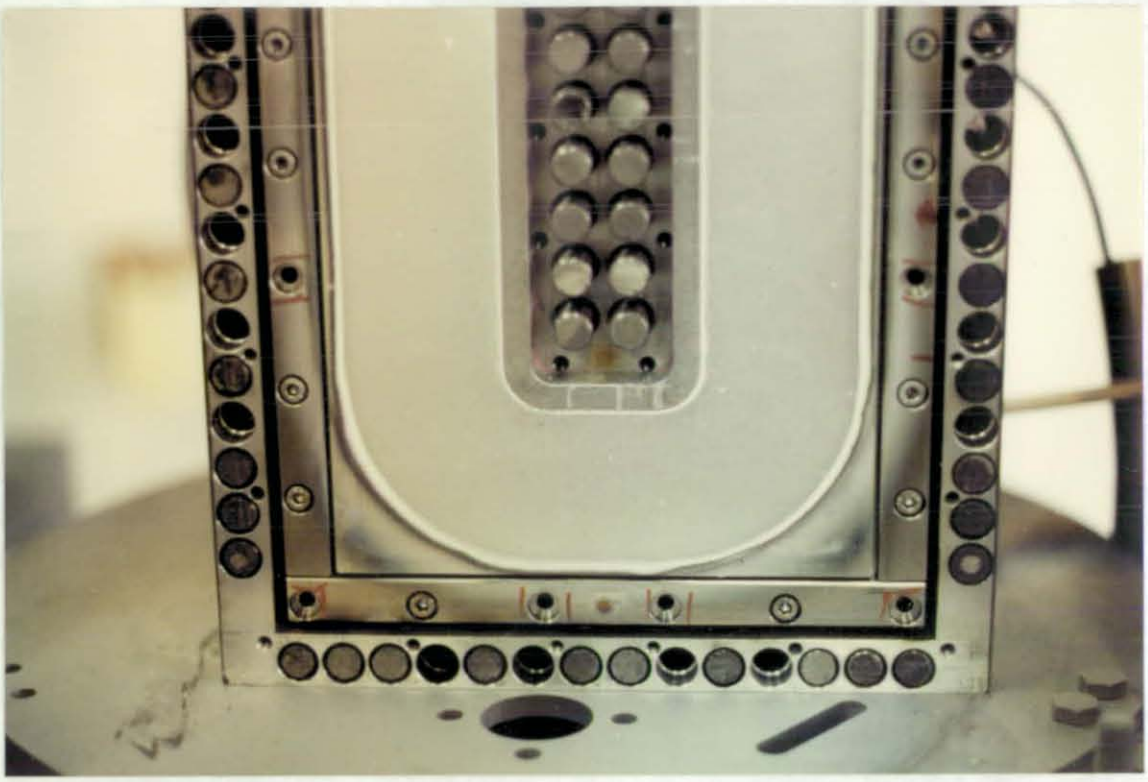

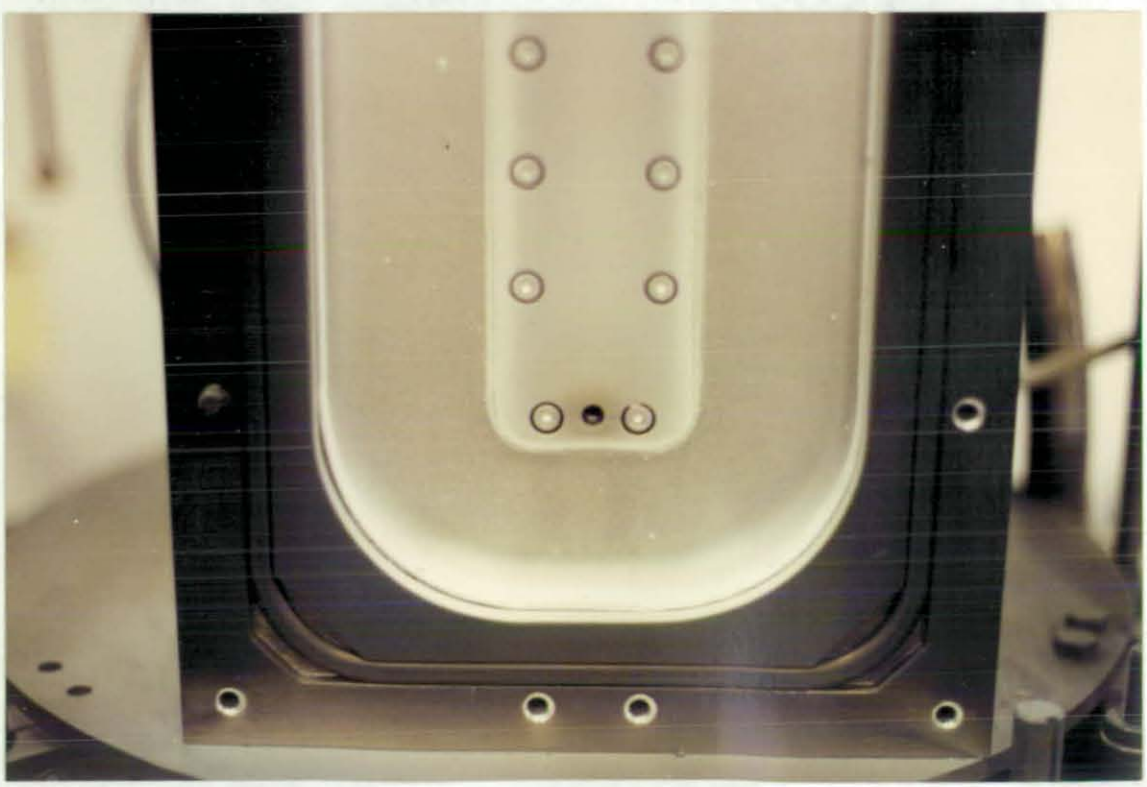

Fig. 5·6 : A cross section of the Everest coating geometry.

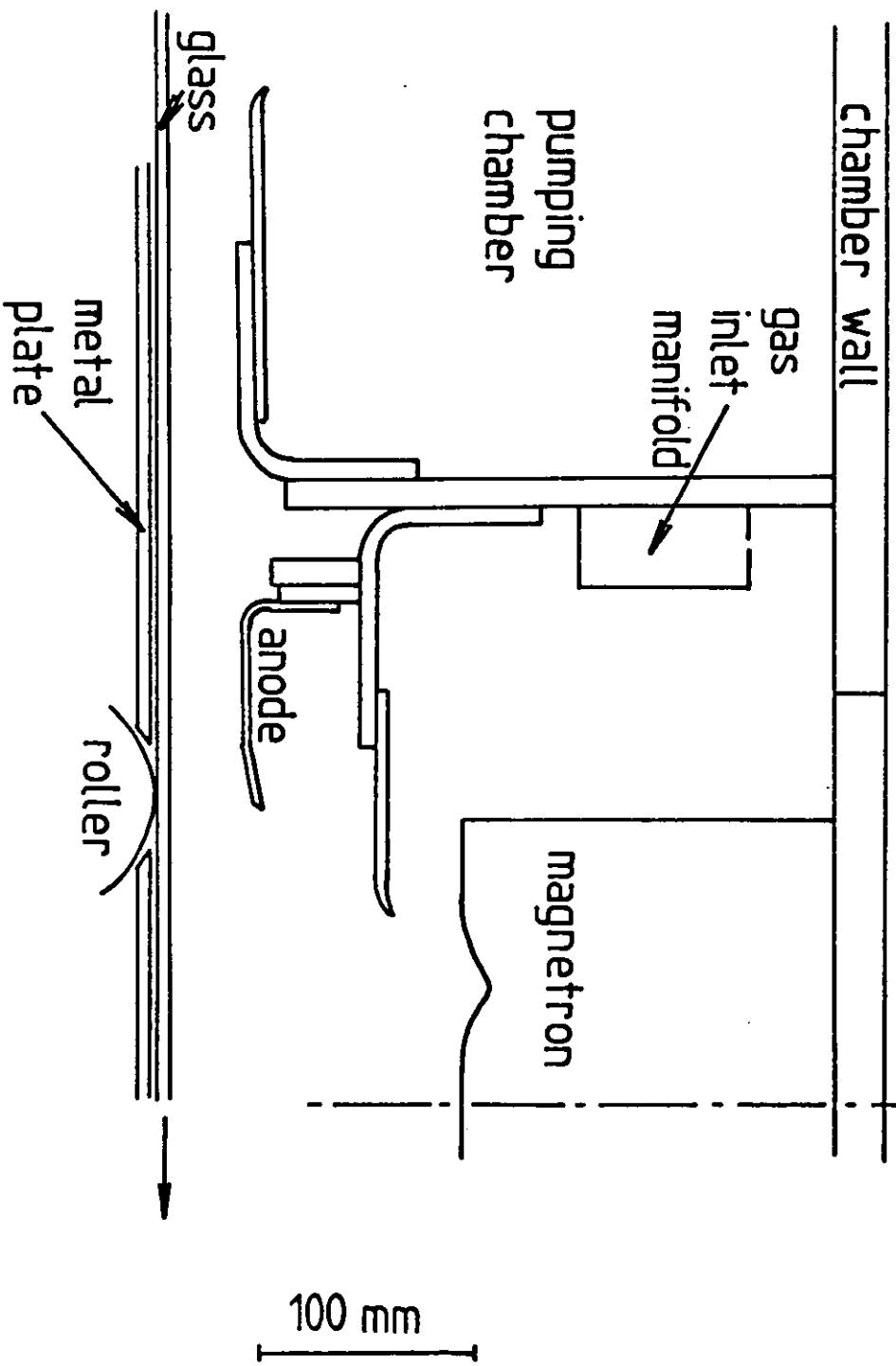

simple domed magnetic field and so results in the roughly triangular erosion profile shown. The peak current density on the target is around 10 W/cm^2 (this varies by +/- 20% as the target ages). The deposition rate averaged across the deposition zone is 1.8 nm/s ie reasonably low.

An input argon gas flow of 193 sccm (322 Pa.l/s) gives a chamber pressure of 4.8×10^{-3} mBar (0.48 Pa) ie the chamber pumping rate is 670 l/s for Ar. The measured pressure in the adjacent pumping chamber gives a pumping speed here of 1400 l/s. The conductance of the slot lock linking the sputter chamber and pumping chamber is then about 1400 l/s. This is much smaller than the front to back conductance of the pumping chamber and so it is likely that the pumping rate within the sputter chamber is fairly uniform. This cannot at present be confirmed as the properties of the coating are not highly pressure dependent and the necessary instrumentation is not present. The standard gas inlet manifold is shown in cross section in fig 5.6. These manifolds are 77 mm x 37 mm x 3010 mm and have 50 holes per manifold each of 1 to 1.5 mm diameter.

Summary

- Initial experiments were performed on a roll coater with a static substrate attachment.
- A batch coater was designed to coat A4 size rigid substrates and to act as a test bed for the Everest coater. The design requirements of this batch coater were long target lifetime, high production rate (neglecting pump out time), high uniformity, the ability to plasma bombard the substrate and no effect of substrate movement on the pumping rate.
- The Everest coater is a large flat glass coater of modular design, the magnetrons are 2.7 m wide coating 2.5 m wide substrates. The deposition chamber is pumped from an adjacent chamber through a slot (670 l/s for Ar). The glass substrates enter the deposition chamber through this slot and so change the pumping rate.

REFERENCES: CHAPTER 5

1. Bishop C.A., "The deposition of coatings onto polymer substrates by planar magnetron sputtering", PhD Thesis, LUT, 1986.

2. Waits R.K., "Planar magnetron sputtering", in 'Thin Film Processes' (Ed. Vossen J.L. and Kern W.), p 125, Academic Press, New York, 1978.

3. Swann S., Vacuum, 38, 791-794, 1988.

4. Schiller S., Biester G. and Sieber W., Thin Solid Films, 111, 259, 1984.

5. Windows B. and Savvides N., J. Vac. Sci. Technol., A4, 196, 1986.

6. Fraser D.B., in 'Thin Film Processes' (Ed. Vossen J.L. and Kern W.), p 125, Academic Press, New York, 1978.

6. RESULTS - SMALL SUBSTRATES

6.1 TARGET COOLING

Indium is a low melting point material (156 ^{0}C) and so when sputtering from an indium target the power input is limited by the target cooling. When sputtering from the magnetron of fig 5.1 with an indium target 3 mm thick we could use a maximum current of 2.2 A before the target melted. It would be useful to increase this current to obtain a higher deposition rate and so the target cooling was analyzed.

This can be done easily because the target melts at the centre of the race track where the heat load is highest. This means that our problem is symmetrical and can be analyzed in one dimension (fig 6.1). With no heat flow sideways out of the model we can put

$$Q/A = dT_1 . \rho_1/L_1 = dT_2 . \rho_2/L_2$$

where Q/A = heat flow/area (W/m^2)
dT = temperature difference (K)
ρ = thermal conductivity (W/m/K)
L = thickness (m)

The total temperature difference ($T_t - T_w$) must equal the temperature across the two slabs ($dT_1 + dT_2$) so using this and re-arranging gives

$$dT_2 = \frac{T_t - T_w}{(1 + (\rho_2 . L_1)/(\rho_1 . L_2))}$$

In the present magnetron we have 3 mm of indium and 3 mm of aluminium. The water temperature (T_w) is 10 ^{0}C and when the target melts the front surface temperature (T_t) is 160 ^{0}C. The thermal conductivities for indium and aluminium are 23.8 and 237 W/m/K respectively. This gives at melting dT_2 = 13.7 K and putting this in our first equation gives

$$Q/A = 1.08 \times 10^6 \text{ W/m}^2 \quad (108 \text{ W/cm}^2)$$

Now the magnetron racetrack is 350 mm long and the erosion profile is close to a triangle 3 mm deep and 12 mm wide. The power input at 2 A (350 V) is 700 W. Weighting the power density by the erosion depth gives a power density at the centre of the racetrack of

Fig. 6·1 : Target heat flow.

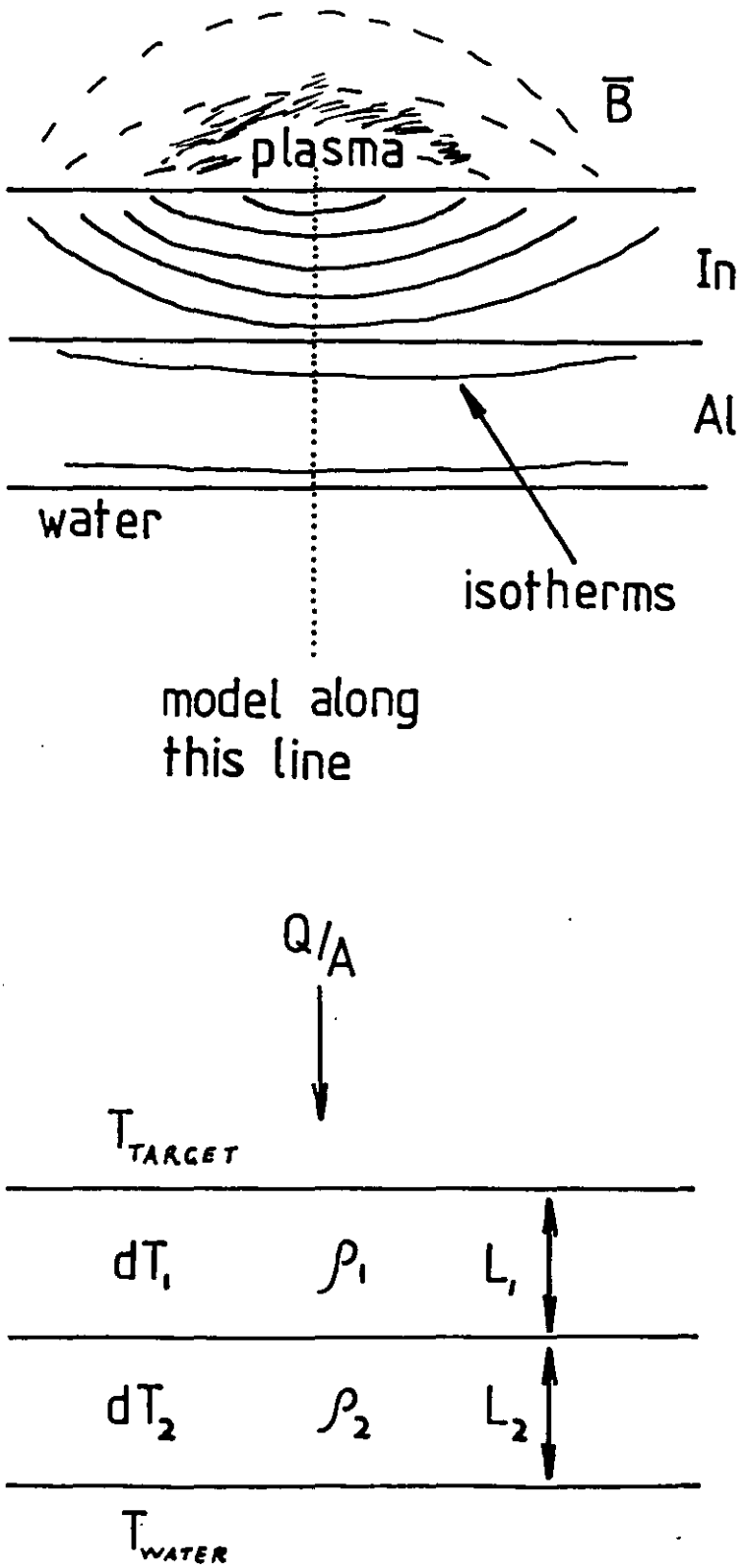

3×10^5 W/m^2. This measured value is roughly a factor of three lower than the calculated heat load for target melting. M.I. Ridge (ref 1) claims to have achieved a power density of 80% of the theoretical limit in his indium target. The discrepancy between our two results is likely to be due to the thermal impedance at the In/Al interface which must be carefully prepared (ref 2).

The target lifetime was only 12 hours at 2 A (350 V); this is a total charge flow of 5.4×10^{23} elemental charges. As we found before (section 3.3) only about 60% of this will lead to sputtering and so we have a useful ion bombardment of 3×10^{23} ions. The sputtered volume was 6 (+/- 1) $\times 10^{-6}$ m^2 and taking a density of 7310 kg/m^2 and an atomic mass of 114.8 amu gives a total number of sputtered atoms of 2.4×10^{23}. The effective sputtering yield is then around 0.8. This is intermediate between the metal sputter yield (calculated from Steinbruchel's formula (section 3.3) for 350 eV ions) of 1.7 and the oxide sputter yield of 0.27 (ref 2a). This is consistent with the picture of a partially oxidized target surface.

To calculate the sputter yield the surface binding energy is needed. This is not available for In or In_2O_3. The bi-molecular In-In bond strength is 1.0 eV per bond and its crystal structure is tetragonal. For a 110 crystal surface this gives 3 direct bonds plus bonding to the adjacent plane (ref 3). A surface binding energy of >3 eV is then expected. The available data for elements nearby in the periodic table (ref 4) also supports a figure slightly greater than 3 eV (fig 6.2).

6.2 In/O RESISTANCE MINIMUM

Before trying to produce a conducting indium oxide over a large area we must first characterize its production on small substrates. Using the Balzers apparatus described previously (fig 5.1) we looked at the width of the resistance minimum and at the properties obtained here. The oxygen partial pressure was obtained by subtracting the argon pressure from the total. The resistance between two probes dragging on the plastic substrate was also monitored. This could be minimized by controlling the reactive gas flow and under these conditions the glass substrate exposed and coated.

Fig. 6·2 : Surface binding energy and estimated indium sputter yield (data from ref. 4).

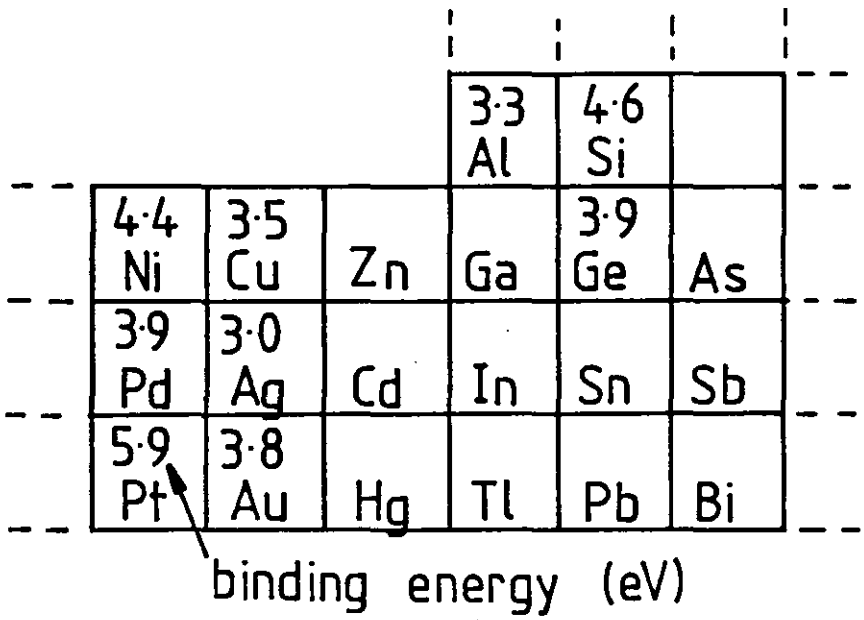

binding energy (eV)	calculated sputter yield Y (at 350 eV)
3	2·2
4	1·6
5	1·3

$$Y_{INDIUM} = 1{\cdot}7 \pm 0{\cdot}5$$

The measured dependence of the film resistance on the oxygen partial pressure is shown in fig 6.3. Taking a production accuracy of R_{MIN} + 10% gives a required oxygen partial pressure accuracy dP/P of 6%. Films deposited onto the glass substrates at this resistance minimum had a deposition rate of 8.3 nm/s, a resistivity of 4.5×10^{-6} ohm.m and a high light transmission. To achieve this on larger area substrates we must aim for a uniformity of reactive gas pressure over the substrate of better than 1-2%. In most cases the oxygen partial pressure is not controlled directly but through the delivered oxygen flow. The same set of results gave a required accuracy in oxygen flow of dQ/Q of only 2%. This shows that the relationship between oxygen flow and oxygen partial pressure is not linear.

6.3 REACTIVE GAS UTILIZATION

According to Schiller et al (section 3.3) for stable production of a compound film we must have at the substrate a constant ratio (metal flux/oxygen flux) and a constant utilization of each. By utilization is meant the fraction of the arriving species (of each type) which remain in the growing film (sometimes termed the effective sticking coefficient). The metal utilization is assumed to be 1 as the surface temperatures are below the metal melting point. We know the oxygen partial pressure and the film growth rate and so can quantify the oxygen utilization.

The arrival rate per unit area of oxygen v_g at a pressure P can be calculated if the gas temperature T is known or assumed (section 3.7). Equation 5 from section 3.7 gives v_g as

$$v_g = P.(2.\pi.k.T.m)^{-1/2}$$

At the resistance minimum we have an oxygen pressure P of 1.1 mTorr (= 0.14 Pa) and oxygen has as molecular mass of 32 amu (= 5.3×10^{-26} kg). Assuming an oxygen temperature of 300 K then gives an arrival rate of

$$v_g = 3.8 \times 10^{21}/s/m^2$$

The conducting oxide is close to stoichiometry and the molecular mass of In_2O_3 is 278 amu. The density of our films is close to the bulk value as the refractive index is high (n_{633} = 2.05). The density of bulk

Fig. 6·3 : The resistance minimum of indium oxide.

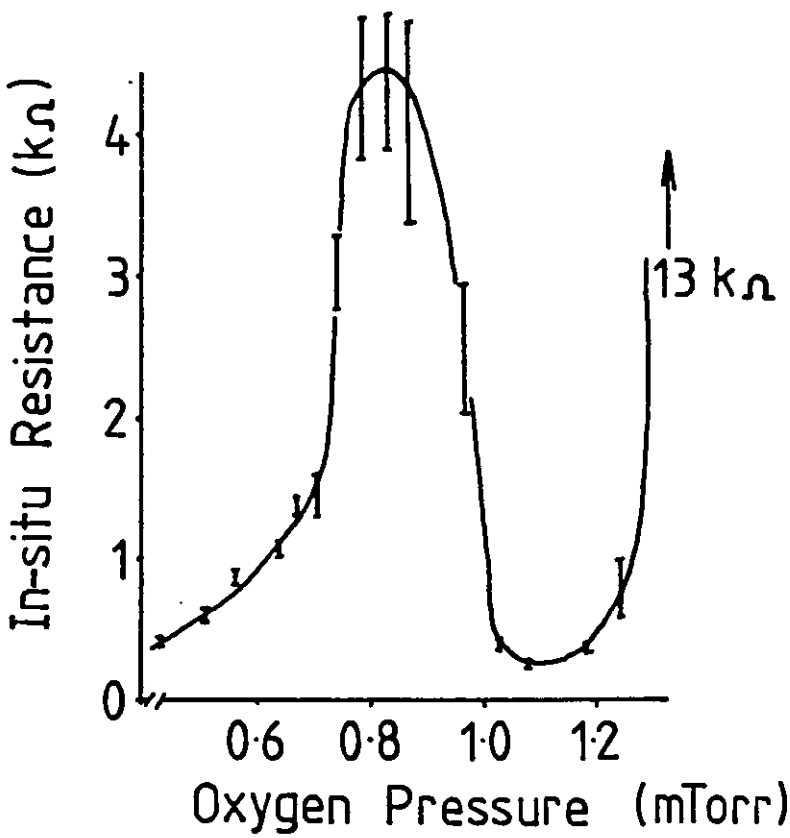

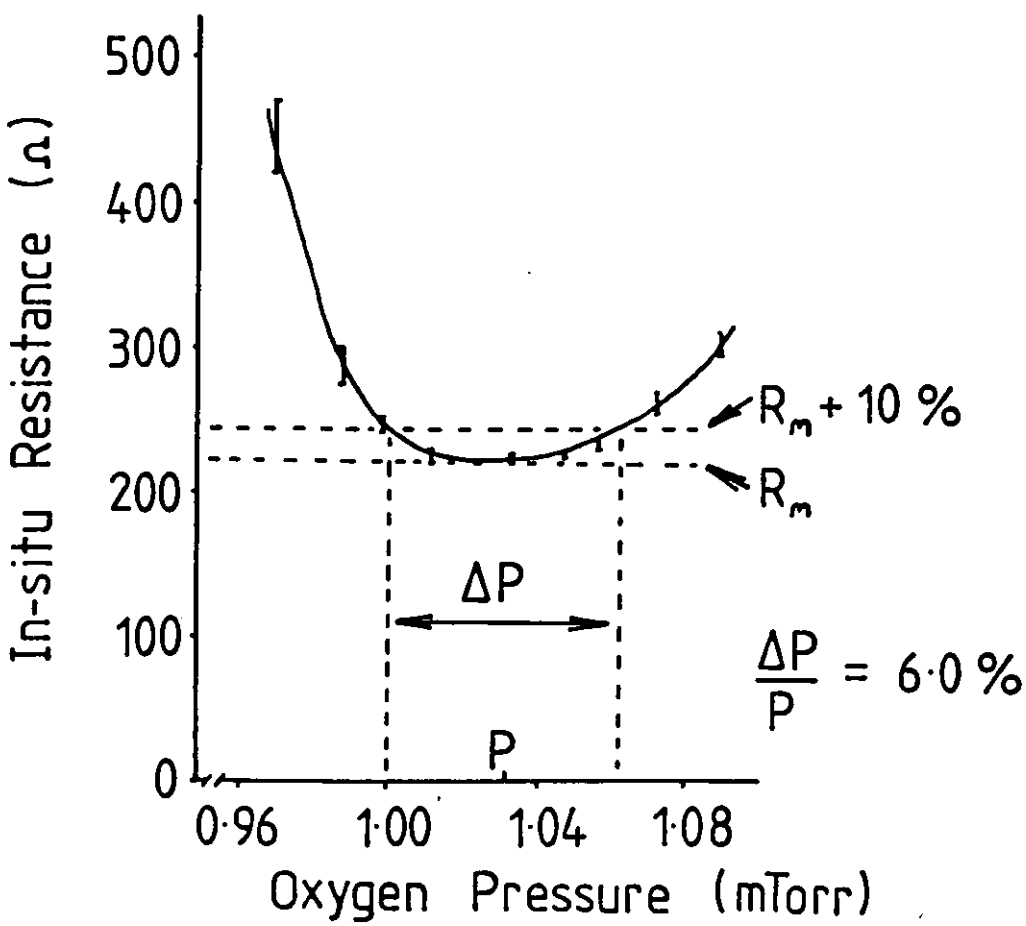

indium oxide is 7180 kg/m^3 (ref 5) so a deposition rate of 8 nm/s is an oxygen atom sticking rate of 6.2 x 10^{-4} moles/s/m^2. This is a molecular sticking rate of 1.9 x 10^{20}/s/m^2. The utilization of the arriving oxygen molecules is then

$$O_2 \text{ utilization} = \frac{\text{sticking rate}}{\text{arrival rate}} = 0.05$$

This is fairly small and obviously implies that much of the available oxygen is desorbed from the surface before reactions can take place. This value is also consistent with the work of Tiedje et al (ref 6) (see section 3.5) who obtained a value of utilization for H_2 in Si of 0.04 +/- 0.02.

To get this figure I have assumed an oxygen temperature of 300 K which may not be right. The expansion into the chamber may decrease this (adiabatic case) or exposure to the plasma increase it. The equation for the arrival rate has a $T^{-1/2}$ dependence so even if the gas temperature is an order of magnitude out the error is only a factor of 3.

Using the value from our system and the theory of Tiedje et al we can obtain a value for the In/O reaction cross section on the growing film surface. They state (ref 6) that

$$N/N_0 = \exp(-\sigma.\theta.V_g/R)$$

where N = number of free reaction sites (/m^2)
N_0 = number of free reaction sites for metallic film (/m^2)
σ = reaction cross section (m^2)
θ = sticking coefficient
v_g = reactive gas arrival rate (/s/m^2)
R = film growth rate (monolayers/s)

The density of In_2O_3 is 7180 kg/m^3 and the molecular mass is 278 amu. The molecular volume is then 6.4 x 10^{-29} m^3 and so a deposition rate of 8 nm/s is 20 monolayers/s. The conducting indium oxide has a carrier density of 4 x 10^{26} m^{-3} (ref 7) with perfect doping (due to oxygen deficiencies (ref 8)), this is a deviation from stoichiometry of 1%.

In practice the optimum In_2O_3 has a departure from stoichiometry closer to 10% (ref 9) ie $N/N_0 = 0.9$. Putting v_g, R and N/N_0 into the equation above gives

$$\sigma.\theta = 1 \times 10^{-20}\ m^2$$

A sticking coefficient of 0.05 is reasonable (see above or ref 10) and this gives a reaction cross section of $2 \times 10^{-19}\ m^2$. This is an average value for all the excitation states and species arriving at the film. I shall refer to this as the effective reaction cross section. Hu et al (ref 11) obtained by a different method a reaction cross section for N_2+ on Ti of $10^{-20}\ m^2$ and for N^2+ on Re of $10^{-22}\ m^2$. The effective reaction cross section above is then not unreasonable in the light of Hu et al's results for less reactive systems.

6.4 PRESSURE INSTABILITY

Indium oxide

The results in section 6.2 indicate that the oxygen partial pressure vs oxygen flow dependence is non-linear. We therefore measured these two with and without the magnetron operating (fig 6.4). The difference between the two must represent the oxygen consumed by the growth of the oxide film. This is shown in fig 6.4 and significantly has a negative gradient (dQ_{FILM}/dp) at the pressure where the conducting oxide is formed (1.1 mTorr - indicated by the small arrow). We identified this negative gradient as the cause of the instabilities seen in reactive magnetron sputtering (ref 12). We termed this a pressure instability and postulated the instability mechanism shown in fig 6.5.

If we are considering scaling up our process the film consumption of oxygen will increase with the deposition area. In this case with a constant pumping speed the film consumption will come to dominate the total oxygen consumption. When this happens we have the situation shown in fig 6.5 and a pressure instability will occur.

To check this we can perform a simple experiment. We have a pressure instability whenever an increasing oxygen pressure leads to a decreasing oxygen consumption (detailed in fig 6.5) ie a deposition system is stable if

Fig. 6·4 : Oxygen consumption in a stable system depositing indium oxide (arrow indicates conducting oxide).

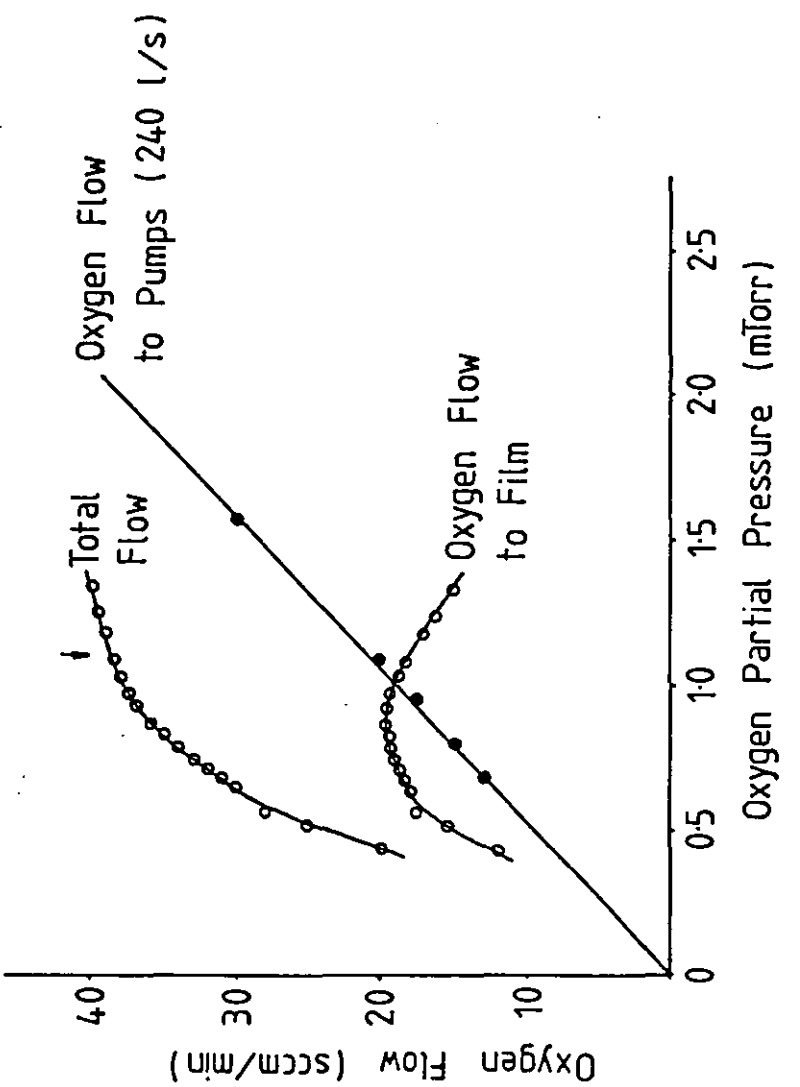

Fig. 6·5 : The mechanism that causes instability.

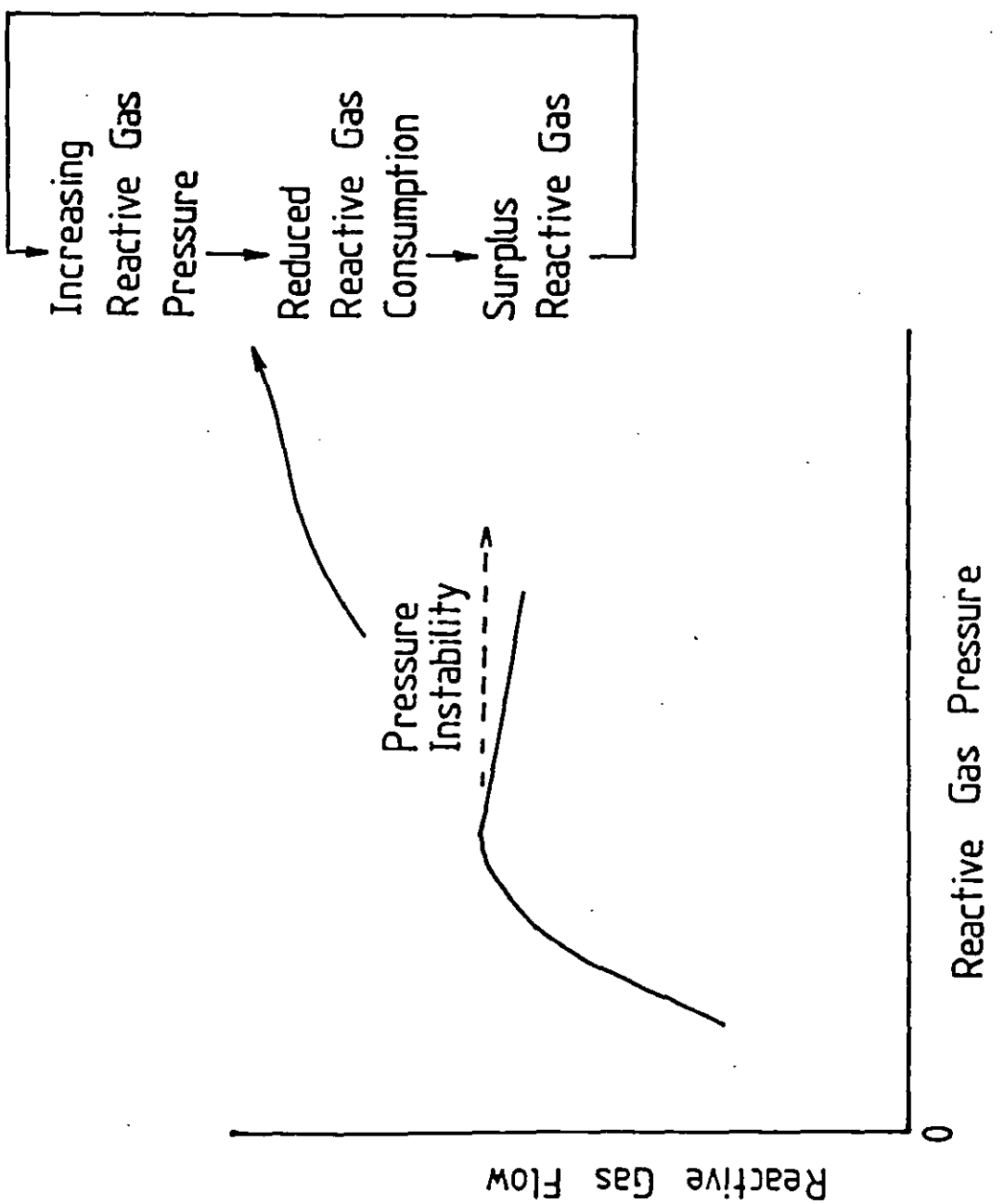

$$Rp > -dQ_{FILM}/dp$$

The negative gradient of the film consumption (Q_{FILM}) in fig 6.4 is dQ_{FILM}/dp = 150 l/s. So if we reduce the pumping rate to less than 150 l/s we will induce a pressure instability. The pumping orifice was baffled to give a pumping rate of 120 l/s and our experiment repeated. Fig 6.6 shows the result and we do indeed have an instability. Also notice that the oxygen pressure of 1.1 mTorr (where our conducting oxide is produced) is now unobtainable.

Al, Ti, and Sn with O in other systems

In conjunction with R.W. Lewin, I measured the oxygen consumption curves for the notoriously unstable materials Al (fig 6.7) and Ti (fig 6.8) (in a circular magnetron running at 2.0 A). The most significant difference between these film consumptions and the indium/oxygen one is at high oxygen pressures. The consumption of reactive gas falls to zero (within our errors) for Ti and Al but stays high for indium/oxygen. Titanium and aluminium are more reactive with oxygen than is indium. The sputter rate for the titanium and aluminium oxide will therefore be much lower than the sputter rate of indium oxide. Also significant is the fact that the maximum film consumptions for Al and Ti differ by a factor 1.75 as do their sputter yields (ref 13).

In the Everest coater with 2.7 m magnetrons we also measured the oxygen curve for tin/oxygen (fig 6.9). This curve is very similar to the indium consumption curve ie similar processes are involved. We could only use a magnetron current of 10 A for this experiment and the magnetron in production runs at around 30 A. In this case as the target ages a pressure instability occurs with the target changing uncontrollably from a poisoned to a metallic surface accompanied by a total pressure change from 3.0 x 10^{-3} mBar to 1.5 x 10^{-3} mBar and a voltage change from 450 V to 610 V. This behaviour is the same process of instability seen in our small magnetron.

Summary

- The power that can be delivered to the magnetron is limited by the thermal impedance of the target and the maximum permitable surface temperature. Experimental results imply that for cast

Fig. 6·6 : The system of fig. 6·4 made unstable by reducing the pumping rate.

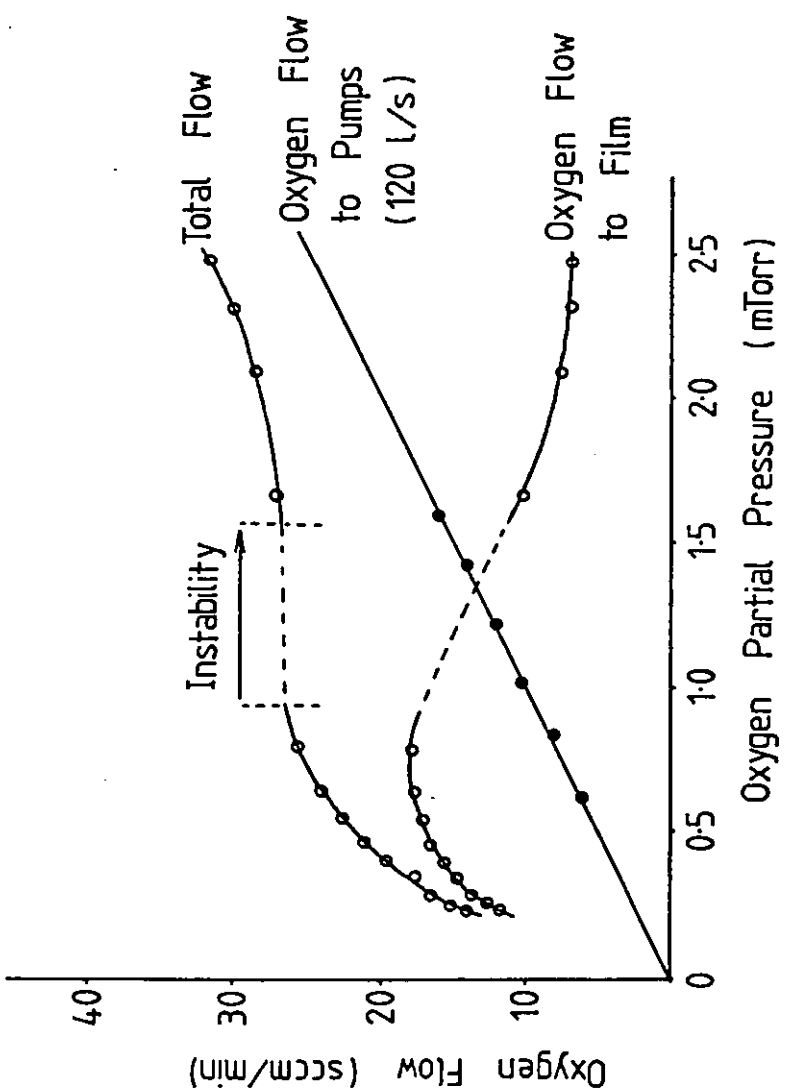

Fig. 6·7 : The oxygen consumption of aluminium.

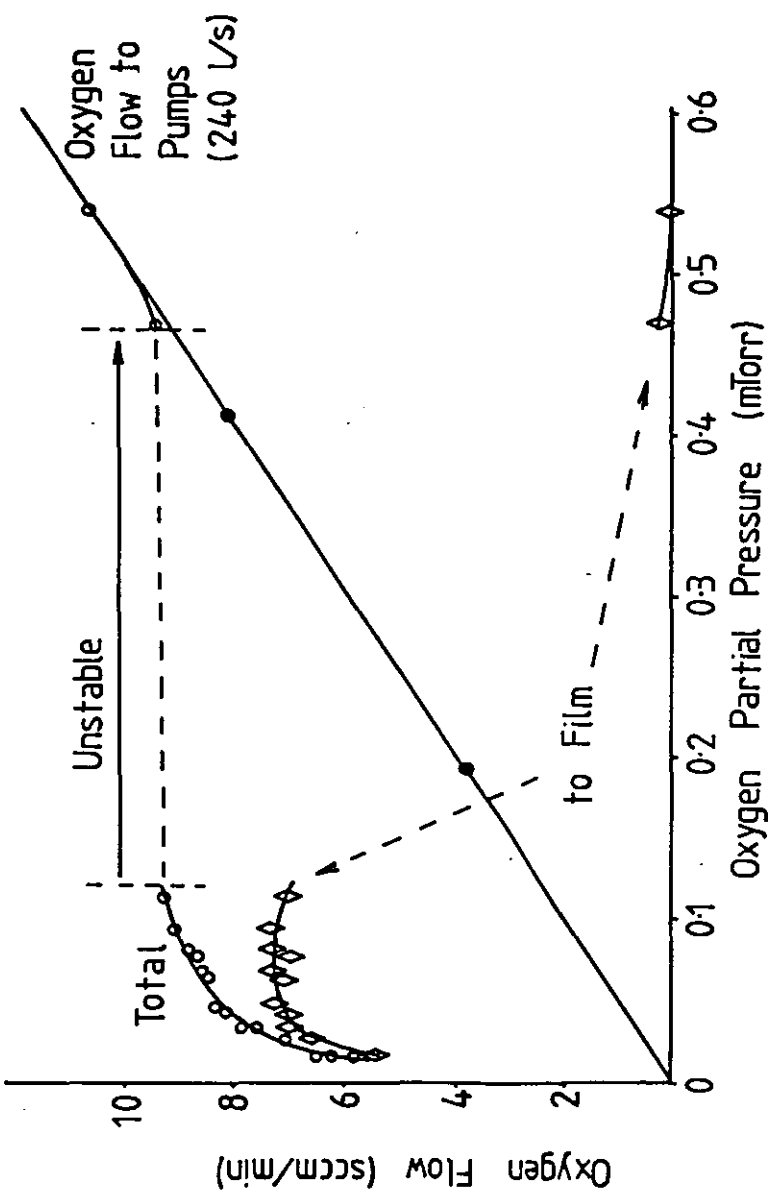

Fig. 6·8 : The oxygen consumption of titanium.

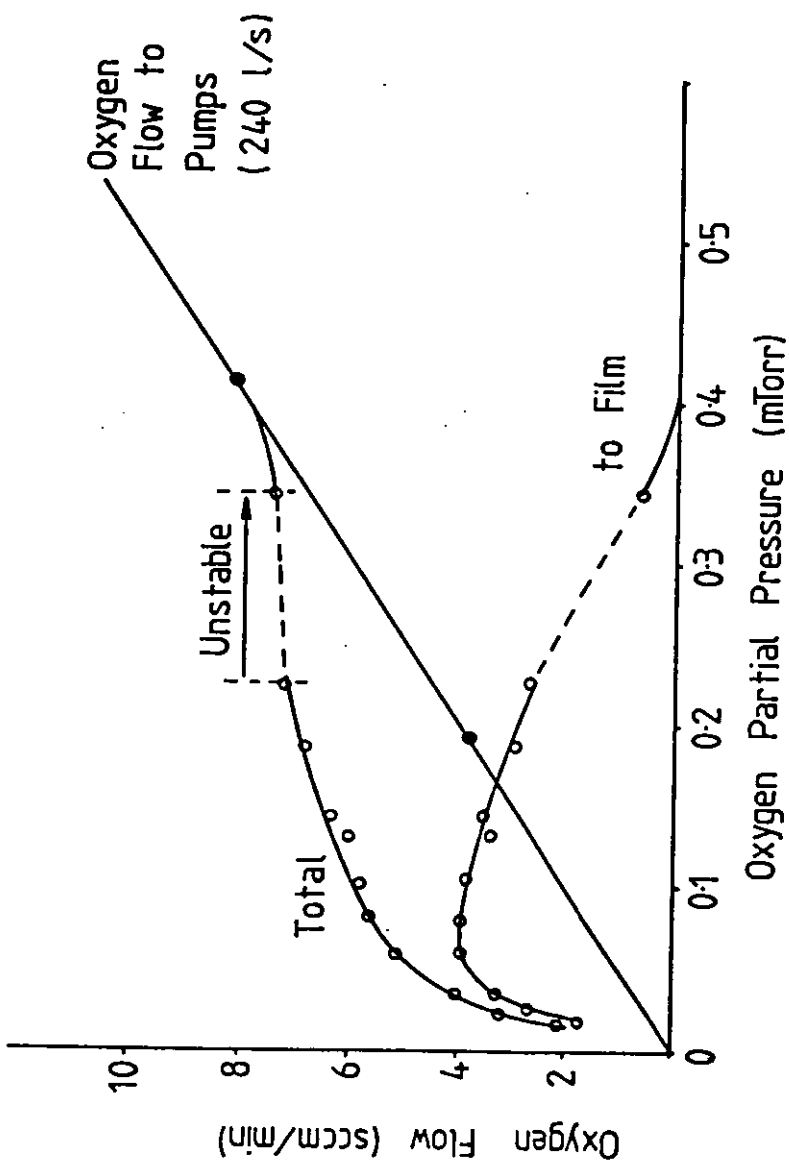

Fig. 6·9 : Oxygen consumption in the Everest coater.

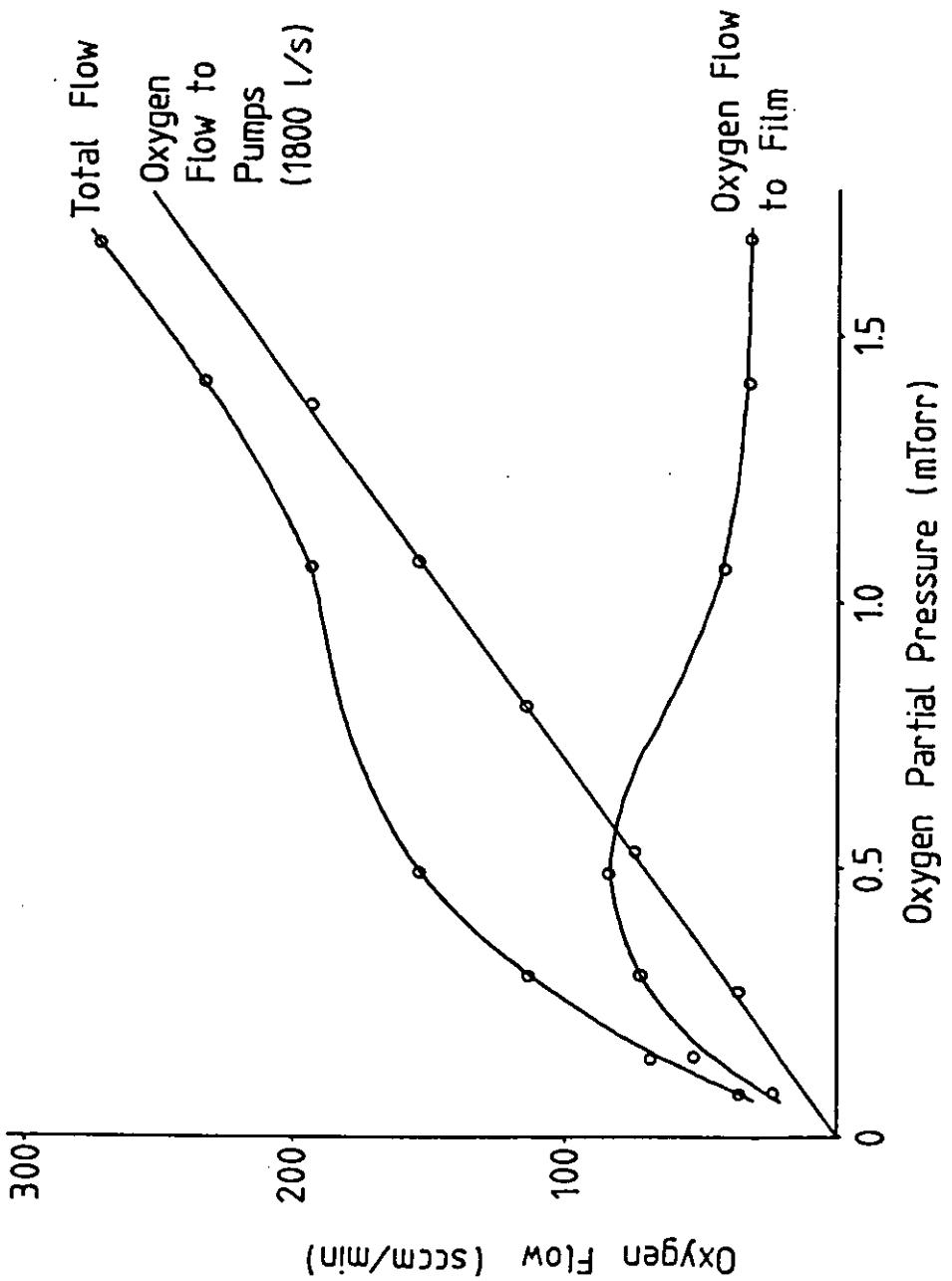

targets there can be significant thermal impedance associated with the target/backing plate interface.

- Films deposited at maximum power and with minimised resistance had a deposition rate of 8 nm/s.
- The effective sputter yield of the target is intermediate between the metal and the oxide sputter yields.
- The width of the indium oxide resistance minimum is different if specified in oxygen flow and oxygen pressure ie oxygen pressure and flow are not linearly related.
- Of the oxygen arriving at the substrate only about 5% is utilized in the growing film. The effective reaction cross section for indium and oxygen is then about 10^{-19} m^2.
- Measurements of the reactive gas pressure and flow show up the amount of reactive gas consumed by the growing film. This is a useful diagnostic technique and once understood can explain the pressure instability widely observed in reactive magnetron sputtering.
- The reactive gas consumption in various sputtering systems and with various metals has been measured and these all conform to the same basic curve.

REFERENCES: CHAPTER 6

1. Ridge M.I., "Visibly transparent heat reflecting oxides deposited by reactive magnetron sputtering", PhD Thesis, LUT, 1984.

2. Lewin R.W., Private Communication.

2a. Natarajan B.R., Eltoukhy A.H., Greene J.E., and Barr T.L., Thin Solid Films, 69, 217-227, 1980.

3. Ashcroft N.W., and Mermin N.D., 'Solid State Physics', Holt Saunders, Tokyo, 1976.

4. Stenbruchel Ch., Appl. Phys., A36, 37-42, 1985.

5. "Handbook of Chemistry and Physics", CRC Press, Boca Rata, U.S.A., 1983.

6. Tiedje T., Moustakas T.D., and Cebulka J.M., Phys. Rev. B, 23, 5634-5637, 1982.

7. Lewin R.W., Howson R.P., Bishop C.A., and Ridge M.I., Vacuum, 36, 95-98, 1986.

8. Hamberg I., and Granqvist D.G., Solar Energy Materials, 14, 241-256, 1986.

9. Frank G., Kauer E., and Kostlin H., Thin Solid Films, 77, 107, 1981.

10. Popov D.N., Kotlarova Tz.K., Uzunov Tz.D., and Gaydarova V.N., Vacuum, 38, 1015-1017, 1988.

11. Hu H.K., Terrence Murray P., Fukuda Y., and Wayne Rabalais J., J. Chem. Phys., 74(4), 2247-2255, 1981.

12. Spencer A.G., Howson R.P., and Lewin R.W., Thin Solid Films, 158, 141-149, 1988.

13. Maissel L.J., and Glang R., "Handbook of Thin Film Technology", McGraw Hill, New York, 1970.

7. RESULTS - A MODEL

The reactive gas consumption curve and the associated pressure instability are applicable to a wide range of materials and deposition systems. To gain some insight into this we developed a conceptual model (ref 1) from the results in Chapter 6.

7.1 A MODEL OF THE PROCESS

The curve of film reactive gas consumption against reactive gas pressure is the result of chemical reactions both on the target and on the substrate. Our results have all been for metal/oxygen systems but we believe the argument below will apply to other reactive gases eg nitrogen or a hydrocarbon gas (ref 2, 3). Ignoring for now the reactive gas removed by the pumps we can consider the amount used up by the growing film:-

At the target the surface is constantly being poisoned and sputtered clean. Where the poisoning rate exceeds the cleaning rate a poisoned surface exists and increasing the reactive gas pressure then increases the proportion of the target that is poisoned (see section 3.3). This poisoned surface will sputter more slowly than the metallic one (also see section 3.3) and so this leads to a reduction in the metal flux with increasing reactive gas pressure. This continues until the target is completely poisoned and then the metal flux remains roughly constant (fig 7.1a). The shape of fig 7.1a is based on work by Schiller et al and Georgiev et al (ref 2, 3).

At the substrate at low reactive gas pressures the formation of the compound (film) is limited by the arrival rate and utilization of the reactive gas and so a metal rich film is formed. As the reactive gas pressure is increased the arrival rate of the reactive gas increases and the film becomes less metallic. This continues until the film is saturated with gas (fig 7.1b). The consumption of the reactive gas is then limited by the metal arrival rate. This was seen experimentally by Nishikama (ref 5) and discussed theoretically by Tiedje et al (ref 6) (see section 3.5).

The processes at the target (fig 7.1a) and at the substrate (fig 7.1b) combine to give the gas consumption curve (fig 7.1c) and we can

Fig. 7·1 : The origins of the reactive gas consumption by the film.

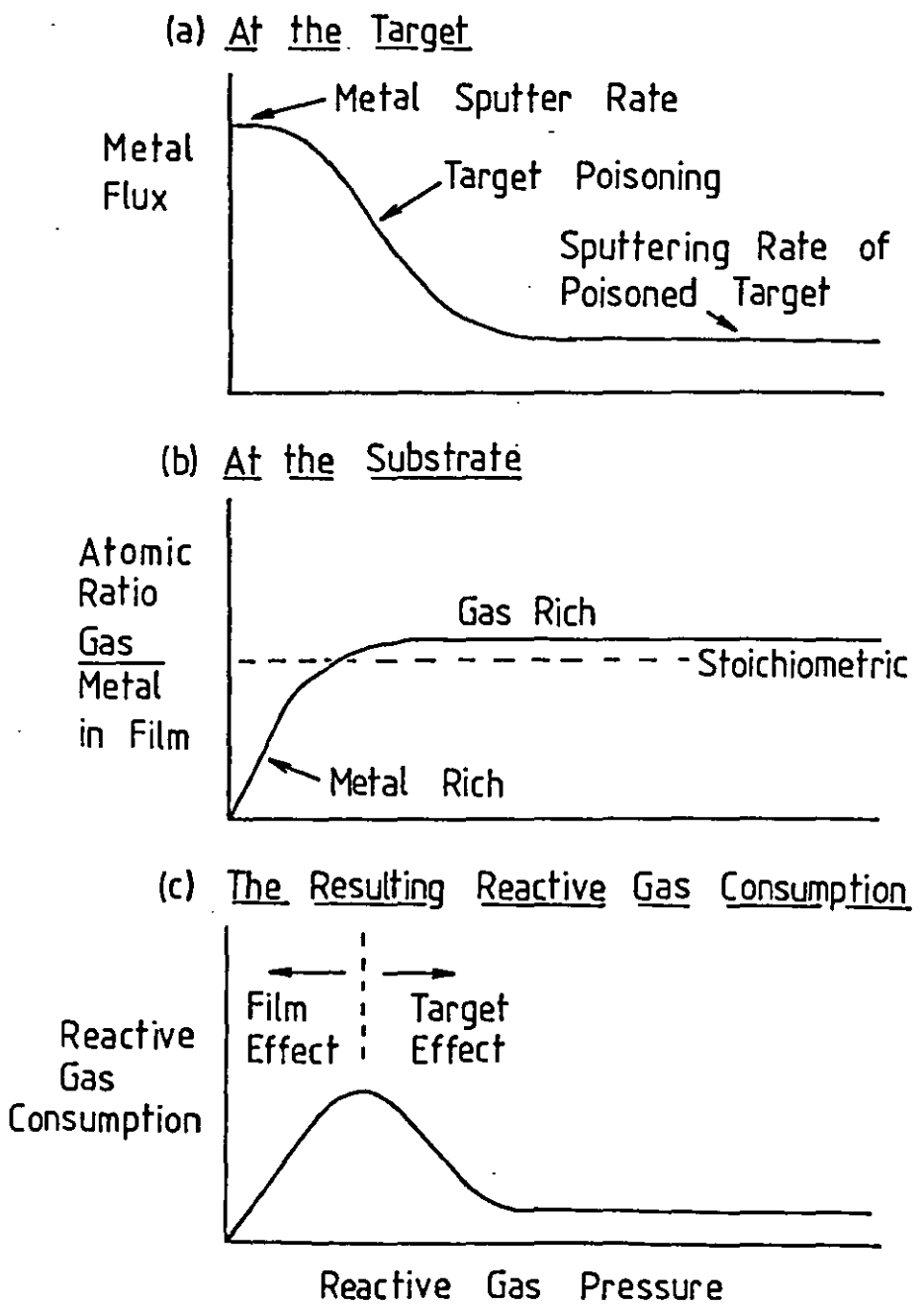

now indicate the limiting factors in each region of the curve (fig 7.2).

7.2 CONSEQUENCES OF THIS MODEL

If this conceptual model is to be of any use we must be able to make predictions about the effects of various parameters.

We have already shown that the pumping rate required for stability can be predicted from the measured gas consumption curves. The rate of change of reactive gas pressure in the instability (and hence the transit time across the instability) can also be predicted. Fig 6.5 shows the cycle occurring in the instability and this is comprised of three effects.

1. The reactive gas pressure increases.
2. The reactive gas consumption decreases.
3. There is a surplus amount of reactive gas and so to 1.

The ion bombardment on the magnetron target is such that each exposed atom is subject to around 10^3 ions/s. We might then expect a monolayer of reaction products to form on a timescale of 10^{-3} ie steps 2 and 3 occur quickly. Given that we now have a surplus mass flow of reactive gas Q_s how quickly will step 1 occur? For a perfect gas this is simple and we have

$$\frac{dP}{dt} = \frac{Q_s}{V} \qquad (1)$$

where P = reactive gas pressure (Pa)

Q_s = surplus reactive gas flow (Pa.l/s)

$= Q_{IN} - Q_{FILM} - Q_{PUMP}$

V = chamber volume (l)

The time T taken for an unstable transition between pressures P_1 and P_2 is then

$$T = \int_{P_1}^{P_2} \frac{dt}{dP} \cdot dP = V \cdot \int_{P_1}^{P_2} \frac{1}{Q_s} \cdot dP \qquad (2)$$

Fig. 7·2 : The limiting factors in each region of reactive gas consumption.

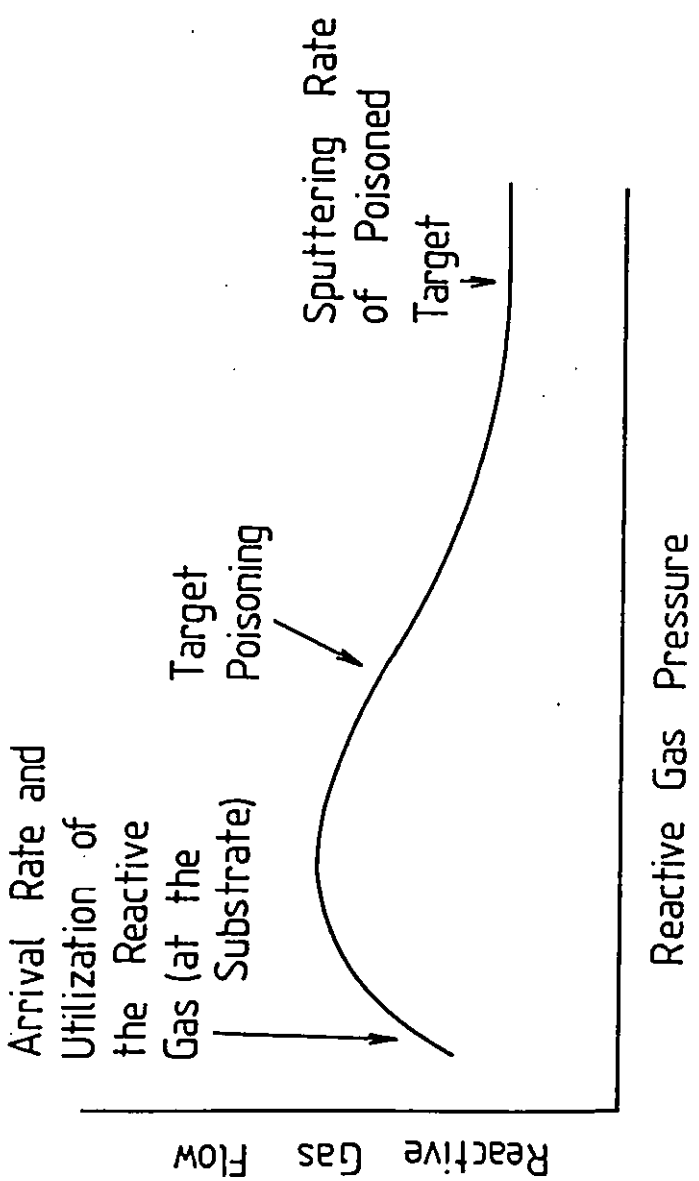

From figures 6.4 and 6.6 we can evaluate Q_s as a function of pressure with a pumping rate of 120 l/s. Integrating this numerically and using a chamber volume of 100 l gives a time for the instability of 16 s. The observed time was 20 s which is close enough to give us some confidence in equations 1 and 2. It is also worth pointing out here that the measured curves are quasi-static ie the gas flow or pressure is allowed to reach equilibrium between each change. If with a pressure controller the set point is suddenly increased we see an initial gas flow increase beyond the eventual steady state value and then over a minute a gradual fall back to the steady value. This we attribute (ref 1) to the material on the chamber walls continuing to absorb reactive gas after deposition.

We can also say in a qualitative fashion what effect surfaces exposed to the coating flux will have on the gas consumption curve. If the surfaces are close to the magnetron they will receive a high flux per unit area of metal species and the film formed will saturate at relatively high reactive gas pressures. A surface further from the magnetron will receive less metal per unit area and so saturate at lower reactive gas pressures. The total sputtered flux will cover less area if the receiving surfaces are close to the magnetron and as pumping rates are proportional to area (see section 3.7) the getter pumping rate will fall ie the initial gradient in fig 7.2 will decrease. Using this reasoning we predicted that pumping surfaces close to the magnetron would still have increasing reactive gas consumption (ie an unsaturated film) while a substrate placed further away would coat with a stoichiometric film.

This experiment was performed in conjunction with R.W. Lewin in the apparatus of fig 7.3 and the results are shown in figs 7.4. As expected we pushed the stable reactive gas pressure up and at 0.19 mTorr could deposit TiO_2 on the substrate. These films had a deposition rate of 0.3 nm/s and a refractive index n_{633} of 2.37. Without the pumping surfaces TiO_2 could only be produced from the poisoned target.

Summary

- A simple conceptual model based on target poisoning and film composition can explain and quantify the pressure instability seen in reactive sputter deposition.

Fig. 7·3 : Apparatus for testing the effects of pumping surfaces.

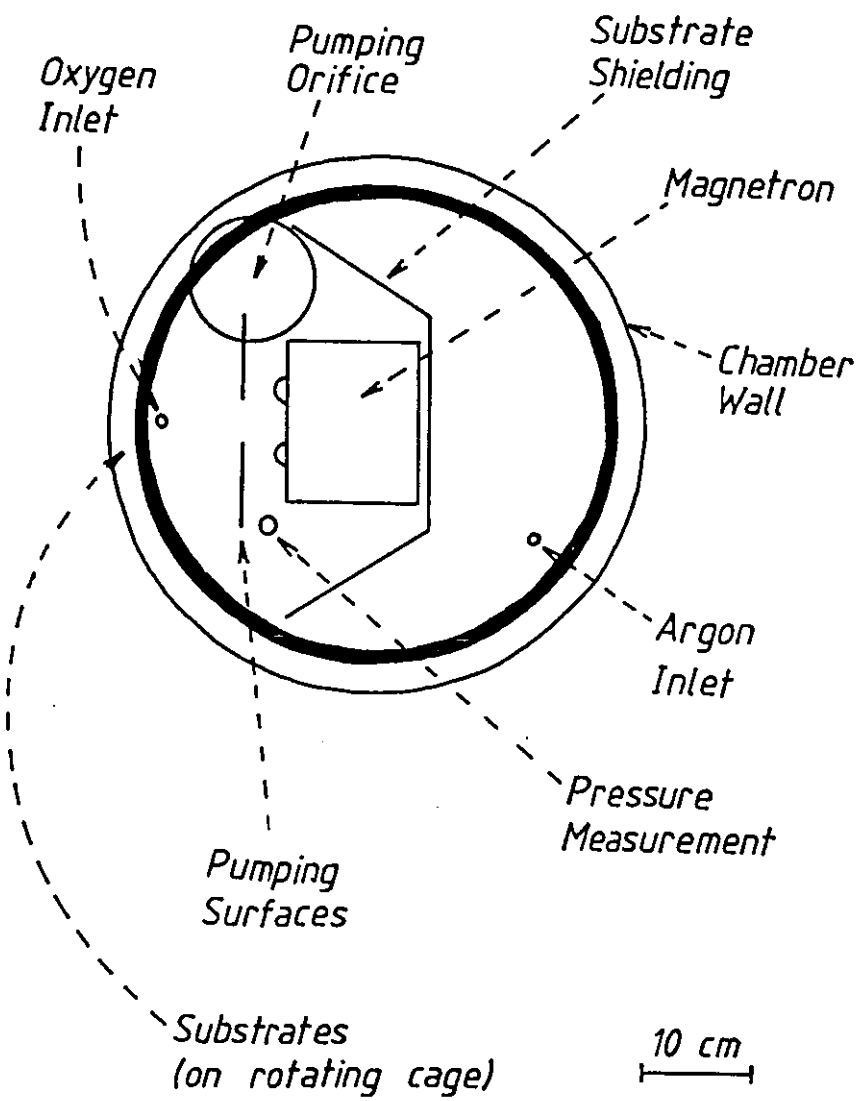

Fig. 7·4a : Oxygen consumption for titanium without pumping surfaces.

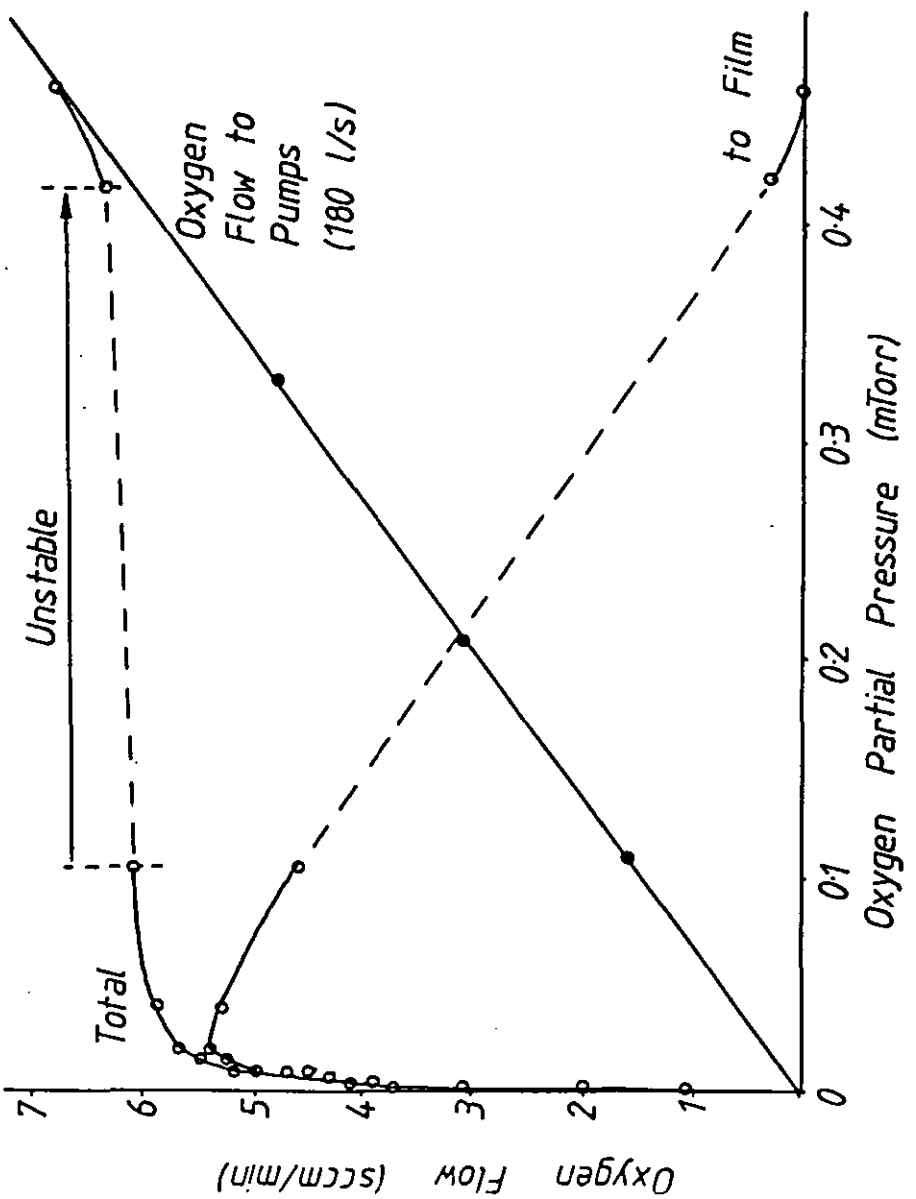

Fig. 7·4b : Oxygen consumption for titanium with pumping surfaces.

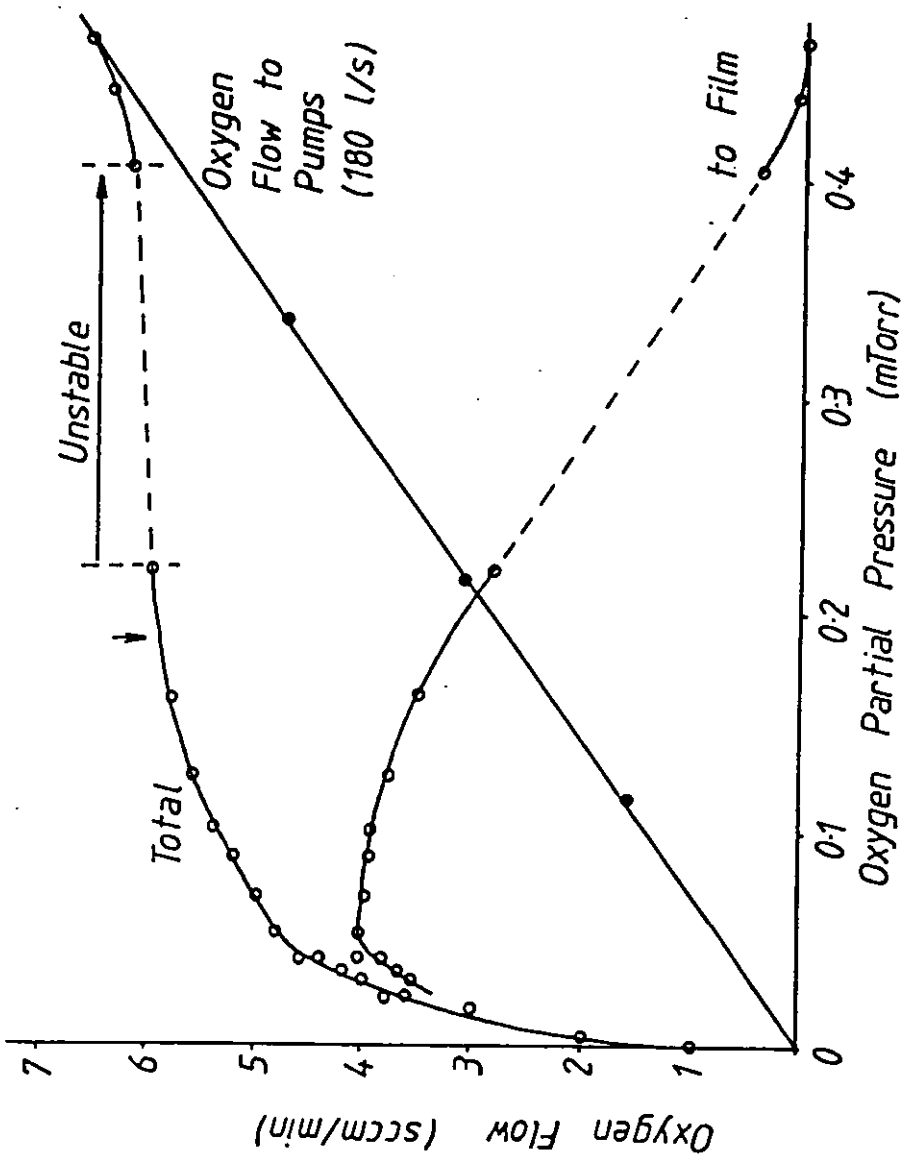

- The speed across the pressure instability is proportional to the amount of surplus reactive gas (= input reactive gas flow - film consumption - pump consumption) and inversely proportional to the chamber volume.
- The curve of film consumption (of reactive gas) versus reactive gas pressure can be modified by varying the positions of the surfaces which intersect the coating flux. In effect this allows stability to be obtained by using some of the sputtered material as a pump instead of for film formation.

REFERENCES: CHAPTER 7

1. Spencer A.G., Howson R.P., and Lewin R.W. Thin Solid Films 158, 141-149, 1988.

2. Schiller S., Beister G., and Sieber W., Thin Solid Films, 111, 259, 1984.

3. Georgiev G., Feschiev N., Popov D., and Uzonov Z., Vacuum, 36, 10, 595, 1986.

4. Schiller S., Heisig U., and Steinfelder K., Strumpfel J. and Sieber W., Vacuumtechnik, 30, 1, 1981.

5. Nishikama S., Thin Solid Films, 135, p 219-228, 1986.

6. Tiedje T., Moustakas T.D., and Cebulka J.M., Phys, Rev., B23, 10, 5634-5637, 1981.

8. RESULTS - IMPLEMENTATION FOR LARGER AREAS

8.1 SYSTEM DESIGN

Our previous results (chapters 6 and 7) show that implementing a reactive sputtering system for large area high rate deposition is not simply a matter of scaling up a small coater. For a stable system the pumping speed should be increased with the area of the deposition zone. Our small system had a magnetron 75 x 180 mm and required for stability an oxygen pumping rate of at least 150 l/s. The Everest large glass coater has a magnetron 230 x 2900 mm and so we would require for stability an oxygen pumping rate of at least 7000 l/s (for a reasonable operating margin about twice this would be desirable). In fact the Everest machine has an oxygen pumping rate of only 750 l/s and for tin oxide does exhibit a pressure instability. Stability could be achieved by greatly increasing the chamber pumping rate but this may not be an economic proposition even when building the machine from scratch.

We have shown that pressure stability is determined by the pumping rate for the reactive gas, and by the position of receiving surfaces within the chamber. It is also likely that it will be affected by the target power density but this dependence is as yet unclear. Given that it would be desirable to control a reactive system in the unstable region we will make our system unstable to act as a test bed for control mechanisms.

Our deposition system is shown in plan view in fig 5.3. We have used a target substrate distance of 1.5 times the racetrack separation ie 3 s in fig 5.2. With only the pumping surfaces (louvres) in place we measured the thickness distribution on a static A4 substrate. The system was saturated with oxygen so that a transparent film was obtained and the thickness then measured by ellipsometry. The thickness profiles obtained are shown in fig 8.1. The metal arrival rate top to bottom is uniform to 5% so to obtain the same uniformity side to side the deposition zone was shuttered to 40 mm either side of the centre.

Ideally the presence of this shuttering should not disturb the thickness profile but merely remove the segments we do not want. To do this the shuttering must be placed as close as possible to the substrate otherwise a highly non-uniform arrival rate results (see fig

Fig. 8·1 : Measured uniformity profiles.

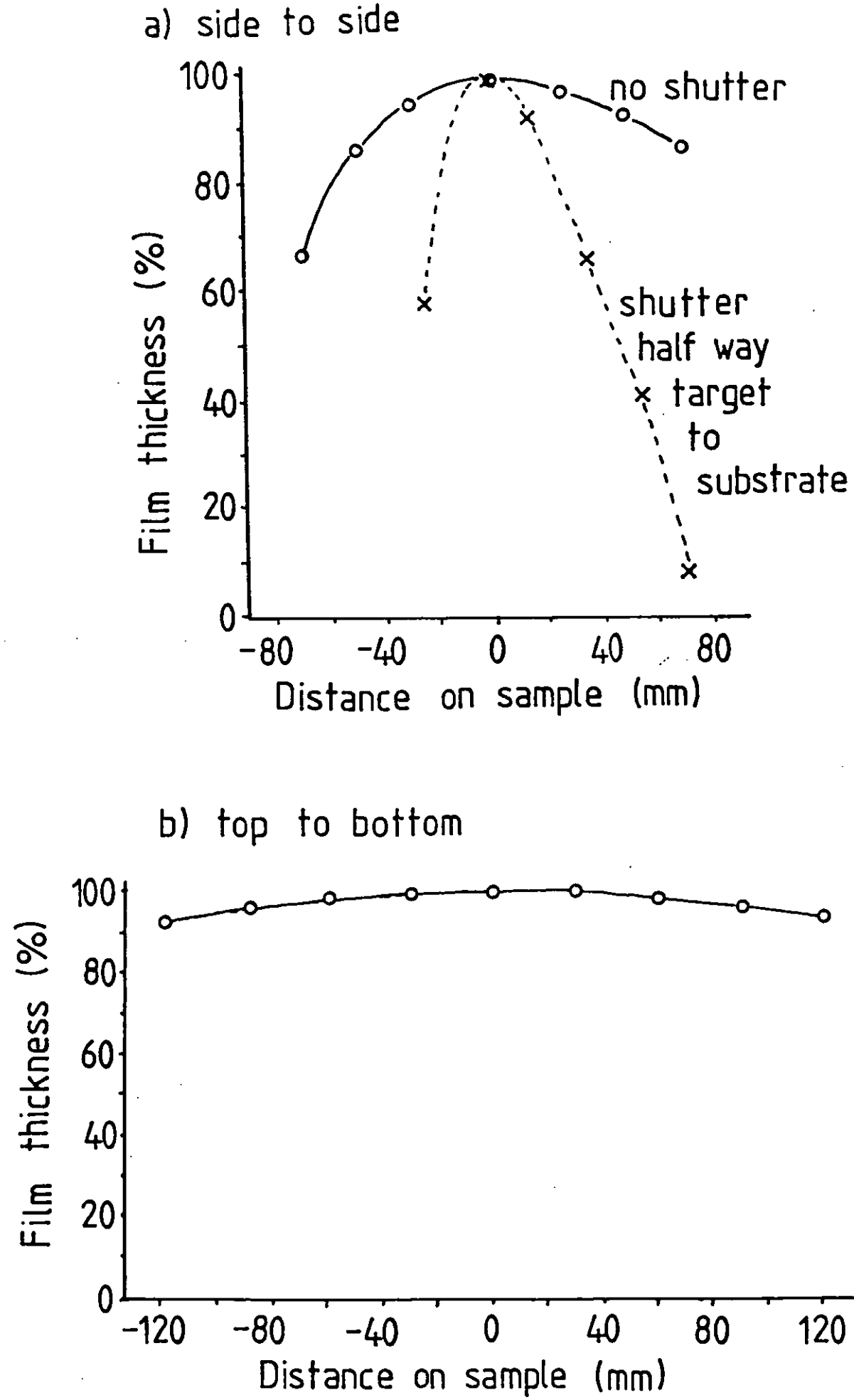

8.1 for shutters placed 20 mm either side of centre and half way between the target and substrate). The shuttering system used in the Everest production coater is then far from ideal for obtaining a uniform film stoichiometry across the deposition zone (fig 5.6). The shutters should be much closer to the substrate.

Having got a roughly uniform metal arrival rate (fine tuning can be done later) the gas arrival rate must be looked at. With the reactive gas admitted through a 4 mm bore pipe and with no shutters we coated a static A4 sample with the conducting oxide. Lines of constant thickness were drawn from the interference colours and the sheet resistance measured with our four point probe. The results are shown in fig 8.2. This shows that the thickness and resistivity (ie film stoichiometry) are now non-uniform. This is due to the pressure gradients around the end of the pipe (see fig 8.3 showing an additional plasma in the high pressure region at end of a pipe). A gas distribution manifold was added (as shown in fig 5.3) and the static deposition showed much better top to bottom uniformity in both sheet resistance and thickness. Lastly adding the shutters (40 mm each side of centre) and moving the substrate past the deposition zone we get the sample in fig 8.4. The side to side uniformity is now better and we are approaching a usable sample. These samples were all made at low power and as the power is turned up the conducting oxide cannot be made due to the occurrence of a pressure instability.

8.2 PLASMA EMISSION MONITORING

For plasma emission monitoring (PEM) control of the process in the unstable region a suitable line intensity should be monitored. Using an EG & G 1451 plasma emission monitor a spectrum of the plasma in the region of the metal lines was taken. The magnetron was run at 8 A 442 V in an Ar/O_2 plasma on the metal side of the instability. The metal lines (451 nm and 410 nm) dominate the spectrum in this region (fig 8.5) and so a high wavelength resolution is not necessary. A simple interference filter is sufficient to isolate the In lines. We obtained such a filter centred at 450 nm with a full width half maximum of 6.5 nm and a peak transmission of 45% (Ealing Electro-optics). The light from the plasma was obtained via a glass fibre optic bundle (light guide). To prevent the end of the light guide being coated the plasma was viewed through a tube (aspect ratio 10:1) (as shown in fig

Fig. 8·2 : Sheet resistance and thickness uniformity without a gas distribution manifold.

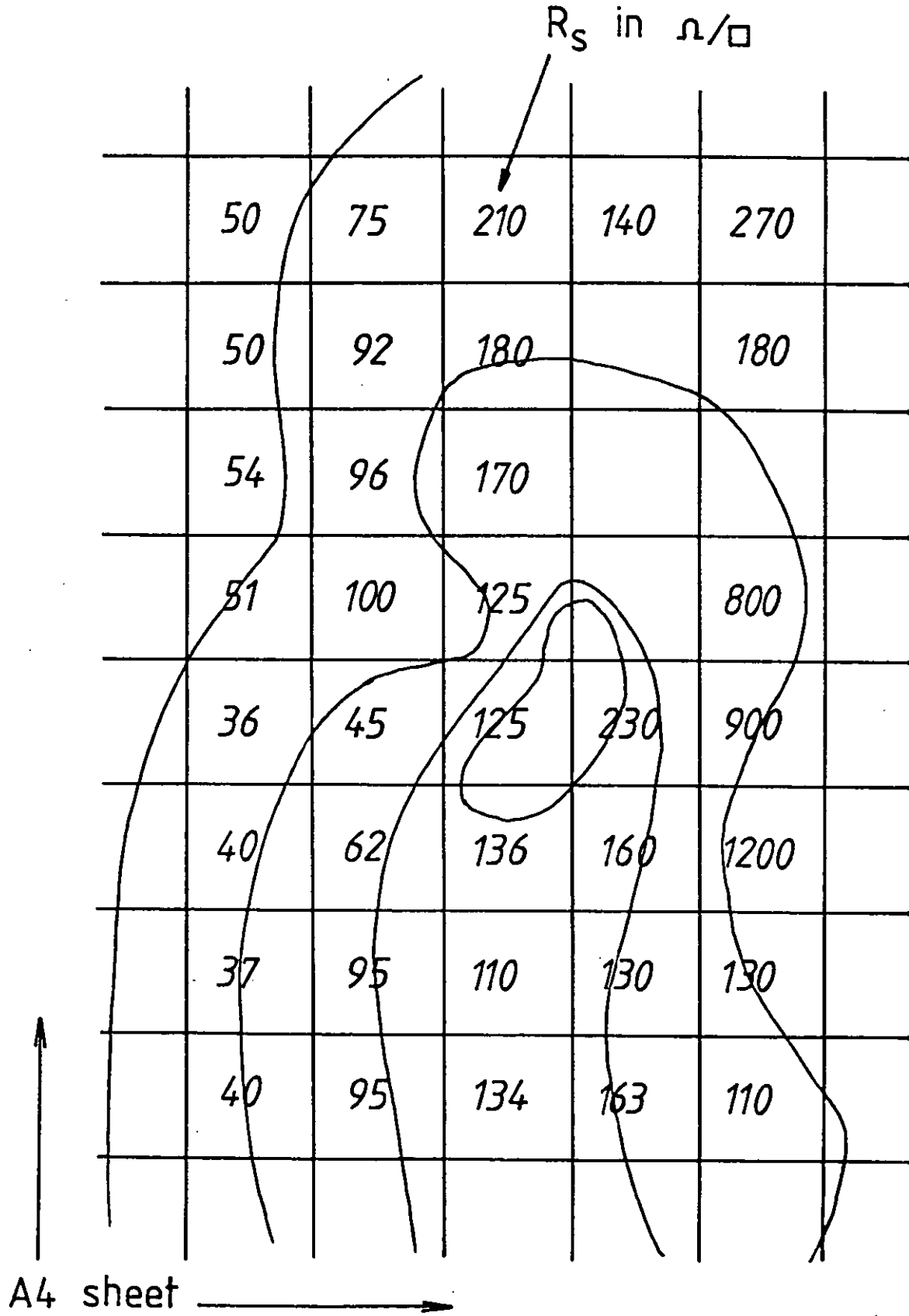

Fig. 8·3 : A top view of the 0·5 m magnetron showing the plasma beam and high pressure at the gas inlet.

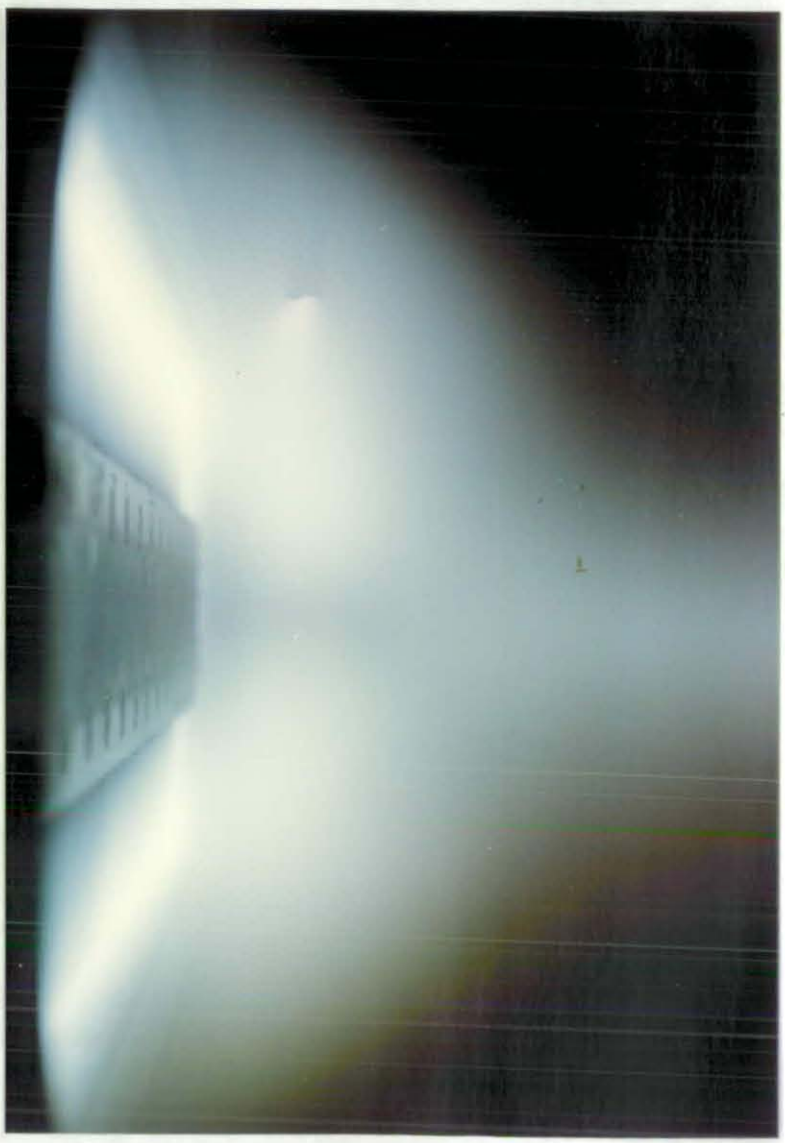

Fig. 8·4 : Sheet resistance uniformity with gas distribution manifold and substrate movement.

	51	74	97	94	154	
	39	46	54	62	104	
	33	35	39	43	67	
	28	30	33	33	49	
	26	29	29	31	41	
	26	29	28	31	38	
	24	26	27	30	40	
	25	25	27	34	42	

Fig. 8·5 : Emission spectrum from 0·5m magnetron (In target, Ar/O_2 gas, 2·8 kW).

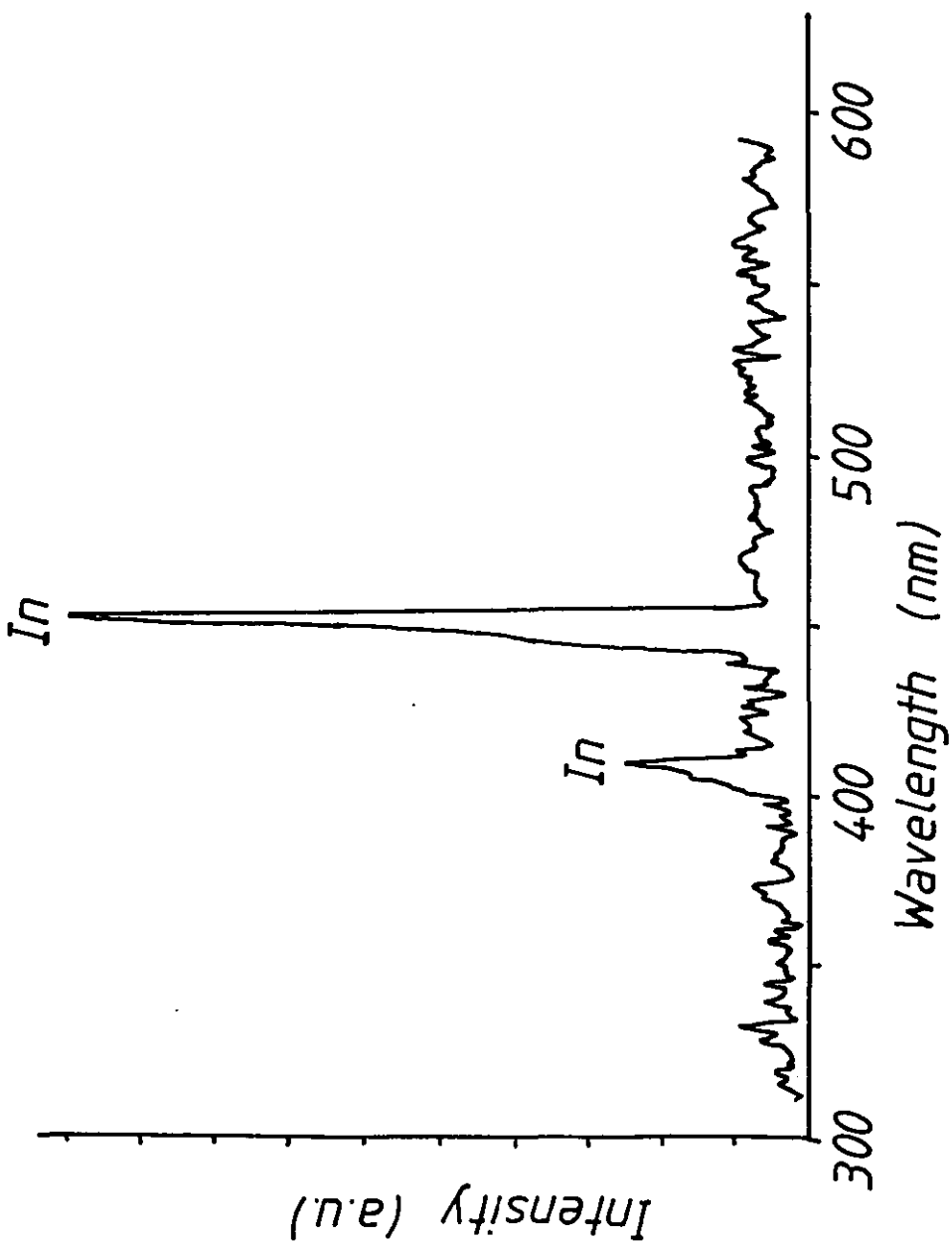

5.3). The filtered light was passed into a photo-multiplier tube (PMT) (mono-light 6117) and the PMT output monitored as the metal emission intensity.

The metal emission intensity, the reactive gas consumption and the magnetron potential were measured as a function of the reactive gas pressure with various magnetron currents. These results are shown in figs 8.6, 8.7 and 8.8 and discussed below.

Reactive gas consumption

The gas consumption curves are shown in fig 8.6. These curves raise several points:-

1. Initial gradient is independent of magnetron current as postulated (see chapter 7).
2. The consumption curves do not scale as current or power (as claimed by Kadlec et al (ref 1) (table 8.1).

Table 8.1: Scaling of reactive gas consumption

Factor	Factor/Current(A)	Factor/Power(kW)
O_2 pressure	0.20 (@ 2 A)	0.53
at roll off	0.12 (@ 4 A)	0.29
(mTorr)	0.083 (@ 6 A)	0.155
	0.078 (@ 8 A)	0.149
Maximum O_2	4.20	11.3
consumption	4.58	11.1
(sccm)	3.97	7.18
	3.45	6.63
O_2 consumption	----	----
of poisoned	0.75	1.90
target	1.00	2.33
(sccm)	1.33	3.07

3. Gradient of roll off ie critical pumping rate is independent of magnetron current.

Fig. 8·6 : Oxygen consumption for indium in the A4 batch coater.

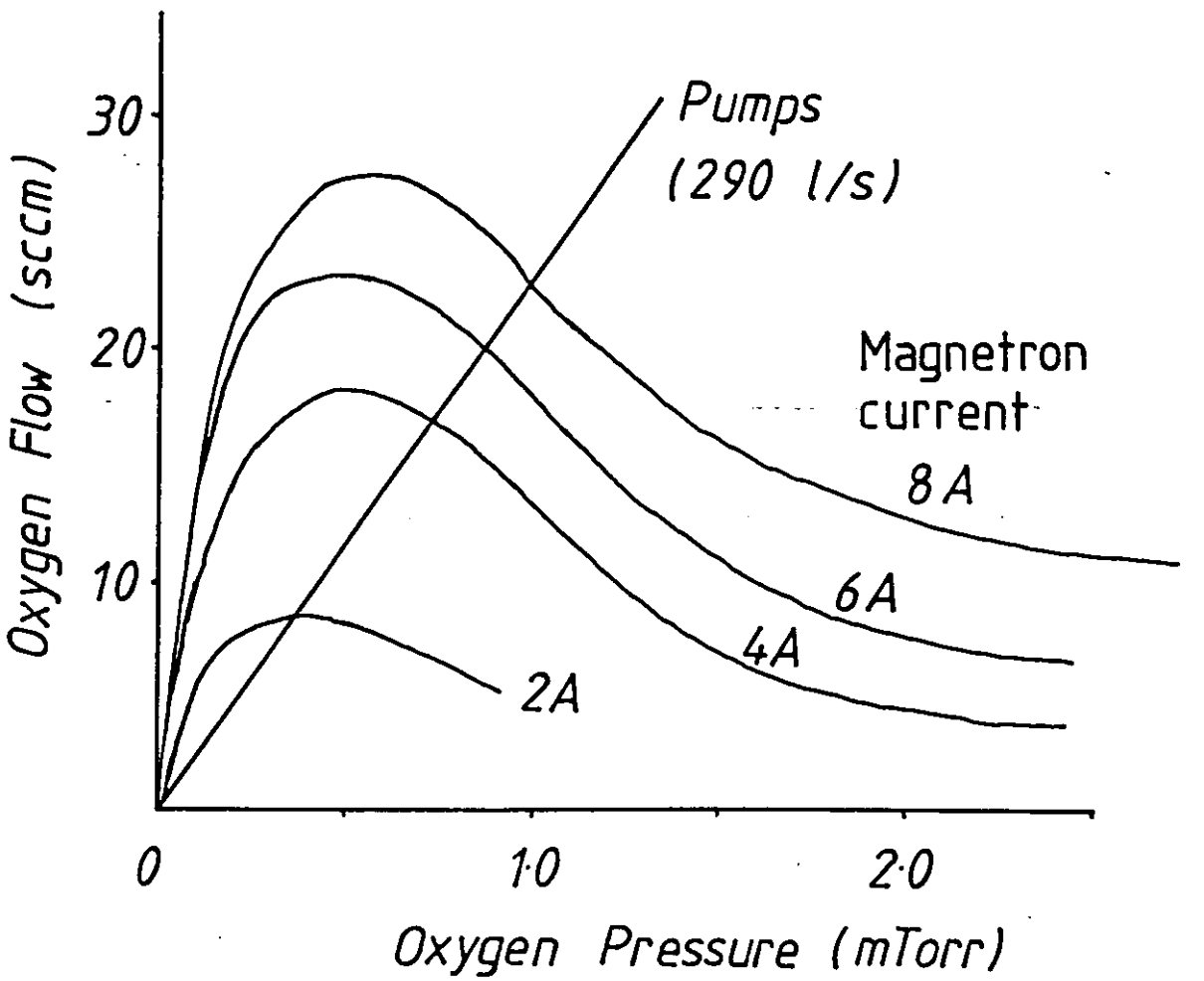

In emission intensity

From fig 8.7 it appears that the normalized emission intensity as a function of reactive gas pressure is independent of the magnetron current. This is surprising in the light of the papers discussed in section 3.3. From these it is expected that at higher magnetron currents the target should poison at higher reactive gas pressures. This should be reflected in the emission intensity falling off at higher pressures as the magnetron current is increased. However this does not seem to be the case. Such a result implies that the target condition f(p) is independent of the magnetron current. This is surprising but does not contradict the theory covered in section 3.3 as this uses a critical reactive gas pressure p*. The relationship between p* and the magnetron current I is of interest here. Our results imply that p* is independent of I.

Magnetron voltage

Changes in the target surface are expected to change the magnetron potential due to the change in the secondary electron coefficient (see section 3.3). However the magnetron potential also depends on other factors. The observed variation of this potential (fig 8.8) is inconclusive as an indicator of the target condition as the magnetron discharge can change modes at low currents. For 4 A and 6 A it looks as if varying the current does influence the target condition. However the curves for 6 A and 8 A fall at similar reactive gas pressures ie varying current does not influence target condition. I presume then that f(p) is not the only quantity changing with the current and reactive gas pressure.

Metal emission intensity

As I am using the metal emission intensity as a diagnostic it is interesting to see how this intensity depends on the magnetron power. If the electron energy distribution is independent of power we would expect (see section 3.6) that the metal emission intensity E is

$$E = \text{const.} N_e . N_{METAL}$$

where N_e = electron density (m^{-3})

N_{METAL} = metal density (m^{-3})

Fig. 8·7 : Indium emission intensity (normalized) against oxygen pressure.

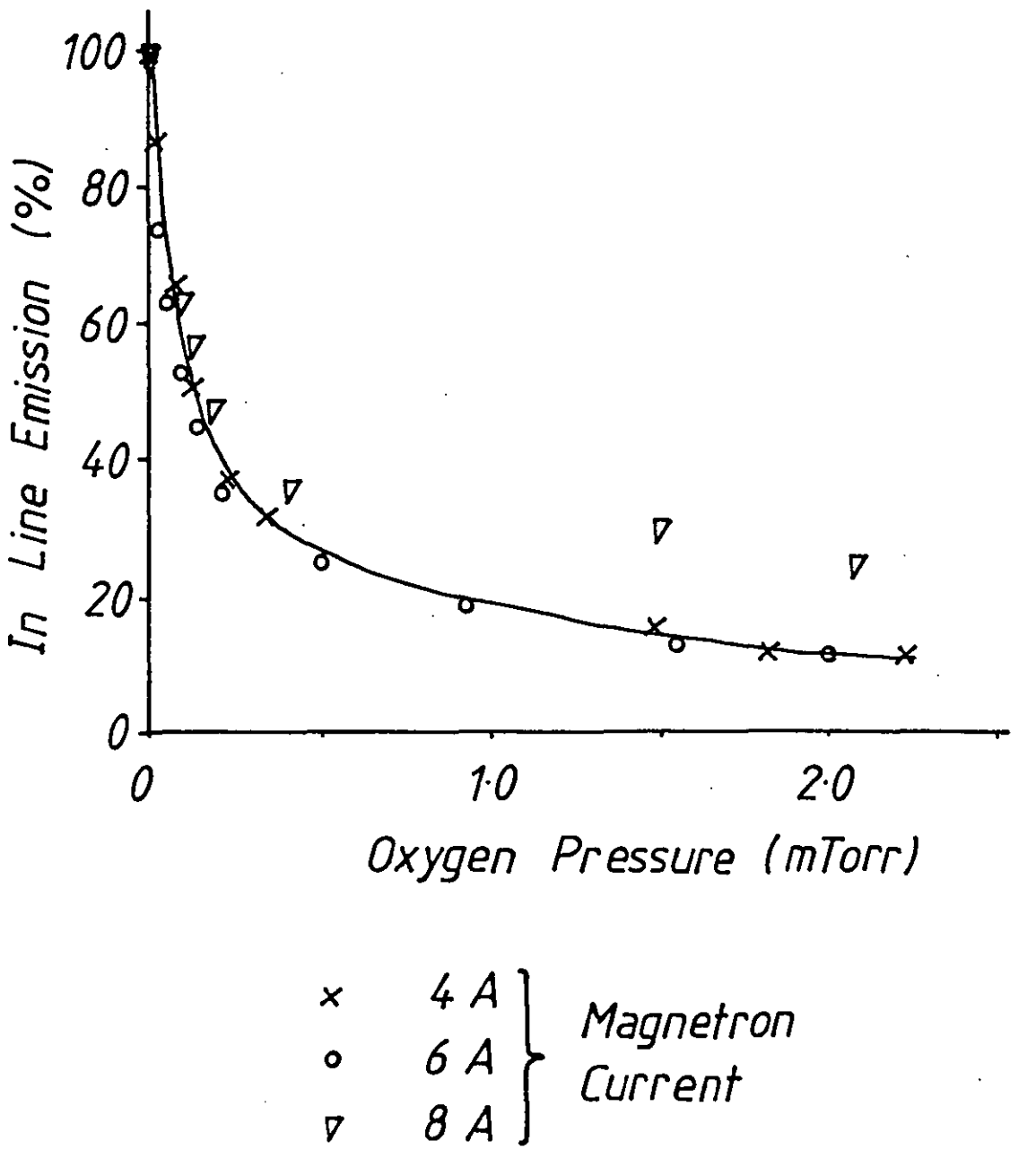

Fig. 8·8 : Magnetron potential against oxygen pressure.

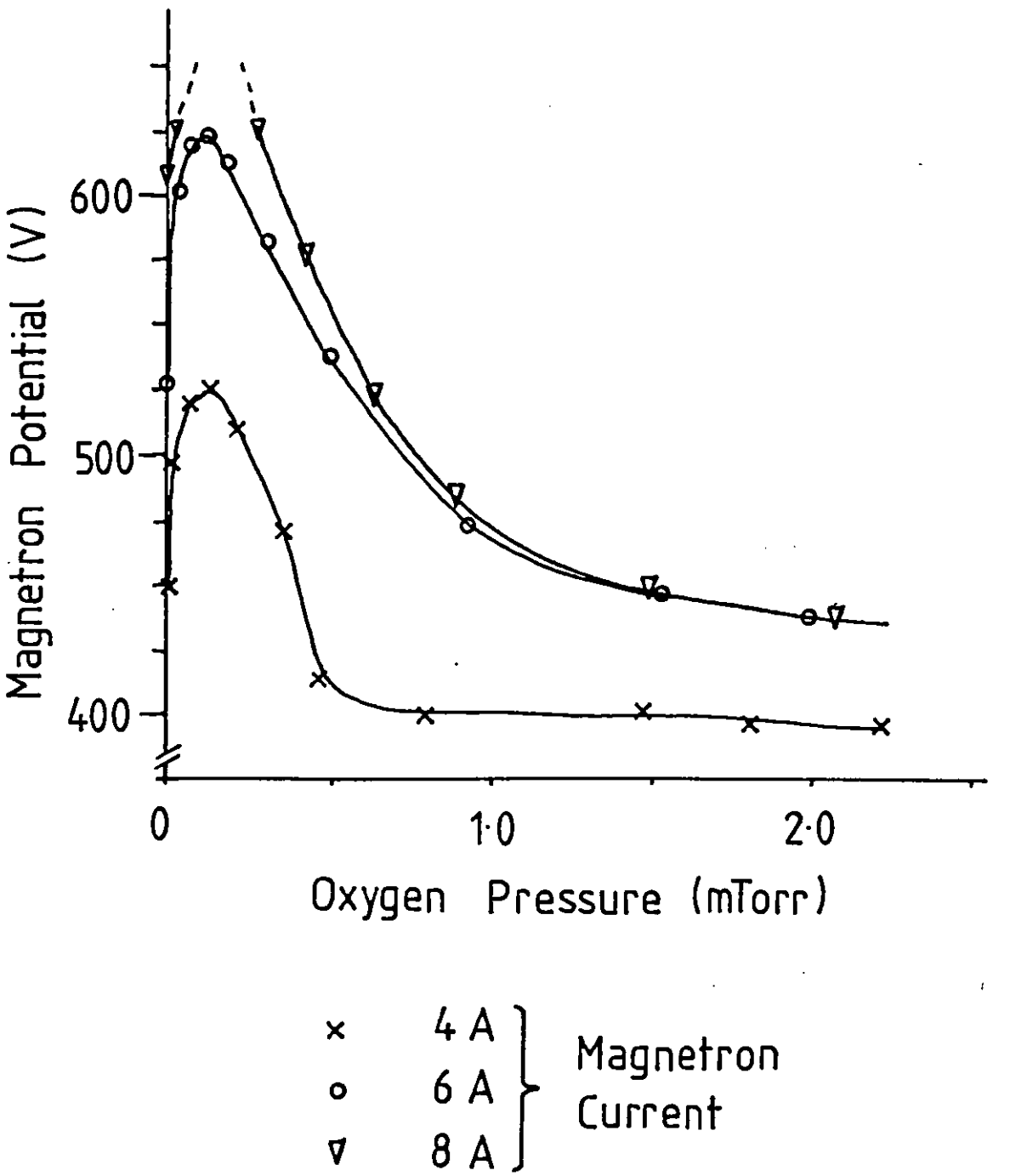

Now under the simple assumptions that N_e and N_{METAL} are proportional to the magnetron power we get

$$E = \text{const.power}^2$$

Running in Ar only we measured the emission intensity as a function of magnetron power. The result is shown in fig 8.9a and least squares fitting a line to a log.log plot of this data gives

$$E = \text{const.power}^{1.7}$$

Emission intensity plotted against power to the 1.7 then gives the plot in fig 8.9b which is close to linear. The same effect was seen recently by Pech et al (ref 2) who found the metal emission intensity was proportional to the magnetron power to 1.6 for a Ti target. These results imply that either or both our assumptions of N_e and N_{METAL} being proportional to power are not true.

The intensity of the Ar line at 763 nm is however linear with magnetron power (fig 8.10). Here the density of the emitting species (now Ar) is constant so any variation will be due to N_e ie as fig 8.10 is linear N_e is proportional to power. These two results then show that

$$N_{METAL} = \text{const.power}^{0.7}$$

PEM of Everest plasmas

Because of the low opacity of magnetron plasmas the emitted light intensity is increased by viewing along an increased length of plasma. In the Everest coater the viewing length is 2.7 m (along the magnetron) instead of 0.05 m (across the magnetron) in our coater. Even with its reduced power density the light intensity from the Everest coater is high. Spectra can then be easily obtained with low background noise. Fig 8.11 shows spectra from the aluminium cathode (Al, Ar) and the tin cathode (Sn, Ar, O). These were obtained with a Rofin rotating grating spectrometer and photographed from the expanded CRT display. The spectra were recorded on separate channels of a storage oscilloscope for cross calibration. The low wavelength end of the spectra are lost due to absorbtion below 340 nm in the glass window. The emission lines chosen for calibration are shown in table 8.2. These were picked as

Fig. 8·9 : Metal emission intensity against magnetron power (In line at 451 nm).

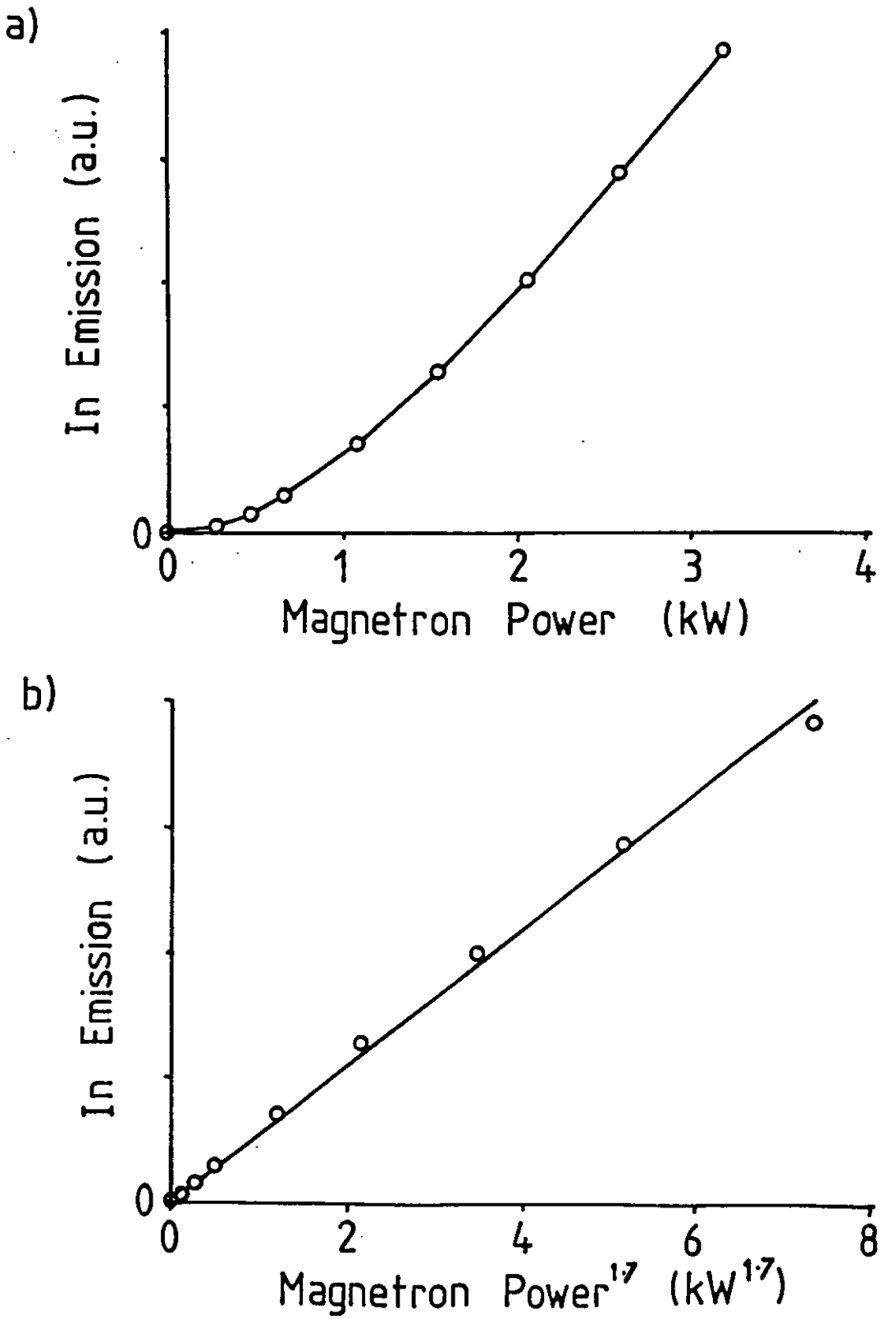

Fig. 8·10 : Argon emission intensity against magnetron power (Ar line at 763 nm).

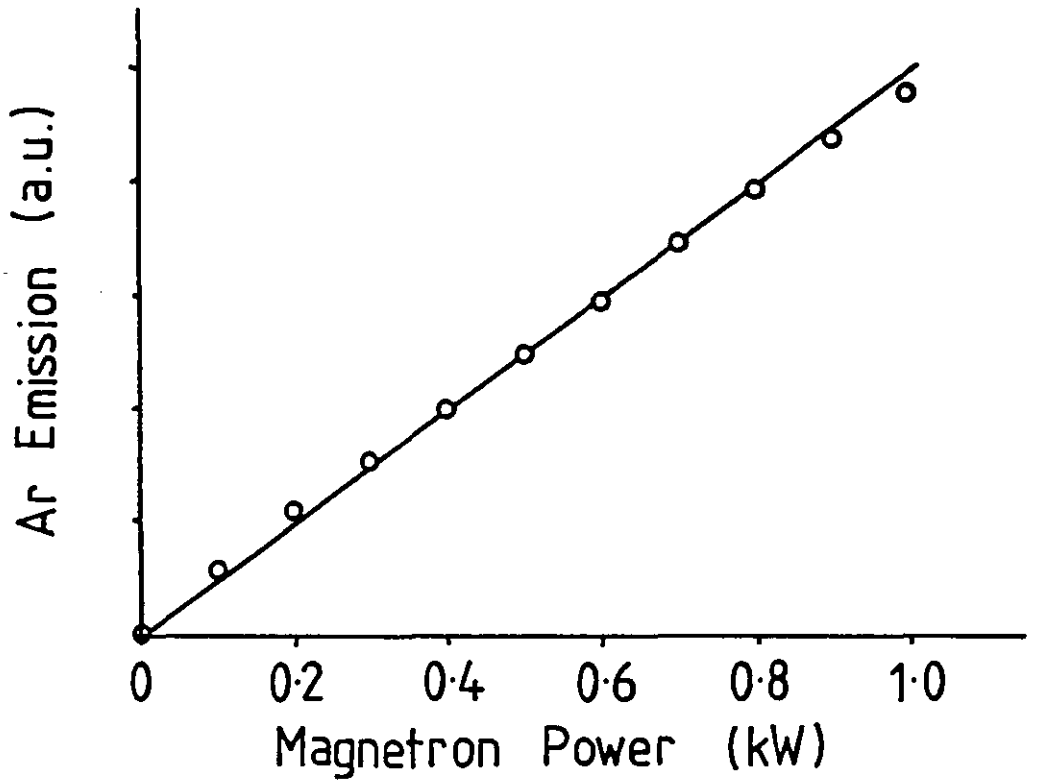

Fig. 8·11 : Emission spectra from the Everest magnetrons.

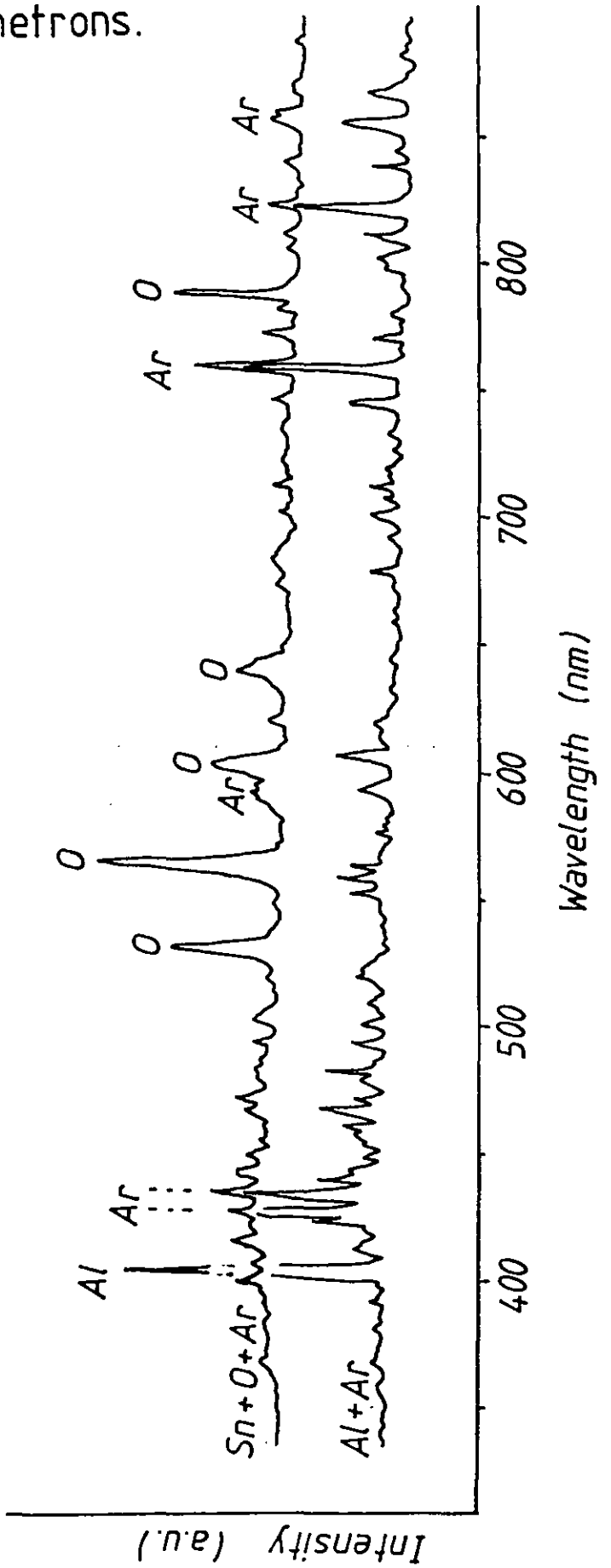

strong lines which cover the complete range of the spectra.

Table 8.2: Calibration lines

Species	Wavelength (nm)
Al	395
O	533
O	600
O	645
O	777
Ar	826

For these lines a linear least squares fit was done between the wavelength and the measured line position. This then gave the wavelength scale plotted. The calibration Rofin spectra gives a resolution of 2 nm. The positional accuracy is worse at about +/- 10 nm, this could probably be improved by a direct print out from the oscilloscope. The lines from the plasma are assigned to species present (refs 3, 4). Only neutral lines were necessary and no molecular or ionized species are required to explain the major features of the plasma emissions. To positively identify molecular or ionized species a much higher wavelength resolution is needed (ref 5). The lines present only in the Sn/O/Ar plasma (cathode K5) are tabulated in table 8.3. The additional lines in the Al/Ar spectrum (cathode K4) are given in table 8.4. No oxygen lines are visible in the Al/Ar spectrum even though it is known that oxygen passes from K5 to K4 (see section 5.3).

Table 8.3: Lines in the Sn/O/Ar Spectrum

Wavelength (nm) Measured	True	Height (a.u.)	Species
400		6	
406	404	2	Ar
531	533	20	O (3 lines)
565	558	34	O
598	596	3	O (2 lines)
640	645	10	O (3 lines)
673		2	
683		3	
788	777	22	O (3 lines)
860		4	

Table 8.4: Lines in the Al/Ar Spectrum

Wavelength (nm) Measured	True	Height (a.u.)	Species
402	395	48	Al
412		4	N(411) or Ar(416)
425	426	26	Ar
433	434	25	Ar
440		8	
460		6	
467		11	
471		4	
481		11	
494		6	
500		4	
508		3	
521	522	5	Ar
552		6	
558		8	
563		6	
577		3	
594		6	Ar (many lines)
606	605	10	Ar (4 lines 603-6)
615		3	
619		5	
679		5	
692		2	
700	697	5	Ar
706	707	2	Ar
713	715	5	Ar
746	750	9	Ar (2 lines)
758	763	28	Ar
771	772	5	Ar (2 lines)
779		2	
798	795	4	Ar
802	801	5	Ar (2 lines)
810	810	8	Ar (2 lines)
823	826	22	Ar
838	841	7	Ar (2 lines)
844		2	
856	852	12	Ar
869	867	8	Ar
881	885	2	Ar

The relative intensities of the spectral lines differ greatly from those values given in references (refs 3, 4). For instance, the oxygen spectrum in the CRC handbook has two lines of similar intensity at 533 nm and 544 nm. The line at 544 nm is entirely absent in our spectrum. This will be due mainly to changes in the excitation probability (section 3.6) with electron energy. I am unable to find the excitation energy for the oxygen 533 and 544 lines but the absence of the 544 line suggests that its excitation energy is greater than the available electron energy. The excitation energy for a selection of the major lines is given in table 8.5 (ref 4). These span a range of energies and it is interesting that those lines with low excitation potentials are stronger. This indicates an electron energy of the order of 10 eV which is in line with the langmuir probe measurements of K. Oka which give T_e = 2-9 eV (ref 6).

Table 8.5: Spectral excitation energy

Wavelength (nm)	Height (a.u.)	Species	Excitation energy (eV)
395	48	Al	3.1
697	5	Ar	13.3
707	2	Ar	13.2
750	9	Ar	13.4
777	22	O	10.7
810	8	Ar	13.0

Lastly there is the possibility of in situ detection of impurities while depositing the film. As the low wavelength regions are not accessible without quartz optics we are currently limited to 350-850 nm. The most troublesome impurities are water (outgassing), nitrogen and oxygen (air leaks) or hydrocarbons (backstreaming and polymer outgassing). The molecular band emissions for water, oxygen and nitrogen are all in the UV (around 200 nm). However, the atomic lines would be expected as the plasma will 'crack' the molecules. Oxygen is visible at 777 nm. Nitrogen is obscured at 411 nm by an Ar line at 416 nm but there may be other weaker nitrogen lines in clearer regions of the spectrum. Hydrogen has a strong line at 656 nm in a clear region of the spectrum. Only carbon has its strong lines in the UV but again there may be weaker lines at more accessible wavelengths.

Summary

- For uniform metal arrival rates any substrate masks should be placed as close to the substrate as possible.
- For uniform reactive gas pressures a distribution manifold must be used.
- The reactive gas consumption curves do not scale with magnetron current or power. The peak reactive gas consumption by the film does scale approximately with magnetron current.
- The fraction of the target remaining metallic f(p) is a strong function of reactive gas pressure but does not appear to change drastically with the magnetron current (or power).
- The metal emission intensity increases with magnetron power to the 1.7. The argon emission intensity increases linearly with magnetron power. This implies that the electron density is proportional to power while the metal density is proportional to power to the 0.7.
- Spectra from the Everest plasma show many emission lines. Of particular use is the strong oxygen line at 777 nm which is away from inert gas or metal emission lines. The tin emission lines are in the UV and necessitate the use of quartz optics. The many Ar lines are catalogued.

REFERENCES: CHAPTER 8

1. Kadlec S., Vyskocil J., and Musil J., "A microphysical model of the reactive sputter deposition of thin films", E-MRS meeting, vol XV, Les Editions de Physiques, Paris, p161-167, 1987.

2. Pech T., Chabrerie J.P., and Ricard A., J. Vac. Sci. Technol., A6(5), 2987-2991, 1988.

3. 'Handbook of Chemistry and Physics', CRC Press, Boca Rata, USA, 1983.

4. Harrison G.R., "MIT wavelength tables", Wiley and Sons, New York, 1939.

5. Martin P.J., Netterfield R.P., McKenzie D.R., Falconer I.S., Pacey C.G., Tomas P., and Sainty W.G., J. Vac. Sci. Technol.,

A5(1), p22-28, 1987.

6. Oka K., "Plasma activated growth of reactively sputtered thin films", PhD Thesis, LUT, 1988.

9. RESULTS - PEM CONTROL

9.1 CONTINUOUS CONTROL

Schiller et al (ref 1) claim that controlling the reactive gas flow to keep the metal emission line intensity constant will eliminate the pressure instability. They term this plasma emission monitor (PEM) control. The mechanism that causes the instability was shown in fig 6.4. This feedback cycle can be broken by matching the reactive gas admission rate and the reactive gas consumption to give zero surplus reactive gas. So our aim must be to produce the effect

$$Q_S = Q_{IN} - Q_{FILM} - Q_{PUMP} = 0$$

Obviously to achieve this effect we can control Q_{IN} (input reactive gas flow), Q_{FILM} (magnetron power), or Q_{PUMP} (chamber pumping rate). To control the chamber pumping rate a dynamic throttle valve must be used and these typically have response time constants of around 0.6 s (2-3 s to reach equilibrium (ref 2)). To control Q_{FILM} we can alter the magnetron power. Q_{FILM} should then change as a new getter surface is formed. The monolayer formation time is 1/R where R is the deposition rate in monolayers/s. We can expect for indium/oxygen that R will reach 20/s or higher (see section 6.3) giving a response time of 0.05 s. Most directly Q_{IN} (the input reactive gas flow) can be controlled. Piezo-electric valves are available with a response time of 0.01 s. As this last control method at first sight provides the fastest response I chose to investigate direct control of Q_{IN}.

We also need a control signal. This can be obtained from any parameter which varies across the pressure instability (ie reactive gas pressure, plasma emission at the metal or reactive gas wavelengths, or magnetron potential). The reactive gas pressure is not suitable due to the inherent time delay on a gauge remote from the reaction zone. The magnetron potential can be used but drifts as the target ages and has low sensitivity in certain regions of partial pressure. This leaves plasma emission as a control signal. A potential problem if using magnetron power as the controlled parameter is the dependence of plasma emission intensity on the magnetron power.

Schiller's control system and previous feedback systems were based on either the plasma line emission intensity (ref 1, 3) or a mass spectrometer signal (ref 4). In the preceding section I obtained a signal proportional to the indium line emission from the plasma and now use this in the control loop of fig 9.1.

This PEM control system was set in operation with proportional control and we found that it operated well at low magnetron currents with only a slight oscillation. However as the current was increased the oscillation amplitude increased (fig 9.2). For the reasons stated in the introduction (chapter 2) it is often necessary to operate the magnetron at high current to obtain an economic production rate. Therefore the fact that our PEM operates well at low magnetron currents is of little direct use. This may also be why the original US patent has not come into widespread use and why Schiller's published results are for such a low power density (1.25 kW into a 0.6 m magnetron).

It has previously been found that any time delay in the feedback loop led to oscillation (ref 4). To check the response time of the gas flow components I changed both the control valve and the gas distribution system. Fig 9.3 shows these results for

(a) electro-mechanical valve, gas manifold, and 0.5 m connecting pipe,

(b) piezo-electric valve, gas manifold, and 0.5 m connecting pipe,

(c) piezo-electric valve, gas manifold and 0.14 m connecting pipe,

(d) piezo-electric valve, and 0.14 m connecting pipe.

As a faster response control system is used we obtain better control. We cannot directly measure the time response of these components but the oscillation period can be used as being dependent on the response time. The information in fig 9.3 is presented in a different form in fig 9.4. At small amplitudes the data is reasonably spaced and implies that for a control accuracy of a few percent, an oscillation period of less than 50 ms is required. The best two points are from the same control system, but with and without the gas distribution manifold. This indicates a problem as the gas distribution manifold appears to have a time constant longer than 100 ms (ie it cannot respond fast enough for a 50 ms oscillation period) and I have previously shown that

Fig. 9·1 : The PEM control loop.

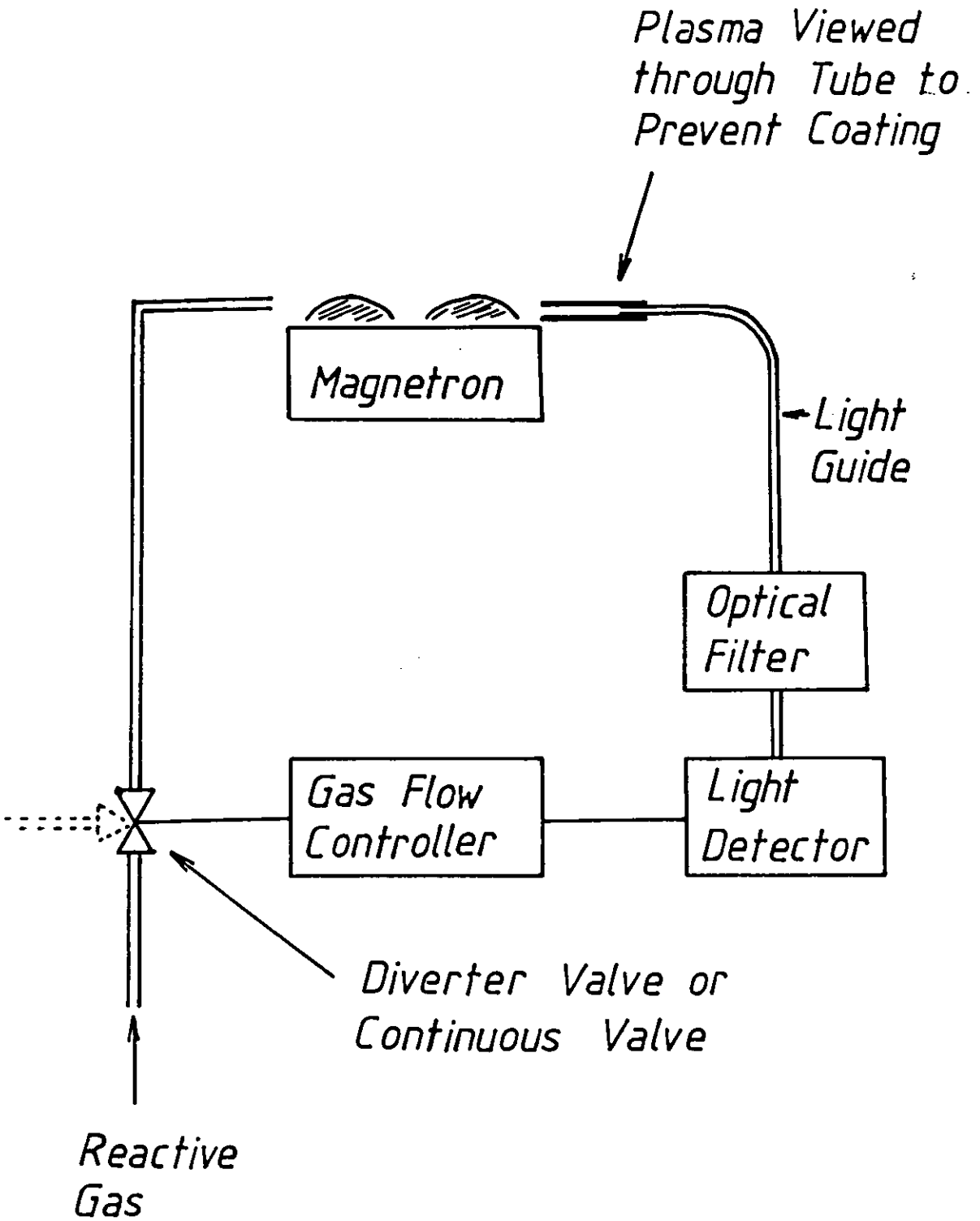

Fig. 9·2 : The effect of magnetron current on control quality.

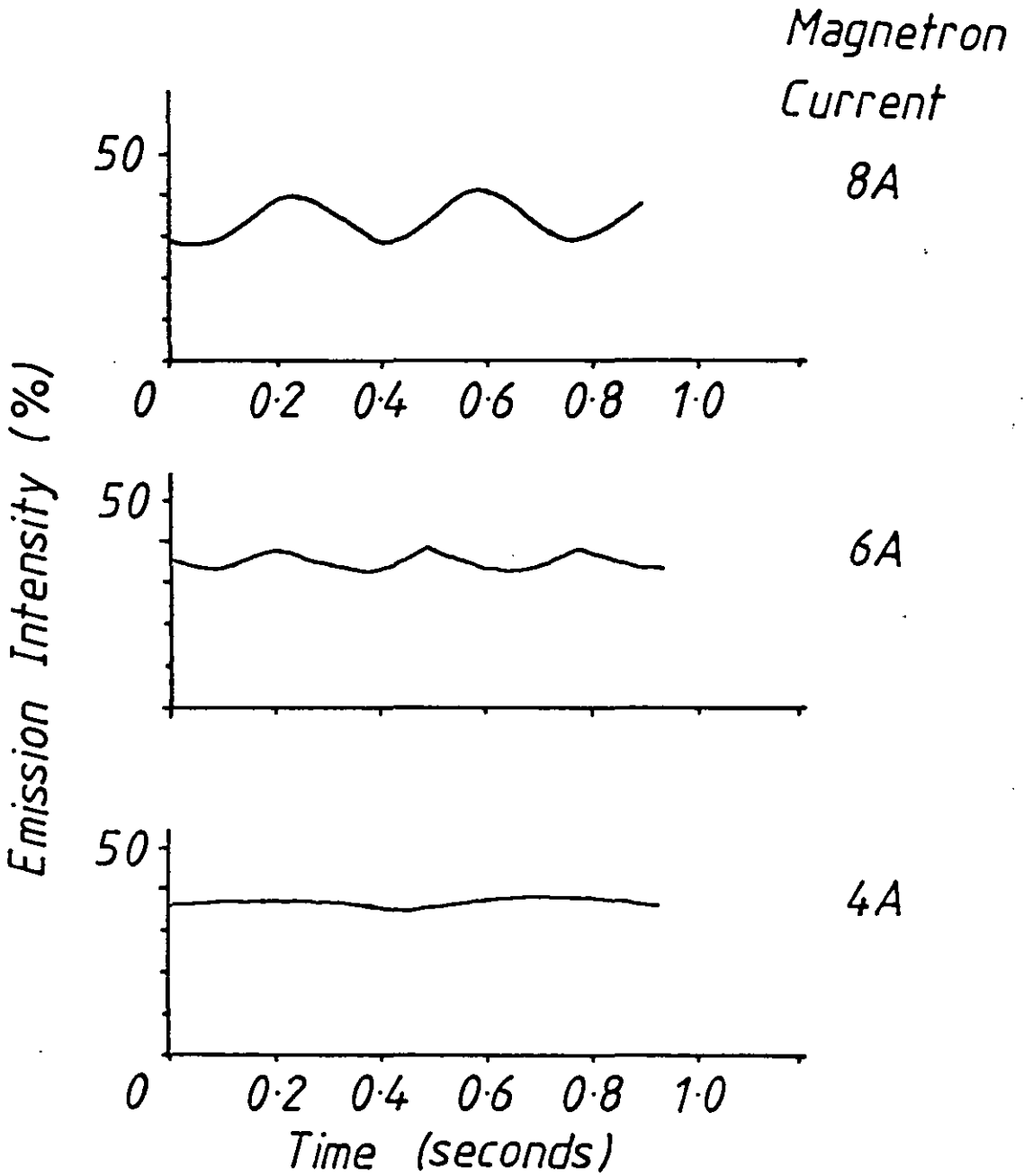

Fig. 9·3 : Control with various gas components.

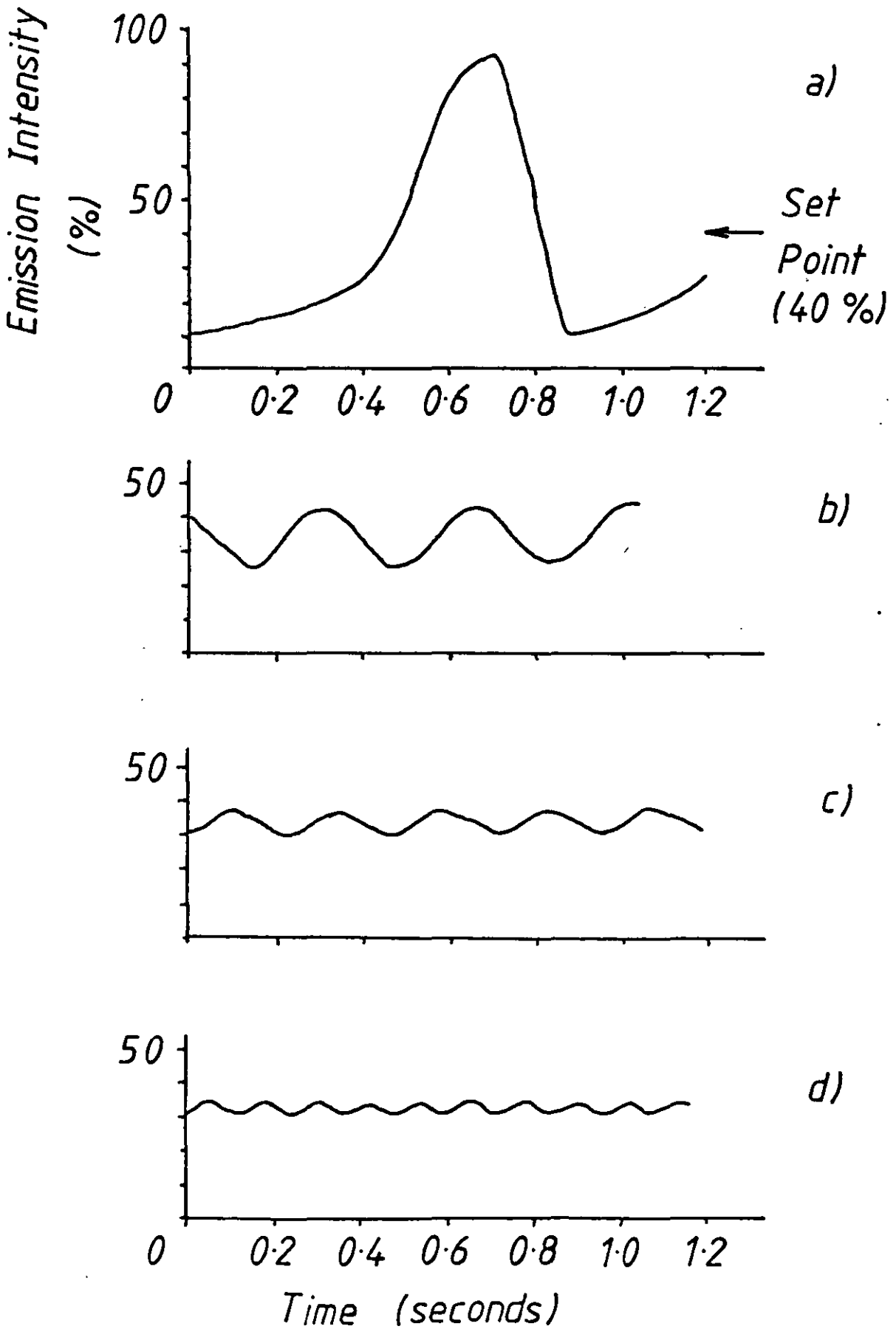

Fig. 9·4 : Oscillation amplitude against period for PEM control (at magnetron current of 8A).

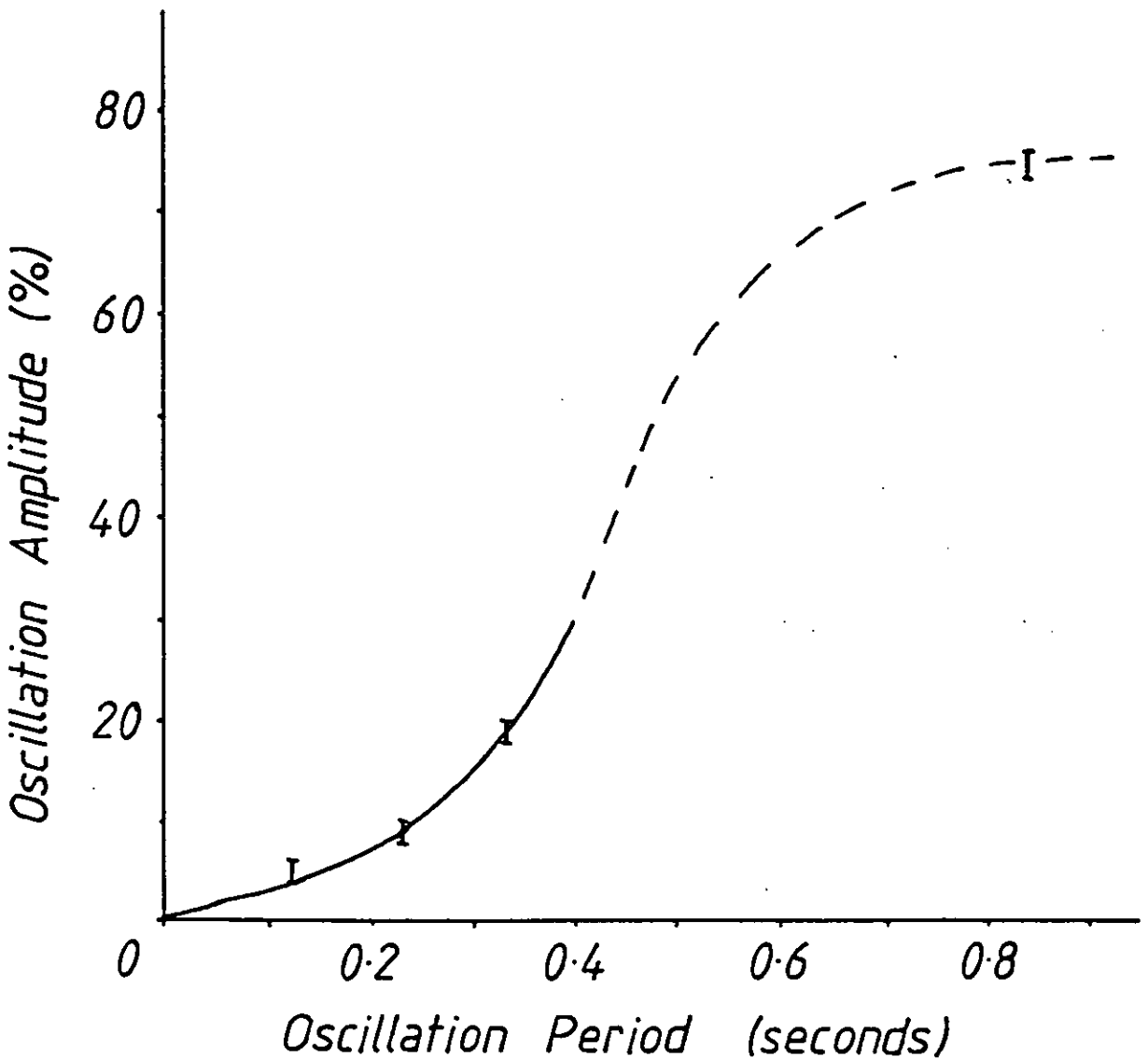

without such a manifold uniform reactive gas pressures (and uniform film properties) are not achieved (section 8.1). The gas distribution manifold then limits the overall response time as the intensity measurement, electronics and valve can all respond much faster than 50 ms.

It was found late on in this investigation that if proportional and integrating control is used then stable operation can be obtained with a manifold. At high gain and low integrating time oscillation occurs but as the gain is reduced and the integrating time increased the oscillations decay to the set point. The response of this type of control loop to a disturbance (an arc) is shown in fig 9.5.

9.2 GAS DISTRIBUTION MANIFOLDS

We have shown that a gas distribution manifold is necessary for uniform film properties (section 8.1) and that the same manifold limits the response time and hence the accuracy of a feedback controller (section 9.1). It would therefore be useful to evaluate the time constant of the gas distribution manifold.

Our gas distribution manifold is a rectangular loop of 8 mm bore pipe, 1.3 m long that encircles the deposition zone. The gas passes from the manifold to the chamber via twenty six 1 mm diameter holes drilled around its inside edge. If pressure gradients within the manifold are neglected and perfect gas behaviour assumed we can calculate a time constant. With the gas flow in (Q_{in}) a function of time ($Q_{in} = Q_0$ at $t < 0$ and $Q_{in} = 0$ at $t >= 0$) we have a gas flow out Q_{out} of

$$Q_{out} = Q_0 \exp(-t.Sm/Vm)$$

where S_m = conductance out of manifold (l/s)
V_m = volume of manifold (l)

This is not useful unless we know S_m and we cannot calculate S_m without an assumption about the flow regime. Therefore we measured the conductance of several hole sizes with realistic gas flows (1-10 sccm per hole).

Fig. 9·5 : The observed return to set point after an arc disturbance.

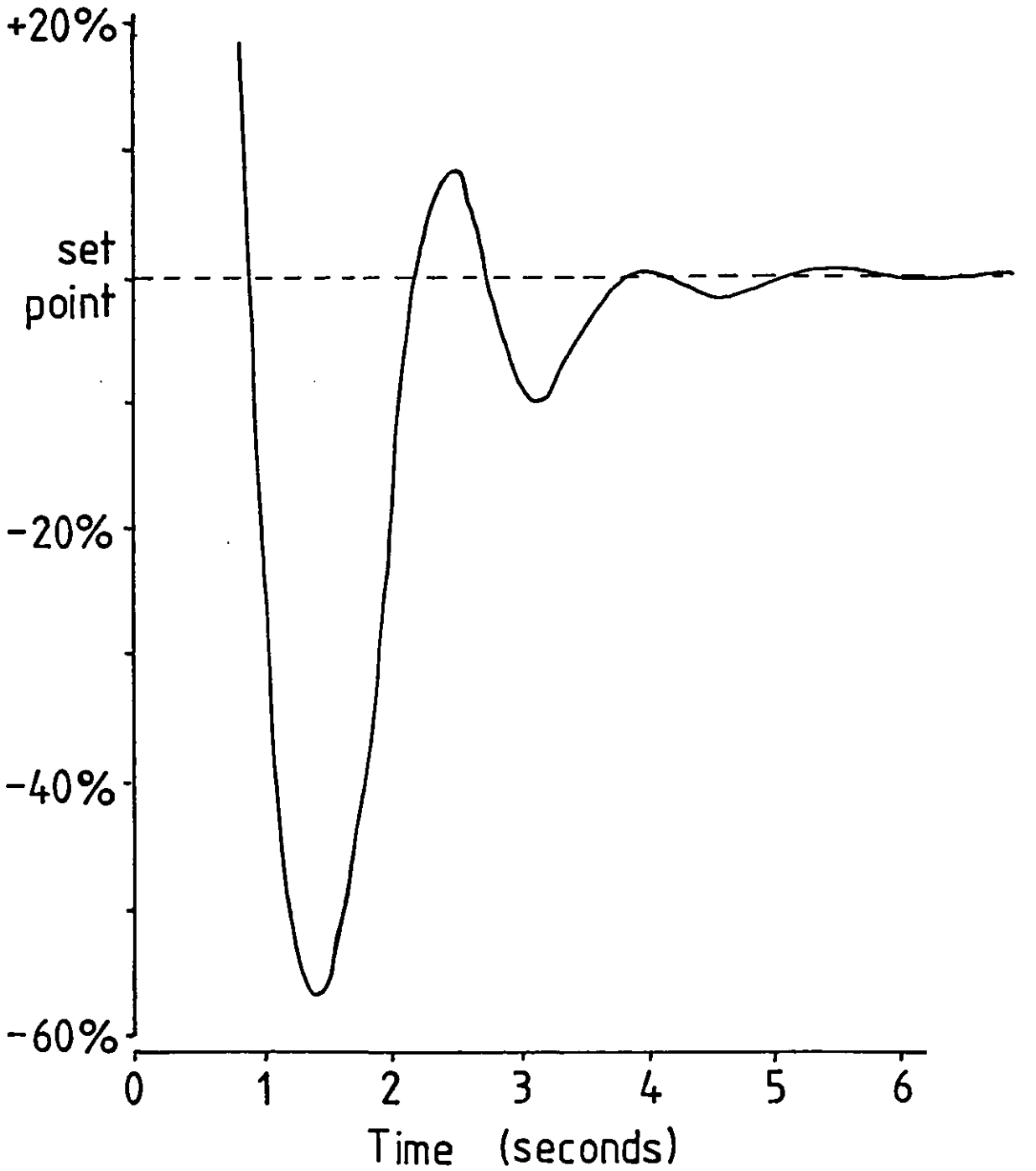

.6) with an internal
les drilled in 1 mm
nanifold. The hole
Photoplan microscope
a VG 78-7 mass flow
5%). For each test
ow. The pressure was
g 9.7) and I obtained
adient and the area of
hole. The results are
e last digit are shown
g (ref 5).

ctances

Reynolds number at 1 sccm
0.36
0.47
0.73
0.86
1.4
2.2

olecular flow regime should
For the largest hole sizes
flow (ie 9.6 l/s/cm^2) and
is reduction could be due to
ratio of the hole, onset of

and the smaller holes will
1 which will reduce the
s well characterized and when
r measurement. The fall in

Measured hole conductance

The apparatus used was a test manifold (fig 9.6) with an internal pressure gauge (capacitance manometer). Test holes drilled in 1 mm thick plate were placed over the end of this manifold. The hole diameters were measured optically on a Vickers M41 Photoplan microscope focused down the hole. Ar gas was supplied from a VG 78-7 mass flow controller (manufacturer's specified accuracy of 5%). For each test hole the pressure was measured as a function of flow. The pressure was found to be almost linear with the gas flow (fig 9.7) and I obtained the least squares gradient of this line. This gradient and the area of the test hole give conductance/area for the test hole. The results are shown in fig 9.8 and in table 9.1. Errors in the last digit are shown in brackets and calculated according the Topping (ref 5).

Table 9.1: Measured hole conductances

Hole dia. (mm)	Pressure per unit flow (mTorr/sccm)	Conductance per unit area ($l/s/cm^2$)	Reynolds number at 1 sccm
4.07(2)	9.4(3)	10.4(4)	0.36
3.07(2)	15.6(6)	10.9(5)	0.47
1.97(2)	47.0(2)	8.8(5)	0.73
1.67(2)	80.0(2)	7.2(4)	0.86
1.07(2)	$2.6(1) \times 10^2$	5.5(4)	1.4
0.68(2)	$1.3(1) \times 10^3$	2.8(3)	2.2

The conductance per unit area in the molecular flow regime should be constant (9.6 $l/s/cm^2$ at 300 K for Ar). For the largest hole sizes the conductance/area is that for molecular flow (ie 9.6 $l/s/cm^2$) and for holes less than 3 mm it falls away. This reduction could be due to several mechanisms; change in the aspect ratio of the hole, onset of turbulent flow or change of flow regime.

The test plate used was 1 mm thick and the smaller holes will then have aspect ratios greater than 1 which will reduce the conductance (refs 6, 7). This reduction is well characterized and when calculated gives higher values than our measurement. The fall in

Fig. 9·6 : The test manifold for measuring hole conductance.

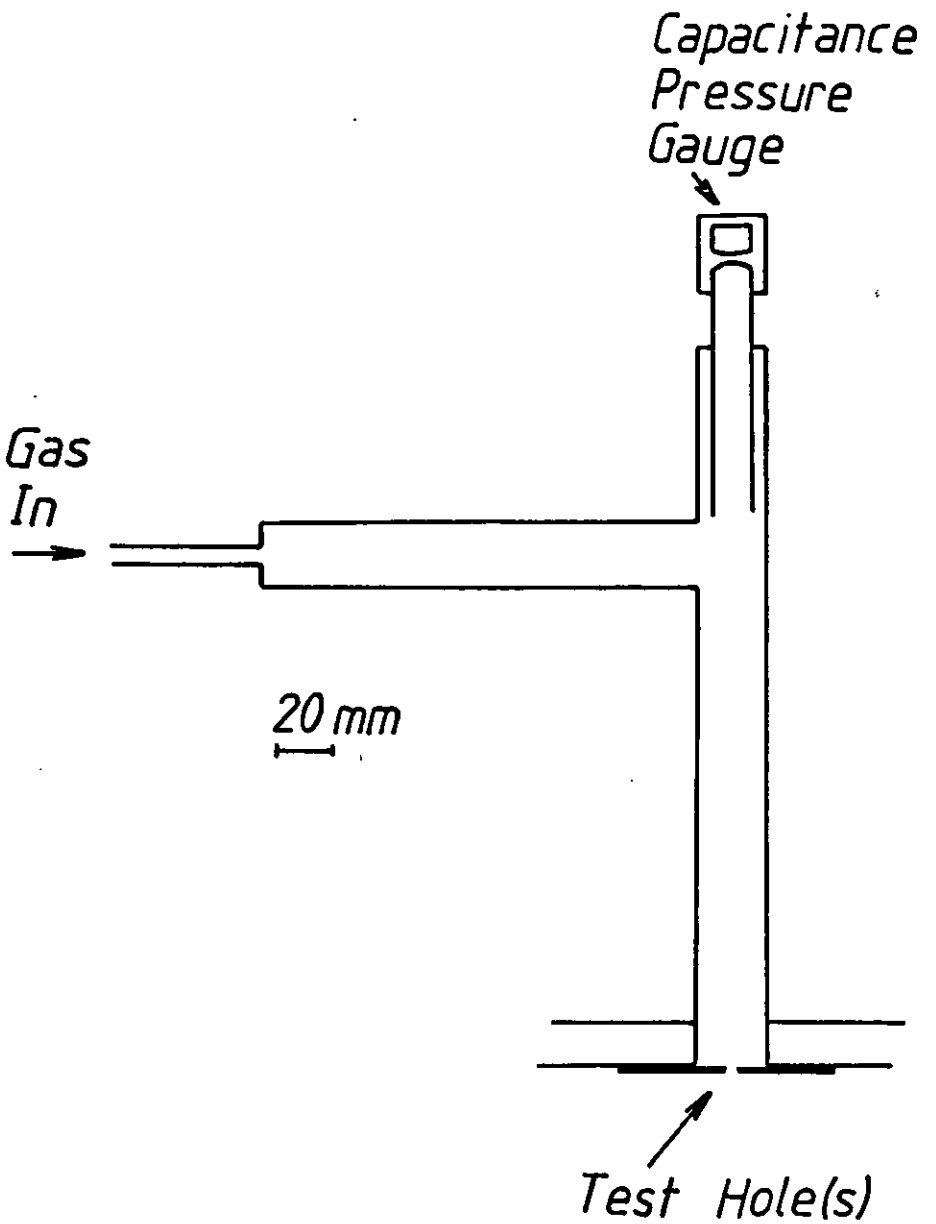

Fig. 9·7 : Measured pressures in the test manifold.

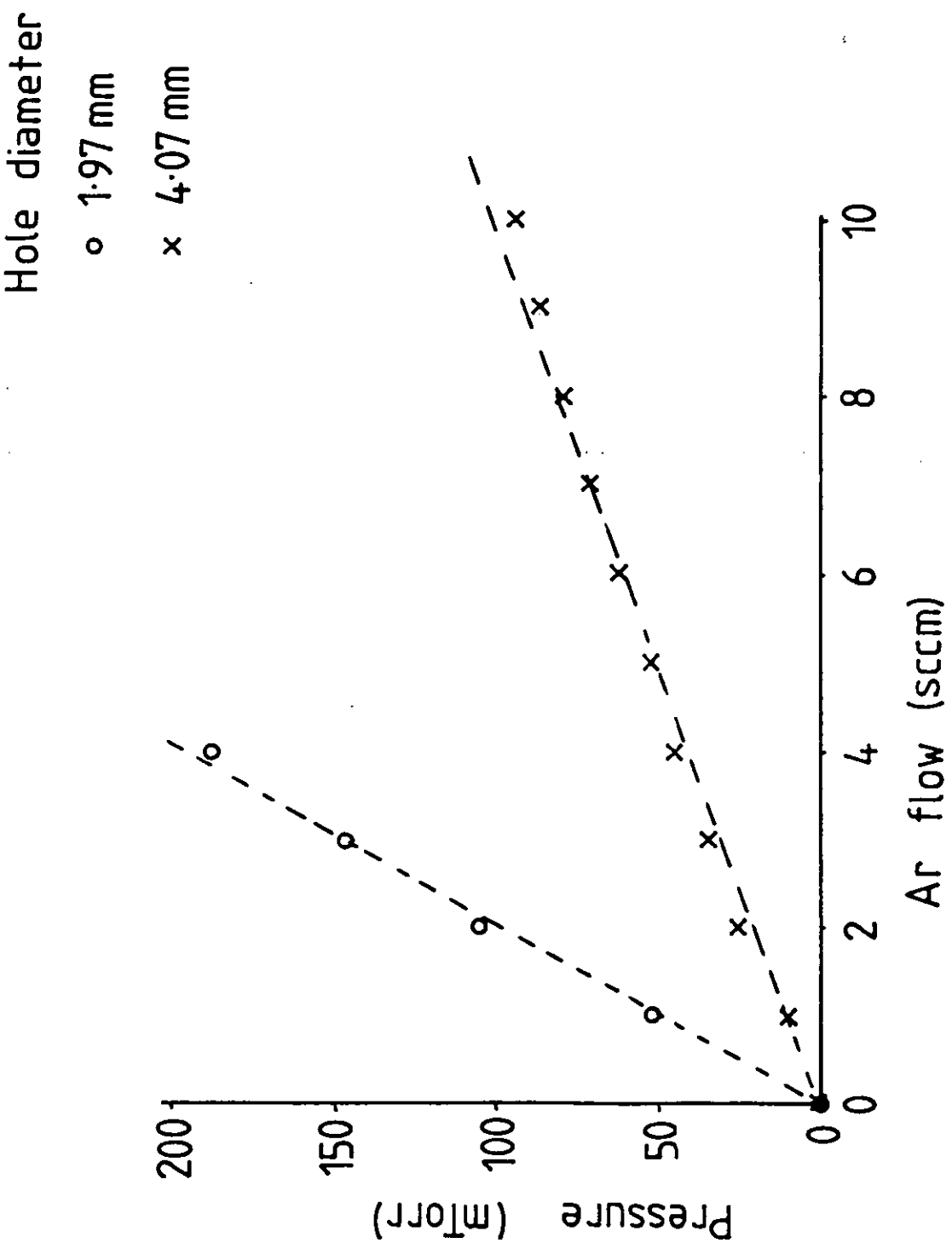

Fig. 9·8 : Measured conductance per unit area against hole size.

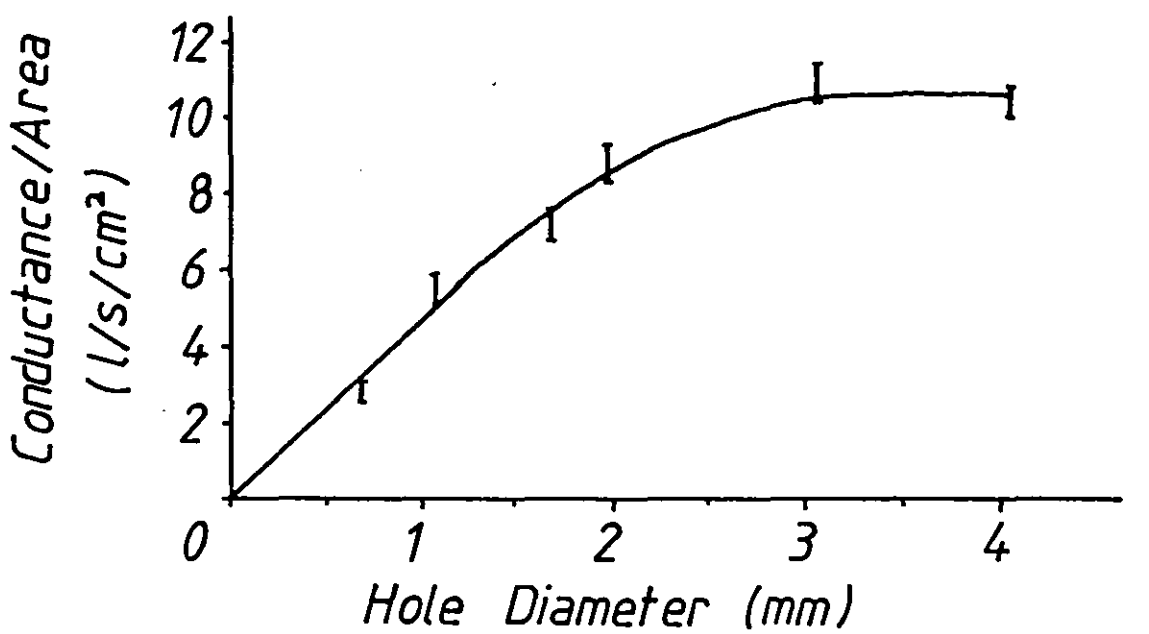

conductance/area due to this effect only becomes significant for holes of 1 mm diameter or less. The observed fall in conductance/area cannot be explained from the change in aspect ratios of the test hole.

The Reynolds number Re of the flow through the hole can be estimated from Q/(4.d) (Q = gas flow in sccm, and d = hole diameter in cm) (ref 8). This is shown in table 9.1 and shows that in all cases we are far from turbulent flow (Re > 2000). The reduction in conductance/area for small holes is not then due to the onset of turbulent flow.

Assuming a gas temperature of 300 K we can calculate the mean free path from the measured pressure (see section 3.7). The flow regime (molecular or viscous) can be decided from the Knudsen number (ref 6). When the mean free path is much larger than the hole size (Knudsen number >> 1) we have molecular flow and when it is much smaller (<< 1) we have viscous flow. At 1 sccm flow per hole the Knudsen number varies between 1 for the 4 mm hole size to 1/20 for the 0.5 mm hole size. These figures are in the transitional flow regime between viscous and molecular flow. This seems the likely explanation for our measured conductance/area. The larger holes have values appropriate for molecular flow and as the hole size is reduced (with a constant gas flow per hole) we move towards viscous flow.

The calculation of gas flow in this intermediate flow regime is possible (refs 9, 10) but such work is really secondary to our requirements. Using our experimental results for the conductance S_B we can calculate a time constant (V_B/S_B) for our manifold. The volume is V_B = 0.07 l. The manifold has 1 mm diameter exit holes so fig 9.8 gives conductance/area of 4.5 l/s/cm^2. This is for argon so correcting by $M^{-1/2}$ (molecular mass see section 3.7) to oxygen give 5.0 l/s/cm^2. Now 26 holes of 1 mm diameter give a conductance of S_B = 1.0 l/s. The manifold time constant is

$$T_B = V_B/S_B = 0.07 \text{ s} \qquad (2)$$

Figures 9.3 and 9.4 show that removing the manifold reduced the oscillation time from 0.23 s to 0.12 s. We cannot directly equate this difference of 0.11 to the manifold time constant but the closeness of the two supports our calculation.

Summary

- For optimum dynamic control of unstable reactive sputtering systems the feedback loop must have the shortest possible time constant. In our system this means less than 10 ms. In practice this is not feasible as the gas distribution manifold has a time constant longer than 10 ms (in our case 70 ms).
- The time constant of the manifold should then be made as short as possible while still maintaining uniformity. As a first step to this we show how the manifold time constant may be calculated.

9.3 ANALYSIS OF CONTINUOUS CONTROL

The analysis of stability and control systems can be found in many textbooks (refs 11, 12). For dynamic control of reactive sputtering this analysis can be done in time space but the result is complex and unwieldy and must be solved numerically (ref 13). In frequency space a more compact solution can be produced. Equations can easily be moved into frequency space by the Laplace transform. As with a Fourier transform for the results to be true all components involved need to be linear.

Time space equations

The equations governing the pressure changes are:-
Firstly by assuming perfect gas behaviour

$$\frac{dP}{dt} = \frac{Q_s}{V} \qquad (1)$$

From the model of chapter 7 I have

$$Q_s = Q_{IN} - Q_{FILM} - Q_{PUMP} \qquad (2)$$

With molecular flow in the pumping orifice we get

$$Q_{PUMP} = P \cdot S_{PUMP} \qquad (3)$$

Lastly by using a straight line for the falling portion of the film consumption (fig 9.9) we can approximate this in the relevant region as

$$Q_{FILM} = Q_{FILM}(0) + S_{FILM} \cdot P \qquad (4)$$

This is making the assumption that the static and dynamic behaviour of Q_{FILM} are the same. If Q_{FILM} does not change significantly on the time scale of the oscillation (200 ms) then $S_{FILM} = 0$. Between these two extremes lies the region where we must consider dQ_{FILM}/dt. This is discussed later in this section.

Substituting equations 2, 3 and 4 into equation 1 gives

Fig. 9·9 : An approximation to the dynamic dependance of Q_{FILM} on the reactive gas pressure (P).

$$Q_{FILM} = Q_{FILM}(0) + S_{FILM} \cdot P$$

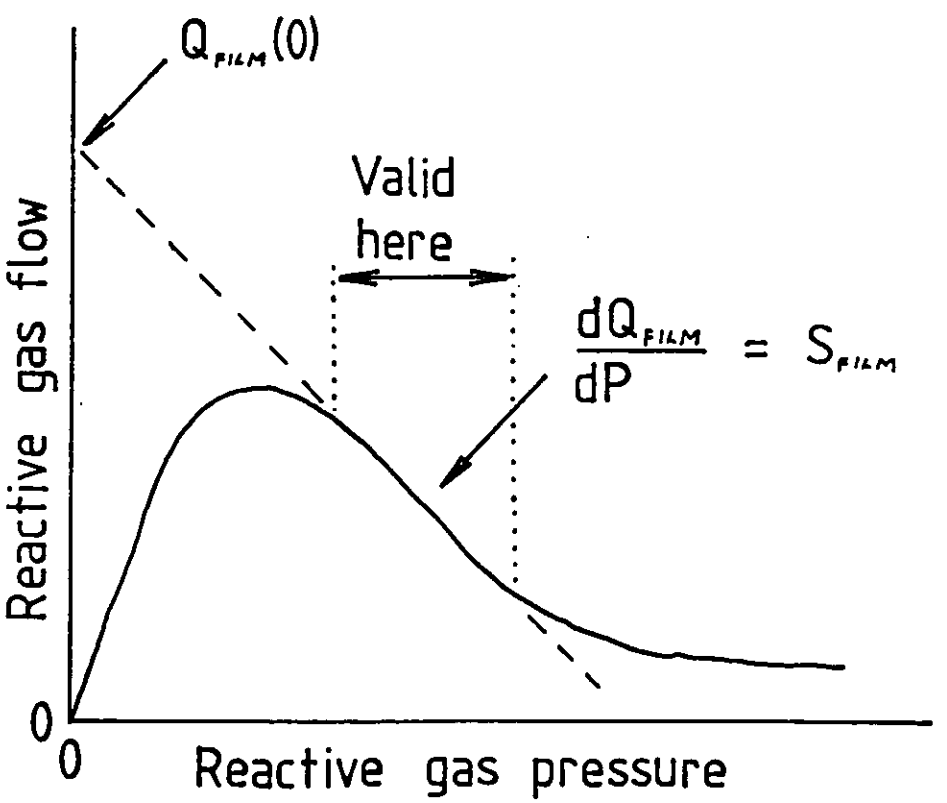

$$\frac{dP}{dt} + A \cdot P + B = 0 \qquad (5)$$

where $A = (S_{FILM} + S_{PUMP})/V$

$B = (Q_{IN} - Q_{FILM}(0))/V$

This equation has a steady state solution

$$P = -B / A$$

This solution is stable if a change ΔP leads to dP/dt opposing this change. We have

$$\frac{dP}{dt} = -A \cdot P - B$$

so putting $P = -B / A + \Delta P$

gives $\frac{dP}{dt} = -A \cdot \Delta P$

ie for stability A must be positive. This is the same stability criterion as found in section 6.4. A simplistic analysis can be done if zero time lag in a feedback loop is assumed and the input gas flow is controlled with a gain K ie $Q_{IN} = Q_{SET} - K.P$. The term A then becomes $(S_{FILM} + S_{PUMP} + K)/V$ and the stability criterion is

$$K > -(S_{FILM} + S_{PUMP})$$

Frequency space equations

In practice Q_{IN} is controlled through a valve and manifold each with a finite response time. To study the response of the complete system with a proportional controller I need to look at the overall frequency response of the combined components (fig 9.10). This response can be obtained from the transfer function G(s) of each component (the ratio in frequency space (s) of output over input for a step input at t=0). The overall open loop gain G(s) is

$$G(s) = Gv(s) \cdot Gp(s) \cdot Gm(s) \cdot Gc(s)$$

Fig. 9·10 : A block diagram of PEM control.

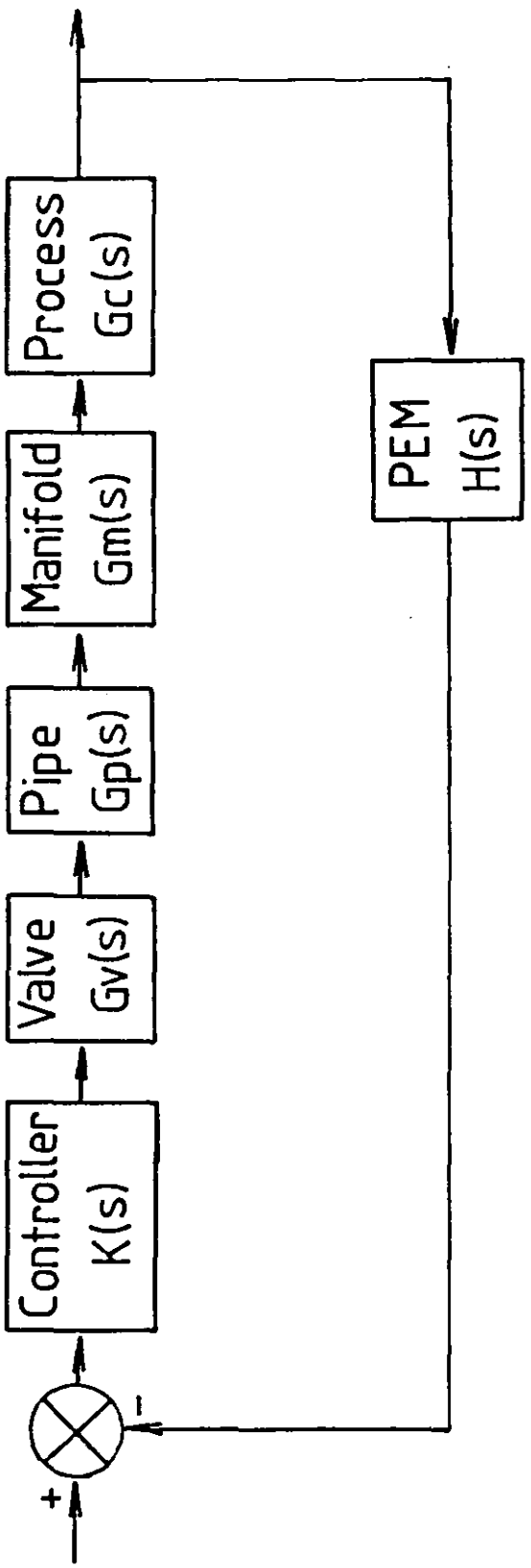

Assuming a fast response valve and short pipe run gives Gv(s) and Gp(s) equal to one. The manifold transfer function can be obtained by Laplace transforming equation 1 after putting $Q_{OUT} = P.S_E$. This gives

$$Gm(s) = \frac{Q_{OUT}(s)}{Q_{IN}(s)} = \frac{1}{(1 + s.T_M)}$$

where $T_M = V_M/S_M$ (as in section 9.1)

The transfer function of the chamber and process Gc(s) can be derived from equation 5. For the transfer function initial conditions are zero so Laplace transforming and inserting the values of A and B gives

$$Gc(s) = \frac{P(s)}{Q_{IN}(s)} = \frac{1}{V.\{s + (S_{FILM} + S_{PUMP})/V\}}$$

The open loop gain can now be obtained as G(s) = Gm(s).Gc(s). With the control loop in place this is modified to give the closed loop gain G'(s).

$$G'(s) = \frac{G(s) \,.\, K(s)}{1 + G(s) \,.\, K(s) \,.\, H(s)}$$

where K(s) = controller gain
H(s) = transducer response

The response time of the photomultiplier is fast (10^{-6} s or better) so H(s) = 1. The denominator of this closed loop gain is the 'characteristic' equation of my control system and its roots describe the control system behaviour. This characteristic equation is

$$1 + G(s) \,.\, K(s) = 0$$

putting in values for G(s) and taking K(s) = K (ie proportional control only) gives

$$1 + \frac{K}{(1 + s.T_M).V.\{s + (S_{FILM} + S_{PUMP})/V\}} = 0$$

Multiplying out gives a quadratic equation in s

$$s^2 + \{\frac{1}{T_B} + \frac{(S_{FILM} + S_{PUMP})}{V}\}.s + \frac{(S_{FILM} + S_{PUMP} + K)}{T_B.V} = 0 \quad (6)$$

This is a standard form for second order systems.

$$s^2 + 2.E.\omega_n.s + \omega_n^2 = 0 \quad (7)$$

where ω_n = undamped natural frequency
E = damping factor.

This standard form responds to a step change in the set point as shown in fig 9.11. This was seen experimentally in fig 9.5 (with ω_n = 17 rad/s, E = 0.05). For rapid control we want a damping factor of around 0.7.

Comparing equations 6 and 7 gives the dimensionally correct terms (K has units of l/s)

$$\omega_n^2 = \frac{(S_{FILM} + S_{PUMP} + k)}{T_B.V}$$

and

$$2.E.\omega_n = \{\frac{1}{T_B} + \frac{(S_{FILM} + S_{PUMP})}{V}\}$$

Interpreting these results gives two points:-

1. There is a minimum feedback gain K = (S_{FILM} + S_{PUMP}) required for stability. This is the same result as from a simplistic analysis ignoring response times.
2. Given a high enough feedback gain the gas distribution manifold must have a time constant such that ($1/T_B$ + (S_{FILM} + S_{PUMP})/V) >0. A large chamber volume is then desirable as a longer manifold time constant can be tolerated.

These results are difficult to visualize beyond this as we have a dependence of ω_n and E on five variables. I have taken the 'typical'

Fig. 9·11 : The time response of a 'classic' second order system.

Characteristic equation

$$s^2 + 2\omega_n E s + \omega_n^2 = 0$$

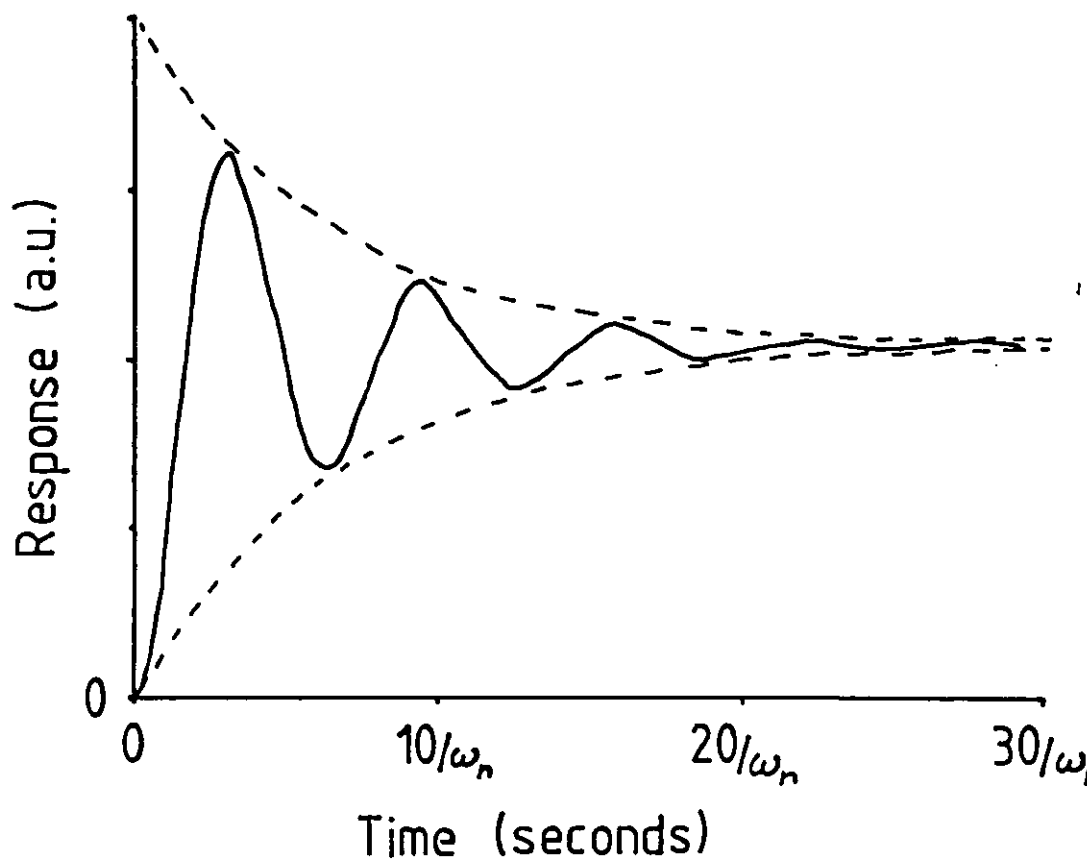

Time response (to a step function) is

$$P(t) = A \exp(-at) \cos(\omega t)$$

where

$$a = \omega_n E$$

$$\omega = \omega_n \sqrt{1 - E^2}$$

values shown in table 9.2 from my batch coater.

Table 9.2: Values for control testing

S_{FILM}	-300 l/s
S_{PUMP}	250 l/s
V	100 l
T_n	0.1 s
K	500 l/s

K was chosen as 500 l/s as this gives the desired damping coefficient E = 0.708. Now each parameter was varied with the others held constant and ω_n and E evaluated. These results are shown in fig 9.12. Instability occurs with either; complex ω_n, or small or negative E. Inspecting fig 9.12 for these effects shows the order of importance for the control parameters to be

1. K (too small: complex ω_n, too large: small E)
2. T_n (too large: small or negative E)
3. V (too small: small or negative E)
4. S_{FILM} (too large (negative): complex ω_n)
5. S_{PUMP} (no gross effects)

Discussion of analysis

As discussed in section 9.1 Q_{FILM} will change on a time scale 1/R where R is the deposition rate in monolayer/s. At a magnetron current of 8 A the deposition rate is 6 nm/s = 15 monolayers/s so 1/R = 0.07 s ie comparable with T_n. A term containing R must be considered as there is at present no mechanism to explain the observed deterioration in control as the magnetron current is increased.

To include the deposition rate (R) I must modify my equation 4 to consider dQ_{FILM}/dt. I have not yet achieved this extended analysis so this result will have to wait for further work. It is likely that this will result in a higher order characteristic equation and that more complex stability conditions will arise from the Routh array (refs 11, 12). A tempting guess for a stability condition is

$$T_n < \frac{1}{R}$$

Fig. 9·12 : Stability of the control loop under various parameter changes.

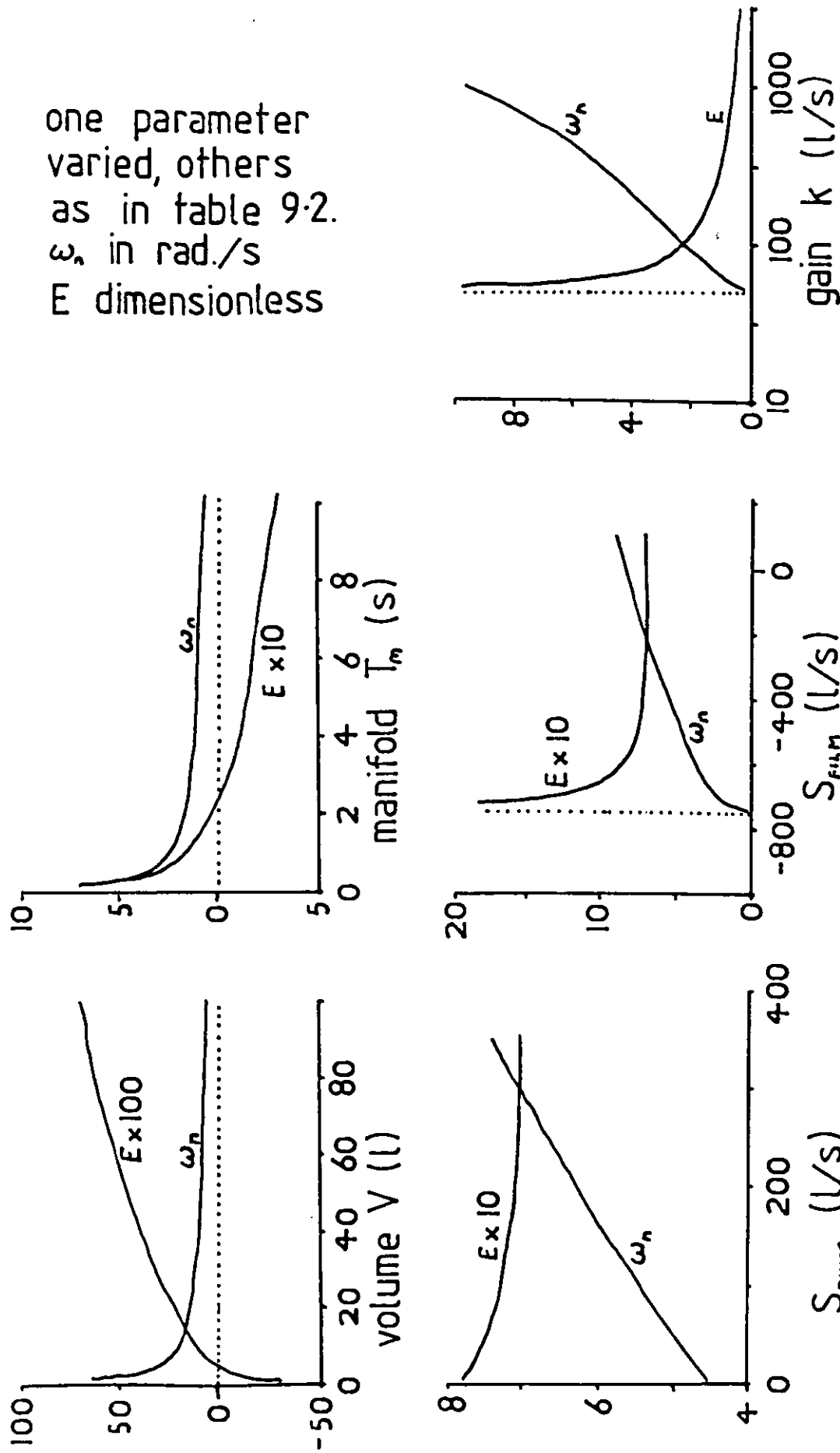

Summary

- The stability of control systems can be discussed in frequency space by looking at the roots of the characteristic equation.
- With simplifying assumptions this analysis shows that
  (i) a minimum gain is required for stability,
  (ii) the manifold time constant should be such that

$$(1/T_n + (S_{FILM} + S_{PUMP})/V) > 0$$

  A large chamber volume is best as a longer manifold time constant can then be tolerated.

9.4 SWITCHED CONTROL

In the pulsed controller of Aronson et al (ref 14) the reactive gas is simply switched between the chamber and a vacuum dump. For TiN this results in a substantially higher deposition rate than from the poisoned target. This system was shown to also work well for TiO_2 (ref 15) with the diverter valve pulsed at a fixed frequency (approximately 1 Hz). Following the work of R W Lewin (ref 16) this pulsed system was modified to switch the reactive gas flow at a given value of the metal emission intensity.

Table 9.3: Conditions for Switched Controller

Ar Pressure	2.0 mTorr (0.26 Pa)
Magnetron Power	2.5 kW
PEM Set Point	40%
Oxygen Flow	> 42 sccm
Oxygen Pressure	0.6 mTorr
Deposition Rate	6.0 nm/s

Using the pulsed controller we controlled our reactive system under the conditions in table 9.3. The system has an oscillating emission signal (fig 9.13) and the individual parts of this curve are now easily identified with time constants in the system. This is discussed in detail in section 9.5 but basically we have the different regions of the control curve as shown in fig 9.14. These are:-

(i) the drift from the metal target to a poisoned target.
(ii) the reactive gas diverted away from the chamber
(iii) the drift to a metallic target.

The main reason our switched control shows large time variations in the metal emission seems to be the 'overshoot' of the drift back to a metallic target ie region (iii). Fig 9.13 shows what effect the gas flow components have on the control curve. When the gas flow has a long time constant the gas is diverted for longer and the overshoot is worse. This can be explained simply:-

At the set point the reactive gas flow is diverted from the chamber. When the target starts to go metallic (the sharp gradient in region (iii)) the reactive gas flow into the manifold is reinstated.

Fig. 9·13 : Pulsed PEM control with various gas flow components.

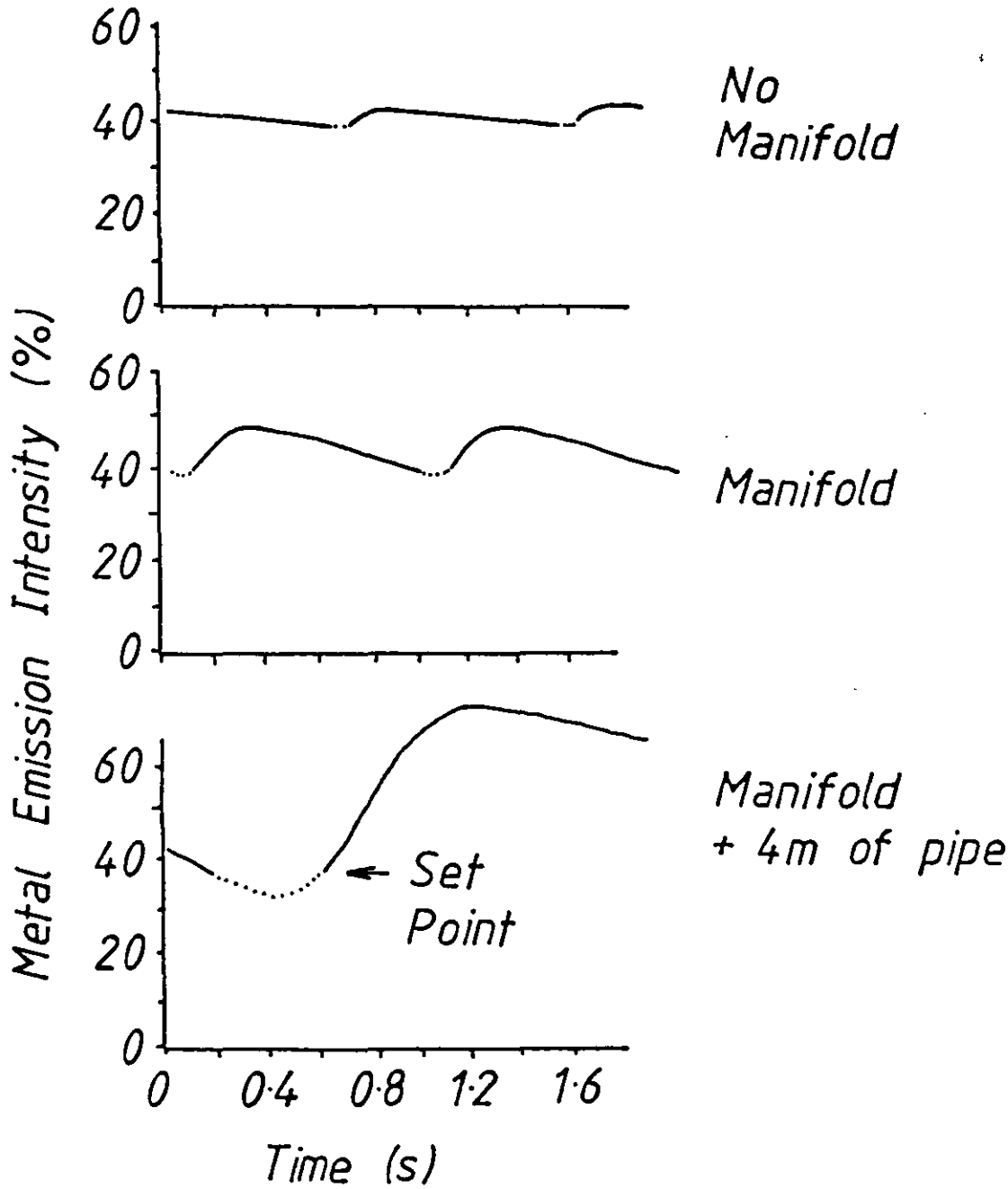

..... Reactive gas diverted

Fig. 9·14 : Different regions of the pulsed control curve.

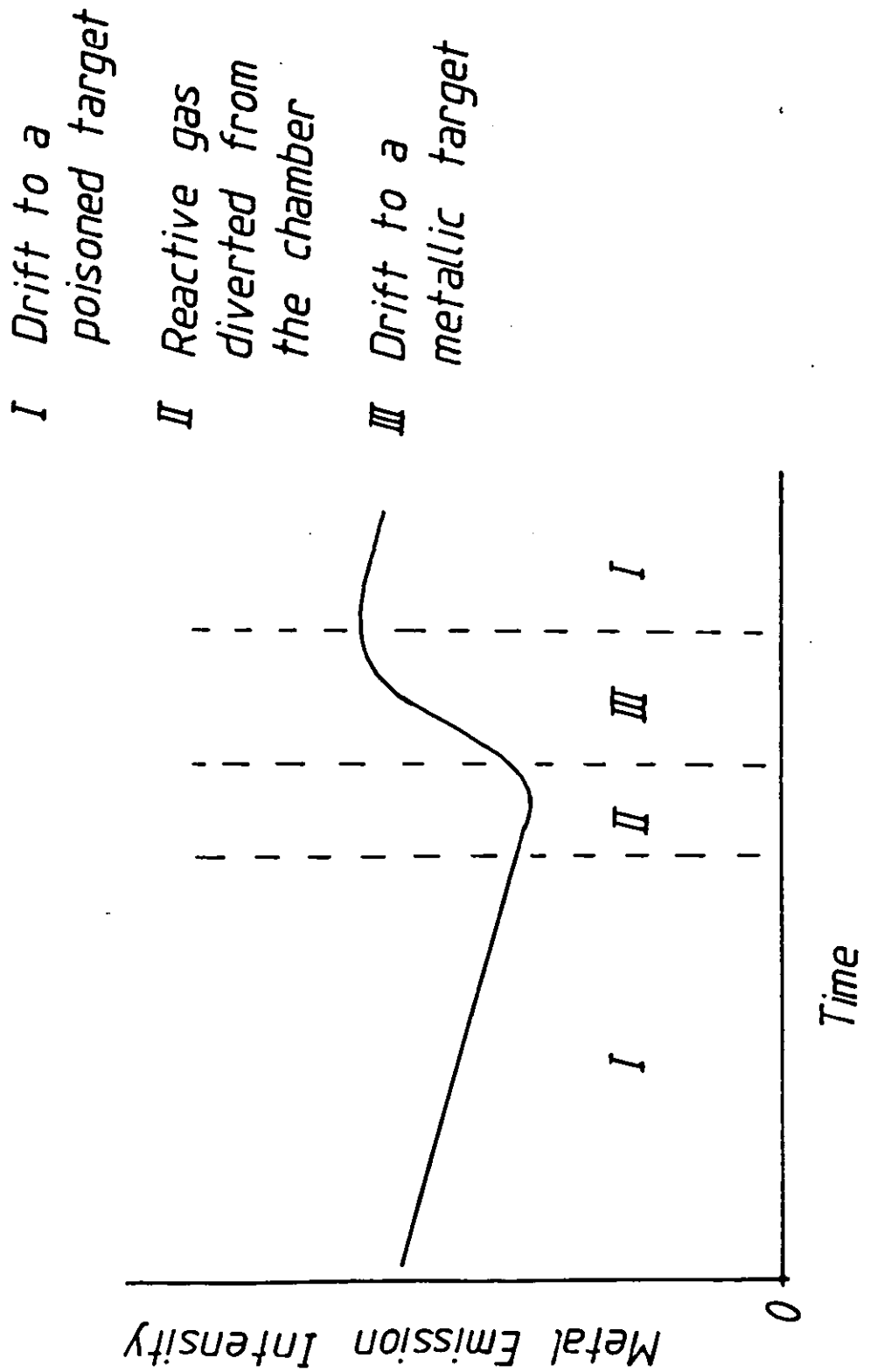

The reactive gas flow into the chamber will only increase on a time scale of Tm and so if the target recovery rate is constant C (%/s) the overshoot will scale with C.Tm.

No significant differences in control could be seen between placing the reactive gas manifold at the substrate or the target (fig 9.15). If the magnetron target was sputter cleaned back to the metal before the controller was set up then a drift in conditions was seen over half an hour with the pulsed controller set point held constant (fig 9.16).

The effects of increasing the reactive gas flow were investigated. With a magnetron power of 2.4 W (7.0 A at set point) the oxygen flow into the system was varied with just the manifold present and also with 4 m of 4 mm bore pipe and the manifold. The resulting control traces are shown in figs 9.17 and 9.18 respectively. Looking at these figures it is apparent that the recovery rate from an oxide to a metal target is independent of both the gas flow configuration and the reactive gas flow. This recovery time must be associated with; the time to pump away the gaseous oxygen in the chamber, and the rates of change of Q_{FILM}, the reactive gas supply, and the target oxidation state. We have already dealt with the fall rate of the reactive gas supply, this being determined by the manifold time constant. The lack of effect on the recovery rate (oxide to metal target) of altering this time constant shows that other effects dominate (compare figs 9.17 and 9.18).

I also introduced a constant background flow of reactive gas so that the controller was only switching a percentage of the total reactive gas flow. The results of this are shown in fig 9.19. This is now affecting the recovery gradient in region iii and this is plotted in fig 9.20. When 10% of the reactive gas flow is switched the oscillation amplitude is similar to that of the continuous control.

Now using our manifold and the PEM control we obtained a deposition rate of 6 nm/s onto A4 glass substrates. The resistivity of these films was 6×10^{-6} Ω.m which is about a 50% increase on the best attainable at these substrate temperatures (ref 17). This discrepancy is due to the variation of deposition conditions about the set point.

Fig. 9·15 : The lack of effect of the manifold position on the control quality.

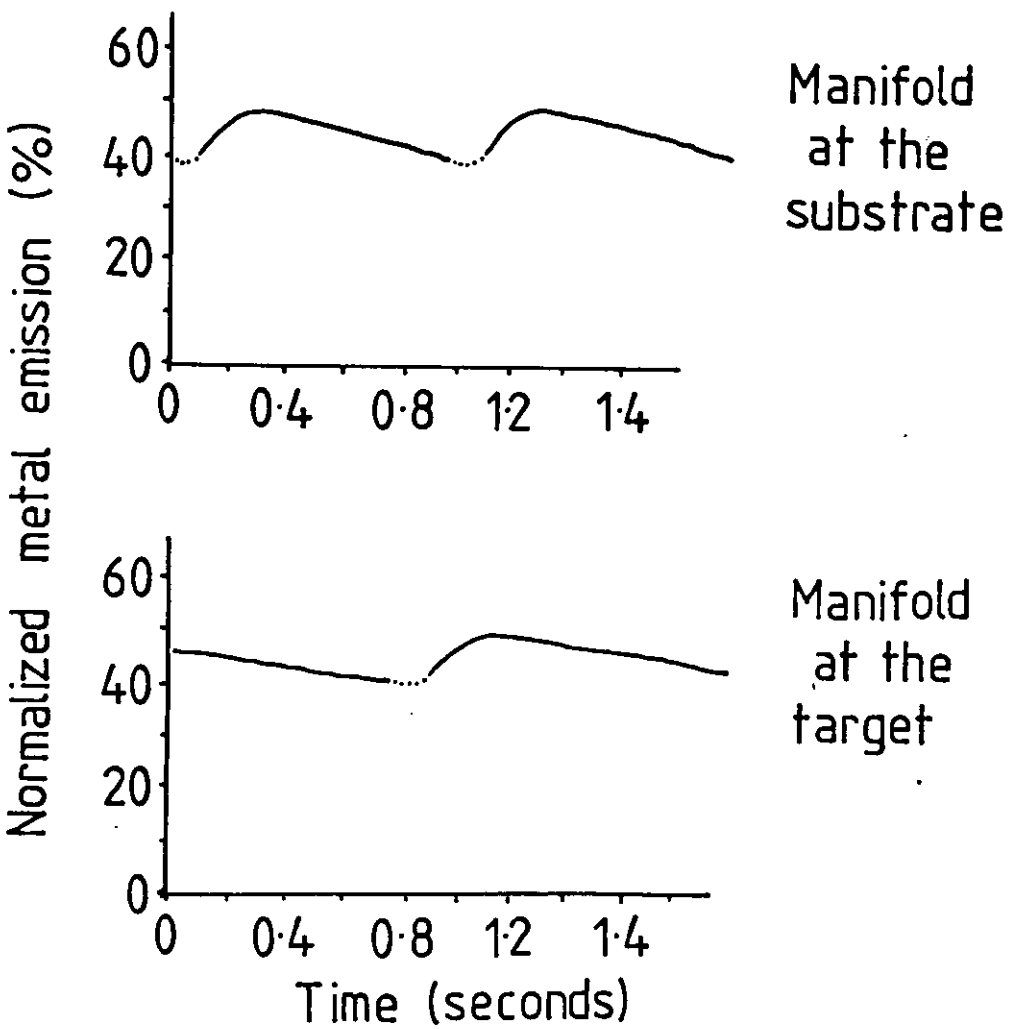

Fig. 9·16 : The drift of our controlled system.

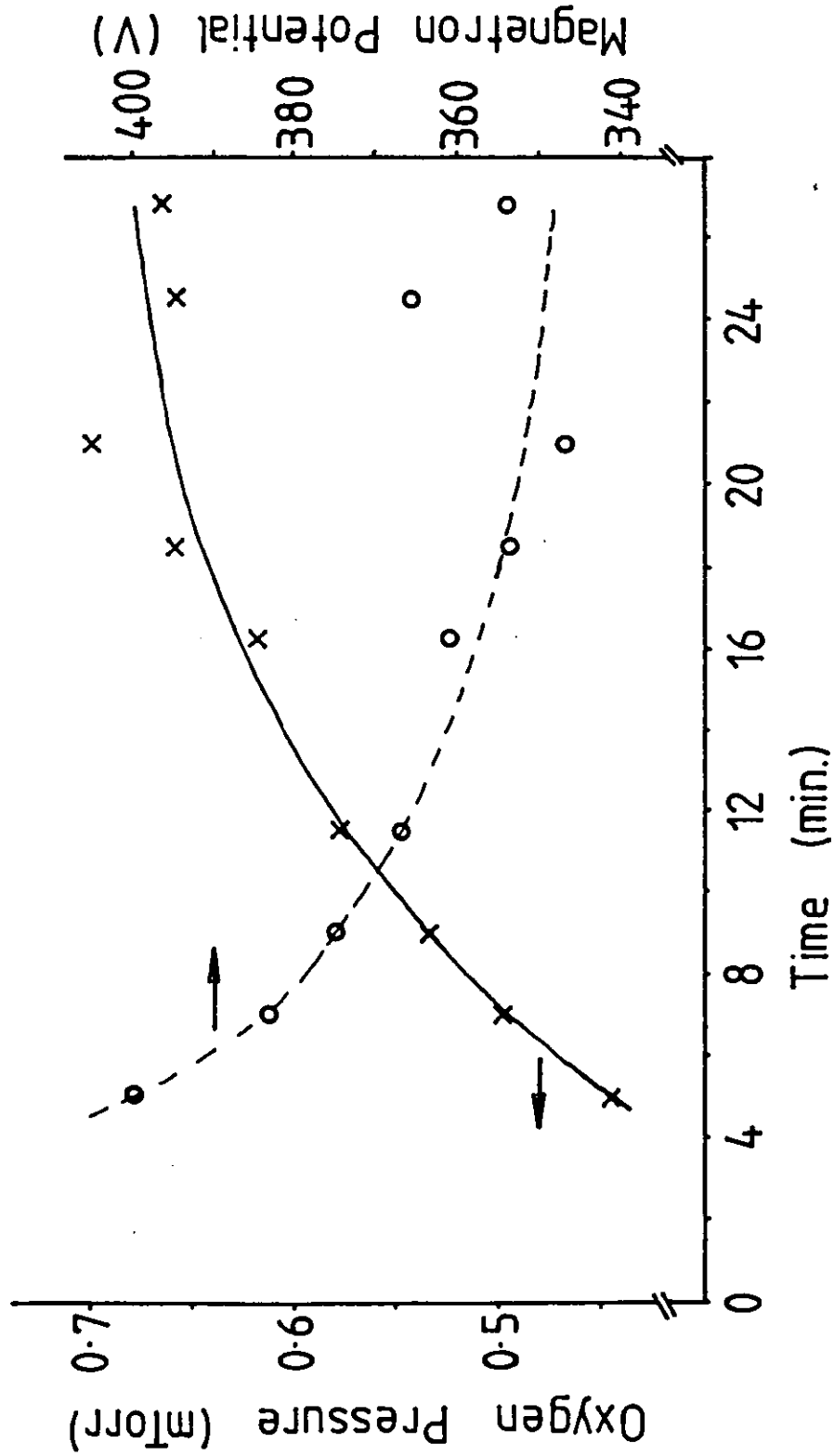

Fig. 9·17 : Switched control of various gas flows through the gas manifold and 4m of pipe.

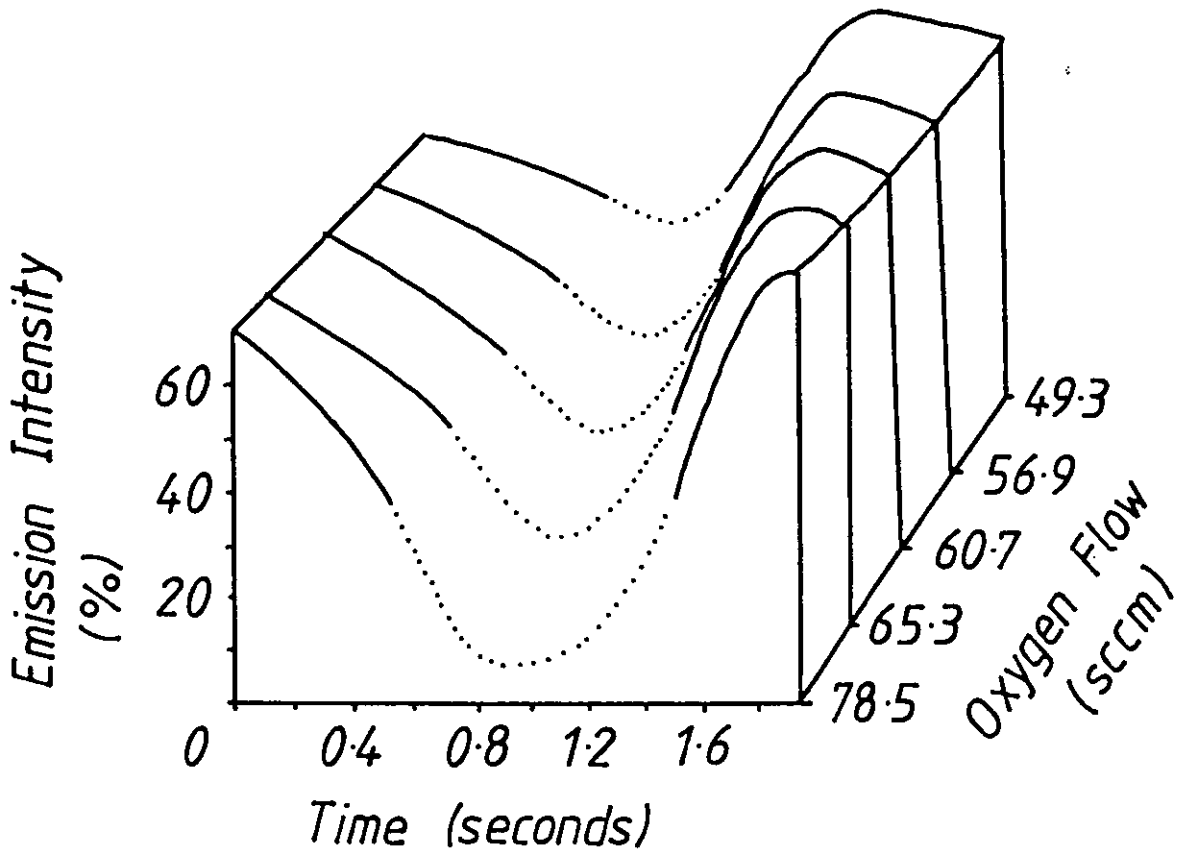

Fig. 9·18 : Switched control of various gas flows through the gas manifold only.

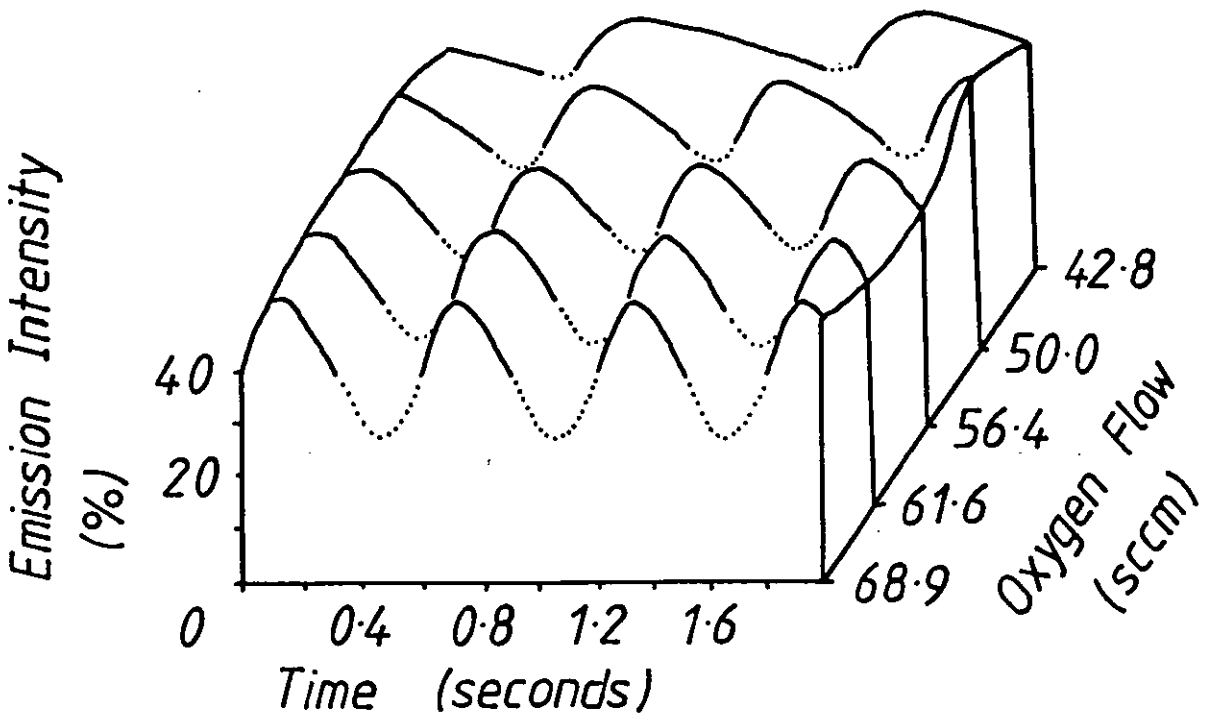

Fig. 9·19 : Control quality improved by the use of switched and constant oxygen flows.

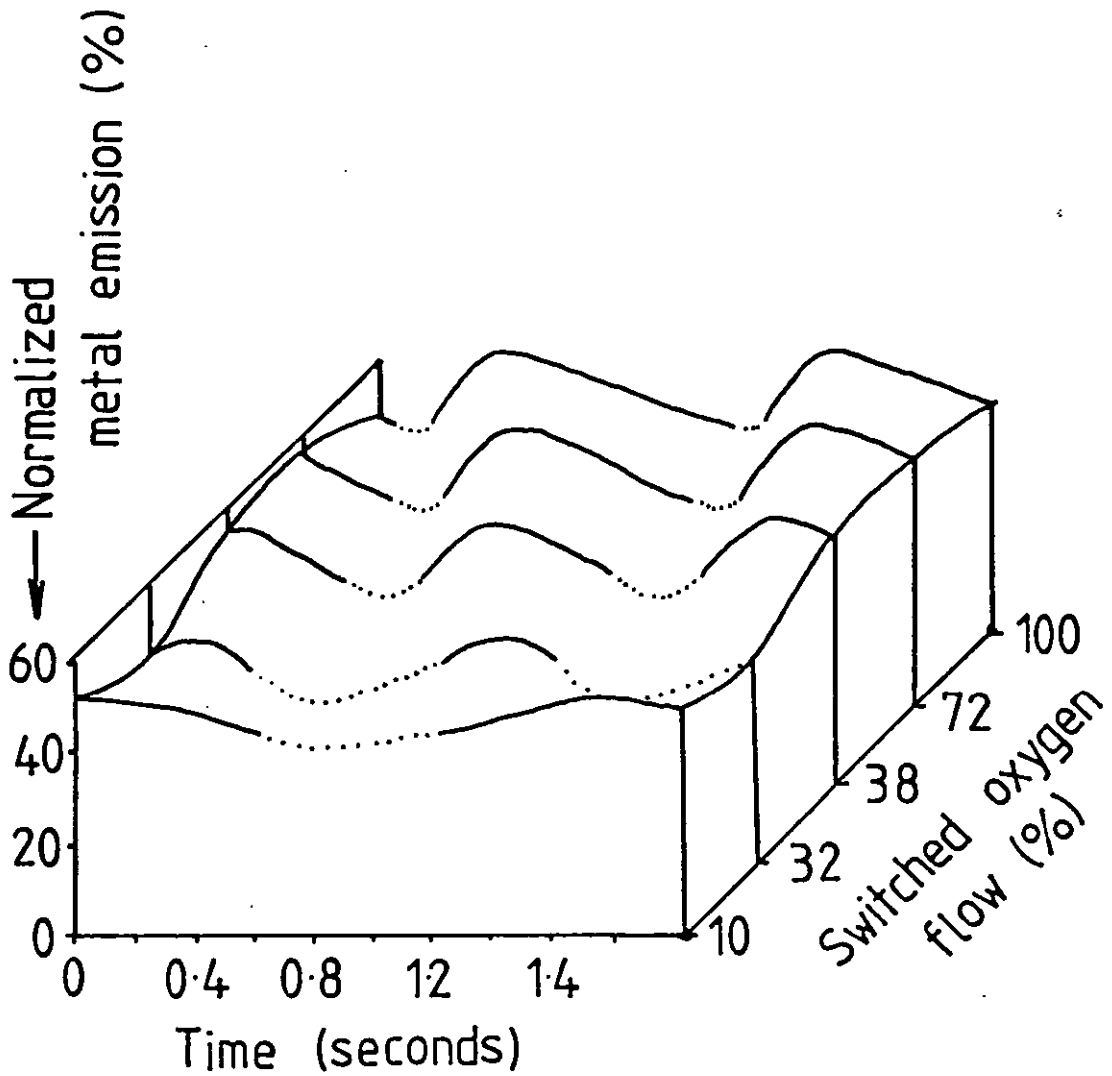

for oxygen flow

100 % = 47 sccm

Fig. 9·20 : The effect of a constant reactive flow on the recovery rate of the poisoned target.

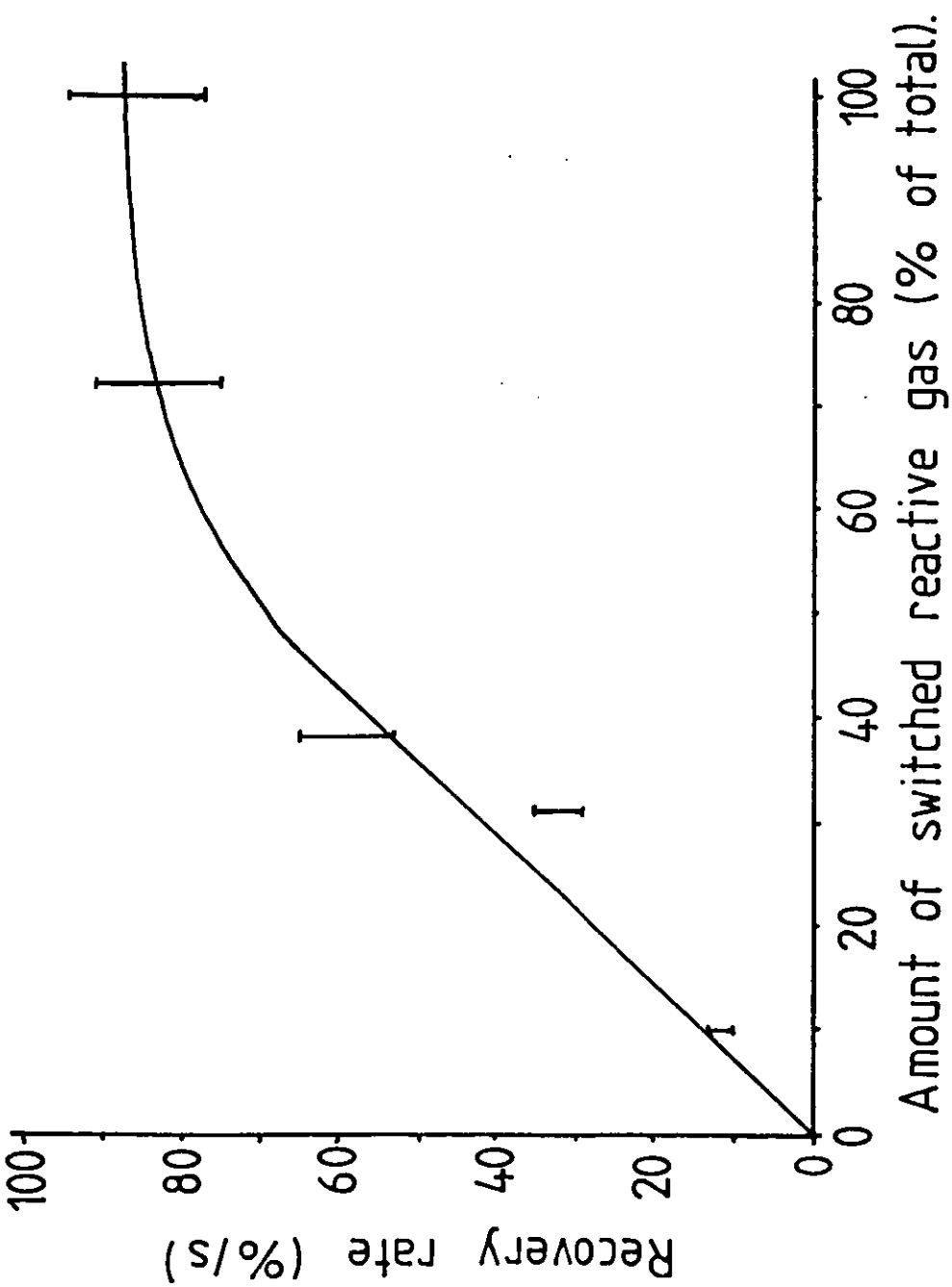

If the magnetron power is decreased then the oscillation amplitude decreases and better resistivities can be obtained but at the expense of a smaller deposition rate.

The process should be unconditionally stable and problems occur with arcing (see section 3.8). When an arc occurs the plasma is extinguished by the magnetron power supply (Advance Energy MDX units were used) and so the reactive gas flow is diverted. When the magnetron relights it comes up on the metallic side of fig 9.21. The total input gas flow should then be sufficient to take it to the point B and so into the desired region of control.

Summary

- Switched control of the reactive gas flow based on PEM gives control of reactive sputtering in the region of the pressure instability.
- As with continuous control there is oscillation of the PEM control signal. With the switched control the time effects in the system are now easily identified with regions of this oscillation.
- The main cause for the oscillation is the high rate of recovery of the target from poisoned to metallic. Once initiated this recovery occurs on a time scale comparable to the manifold time constant and therefore the reactive gas flow cannot be reinstated quickly enough to catch the recovering target.
- This target recovery rate is independent of the manifold time constant but can be reduced by using a constant background flow of reactive gas.
- Using the switched controller conducting indium oxide was deposited at a rate of 6 nm/s and with a conductivity of 6×10^{-6} Ω.m.

Fig. 9·21 : The critical points for the instabilities.

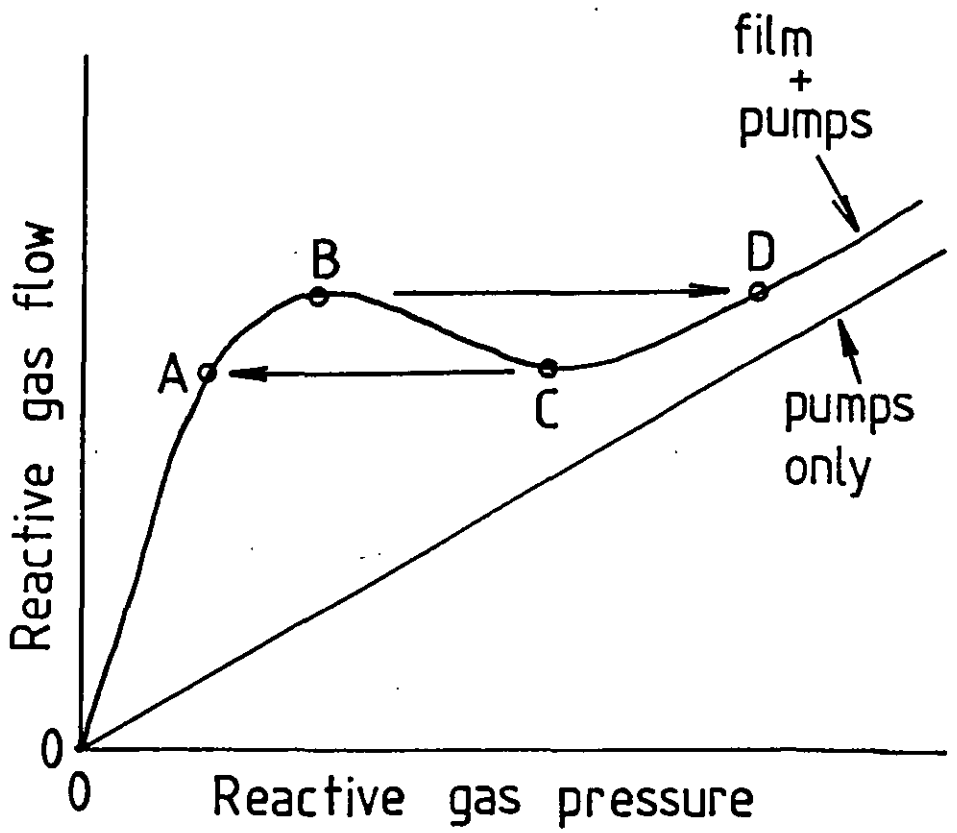

9.5 ANALYSIS OF SWITCHED CONTROL

The different regions of the switched control curve are shown in fig 9.14. We have:-

(i) the drift from the metal target to a poisoned target.

(ii) the reactive gas diverted away from the chamber.

(iii) the drift to a metallic target.

Region i

The drift to the poisoned target is simply the transition speed across the pressure instability. This is predicted by my model of the reactive sputtering process (chapter 7) and so can be used to test our model and to understand the controller. The transition should be governed by

$$\frac{dP}{dt} = \frac{Q_s}{V}$$

where P = reactive gas pressure (units eg Pa)

Q_s = surplus reactive gas flow (units eg Pa.l/s)

$= Q_{IN} - Q_{FILM} - Q_{PUMP}$

V = chamber volume (units eg l)

This predicts that as the input reactive gas flow is reduced the rate of drift will reach zero (this is still an unstable state) when the input flow equals the consumption by process and pumps. We cannot directly measure dP/dt but with an emission intensity E we can easily measure dE/dt. The formation of reaction products on the target was postulated (section 7.1) as a fast process being limited in the transition by dP/dt. The metal emission intensity (E) is an indicator of target state which is directly related to the reactive gas pressure and so it is useful to measure dE/dt.

In the transition from a metal to an oxide target (ie falling emission intensity) dE/dt does indeed fall as the reactive gas flow is reduced. We measure graphically dE/dt at the set point (falling E) in figs 9.17 and 9.18 and the results are shown in fig 9.22.

Fig. 9·22 : Experimental confirmation that dP/dt is proportion to surplus reactive gas flow.

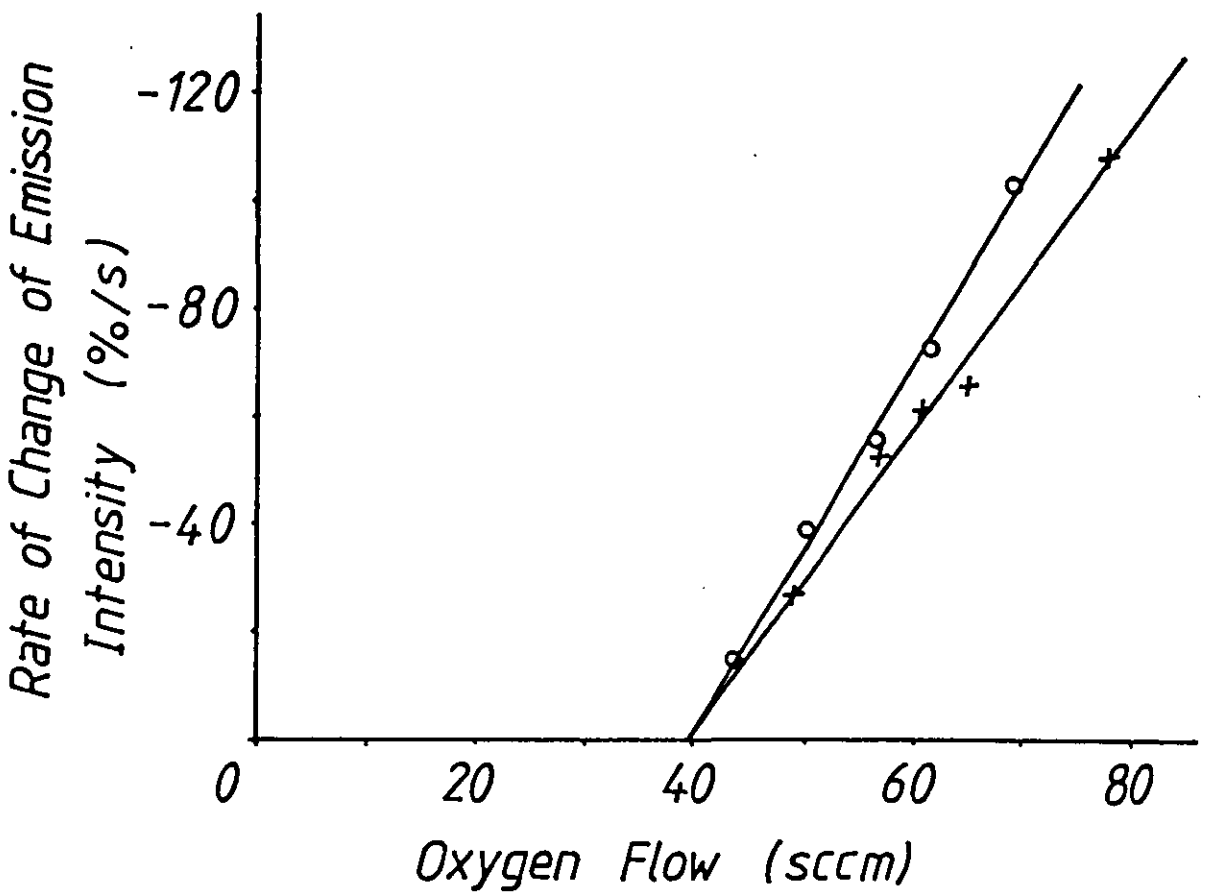

This line has the form predicted by my equation ($dP/dt = Q_s/V$) which also predicts that the x intercept ($dE/dt = 0$) should be the total reactive gas consumption by the film and pumps ie $Q_s = 0$. The x intercept for both lines is 39 +/- 2 sccm. The measured oxygen partial pressure for both cases (this is assumed to be a time average for the whole trace) was 0.60 +/- 0.02 mTorr. At this pressure and a current of 7 A we expect from fig 8.6 a pump consumption of 14 sccm and a film consumption of 25 sccm. This is a total reactive gas consumption of 39 sccm ie exactly as predicted from fig 9.22. Using fig 8.7 as a conversion from emission intensity to partial pressure and putting the gradient from fig 9.22 into equation 3 gives an effective chamber volume of 30 l. This compares with the total chamber volume of 100 l and the volume enclosed by the shuttering of 10 l. This reduced effective volume has implications for continuous control (see section 9.3).

Region ii

In region ii the reactive gas is diverted from the chamber. When the reactive gas flow is switched off the flow from the manifold into the chamber will decay as $\exp(-t.S_g/V_g)$ (see section 9.2). The reactive gas flow into the chamber will then look like fig 9.23. This would explain the behaviour seen in fig 9.13 where the diversion time increases with the manifold time constant.

Region iii

Looking at figs 9.17 and 9.18 it is also apparent that the recovery rate from an oxide to a metal target is independent of both the gas flow configuration and the reactive gas flow.

The pumping out of the chamber will have a time constant V/S where V is the chamber volume and S is the total pumping speed from the chamber. I must distinguish here between the total pumping rate and the differential pumping rate (local gradient) used in section 9.3. As shown in sections 6.4 and 8.1 S is a function of the magnetron power and target condition (reactive gas pressure). At 0.6 mTorr fig 8.6 gives a total pumping speed (film and pumps) of around 1000 l/s so we may expect an evacuation time of around 0.1 s.

Fig. 9·23 : Analysis of switched reactive gas flow control.

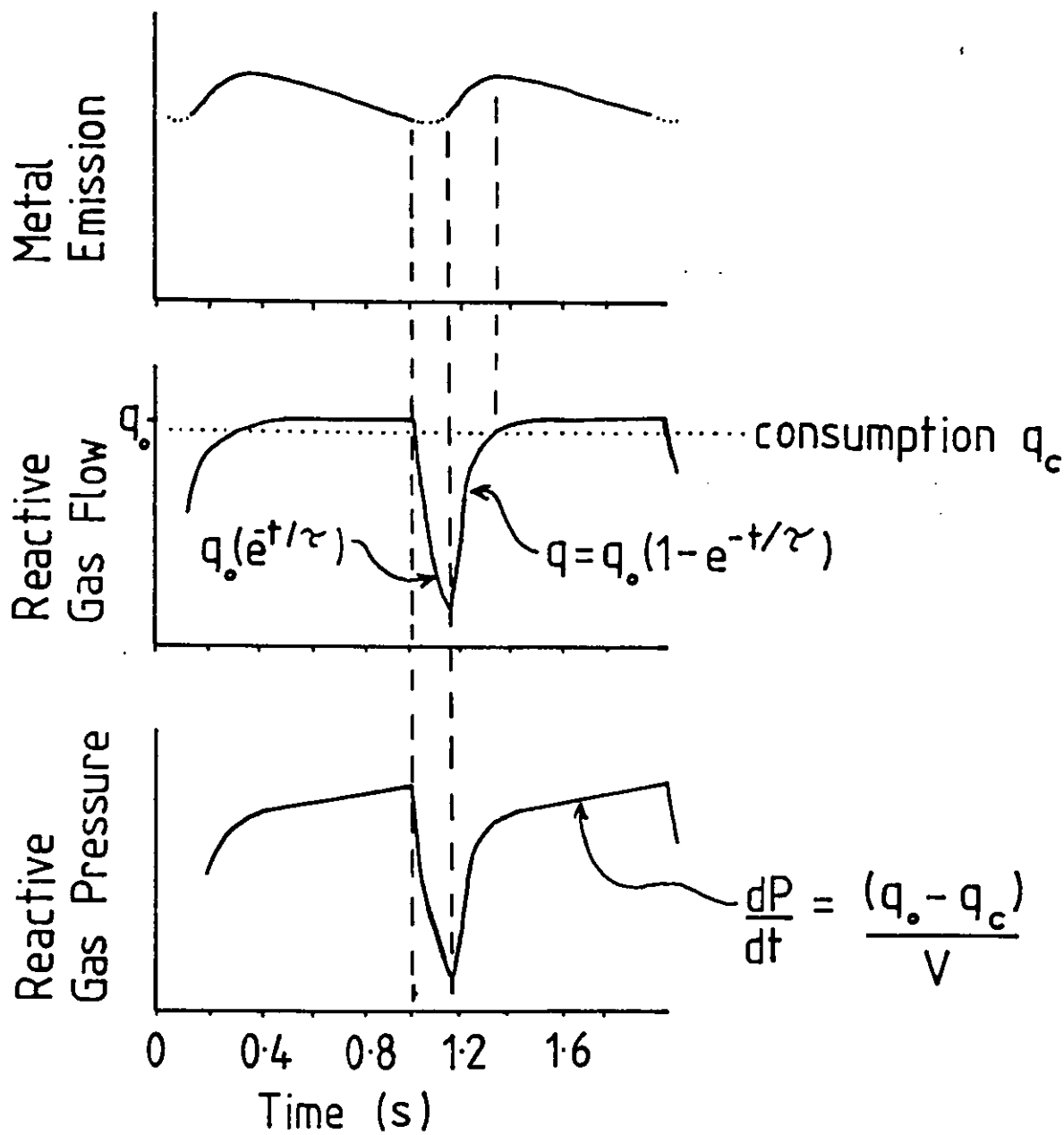

Given that we may expect the oxygen partial pressure to fall in 0.1 s can the target condition change this rapidly? We can only estimate the target recovery time as the oxide layer thickness is unknown. Taking the oxide layer thickness to be consistent with the ion penetration depth ie a few inter-atomic spacings or approximately 1 nm (ref 18). The indium atomic diameter is about 0.3 nm so the surface area per atom will be around 9×10^{-20} m^2. The sputter yield for In_2O_3 is 0.3 (section 3.3). Our current density to the magnetron is 350 A/m^2 ie 200 elemental charges per second to the surface area of one In atom. If 60% (see section 3.3) of this is ion bombardment a sputter yield of 0.3 will give an oxide sputter rate of 35 monolayers/s. A surface oxide a few monolayers thick should then last around 0.03 s.

Discussion of switched control

From the estimates above it is likely that the pump out time of the chamber dominates the recovery from a poisoned target.

The time delays associated with dynamic control of reactive magnetron sputtering are summarized in table 1. Of these parameters the target poisoned to metal transition is outside of our control. The reactive gas control valve should be placed as close as possible to the chamber to minimize propagation delays along the pipework. The gas inlet manifold time constant (volume/conductance) must be minimized for optimum control. To maintain a uniform gas distribution we must have a large ratio of conductance between outlet holes/conductance of outlet holes. Having chosen a pipe size for the manifold the time constant can be varied by changing the hole size to the chamber. The hole size should be increased until uniformity starts to suffer.

The metal to poisoned transition occurs at a rate determined by the amount of surplus reactive gas and the reaction chamber volume. We have used louvred pumping surfaces to move us closer to stability and the effective volume of our reaction chamber is intermediate between the enclosed volume and the chamber volume. Schiller et al advocate the use of enclosed reaction chambers but their deposition rate even without loss of material to the pumping surfaces is only 4 nm/s for indium oxide. The use of an enclosed reaction chamber will speed up the transition from metal to oxide and also reduce the time to remove

oxygen from the chamber. It is not yet clear which type of chamber will provide the best control.

Table 9.4 : Time constants (T) in dynamic control of reactive sputtering

Time Delay	Factors Involved
Gas Inlet Manifold	Manifold Volume V_m (l) Conductance to Chamber S_m (l/s) $T_m = V_m/S_m$
Chamber time constant	Reaction Chamber Volume V (l) Pumping rate S (l/s) Evacuation time T = V/S Perturbation response $T = V/(S_{FILM} + S_{PUMP})$
Metal to poisoned target	Reaction Chamber Volume V (l) Surplus Reactive Gas Flow Q_s (a mass flow rate in appropriate) (units eg Pa.l/s) $\frac{dP}{dt} = \frac{Q_s}{V}$ P = reactive gas pressure (units to match Q_s) (eg Pa)
Poisoned layer from target	Thickness of reaction products on target D_p (in monolayers) Target sputter rate R = Y.I/S (in monolayers per sec) Target poisoning rate R_p proportional to reactive gas pressure? (also in monolayers per sec) Sputter yield of reaction products Y Ion bombardment density I (m^{-2}) surface area per atom A (m^2) $T = Dp/(R - R_p)$ In absence of reactive gas $T = \frac{D_p . A}{Y . I}$
Delay due to pipework	Pipe length L (m) Pipe cross section area A (m^2) Conductance to chamber S (l/s) $T = \frac{k \, . \, L \, . \, A}{S}$

Summary

- The switched gas control is more easily analyzed and we draw several conclusions from the control traces of this system.
- It is confirmed experimentally that the drift rate from a metallic to a poisoned target is governed by

$$\frac{dP}{dt} = \frac{Q_s}{V}$$

- From this our results give an effective chamber volume (30 l) between the total chamber volume (100 l) and the reaction chamber volume (10 l).
- Time constants for the chamber, the cleaning of the poisoned target, and the rate of change of the reactive gas consumption (Q_{FILM}) are estimated. These all lie between 0.1 and 0.03 s (comparable with the manifold time constant T_0 of 0.07 s).

9.6 CONTROL OF THE EVEREST COATER

The results of PEM control on our smaller batch coater were transferred to the large Everest production coater. A tin cathode in the second tin oxide module (see section 5.3) was selected for control tests. These cathodes show a pressure instability (see section 6.4) and this limits the target life as the targets go metallic when only 60% of the available target thickness has been used. Extensive testing and modification could not be carried out as the coater is in production and lost production and coater time is expensive. Therefore the tests done were restricted by the production schedule.

The emission spectrum from a tin cathode is shown and analyzed in section 8.2. The tin emission lines are not in an accessible region of the spectrum. They lie around 250 nm while the chamber windows are glass and only transmit above 350 nm. The oxygen line at 777 nm is easily measured and is away from any significant Ar emission lines. A control signal was obtained by placing an interference filter for 777 nm over the photo-multiplier which viewed the plasma through the chamber window (this is not a permanent arrangement as the window will coat causing a long term drift). Obviously now we must use the opposite sense in our control loop as the oxygen emission signal will rise with increasing oxygen pressure not fall as does the metal signal. The switched controller was used as the results from this are more easily analyzed and in operation it is more forgiving.

The gas admission manifold in the Everest coater has a volume of 8.6 l. The admission to the chamber is through 59 holes of 1 mm diameter giving a conductance to the chamber of 2.3 l/s (see section 9.2). The time constant associated with this manifold is then 3.7 s. This is inconveniently long but cannot be readily altered during production. The sputter chamber has a volume of 1200 l and an oxygen pump rate of 750 l/s giving a chamber time constant of 1.7 s. With the cathode in operation an additional oxygen pump rate of around 750 l/s (see section 6.4) can be expected. In operation the chamber evacuation time would be around 0.9 s.

These time constants are inconveniently long but despite this control was attempted. If the manifold was redesigned for PEM control

its time constant could be reduced. The tin cathode was set up as normal with the parameters shown in table 9.5.

Table 9.5: Tin cathode settings

Ar flow	40 sccm
Oxygen flow	210 sccm
Total pressure	0.34 Pa
Magnetron current	35 A
potential	453 V

The oxygen emission intensity under these conditions was nominally called 100%. The controller was turned on and the set point gradually reduced from the 100% level (table 9.6). As the set point was reduced the oxygen emission began to oscillate with increasing amplitude (fig 9.24) and the divert time increased. At a set point of 70% the coater was initially stable but after a few minutes it went metallic and stayed there.

Table 9.6: PEM control of Everest coater

Oxygen emission (a.u.)	Total pressure (Pa)	Magnetron potential (V)
100	0.34	453
90	0.31	449
80	0.28	438
73	0.25	420
70	0.23	411
--- after a short period went metallic and stuck there		
	0.13	630

On a schematic of the pressure instability (fig 9.21) this can be easily explained. The unstable transition C -> A has occurred and the oxygen flow of 210 sccm is insufficient to induce the transition B -> D back into the control region. The maximum available oxygen flow is 400 sccm and this is still insufficient to induce the transition. (The plant operators know this from experience - they generally get back to

Fig. 9·24 : Switched control of the Everest coater.

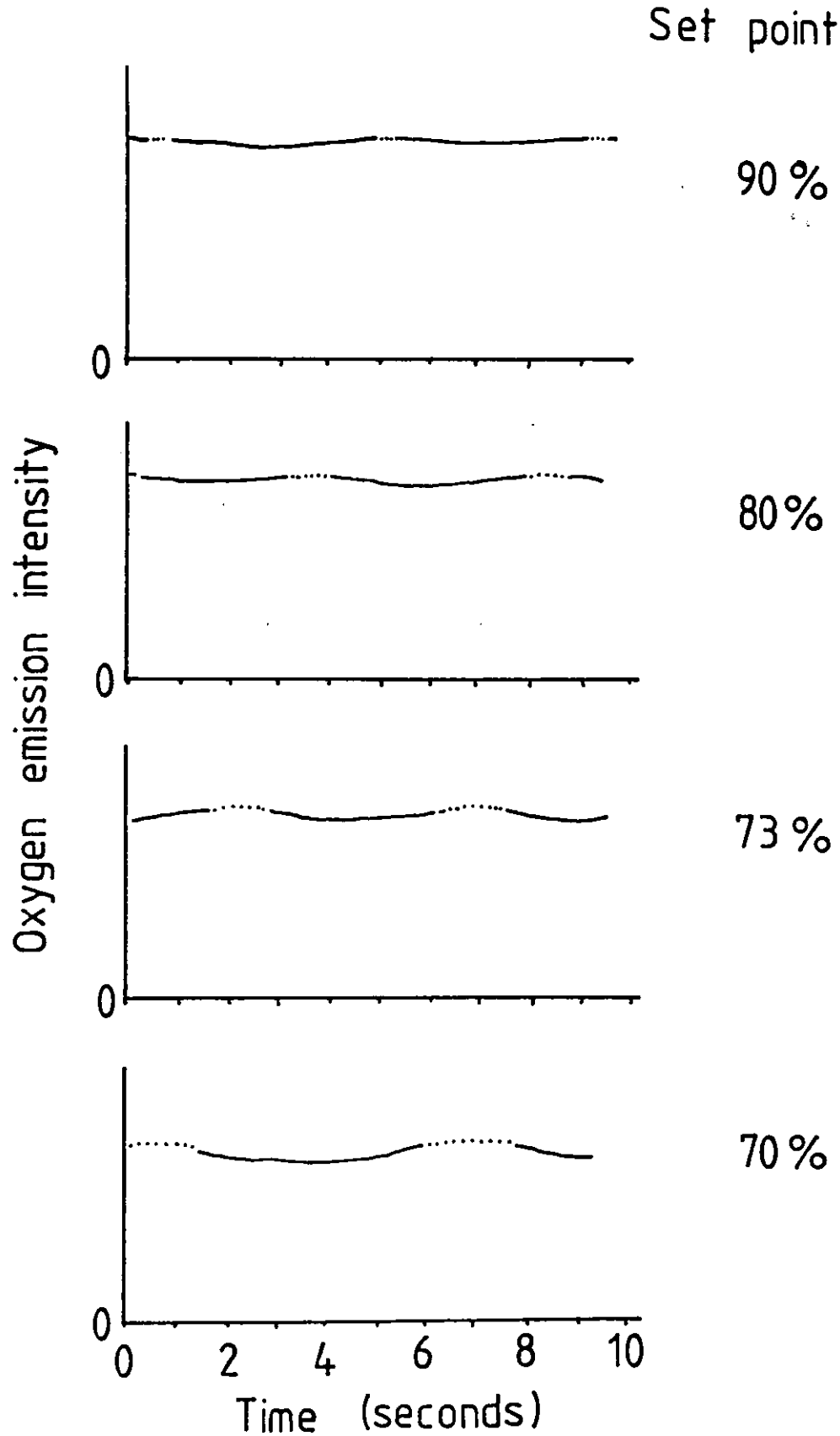

an oxide target by reducing the magnetron current to around 15 A then increasing it back to 35 A).

The Everest coater behaves in a similar fashion to our batch coater as the reactive gas flow is increased - the oscillation amplitude increases (fig 9.25). Now as the transition C -> A occurs the system goes into oscillation (fig 9.26) in the region B -C instead of sticking on the slope A - B.

To obtain some form of control a steady bleed of oxygen was added. Just as in our batch coater this improved the control (table 9.7) and allowed operation of the magnetron in the normally unstable region. The layers of tin oxide thus produced were measured for thickness by ellipsometry and this showed and increase in deposition rate by a factor of 2.6.

Table 9.7: PEM control of Everest coater

Oxygen emission (a.u.)	Total pressure (Pa)	Magnetron potential (V)	Film thickness (nm)
100	0.30	450	21.4
90	0.25	452	33.2
79	0.19	429	
63.6	0.15	419-430	
59.5	0.15	552-560	
57.9	0.15	611	42.1
56.2	0.15	620	56.1

This set up was then used for 30 minutes to produce the full oxide/silver/oxide coating (set point 70%, oxygen flow 350 sccm). The colour of this coating is tightly controlled as perceptible variations in colour within one house or across one window must be avoided. The colour variation permissible across one window is particularly small. The glass produced while using my controller showed a consistent reddening (in reflection) at the trailing edge of every batch ie the tin oxide is thinner at this edge.

The cause of this can be seen in fig 9.27. As the glass passes

Fig. 9·25 : Increasing oscillation amplitude with increasing oxygen flow. (set point 70 %)

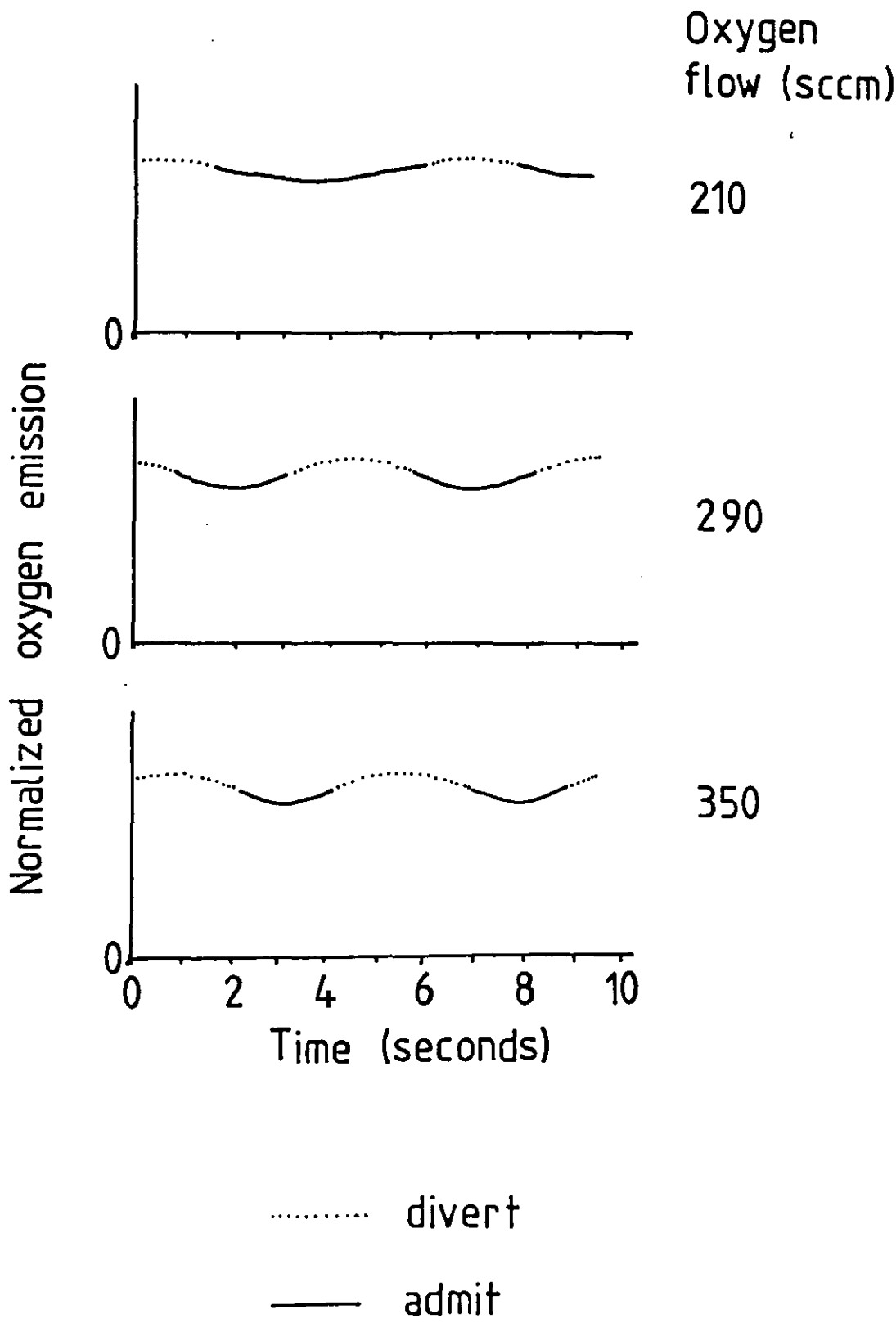

Fig. 9·26 : Control at Everest with all reactive gas flow switched.

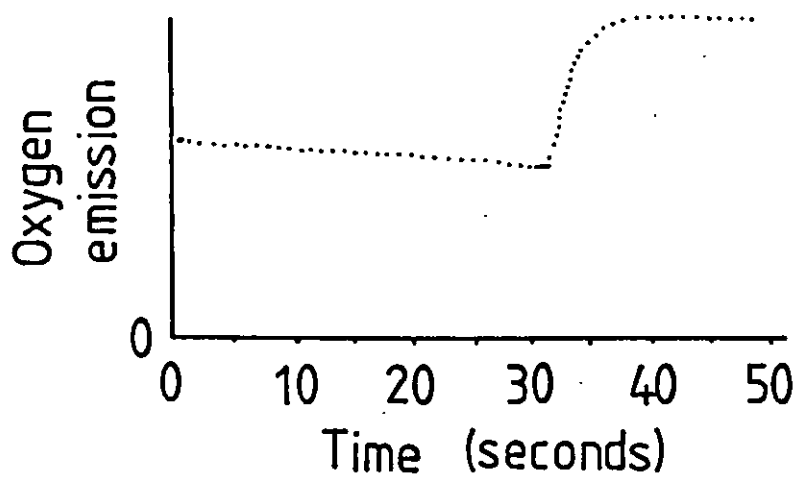

Set point 53 %

Fig. 9·27 : The change in oxygen emission intensity (under constant oxygen flow) as glass enters the slot lock.

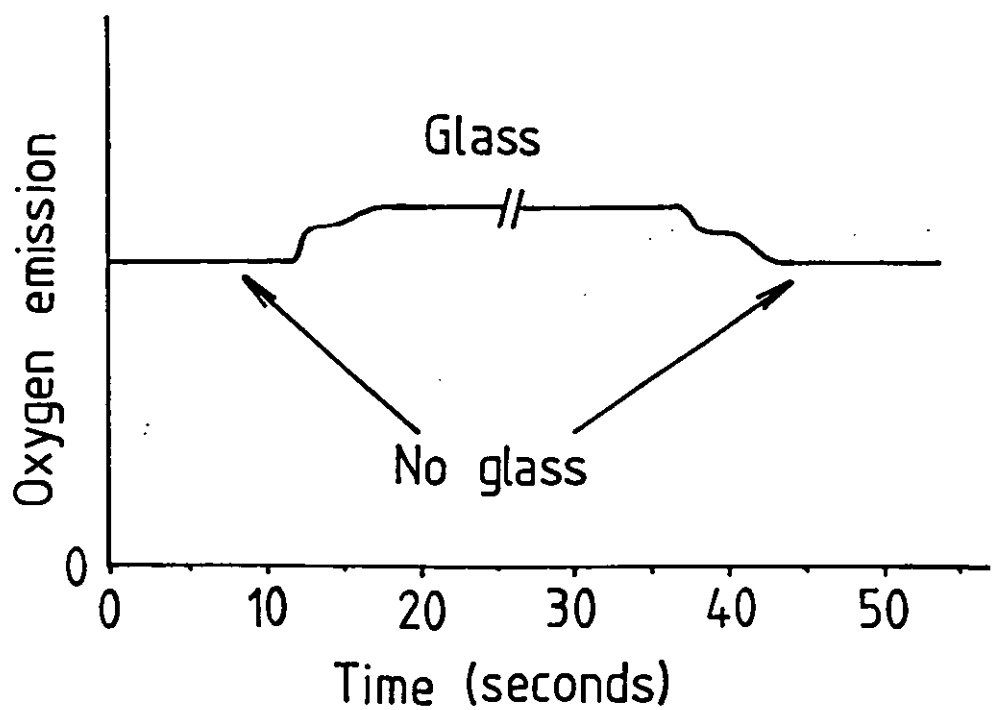

through the slot lock joining the sputter chamber to the pumping chamber it restricts the pumping rate of the sputter chamber. This causes an increase in the oxygen emission signal (oxygen partial pressure). The controller acts to correct this by reducing the oxygen glow. At the leading edge there is no problem because the glass is already in the slot lock before it reaches the coating zone. However on the trailing edge the glass is still in the coating zone while no longer in the slot lock. This causes an increase in the oxygen flow and the observed thinner oxide.

These results show that PEM control can be applied even to very large machines. To fully use PEM control in the Everest machine a few modifications would be necessary. The gas inlet manifold should be reduced in volume (it would be possible to reduce the manifold time constant to around 0.5 s). A proper optical lead through provided to prevent coating of the viewer and the consequent drift of the signal (a minor modification). Lastly (and of most difficulty) the pumping arrangement modified so that the passage of the glass through the slot lock does not significantly alter the emission signal. Alternatively it may be possible to use the Ar emission intensity to compensate the control signal.

Summary

- PEM control of a large production coater is possible and allows increased dielectric deposition rates for a given power. It will also make new regions of film stoichiometry available and allows full use of the reactive sputtering process for large substrates without the need to drastically 'overpump' the chamber.
- Even with very long manifold time constants control can be achieved by the use of pulsed control and a constant reactive gas bleed.

REFERENCES: CHAPTER 9

1. S. Schiller, U. Heisig, K. Steinfelder, J. Strumpfel, A. Freidrich, and R. Fricke, "On the use of a plasma-emission monitor for the control of the reactive sputter process and its application in the production of indium-tin layers", Proc. Int. Conf. on Ion and Plasma Assisted Techniques, Brighton, CEP Consultants, Edinburgh, 23-31, 1987.

2. Clark W.R. and Sullivan J.J., Solid State Technol., 3, 105-107, 1982.

3. J. Chapin and C.R. Condon, "Feedback control for vacuum deposition apparatus", U.S. Patent 4, 166,784, 1979.

4. A.F. Hmiel, "Partial pressure control of reactively sputtered titanium nitride", J. Vac. Sci. Technol., A3(3), 592-595, 1985.

5. Topping J., "Errors of observation and their treatment", Chapman and Hall, London, 1979.

6. L.G. Carpenter, Vacuum Technology, Adam Hilger, Bristol, 1983.

7. Santeler D.J., J. Vac. Sci. Technol., A4 (3), 338-343, 1986.

8. Leybold Heraeus handbook "Vacuum Technology: its foundations, formulae and tables", Hanau, FDR, 1987.

9. Santeler D.J., J. Vac. Sci. Technol., A4 (3), 348-352, 1986.

10. DeMuth S.F. and Watson J.S., Ibid, 344-347.

11. Marshall S.A., "Introduction to Control Theory", MacMillan, London, 1978.

12. Hostetter G.H., Savant C.J. and Stefani R.T., "Design of Feedback Control Systems", Holt, Rinehart and Winston, New York, 1982.

13. C. Nender, "Dynamic modelling of reactive sputtering of nitrides", PhD Thesis, Uppsala University, Sweden, 1988, to be published.

14. Aronson A.J., "Sputtering thin film titanium nitride", Microelectronic Manufacturing and Testing, Jan., 25-26, 1988.

15. Howson R.P., Suzuki K., Bishop C.A., and Ridge M.I., Vacuum, 34, 291-294, 1984.

16. R.W. Lewin, A.G. Spencer, and R.P. Howson, "A control process for stable operation of a high rate d.c. reactive magnetron sputtering system", presented at European Vacuum Conference, Salford, U.K. April 1988, Abstract published in Vacuum, 38, 947, 1988.

17. Lewin R.W. and Howson R.P., "The reactive sputtering of alloy metal oxide thin films of the indium tin system", Proc. Int. Conf. on Ion and Plasma Assisted Techniques, Brighton, CEP Consultants, Edinburgh, 464-469, 1987.

18. Muller K.H., "Modelling ion-assisted deposition of CeO_2 Films", Appl. Phys., A 40, 209-213, 1986.

10. RESULTS - PLASMA ACTIVATION

10.1 PLASMA BEAM BOMBARDMENT

The magnetron of C.A. Bishop (ref 1) is unbalanced and produces a plasma beam. With polymer substrates this was a problem as the extra heat load (ref 2) melted the polymer. C.A. Bishop therefore removed the plasma beam by placing an earthed anode in its path. I modified this arrangement by using a variable resistor between the anode and earth. When this resistance is zero the whole magnetron current flows to earth via the anode (2.00 +/- 0.01 A into the magnetron and 2.00 +/- 0.01 A through the anode). Now if the resistance to earth is increased I would expect a self bias on the anode. Biasing the anode has been shown to alter plasma bombardment of substrates (ref 3) and in the same manner this self bias alters the plasma beam (fig 10.1) (refs 4, 5).

Our A4 magnetron is also unbalanced (see fig 8.3) and so we could control the plasma bombardment of the substrate by a variable resistance between the anode and earth. Langmuir probe measurements at the substrate position were made by K. Oka (ref 2). With a magnetron current of 6 A (390 V), an argon pressure of 1.75 mTorr and oxygen pressure of 0.45 mTorr these showed the beam profile of fig 10.2 (anode isolated). At the centre of the beam the substrate floating potential, and the ion and electron currents varied with the magnetron current and anode/earth impedance as shown in fig 10.3. We now have a controllable plasma bombardment of the substrate during deposition of our films.

10.2 EFFECTS ON REACTIVE FILM GROWTH

Conducting indium oxide has a film resistivity which is a strong function of the film stoichiometry (refs 6, 7) (see fig 10.4) we can therefore use the variation in film resistivity to pinpoint the formation of a specific film stoichiometry. The A4 glass coater is a batch coater and from the size of the machine and the width of the deposition zone we can coat a maximum of 6 samples in one run. For this reason we can locate the resistance minimum to +/- 10% in oxygen pressure or deposition rate (fig 10.4).

Fig. 10·1 : The effects of electrode self-bias on the plasma beam.

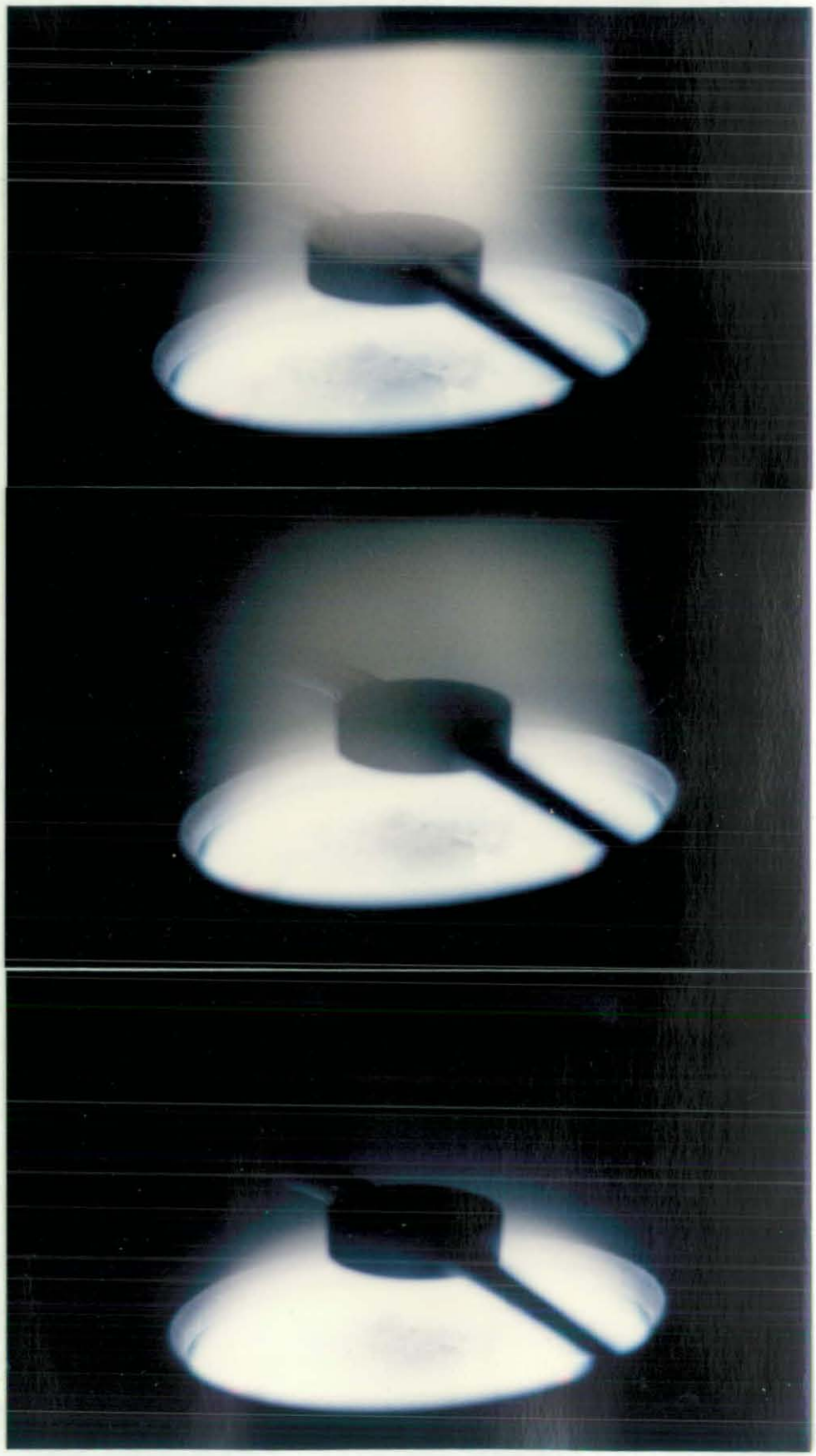

Fig. 10·2 : The plasma beam profile.

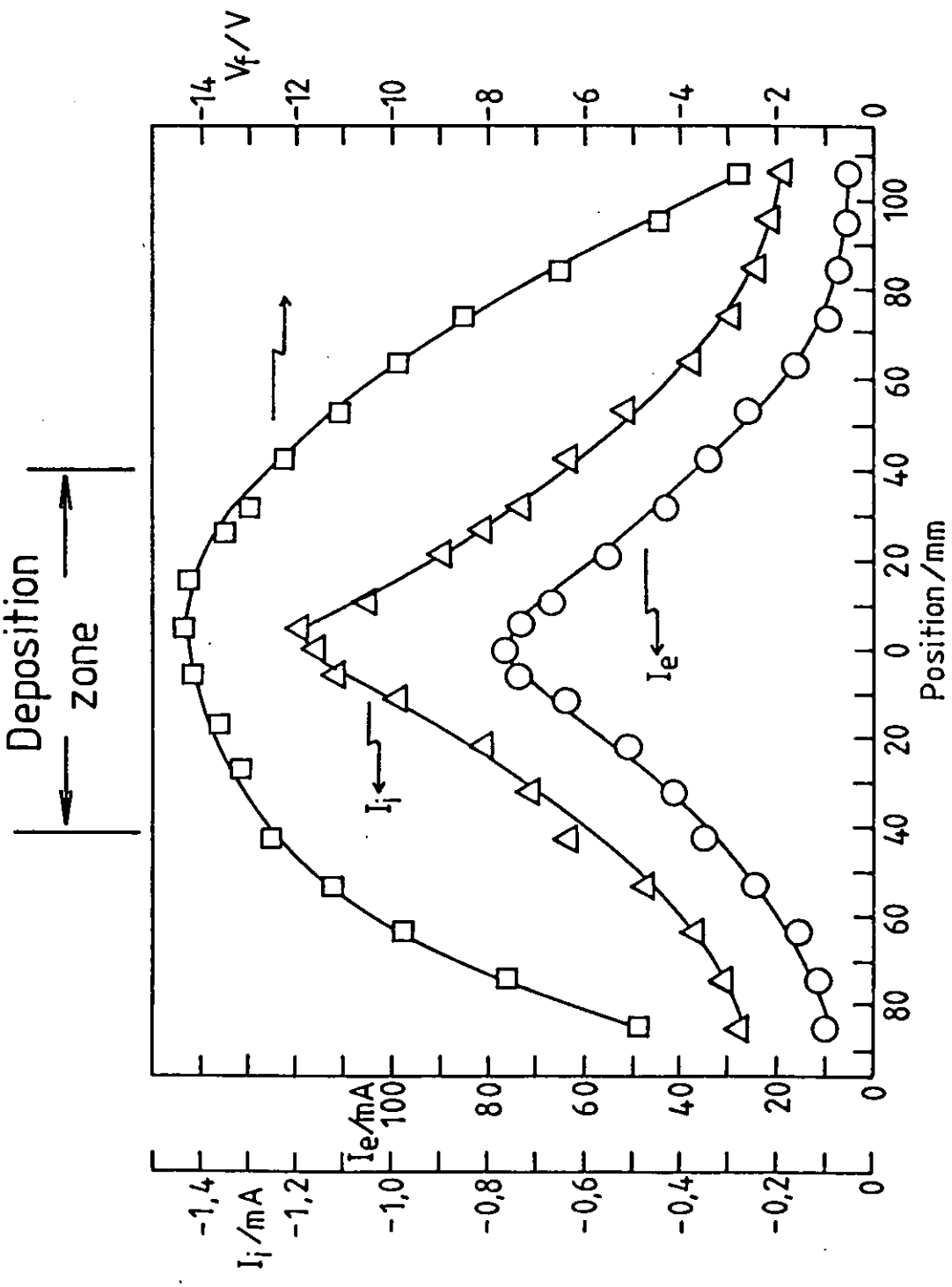

Fig. 10·3 : Plasma bombardment of the substrate by the 0·5m magnetron. (6mm diameter probe)

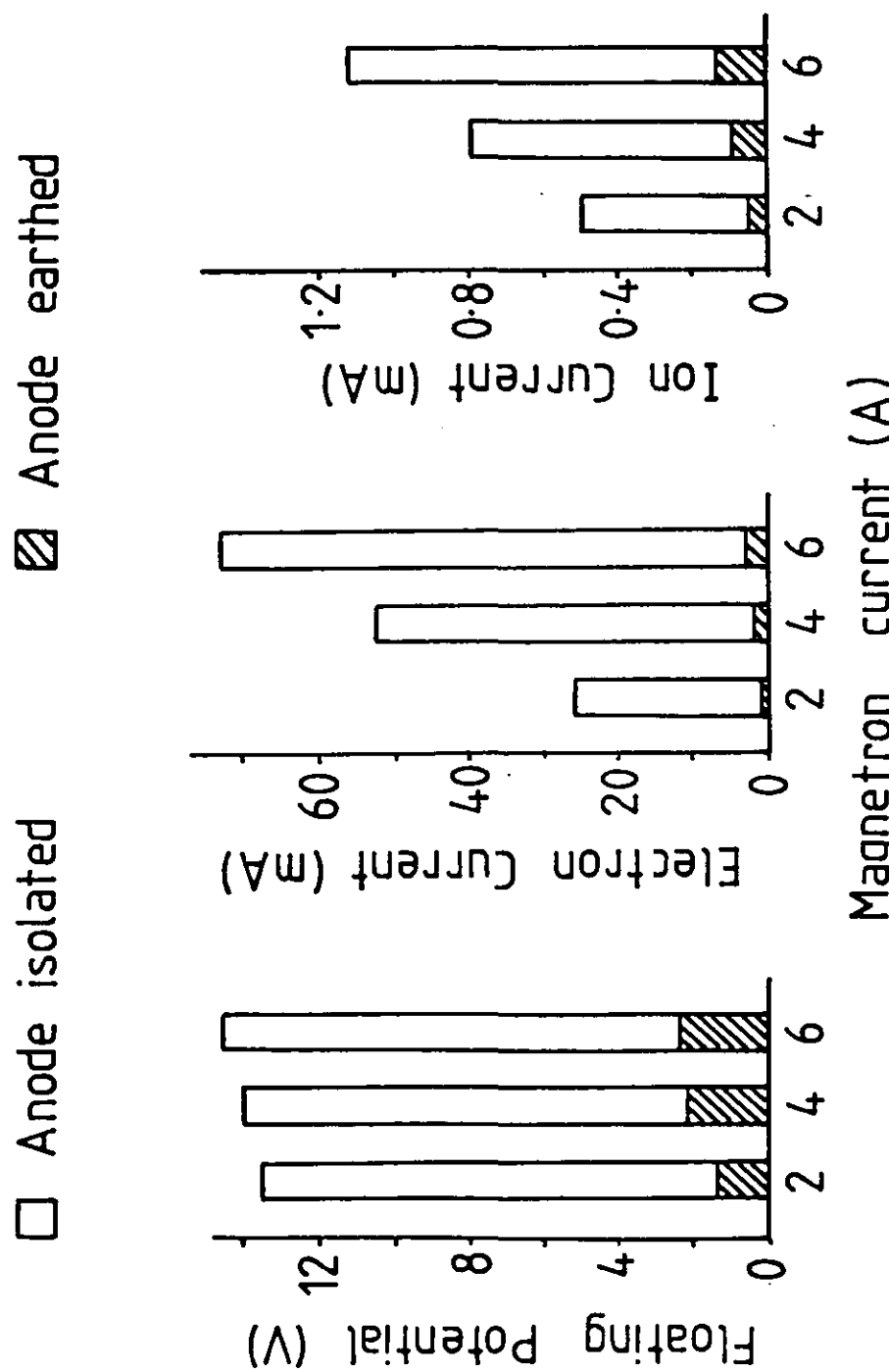

Fig. 10·4 : Measurements to determine the position of the In_2O_3 resistance minimum.

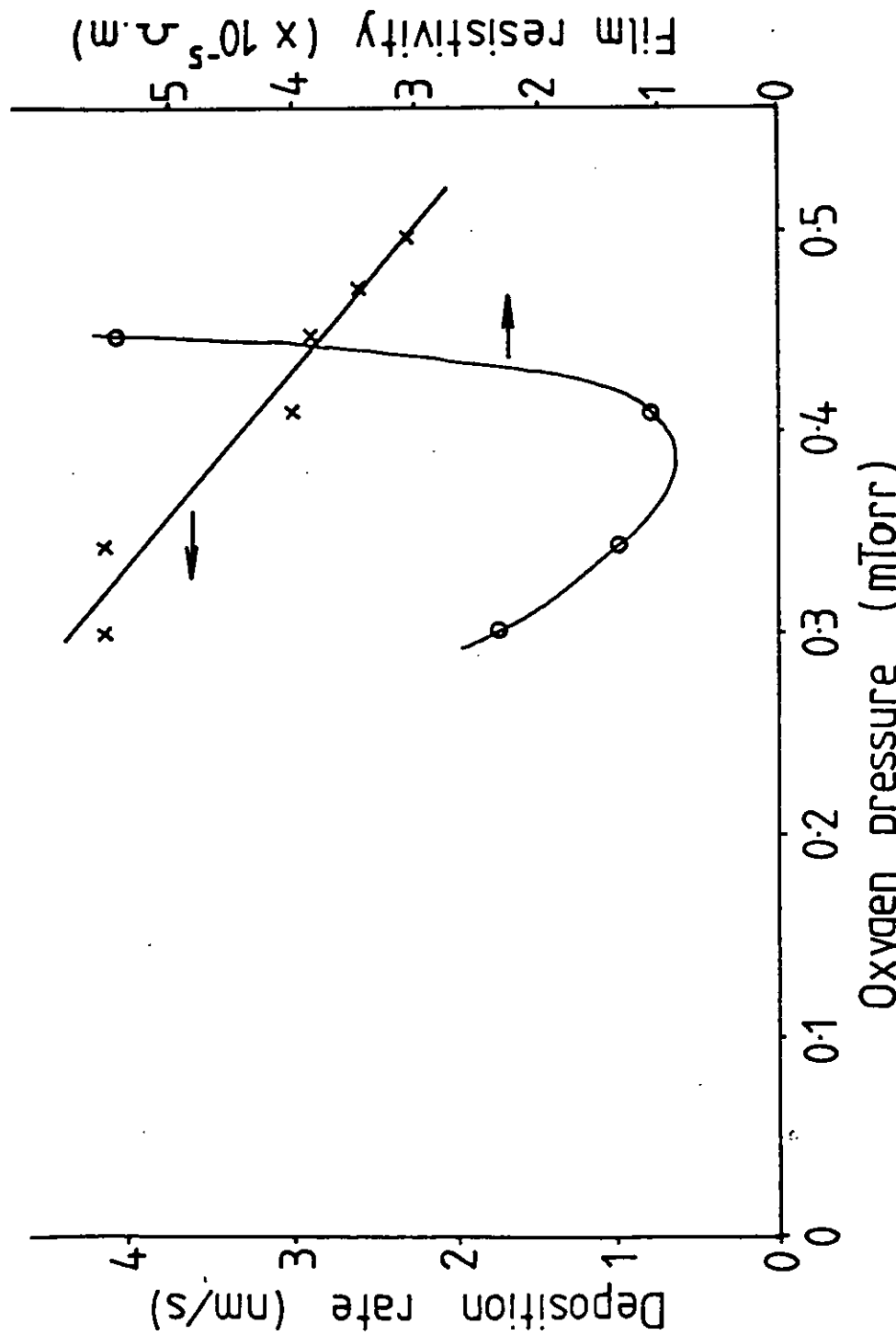

Now we can test various ideas about reactive sputter deposition. The two postulates identified in sections 3.3 and 3.5 were either that ratio of the arrival rates of the film components should be a constant or that the amount of gas consumed should be proportional to the amount of sputtered metal. In practice these two come down to an emphasis on the reactive gas pressure or the reactive gas flow.

Firstly we have the requirement for constant stoichiometry that (refs 8, 9) (see sections 3.3 and 3.5)

$$\frac{\text{Utilization} \cdot v_g}{v_m} = \text{constant}$$

where v_g = reactive gas arrival rate (atoms/s/unit area)
v_m = metal arrival rate (atoms/s/unit area)

For a constant reactive gas temperature v_g is proportional to the reactive gas pressure (section 3.7). For a constant film stoichiometry v_m is proportional to the deposition rate. Therefore with a constant utilization we would expect a graph of reactive gas pressure versus deposition rate to be linear with an intercept at the origin.

Plotting this for our films with and without the plasma beam we obtained fig 10.5. The two lines obtained clearly show an increase in utilization for plasma bombardment but as the curves do not pass through the origin our results do not accord a constant value of utilization for varying deposition rates.

Comparing our plasma beam (figs 8.3 and 10.1) with the discussion of decaying plasmas by Bardos (ref 10) it is apparent that the substrate will be bombarded with a decaying plasma rich in metastable species. The observed displacement of the optimum conditions to lower reactive gas pressures shows that this decaying plasma activates reactions at the substrate. This implies either (i) that excited species (probably metastables) have a higher reaction cross section than do simple gaseous or sputtered species, or (ii) that ion and/or electron bombardment activates surface reactions (ref 11).

Honke *et al* (ref 12) (see also section 3.3) derived the factor W/Q_{IN} (W = magnetron power, Q_{IN} = reactive gas flow) which they said

Fig. 10·5 : The position of the resistance minimum (In_2O_3) at different magnetron powers.

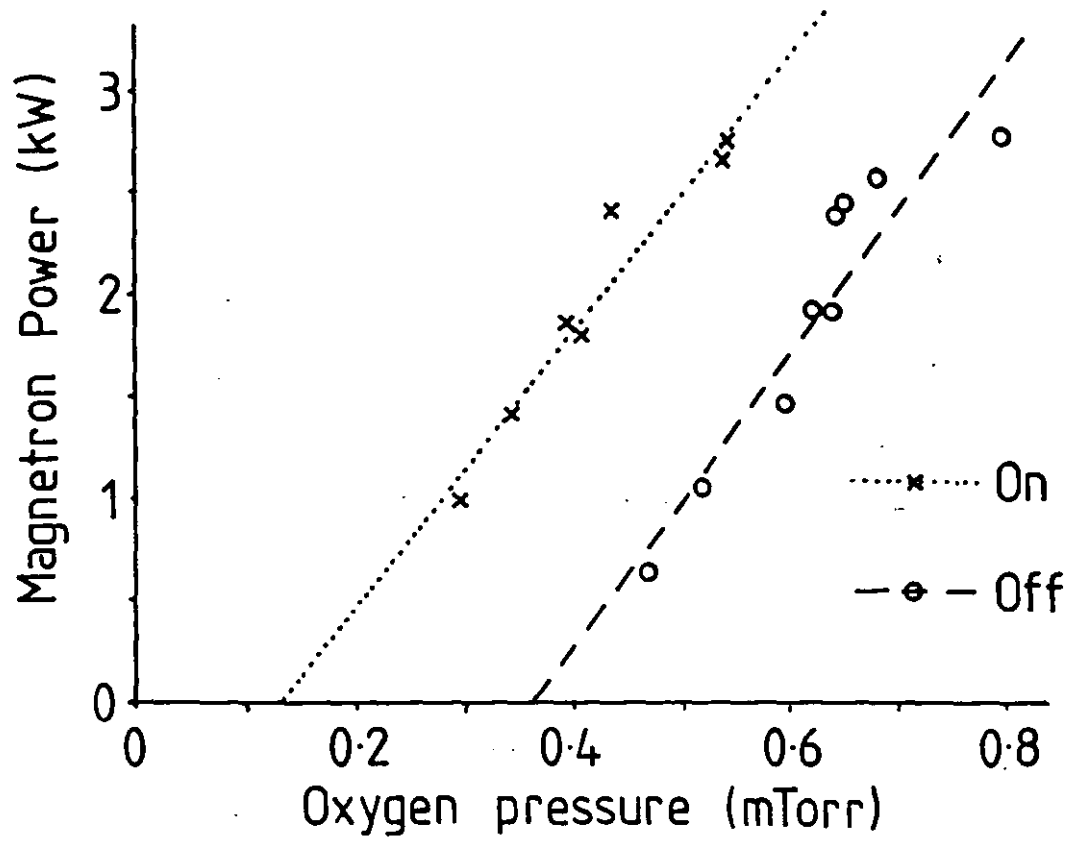

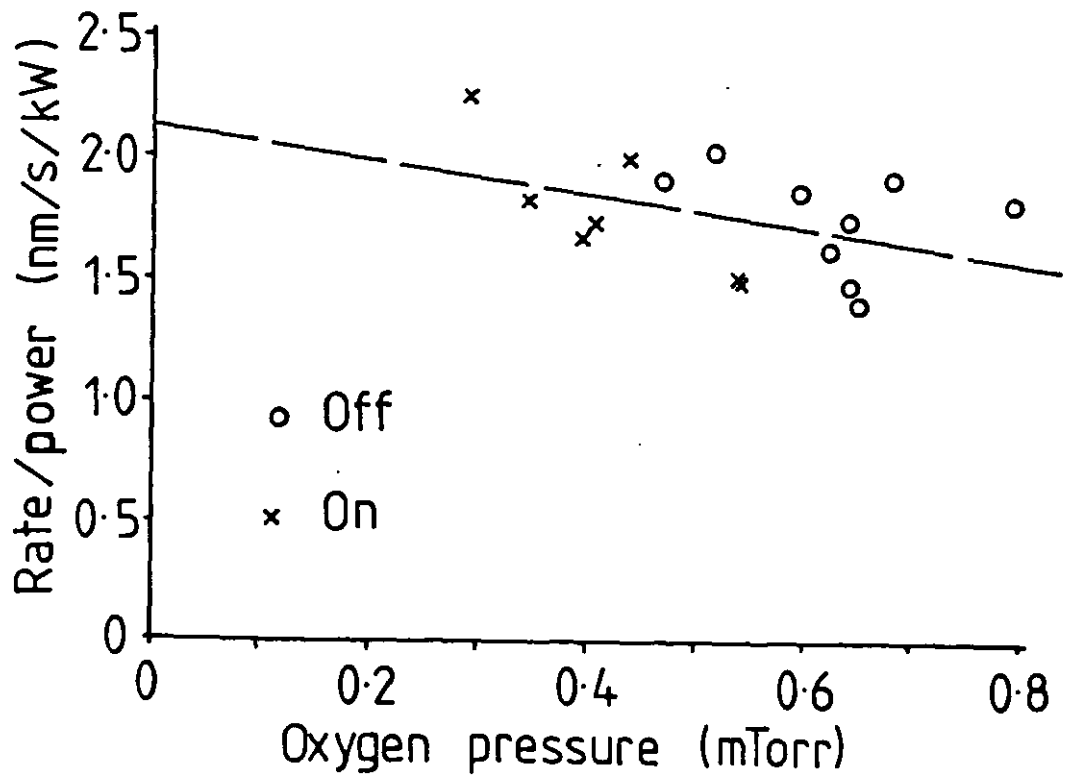

should remain constant for constant stoichiometry. I have plotted W vs Q_{IN} in fig 10.6a and this shows a linear relationship but a non-zero intercept and a separation with the differing activations. This is because the gas consumed by the vacuum pumps is not considered in their analysis. If we correct Q_{IN} for the pump consumption we obtain the film consumption $Q_{FILM} = Q_{IN} - P \cdot S_{PUMP}$. This is plotted in fig 10.6b. This gives a straight line, zero intercept and no separation with varying activation. The lack of separation implies a constant target condition ie f(p) is constant. This is borne out by the graph showing deposition rate/power (fig 10.5b). The least squares fit to this data shows only a small dependence on reactive gas pressure.

This method of calculating the film consumption of reactive gas then gives a better method of predicting the film stoichiometry than does simply monitoring the reactive gas pressure or the reactive gas flow.

Summary

- An unbalanced magnetron provides a simple controllable source of low energy ions at a high current density.
- This plasma activates surface reactions in reactive sputter deposition.
- By calculating the reactive gas consumption of the growing film, lines of constant stoichiometry for varying magnetron power can be produced.
- The reactive gas utilization is not constant with varying magnetron power and reactive gas pressure.

REFERENCES: CHAPTER 10

1. Bishop C.A., "The deposition of coatings onto polymer substrates by planar magnetron sputtering", PhD Thesis, LUT, (1986).

2. Oka K., "Plasma activated growth of reactively sputtered optical thin films", PhD Thesis, LUT, (1988).

3. Fraser D.B., "Thin Film Processes", Ed. Vossen J.L. and Kern W., p125, Academic Press, New York, (1978).

Fig. 10·6 : The position of the resistance minimum (In_2O_3) at different magnetron powers.

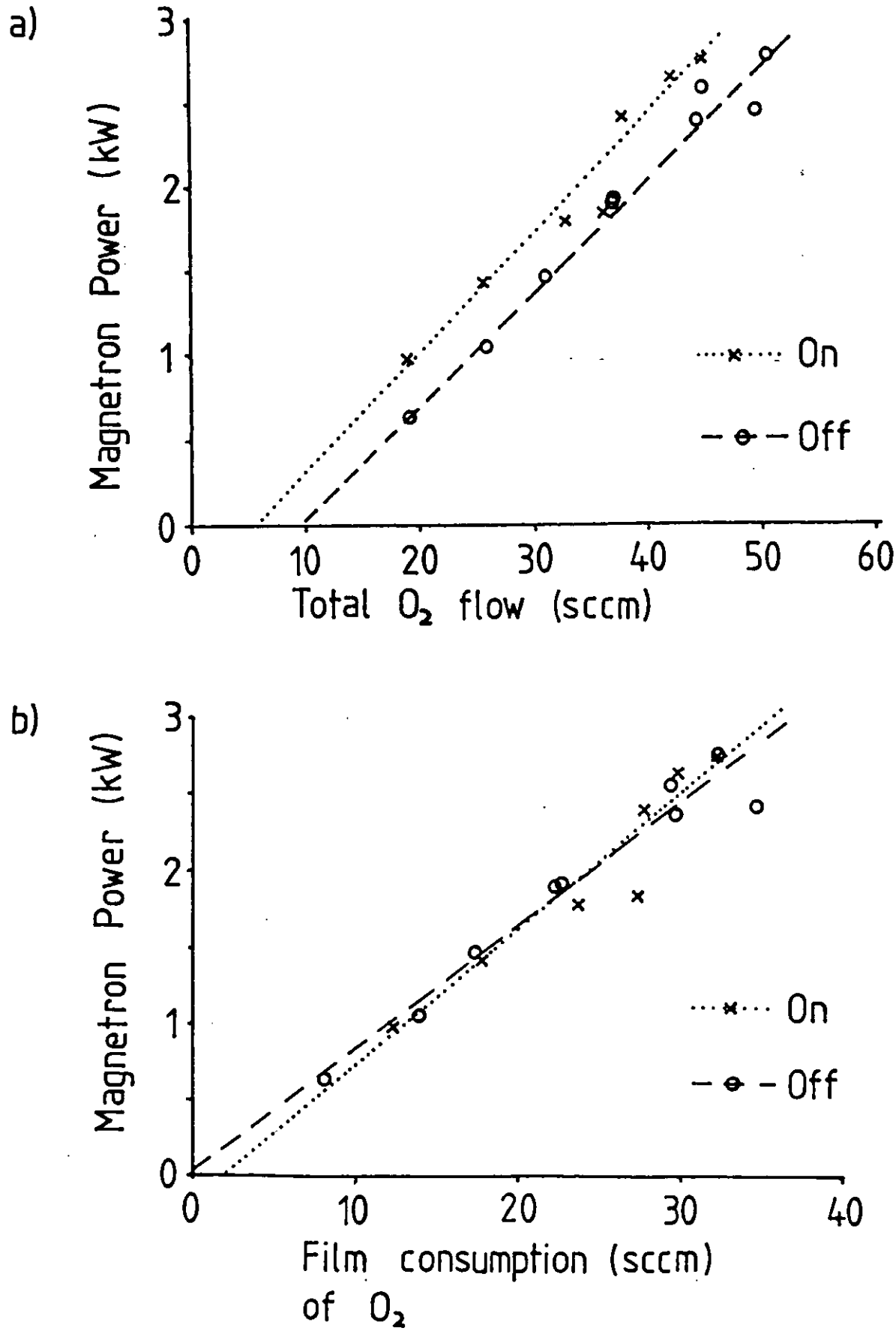

4. Spencer A.G., Oka K., Howson R.P., and Lewin R.W., Vacuum, 38, 857-859, (1988).

5. Warner E.S., Thesis to be submitted for M.Phil, Dept. of Physics, LUT, (1989).

6. Ridge M.I. and Howson R.P., Thin Solid Films, 96, 121-127, (1982).

7. Hamberg and Granqvist C.G., Solar Energy Materials, 14, 241-256, (1986).

8. Schiller S., Heisig U., Beister G., Steinfelder K., Strumpfel J., Korndorfer Chr., and Seiber W., Thin Solid Films, 118, 255-270, (1984).

9. Boenig H.V., "Fundamentals of plasma chemistry and technology", Technomic, Lancaster, USA, (1987).

10. Bardos L., Vacuum, 38, 637-642, (1988).

11. Coburn J.W. and Winters H.F., J. Appl. Phys., 50(5), 3189-96, (1979).

12. Honke D.K., Schmatz D.J., and Hurley M.D., Thin Solid Films, 118, 301-310, (1984).

11. DISCUSSION

My aim (perhaps over ambitious) was to find general aspects of reactive sputter deposition that could be applied to any reactive sputter deposition process. As discussed in the introduction the emphasis is on high rate processes. The areas covered in this thesis have been modelling, control and activation of reactive magnetron sputtering.

My model of the process identifies the origin of the instability seen in reactive magnetron sputtering and gives relationships between many factors (reactive gas consumption, speed of transition, film growth rate, effects of surfaces within the reaction chamber, etc). The instability comes down to a requirement for a positive gradient dQ/dP (because often the reactive gas pressure P is controlled simply by varying the input gas flow Q). For the vacuum pumps alone $dQ/dP = S_{PUMP}$ where S_{PUMP} is the pumping speed. The consumption of reactive gas by the film growth can be considerable and this exhibits a negative gradient in some reactive gas pressure regions. The instability occurs when $S_{PUMP} < - dQ_{FILM}/dt$ and so can be avoided by 'overpumping' the vacuum chamber ie large S_{PUMP}. In practice this often requires enormous pumps and is either not practical in existing systems or is expensive in new systems. One aspect not covered is the dependence of dQ_{FILM}/dP ($= S_{FILM}$) on magnetron design. From previous work (section 3.3) it is expected that higher current densities will result in the region of negative dQ_{FILM}/dP being shifted to higher reactive gas pressures. Experience at Everest suggests that this occurs as the target ages.

My experimental control of the reactive gas pressure in the unstable region has identified the gas distribution manifold as a major source of time delay (and hence oscillation) in the control loop. Theoretically I have confirmed this and produced two stability conditions for a control loop with gain K.

$$K > -(S_{FILM} + S_{PUMP})$$

$$1/T_g + \frac{(S_{FILM} + S_{PUMP})}{V} > 0$$

This shows the requirement for a small manifold time constant T_n and a large chamber volume V. The use of an enclosed reaction chamber would be beneficial to film purity (getter pumping for reactive impurities). Experiments to test the control loop in such a small volume would be useful.

It is found that as the magnetron power is increased the system becomes difficult to control. This implies that there is another stability condition involving the deposition rate. The measured deposition rate R (in monolayers/s) and the manifold time constant are such that a stability condition of the form $T_n < 1/R$ would be reasonable.

My results and analysis were for proportional control only. An initial result with proportional and integrating control suggests that this type of controller will perform much better. A PID (proportional, integrating, differential) controller may be used (gain = Kp + Ki/s + Kd.s) offering the possibility to 'tune' the controller to the deposition system.

With pulsed control a problem was identified in the rapid recovery of the target from poisoned to metallic. The gas distribution manifold had too long a time constant to 'catch' this recovery. Ironically the most reactive and unstable materials will have the slowest sputter rate from the poisoned target and will recover more slowly and be easiest to control. The rate of target recovery could also be slowed down by a permanent background of reactive gas. This greatly improved the performance of the switched control.

Activation of reactions at the substrate was demonstrated by the use of plasma bombardment from an unbalanced magnetron. This bombardment could be easily controlled by varying the self-bias on an electrode placed in the plasma. This activation offers the hope of moving the deposition of the required film out of the region of negative dQ_{FILM}/dP. The magnetron power and reactive gas pressure were varied while keeping the film stoichiometry constant. The results were not consistent with a constant utilization of the reactive gas ie the fraction of the reactive gas arriving at the substrate that is incorporated into the growing film is not a constant.

12. CONCLUSIONS

The main problem in high rate D.C. reactive magnetron sputtering is the stability of the process. Higher deposition rates and controllable film stoichiometry can be obtained if the process can be stopped from making the transition from a metal to a compound target surface. This can be done at the design stage by 'overpumping' the vacuum system but involves increased capital outlay. Without a high pumping rate for the reactive gas the transition from a metallic to a compound target surface becomes unstable. It would be desirable to control this unstable transition for two reasons. Firstly such a controller could be fitted to existing unstable systems to improve their performance. Secondly with such a controller the capital cost of new equipment could be reduced by removing the need for overpumping.

A model for the unstable transition is presented and this model explains many features of the instability and allows the calculation of (among other things) transition rates across the instability, the effects of increased pumping rate, and the effects of scaling up the process. During the unstable transition the metal flux from the target falls and the reactive gas partial pressure rises. These effects can be seen in the plasma light emission as a decrease or increase in the appropriate line intensity. By monitoring either the metal or reactive gas emission lines a control signal can be obtained.

A 0.5 m long magnetron was designed and used in a deposition system for 0.3 m substrates. This deposition system was unstable and was used as a test bed for various control systems.

Continuous or switched control mechanisms for the reactive gas flow based on the plasma emission were tested. We found that the greatest limitation was the time constant associated with the gas distribution manifold. Such a manifold is necessary to give a uniform reactive gas pressure but acts as a reservoir for the reactive gas and so restricts the response time of the control loop. By minimising the time constant of the manifold a control accuracy of a few percent can be obtained. The dependence on the manifold time constant was confirmed theoretically and this analysis also indicates that larger chamber volumes are easier to control.

At low magnetron powers very tight control can be obtained and this becomes worse as the magnetron power is increased. Depending on the control of film properties necessary the magnetron power can be increased until the degree of control becomes unacceptable. At present this limits the deposition rates obtainable and future work should concentrate on improving the control to allow higher magnetron powers. Modification of the controller gain to include integral or differential terms (PID control) offers the possibility of this improvement.

Activation of the reactive film growth by plasma bombardment was shown to occur. Such plasma bombardment can be easily obtained by using an unbalanced magnetron in which magnetic field lines leave the vicinity of the plasma trap and intersect the substrate. Once obtained such plasma bombardment can be controlled by the use of an electrode placed in this plasma. I investigated the magnetron power and reactive gas pressure at which a given film stoichiometry is formed (with and without plasma bombardment). It was found that the amount of reactive gas consumed by the growing film (as opposed to the total reactive gas flow) was proportional to the magnetron power and film growth rate. For constant film stoichiometry the ratio of reactive gas partial pressure to the deposition rate was not constant as has been suggested previously.

PUBLICATIONS LIST

"The properties of magnetron sputtered CoNi thin films",
A.G. Spencer and R.P. Howson, Vacuum, 36, 103-105, 1986.

"The Design and performance of planar magnetron sputtering cathodes"
A.G. Spencer, C.A. Bishop, and R.P. Howson, "Vacuum", 37, 363, 1987.

"Pressure stability in reactive magnetron sputtering"
A.G. Spencer, R.P. Howson and R.W. Lewin,
"Thin Solid Films", 158, 141-149, 1988.

"RF oscillations in DC planar sputtering magnetrons",
A.G. Spencer and R.P. Howson,
"Vacuum", 38, 6, 497-498, 1988.

"Activation of reactive sputtering by a plasma beam from an unbalanced magnetron",
A.G. Spencer, K. Oka, R.W. Lewin and R.P. Howson,
"Vacuum", 38, 857-859, 1988.

"A control process for stable operation of a high rate DC reactive planar magnetron sputtering system",
R.W. Lewin, A.G. Spencer and R.P. Howson.
Presented at European Vacuum Conference, Salford, 1988.
Abstract published in"Vacuum", 38, 947, 1988.

"High rate DC magnetron sputtering - A review",
R.P. Howson, A.G. Spencer and R.W. Lewin.
Presented at European Vacuum Conference, Salford, 1988.
Abstract published in "Vacuum", 38, 947, 1988.

"Design and use of a vacuum system for high rate reactive sputtering of $TiO_2/TiN/TiO_2$ solar control films",
A.G. Spencer, M. Georgson, C.A. Bishop, E. Stenberg and R.P. Howson.
"Solar Energy Materials", 18, 87-95, 1988.

"The formation and control of DC magnetron discharges for the high rate reactive processing of thin films",
R.P. Howson, A.G. Spencer and K. Oka.
Presented at AVS annual meeting, October 1988, Atlanta, USA. To be published in J. Vac. Sci. Technol.

"System design for high rate reactive sputtering of indium oxide solar coatings",
A.G. Spencer and R.P. Howson, SPIE, Sept. 1988, Hamburg, FDR.

"Control and activation techniques for the optimization of the reactive sputtering of TiO_2",
K. Oka, R.P. Howson, R.W. Lewin and A.G. Spencer, SPIE, Sept. 1988, Hamburg, FDR.

"Deposition of amorphous CoNbFe magnetic thin films by unbalanced DC magnetron sputtering",
G.H. Pan, A.G. Spencer and R.P. Howson. To be presented at IPAT 89, Geneva.

"High rate magnetron sputtering without a high vacuum pump", R.P. Howson, A.G. Spencer, S.A. Kazandjiev and E.M. Stenlake. To be presented at IPAT 89, Geneva.

"High rate reactive sputtering onto flexible polymer sheet",
R.P. Howson, A.G. Spencer, K. Oka and R.W. Lewin.
To be published in Proc. Electrochem. Soc., USA, 1989.